Tampere University

JENNI ALANEN

Aerosol Particle Emissions from Natural Gas Engines

Tampere University Dissertations 581

Tampere University Dissertations 581

JENNI ALANEN

Aerosol Particle Emissions from Natural Gas Engines

ACADEMIC DISSERTATION
To be presented, with the permission of
the Faculty of Engineering and Natural Sciences
of Tampere University,
for public discussion in the auditorium TB109
of the Tietotalo Building, Korkeakoulunkatu 3, Tampere,
on the 6th of May 2022, at 12 o'clock.

ACADEMIC DISSERTATION
Tampere University, Faculty of Engineering and Natural Sciences
Finland

Responsible supervisor and Custos	Professor Topi Rönkkö Tampere University Finland	
Supervisor	Professor Jorma Keskinen Tampere University Finland	
Pre-examiners	Associate Professor Katrianne Lehtipalo University of Helsinki Finland	Ph.D. Barouch Giechaskiel Joint Research Centre (JRC) Italy
Opponent	Professor Hanna Vehkamäki University of Helsinki Finland	

The originality of this thesis has been checked using the Turnitin OriginalityCheck service.

Cover design: Roihu Inc.

ISBN 978-952-03-2355-4 (print)
ISBN 978-952-03-2356-1 (pdf)
ISSN 2489-9860 (print)
ISSN 2490-0028 (pdf)
http://urn.fi/URN:ISBN:978-952-03-2356-1

PunaMusta Oy – Yliopistopaino
Joensuu 2022

PREFACE

The work for this thesis started with the first measurement campaign in 2014 at the Aerosol Physics Laboratory of Tampere University of Technology (TUT), now Tampere University (TUNI). This thesis has been written during the Tekes (Finnish Funding Agency for Technology and Innovation; currently Business Finland) funded projects CENGE and HERE, funded also by Neste Oil, AGCO Power, Wärtsilä, Dinex Ecocat, Dekati, Suomi Analytics, Viking Line, Dekati and Pegasor. Personal financial support from Gasum kaasurahasto (2014, 2016 and 2017) is also acknowledged.

This thesis would not have been finished without the collaboration and support from various people and organisations, in addition to persistence and my interest towards the world around us. First of all, I want to express my sincere gratitude to my supervisor Prof. Topi Rönkkö for believing in me and my work, for helping to articulate the results and for encouraging me when I was in doubt. Prof. Jorma Keskinen and the whole Aerosol group, thank you for a great place to work. It was a privilege to work with such highly skilled and enthusiastic scientists. I am very thankful for your friendship, help, and peer support. Special thanks to my roommate Fanni Mylläri.

I want to express my gratitude to all my co-authors, your input and expertise were invaluable. Especially I want to thank Dr. Erkka Saukko for the guidance during my first steps in the field of aerosol science, and for the inspiring and fun conversations. Special thanks also to Mr. Pauli Simonen and Ms. Niina Kuittinen for the diligent teamwork during the long days of the measurement campaigns and in between. All the papers in this thesis are a result of the interlaboratory and interdisciplinary collaboration between Tampere University, Finnish Meteorological Institute, and VTT Technical Research Centre of Finland. Therefore, thank you Dr. Hilkka Timonen, Dr. Sanna Saarikoski, Dr. Kati Lehtoranta, Mr. Timo Murtonen, Mr. Hannu Vesala, and others.

I am sincerely grateful to Ass. Prof. Katrianne Lehtipalo and Dr. Barouch Giechaskiel for pre-examining this thesis, thus improving its quality. Thank you Prof. Hanna Vehkamäki for agreeing to be the dissertation opponent and for taking the time to get acquainted with my thesis. I also want to thank my current manager Markus Iivonen and team lead Matti Happonen for the understanding during the final writing process.

For your love and support, and the encouragement towards reading and learning, I want to thank my family. I am very grateful to my friends for being in my life. My husband Mikko, thank you for everything, you have made this possible. Our sons Jori and Viljami, thank you for making life happy and for showing what really matters.

Ylöjärvi, March 2022

Jenni Alanen

ABSTRACT

Fine particle pollution emitted from anthropogenic sources such as traffic and energy production causes globally millions of premature deaths annually and, for example, cardiovascular and lung diseases. Airborne particles also contribute to the greenhouse effect either by absorbing or reflecting radiation and by serving as cloud condensation nuclei. In this thesis, the particle emissions from two retrofitted natural gas engines – one the size of a passenger car engine and the other the size of a ship's engine – from the exhaust line to the aged exhaust in the atmosphere are presented.

The size distribution measurement of tiny particles (1–5 nm) proved to be very important: With the smaller-scale engine, the particle emission was dominated by particles with a number size distribution peak diameter of 1–5 nm. With the larger engine, a high mode of nonvolatile core particles below 3 nm was found. All natural gas exhaust particles did not evaporate in thermal treatment, but only decreased in size, forming a trimodal size distribution that comprised a fuel-originated core mode with <10 nm particles, a lubricating-oil-originated core mode with spherical particles with a mean diameter of 6–20 nm, and a third mode that consisted of soot agglomerates and larger lubricating oil particles. In the dilution process, which mimicked the real-world fresh emission, a nucleation mode formed by nucleation and by condensation onto the core particles. The nucleation mode dominated the particle population, and its number concentration was further increased by a hot catalyst. Soot emission from the natural gas engines was small, but the particle number emission of the tiniest particles was not.

A flow-through reactor simulating the atmospheric photo-oxidation of several days was utilized to study the secondary aerosol formation potential of the exhaust. The measured formation potential of secondary aerosol mass was substantial, 1-2 magnitudes larger than the fresh exhaust particle mass and at a similar level to the secondary aerosol formation potential of clean diesel or gasoline engines. It was concluded that the urea used in the exhaust after-treatment system was the main source for secondary inorganic (mainly ammonium sulfate and ammonium nitrate) and the lubricating oil for the secondary organic aerosol mass.

This thesis produced a novel understanding of the number concentration, size distribution, composition, volatility, morphology, electric charge, and origin of particle emissions from natural gas engines and the effect of catalysts on the emissions. Also, new knowledge on the secondary aerosol formation potential of natural gas engine exhaust and its composition and volatility characteristics was obtained.

TIIVISTELMÄ

Pienhiukkaspäästöt esimerkiksi liikenteestä ja erergiantuotannosta aiheuttavat maailmanlaajuisesti miljoonia ennenaikaisia kuolemia ja esimerkiksi keuhko- ja verisuonisairauksia. Ilmakehässä hiukkaset voivat toimia pilvien tiivistymisytiminä ja ominaisuuksistaan riippuen joko kiihdyttää tai hidastaa ilmaston lämpenemistä. Tässä väitöskirjassa tutkittiin maakaasumoottoreiden hiukkaspäästöä ja sen elinkaarta pakoputkesta ilmakehään. Mittaukset suoritettiin kahdella jälkikäteen maakaasukäyttöiseksi asennetulla moottorilla, joista toinen oli henkilöauton ja toinen laivan moottorin kokoluokkaa.

Erittäin pienten, halkaisijaltaan 1–5 nm hiukkasten kokojakauman mittaus osoittautui tärkeäksi. Pienemmällä moottorilla lukumäärältään suuri hiukkaskokojakauman huippu havaittiin 1–5 nm:ssä ja suuremmalla moottorilla mittaus paljasti suurilukuisen haihtumattomien ydinhiukkasten moodin jatkuvan alle 3 nm hiukkaskokoon. Kuumennetussa näytteessä, joka kuvaa raakapakokaasua, kaikki hiukkaset eivät haihtuneet vaan pienenivät muodostaen kolmemoodisen kokojakauman. Pienimpien hiukkasten moodi koostui polttoaineperäisistä alle 10 nm haihtumattomista hiukkasista, keskimmäinen voiteluaineperäisistä keskikooltaan 6–20 nm pallomaisista hiukkasista ja suurin moodi nokihiukkasista ja suuremmista voiteluaineperäisistä hiukkasista. Laimetessaan ja jäähtyessään pakokaasusta muodostui nukleaation tai ydinhiukkasten ympärille tapahtuvan tiivistymisen kautta lukumäärää dominoiva nukleaatiomoodi, jota kuuma katalysaattori kasvatti. Maakaasumoottorien nokipäästö oli hyvin pieni, mutta erityisesti aivan pienimpien hiukkasten lukumääräpäästö ei.

Pakokaasun ikääntymistä ilmakehässä eli sekundääriaerosolin muodostuspotentiaalia tutkittiin luomalla erittäin hapettavat olosuhteet läpivirtausreaktorissa. Mitattu sekundäärisen aerosolin massa ylitti yllätten tuoreen pakokaasun hiukkasmassan jopa yli satakertaisesti ja vastasi diesel- ja bensiinimoottorin sekundäärisen aerosolin muodostuspotentiaalia. Jälkikäsittelylaitteessa käytetty urea oli merkittävä epäorgaanisen (pääosin ammoniumsulfaattia ja -nitraattia) ja moottorin voiteluöljy orgaanisen sekundääriaerosolin lähde.

Väitöskirja tuotti uutta ymmärrystä maakaasumoottorin hiukkaspäästön lukumääräpitoisuudesta, kokojakaumasta, haihtuvuudesta, koostumuksesta, morfologiasta, sähkövarauksesta ja alkuperästä, katalysaattorien vaikutuksesta hiukkaspäästöön sekä sekundääriaerosolin muodostumispotentiaalista ja sen koostumuksesta ja haihtuvuusominaisuuksista.

CONTENTS

ABBREVIATIONS

CI	compression ignition
CNG	compressed natural gas
CPC	condensation particle counter
CS	catalytic stripper
DF	dual-fuel
DI	direct injection
DR	dilution ratio
EDS	energy dispersive X-ray spectrometer
EEPS	engine exhaust particle sizer
EF	emission factor
ESP	electrostatic precipitator
FC	fuel-originated core
HC	hydrocarbon
LC	lubricating-oil-originated core
LNG	liquefied natural gas
LPG	liquefied petroleum gas
MDO	marine diesel oil
MGO	marine gas oil
NG	natural gas
OC	oxidation catalyst
PAM	potential aerosol mass reactor
PDR	primary dilution ratio, here over the PTD
PIQ	pilot fuel injection quantity
PM	particulate mass
PN	particle number (concentration)
PSM	particle size magnifier
PTD	porous tube diluter
RH	relative humidity
SCR	selective catalytic reduction
SI	spark ignition
SMPS	scanning mobility particle sizer
SOA	secondary organic aerosol
SP-AMS	soot-particle aerosol mass spectrometer
SPN	solid particle number (concentration)
TD	thermodenuder
TEM	transmission electron microscope
UV	ultraviolet radiation

ORIGINAL PUBLICATIONS

Paper 1 Alanen, J., Saukko, E., Lehtoranta, K., Murtonen, T., Timonen, H., Hillamo, R., Karjalainen, P., , H., Harra, J., Keskinen, J. and Rönkkö, T. (2015). The formation and physical properties of the particle emissions from a natural gas engine. *Fuel* 162, 155–161. DOI: 10.1016/j.fuel.2015.09.003.

Paper 2 Alanen, J., Isotalo, M., Kuittinen, N., Simonen, P., Martikainen, S., Kuuluvainen, H., Honkanen, M., Lehtoranta, K., Nyyssönen, S., Vesala, H., Timonen, H., Aurela, M., Keskinen, J. and Rönkkö, T. (2020). Physical Characteristics of Particle Emissions from a Medium Speed Ship Engine Fueled with Natural Gas and Low-Sulfur Liquid Fuels. *Environmental Science and Technology* 54, 5376–5384. DOI: 10.1021/acs.est.9b06460.

Paper 3 Lehtoranta, K., Murtonen, T., Vesala, H., Koponen, P., Alanen, J., Simonen, P., Rönkkö, T., Timonen, H., Saarikoski, S., Maunula, T., Kallinen, K. and Korhonen, S. (2017). Natural Gas Engine Emission Reduction by Catalysts. *Emission Control Science and Technology* 3, 142–152. DOI: 10.1007/s40825-016-0057-8.

Paper 4 Alanen, J., Simonen, P., Saarikoski, S., Timonen, H., Kangasniemi, O., Saukko, E., Hillamo, R., Lehtoranta, K., Murtonen, T., Vesala, H., Keskinen, J. and Rönkkö, T. (2017). Comparison of primary and secondary particle formation from natural gas engine exhaust and of their volatility characteristics. *Atmospheric Chemistry and Physics* 17, 8739–8755. DOI: 10.5194/acp-17-8739-2017.

AUTHOR'S CONTRIBUTION

This compound thesis consists of the following journal articles. All the publications are the result of the collaboration of several researchers. The author has contributed to all of the publications but takes credit only for the parts for which she is responsible. The contribution of other doctoral students is also specified below. The publications are cited based on the labels below.

Paper 1 The author participated in the measurements and data analysis, taking a major role. The article figures were drawn and most of the publication was written by the author.

Paper 2 The author planned and coordinated Tampere University's part of the measurements with an equal contribution with Ms. Niina Kuittinen, and participated in the data analysis, taking a major role. The figures were drawn and most of the publication was written by the author. Doctoral students Ms. Mia Isotalo, Mr. Sampsa Martikainen, Mr. Pauli Simonen and Ms. Niina Kuittinen also participated on the measurement campaign, Ms. Mia Isotalo carried out a preliminary data preparation and Ms. Niina Kuittinen and Mr. Pauli Simonen contributed to the preparation of the manuscript.

Paper 3 The author planned Tampere University's part of the measurements, worked as a project manager for Tampere University's part of the research project, and participated in the writing process, taking a minor role. Doctoral student Mr. Pauli Simonen participated in the measurement campaign and the data analysis.

Paper 4 The author participated in the planning and implementation of the experiments, worked as a project manager for Tampere University's part of the research project, analysed most of the data, and wrote most of the publication. Doctoral students Mr. Pauli Simonen operated the PAM chamber in major role and Mr. Oskari Kangasniemi conducted the calculation of the equivalent atmospheric aging.

1 INTRODUCTION

Natural gas (NG) engines are used in various applications, from small vehicles to very large marine and energy production applications. Although the first engines ran on gaseous fuel already in the 19th century, natural gas is still considered an alternative fuel in many applications. However, interest towards the utilization of natural gas has significantly grown over the past decades, and the growth will continue. In general, worldwide natural gas consumption has more than doubled over the last 30 years (*Gas consumption* 2019). For example, in the US, the capacity of natural gas fired engines has approximately tripled over the last 20 years (Ray 2019). In Finland, the number of new CNG (compressed natural gas) vehicles more than doubled every year in 2016–2020 (*First registrations of motor vehicles* 2021). In marine vessels, the share of LNG (liquefied natural gas) as fuel is only a few percentages, but LNG consumption and the number of LNG-fueled ships is expected to multiply in the next ten years (*Gas 2020* 2020; Fevre 2018). The increase in natural gas and NG engine usage is partly due to the increased need for engines as a reserve power source for wind and solar power – preferably with a low environmental burden. In the transport sector, it is hoped natural gas will provide a relatively clean alternative and a way to meet the ever more stringent emission regulations. Also economic aspects may partly encourage natural gas usage as a power source (e.g., Fevre 2018).

The increased usage of natural gas has awakened growing interest towards the emissions from NG engines. Particle mass emissions emitted by natural gas engines are usually lower than, e.g., those emitted by heavy fuel oil or gasoline fueled engines (e.g., Wang et al. 1997), which can make NG engines better for human health and the environment. However, natural gas engines also emit particles and the natural gas exhaust species react in the atmosphere, forming particles when the exhaust ages. When natural gas fueled engines become more widespread in transportation and energy production, their particle emissions become more relevant and important to study and mitigate. This applies to the whole exhaust lifespan, from the primary to the aged aerosol particles.

Exhaust particles undergo several transformation processes during their lifespan, each of which has importance from the aspects of emission legislation, human health, air quality, and climate. In this thesis, the concepts of primary and fresh exhaust particles and secondary aerosol formation are used. The term "primary particles" refers to the particles that are in the particle phase in the undiluted hot exhaust, such as soot and core mode particles. The primary particles form in the combustion process, inside or close to the engine cylinders. The term "fresh exhaust" refers to the exhaust that has just been emitted to the atmosphere and has experienced ambient temperature, humidity, and dilution processes, including nucleation (new particle formation), coagulation (particle aggregation), and condensation of gaseous species on the particle surfaces. Therefore, fresh exhaust particles consist of primary particles and particles formed in the dilution (i.e., delayed primary). When aging in the atmosphere, exhaust species go through oxidation reactions. The reaction products may transfer to the particulate phase, thus forming secondary aerosol mass. Total aged particles consist of secondary aerosol mass and the fresh exhaust particles that have remained in the particle phase after the exhaust aging. The different stages of the lifespan of the exhaust particles possess their own methods and challenges for measurement technologies.

Fresh exhaust aerosol particles often appear in two modes of the particle size distribution, that is, a nucleation mode with smaller particle diameters, and a soot (or accumulation) mode with larger particle diameters. The term "core mode particles" refers to the non-volatile core of the nucleation mode particles, which have been found and studied by several researchers (Rönkkö et al. 2007; De Filippo and Maricq 2008; Karjalainen et al. 2016; Saffaripour et al. 2015). Furthermore, the term "nanocluster" refers to particles in the size range of 1–3 nm. Nanoclusters are important in the processes initiating atmospheric aerosol formation (Kulmala et al. 2007) and are found in large fractions in particles emitted by road transportation (Rönkkö et al. 2017). Nanoclusters from engine exhausts – especially their size distribution – have been studied only recently and, to the author's knowledge, no such measurements have been reported for natural gas engine exhaust before this study.

Although the primary and fresh aerosol emissions are very important from the aspects of local emission, emission control, and human health, the significance of the secondary aerosol formation on the total air quality may be even more pronounced. For instance, the majority of the shipping-related $PM_{2.5}$ (particle mass of particles with a diameter of less than 2.5 μm) air pollution is of secondary origin (Viana et

al. 2014; Cesari et al. 2014), and during severe haze pollution events in China, secondary aerosol formation has been found to be responsible for 30–77% of the $PM_{2.5}$ (Huang et al. 2014). Furthermore, secondary organic aerosol (SOA) formation has been found to exceed primary particulate matter emissions from light-duty gasoline vehicles (Gordon et al. 2014). To the author's knowledge, no studies focusing on the secondary aerosol formation potential from natural gas engine exhaust has been reported in the literature before this study.

Aerosol particles influence radiative forcing, i.e., how much more energy is received by the Earth's surface than is radiated back into space, either with a cooling or warming effect on the climate (Boucher et al. 2013). The total radiative forcing of aerosol particles is cooling, although the radiative forcing effect of aerosol particles still has large uncertainties. For instance, sulfates and sea spray scatter solar radiation and thus tend to have a cooling effect, whereas soot particles in the atmosphere have a warming effect on the climate. Furthermore, soot particles on polar glaciers and other ice- and snow-covered surfaces cause the layer to absorb radiation instead of reflecting it, and thus to melt faster. Light-absorbing black carbon, a major constituent of soot, is the second largest climate change agent (Bond et al. 2013). Aerosols also work as cloud condensation nuclei, affecting the droplet size of clouds and their radiative forcing (Boucher et al. 2013). Soot emission from natural gas engines is typically much lower than from other internal combustion engines (e.g., Lehtoranta et al. 2019; Peng et al. 2020). Therefore, the particle emission of NG engines may contribute less to global heating.

Air pollution, mostly the fine particles $PM_{2.5}$, are estimated to cause 3.3 million, 4.2 million, or even 8.8 deaths globally a year (Lelieveld et al. 2015; Cohen et al. 2017; Lelieveld et al. 2020, respectively). The mortality, lung and cardiovascular diseases, and adverse health effects caused by air pollution are a huge problem, especially in highly polluted low- and middle-income countries (Cohen et al. 2017). However, there is strong evidence that fine, combustion-related particles increase mortality even in low mass concentrations (e.g., Hoek et al. 2013; Beelen et al. 2014). The smallest nanoparticles, which are typically significant in terms of number concentration, are hazardous because they may enter the human nervous and vascular system (Oberdörster et al. 2004; Pope III and Dockery 2006). Their relative surface area is also larger than that of larger particles, leading to potentially higher toxicity per unit mass (e.g., L. Salo et al. 2021). Particle pollution also deteriorates air quality and visibility. Reduction of particle emissions can improve air quality and save human lives.

The introduction of natural gas to the transport and energy sector has the potential to reduce airborne particle mass due to the relatively low particle mass emissions of gas engines (Goyal and Sidhartha 2003; Dong et al. 2018).

Particle characteristics (e.g., volatility, composition, and morphology) have an impact on the atmospheric and health related effects of the particles. For example, volatility affects gas-particle partitioning (e.g., Donahue et al. 2013), i.e., if the particles appear in the gaseous or particulate phase in the atmosphere when aging. The more surface area an aerosol particle possesses and the more toxic species are condensed on the particle surface, the more toxic it is. The particle characteristics also implicate the formation process of particles, the knowledge of which can be used when designing the best emission-mitigation strategies. In this thesis, the particle characteristics of fresh and aged exhaust particles are studied and compared for the first time for natural gas engines.

The prevention of global heating (formerly global warming) needs solutions. The CO_2 emissions from clean NG combustion can be smaller than from, e.g., diesel combustion because of the higher hydrogen-to-carbon ratio of the fuel (mostly methane CH_4) (e.g., Cho and He 2007). Natural gas is a nonrenewable fossil fuel, but it is often thought of as a "bridge" to the usage of renewable biogas. In fact, natural gas engines sometimes run with a mixture of natural gas and biogas that is injected in the natural gas grid (Köppel, Götz and Graf 2009; Savickis et al. 2020). Naturally, the combustion of renewable biogas may cause even smaller CO_2 emissions. Despite the potentially lower CO_2 emission, the total greenhouse gas emissions from an NG engine may still be high due to the methane slip that is difficult to control (Wei and Geng 2016), especially at low loads (Peng et al. 2020). The amount of the methane slip depends on, e.g., the fuel-air ratio and operation mode of the engine. Lean-burn (air excess) engines and low-load operation emit more methane than stoichiometric and high-load operation (Ushakov, Stenersen and Einang 2019).

NG engines also emit pollutants such as CO and NO_x that may need to be controlled, e.g., by oxidative and SCR (selective catalytic reduction; for NO_x reduction) catalysts. Therefore, also the catalysts and their state influence the emission levels. For example, oxidative exhaust after-treatment oxidizes SO_2 and enables sulfuric acid formation (Rönkkö et al. 2013), and the urea used in the SCR technology may form particles (Legala et al. 2021). In this thesis, the effects of two exhaust after-treatment systems targeting the oxidation of hydrocarbons and reduction of nitrogen oxides

were examined at a wide range of exhaust temperatures. The effect of catalysts on both the fresh and the aged exhaust particles was studied.

1.1 Aim and scope

The aim of this thesis was to study the characteristics of the particle emission from natural gas engines. The measurements were conducted on two different-sized retrofitted natural gas engines running at two steady-state engine operation modes. The smaller engine was a spark-ignited (SI) old passenger car gasoline engine and the larger engine was a compression-ignition (CI) engine with a liquid fuel pilot.

The focus of the thesis was on particle number emission, number size distribution, and the volatility of the nanoparticles emitted by the natural gas engines, and on secondary aerosol formation from the natural gas engine exhaust. Particle morphology, composition, volatility, and electric charge measurements allowed the analysis of the particles' origin. The effect of catalysts on the fresh and aged exhaust particles was also studied. Emission comparison to low-sulfur liquid fuels was enabled by measurements on the larger engine. Finally, a method for measuring and comparing the volatility characteristics of different chemical species of the fresh and aged exhaust particles was applied. The methods, results, and research outcomes of the thesis are summarised in Figure 1.1. The broad variety of aerosol instruments at the Aerosol physics unit and the excellent collaboration between research groups allowed a profound analysis of the emissions.

The scope of the thesis was on experimental work. The engines studied were a large-bore power plant or marine engine and a small-scale engine designed to resemble a large-bore engine's exhaust. The scope of the background projects that made the thesis possible was on steady-state power-plant-relevant engine operation. However, the results provided valuable information also on natural gas engine exhaust particles and exhaust particle formation phenomena in general.

The research questions were the following:

- Where are natural gas engine exhaust particles generated, and what are their composition and physical characteristics?
- How does exhaust after-treatment affect the particulate emission?

- How much secondary aerosol mass does the natural gas engine exhaust form in the atmosphere, and what are the origin, composition and volatility characteristics of the secondary aerosol?
- How does the particle emission of a large-scale compression ignition natural gas engine differ from one run with other fuels?

Chapter 2, *Natural gas engine emission studies*, introduces the literature of exhaust particles from natural gas engines. The engines, exhaust after-treatment, and particle emission technologies are presented in Chapter 3, *Experimentation*.

Deeper analysis on the particle lifespan from primary to aged exhaust is presented in Chapter 4, *Results and discussion*, which first studies the primary particles present in the primary exhaust in the exhaust line and then moves to the particles in the freshly emitted exhaust that are formed and grown in the dilution and cooling process of the exhaust. The effect of catalysts and catalyst temperature on the primary and fresh exhaust particle formation is discussed in Section 4.3, *The effect of catalysts*. These sections discuss particle concentrations primarily in terms of number concentration.

Secondary aerosol formation in the atmosphere and the physical characteristics of the secondary aerosol are discussed in the fourth section of Chapter 4, *Results and discussion*. The results of the thermal evaporation method at a temperature range from room temperature to near 300 °C combined with aerosol spectrometer and a comparison of fresh and aged aerosol particles are also given in Section 4.4, *Aged exhaust particle mass*. Chapter 5, *Comparison to liquid-fuel combustion*, compares the obtained results to the literature and to the low-sulfur liquid fuel combustion of the larger-scale engine. The implications of the work are discussed in Chapter 6, *Summary*.

The primary particle origin is discussed in **Papers 1 and 2** and the effect of exhaust after-treatment in **Papers 3 and 4**. The fresh exhaust particles and their properties are discussed in **Papers 1, 2, 3, and 4**, and the secondary aerosol formation and characteristics in **Paper 4**.

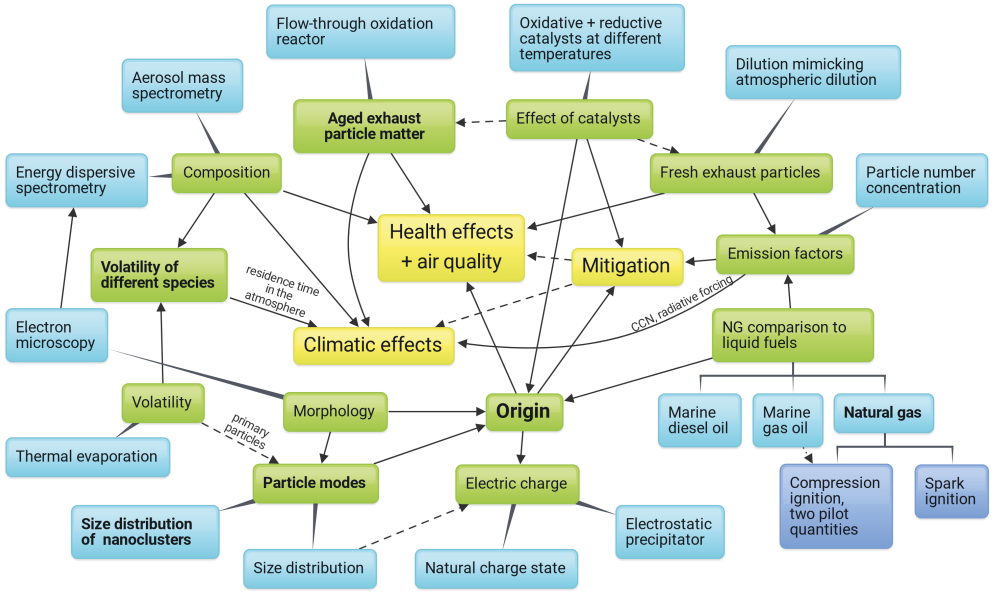

Figure 1.1 This thesis studied the exhaust particles from natural gas engines. The methods (blue), results (green), and future outcomes (yellow) of the thesis are presented here. The most important and novel findings and methods of the thesis are highlighted in bold text. CCN = cloud condensation nuclei. The mind map was created at the website bubbl.us

2 NATURAL GAS ENGINE EMISSION STUDIES

The research of particle number emission from natural gas engines has accelerated over the last few years (Table 2.1). Especially at the time of our first publication in 2015, the number of natural gas engine emission studies focusing on particle number was very small. Even today, the particle number emission from large-scale natural gas engines is reported only by a few studies.

Natural gas engines may be either spark-ignited (SI), or compression-ignition (CI) engines with an igniting injection of a liquid pilot fuel (Jääskeläinen 2021). That is, in compression ignition engines, a small quantity of the liquid pilot fuel is also combusted in the engine. The quantity of the pilot fuel may vary from <5% to 100% (liquid fuel only combustion), the small quantities being more common. The air-to-fuel mixture in natural gas engines may be either lean or stoichiometric, and the fuel may be either premixed or non-premixed. In general, spark ignition, premixing, and stoichiometric configurations are more common in passenger car engines, whereas lean-burn, diesel-pilot-ignited engines are more common in power plant, marine, and non-road applications (Jääskeläinen 2021). In Table 2.1, the ignition method is given, where available.

It is generally known that the particulate mass (PM) emissions from natural gas engines are small (e.g., Hallquist et al. 2013; Frailey et al. 2000). However, the particle number emission is not necessarily low when compared to modern diesel and gasoline engines, especially when particles down to 10 nm or smaller are counted (e.g., Toumasatos et al. 2021; Gómez et al. 2021). In particular, the particle number (PN) emissions from retrofitted engines, not originally optimized for NG combustion, may be relatively high (Lehtoranta et al. 2019).

The PN emission factors (EF; particles emitted per produced energy, consumed fuel, or distance) found in the literature are presented in Table 2.1 together with the ones measured in the papers of this thesis. The reported particle number emissions from NG engines varied a great deal. Particle concentrations, calculated to the undiluted

exhaust concentration, of 0.001–100 $\times 10^5$ cm^{-3} have been reported. The emission factors of engines were usually given in unit kWh^{-1}, being 0.1–330 $\times 10^{12}$ kWh^{-1}. The largest emission was produced by idling (i.e., without load) large-scale engines and the lowest emission (Lehtoranta et al. 2019) was reported for the solid >23 nm particles only from a dual-fuel (DF) engine. The EFs of vehicles, usually reported per distance travelled, were 0.01–1,400 $\times 10^{12}$ km^{-1}. The cleanest vehicles were modern passenger cars (Dimopoulos Eggenschwiler, Schreiber and Schröter 2021; Kontses et al. 2020) and the dirtiest were older buses (Jayaratne et al. 2009; Hallquist et al. 2013).

Five of the studies have measured the particle number concentration of particles down to 2.5–3 nm, but in the majority of the studies, measurement instruments were not able to detect the particles below 5–10 nm in size. In this thesis, the particle number (PN) size range measured was down to ca. 1 nm. The majority of the vehicle studies were conducted in real-world conditions and the rest of the vehicle studies and the engine studies were conducted under laboratory conditions. In the laboratory, the effect of the sampling and dilution system on the particle concentration is significant (e.g., Ntziachristos et al. 2016), especially on the volatile particles. This study was conducted in a laboratory with a dilution system that aimed to reproduce real-world particle emission formation.

In comparison to the NG exhaust literature for a similar engine size range, the particle number emission factors measured from the small-scale engine (**Paper 1**) were usually at the same level or higher (Table 2.1). Also from the large-scale engine (retrofitted DF 1.4 MW engine, **Paper 2**), the total particle number emission was clearly higher than reported in the literature for large-scale natural gas engines (Anderson, K. Salo and Fridell 2015; Corbin et al. 2020), although lower than from liquid fuel combustion in the same engine (**Paper 2**; Kuittinen et al. 2021). In this thesis, the engines were retrofitted to run with natural gas; the combustion parameters might not have been perfect for NG combustion. Secondly, the wider particle size range measured in this thesis may explain difference to the literature. Thirdly, in this thesis, all particles (not only solid) were measured, and the dilution conditions favored particle formation in the dilution in order to mimic atmospheric dilution. Therefore, the higher emissions can be explained by the different sampling conditions compared to the literature. The results of this thesis are more thoroughly addressed in Chapters 4 and 5.

Table 2.1 Particle number emissions of NG engines and vehicles in the literature and this thesis, calculated to exhaust line/stack concentrations. The values are extracted from plots if not given in numbers in the text. Exhaust after-treatment methods and combustion ignition method given where available.

Study	Application	PN (cm^{-3})	EF (kWh^{-1})	EF (kg_{fuel}^{-1})	EF (km^{-1})	PN size range
Ristovski et al. (2000)	525 and 1082 kW engines, SI	$0.2–100 \times 10^5$	-	-	-	15–700 nm
Holmén and Ayala (2002)	CNG bus, SI	$0.1–0.8 \times 10^5$		-	-	6–237 nm
Holmén and Qu (2004)	CNG bus, SI	$0.06–0.2 \times 10^5$	-	-	-	29–164 nm
Schreiber et al. (2007)	3 retrof. DF buses, SI	-	-	-	$1.8–410 \times 10^{11}$	>7 nm, solid
Quillen et al. (2008)	298 kW engine, SI	ca. 3×10^5	ca. 2.5×10^{12}	-	-	7–1000 nm
Jayaratne et al. (2009)	13 buses, OC or TWC	$0.1–1.8 \times 10^5$	-	-	$1–14 \times 10^{14}$	>5 nm
Hallquist et al. (2013)	7 buses	-	-	$7.8 \pm 5.7 \times 10^{15}$	$40 \pm 29 \times 10^{14}$	5.6–560 nm
Hajbabaei et al. (2013)*	3 buses, SI, TWC or OC	-	-	$1.5–7.5 \times 10^{12}$	$1.5–7 \times 10^{12}$	>2.5 nm
Karavalakis et al. (2013)*	waste hauler, SI	-	$2–9 \times 10^{11}$	-	$1–21 \times 10^{12}$	>2.5 nm
Anderson, K. Salo and Fridell (2015)	DF 7.6 MW engine, CI	-	$2.3–5.7 \times 10^{12}$	-	-	5.6–560 nm
Anderson, K. Salo and Fridell (2015)	DF 2.8 MW engine	-	$58–64 \times 10^{12}$	-	-	5.6–560 nm
Pirjola et al. (2016)	5 buses, TWC	$0.01–38 \times 10^5$	-	$29 \pm 5 \times 10^{12}$	-	>2.5 nm
Amirante et al. (2017a)	single-cylinder engine, SI	$0.7–100 \times 10^5$	-	-	-	5.6–560 nm
Giechaskiel (2018)	trucks and buses, TWC	-	-	-	$3–45 \times 10^{11}$	>23 nm, solid
Giechaskiel et al. (2018)	trucks and buses, Euro VI, TWC	-	$0.6–10 \times 10^{11}$	-	-	>23 nm, solid
Giechaskiel, Lähde and Drossinos (2019)	2 cars, SI, Euro 6	-	-	-	$0.2–20 \times 10^{11}$	>10 nm, solid
Giechaskiel et al. (2019)	2 cars, SI, TWC	-	-	-	ca. $1–16 \times 10^{11}$	>10 nm, solid
Lehtoranta et al. (2019)	retrof. DF 1.4 MW engine, CI	-	ca. 1×10^{12}	-	-	>23 nm, solid
Lehtoranta et al. (2019)	DF 1 MW engine, CI	-	1.3×10^{11}	-	-	>23 nm, solid
Giechaskiel et al. (2020b)	car, SI, Euro 5	-	-	-	ca. 9×10^{10}	>10 nm, solid
Distaso et al. (2020)	100 kW engine	-	ca. 3×10^{12}	-	-	5–1000 nm
Corbin et al. (2020)	2 DF 4.3 MW engines, CI	-	$6.0 \pm 2.7 \times 10^{13}$	-	-	5.6–560 nm
Corbin et al. (2020)	2 DF 4.3 MW engines, CI, idle	-	$3.3 \pm 0.3 \times 10^{14}$	-	-	5.6–560 nm
Kontses et al. (2020)	car, SI, TWC	-	-	-	$2.4–14 \times 10^{10}$	>23 nm, solid
Zhu et al. (2020)*	2 heavy-duty vehicles, SI, TWC	-	-	-	$5–100 \times 10^{12}$	>3 nm
Dimopoulos Eggenschwiler, Schreiber and Schröter (2021)	car, SI, TWC	-	-	-	$0.7–7 \times 10^{10}$	>10 nm, solid
Gómez et al. (2021)	bus, SI, TWC	-	$3–4 \times 10^{11}$	-	$2–5 \times 10^{11}$	>10 nm
Toumasatos et al. (2021)	3 cars, SI, Euro 6	-	-	-	$1.8–39 \times 10^{11}$	>2.5 nm, solid
Lähde and Giechaskiel (2021)	2 cars, Euro 6, SI, TWC	-	-	-	ca. $2–50 \times 10^{11}$	>4 nm, solid
Paper 1	retrof. 100 kW engine, SI	$38–346 \times 10^5$	$19–260 \times 10^{12}$	$78–710 \times 10^{12}$	-	>1.5 nm
Paper 1	retrof. 100 kW engine, SI	$2.5–45 \times 10^5$	$1.3–34 \times 10^{12}$	$5.1–93 \times 10^{12}$	-	>1.5 nm, solid
Paper 2	retrof. DF 1.4 MW engine, CI	$6.1–12 \times 10^8$	$2.7–7.1 \times 10^{15}$	$16–32 \times 10^{15}$	-	>1.2 nm
Paper 2	retrof. DF 1.4 MW engine, CI	$0.09–1.6 \times 10^8$	$0.04–0.8 \times 10^{15}$	$0.2–4.1 \times 10^{15}$	-	>1.2 nm, solid
Paper 3	retrof. 100 kW engine, SI, OC+SCR	$7–1200 \times 10^5$	$5–880 \times 10^{12}$	$14–2390 \times 10^{12}$	-	>1.2 nm
Paper 3	retrof. 100 kW engine, SI, OC+SCR	$0.3–64 \times 10^5$	$0.2–48 \times 10^{12}$	$0.6–130 \times 10^{12}$	-	>1.2 n, solid

* Recalculation of values demanded, e.g., miles to km or GGE to kg_{fuel}.
DF = dual-fuel, PN = particle number, EF = emission factor, SI = spark ignition, CI = compression ignition, TWC = three-way catalyst, OC = oxidation catalyst, SCR = selective catalytic reduction

According to the studies published before the articles in this thesis, particles with a diameter below 50 nm dominate the particle size distribution of NG exhaust (e.g., Quillen et al. 2008; Ristovski et al. 2000). Size distribution peaks of tiny particles below 12 nm were reported by, e.g., Jayaratne et al. (2009) and Hallquist et al. (2013). However, especially the particle size distributions measured by Hajbabaei et al. (2013) indicate that instrument limitations prevented the measurement of even smaller peak particle diameters. The size distribution and particle concentration measurement comparison by Toumasatos et al. (2021) has confirmed this observation. Before this thesis, no measurements of a particle size distribution of <4 nm were reported.

The composition of the NG engine emission particles has been speculated over and analysed by many. Natural gas engine emitted particles may consist of lubrication oil additives and engine wear metals (Thiruvengadam et al. 2014), lubricant oil droplets (Amirante et al. 2017b; Giechaskiel, Lähde and Drossinos 2019), volatile organic compounds (Jayaratne et al. 2009; Pirjola et al. 2016), ash (Jayaratne et al. 2012), or sulfuric acid/water nucleation particles (Holmén and Ayala 2002). Burner studies have also shown that natural gas combustion can generate carbonaceous nanoparticles (e.g., Commodo et al. 2013).

Several studies indicate lubricating oil is the primary source of the particulate matter in natural gas engine exhaust, both non-volatile and volatile (e.g., Holmén and Ayala 2002; Jayaratne et al. 2012; Hajbabaei et al. 2013; Anderson, K. Salo and Fridell 2015; Pirjola et al. 2016). The evidence for the lubricating oil contribution is strong: e.g., an additional injection of lubricating oil into the engine cylinder was found to increase the emission of predominantly very small particles (Amirante et al. 2017b). Also, the particle number of soot or "accumulation" mode (>20–30 nm) was increased with a large amount of lubricant oil, especially if the conditions allowed the oil to survive the combustion process as droplets.

Although natural gas mainly consists of short-chain hydrocarbons, the literature has shown that also the gaseous fuel plays a role in the magnitude of the particle emission from natural gas engines (Karavalakis et al. 2013; Hajbabaei et al. 2013). Strong evidence of natural gas as the source of NG exhaust nanoparticles is presented by Amirante et al. (2017b): lubricating oil free spark-ignition natural gas combustion on a special test engine was found to emit ca. 1.5×10^6 cm^{-3} particles with a bimodal number distribution. The relative contribution of the gaseous fuel was still minor: with a lubricating oil injection to the intake manifold, the number concentration was up to 100 times higher and three particle modes were present in the size distribution.

The volatility of the NG engine exhaust particles has also been studied by several researchers, who have concluded that the fresh NG exhaust particles are very volatile. In number basis, volatile fractions of at least 98% (Jayaratne et al. 2012), 8–92% (Anderson, K. Salo and Fridell 2015), and 5–45% (Graves et al. 2015) have been reported. In volume basis, volatile fractions of over 95% and 58% have been reported (Bullock and Olfert 2014; Pirjola et al. 2016, respectively). The volatile fraction depends on several aspects, such as engine operation conditions, air humidity, and temperature. Also, if measured under laboratory conditions, the sampling system has a considerable effect. Not all sampling systems are developed to replicate atmospheric

dilution processes. Therefore, the volatilities measured in the laboratory may not represent real-world conditions.

There is a shortfall of thorough research on the effect of exhaust after-treatment systems on the particle number emission of natural gas engines. In the study of Guo et al. (2014), compressed natural gas (CNG) buses were found to emit less PN and PM with the presence of oxidation catalysts (OC). Distaso et al. (2020), on the other hand, measured an increased PN emission downstream of an oxidative pre-catalyst and then a decreased PN emission downstream of a three-way catalyst (TWC).

In addition to **Paper 2** of this thesis, one study focusing on the secondary aerosol formation from NG exhaust was found. Le Breton et al. (2019) measured a secondary aerosol mass production 150 times higher than the fresh exhaust particle mass emission from a NG engine – 2140 mg kg^{-1} and 14.2 mg kg^{-1}, respectively. The secondary aerosol mass formation potential from the NG-fueled buses was at a similar level to diesel and rapeseed methyl ester-fueled buses, and it was hypothesized to originate from lubrication oil and SCR technology.

3 EXPERIMENTATION

The measurements for **Papers 1, 3, and 4** were run on an old passenger car gasoline spark-ignition engine (maximum power 100 kW/5500 rpm, 2.0L displacement), retrofitted to run with natural gas. The engine was run in a manner that aimed to generate the exhaust matrix of a large-bore power plant engine (see Murtonen et al. 2016). This was done by adjusting the engine to produce the desired NO_x and CO levels and, during one of the two engine operation modes, by injecting extra hydrocarbons into the exhaust. The small engine was used instead of a large-bore power plant engine in order to save space, costs, fuel, and catalyst material. The first of the steady-state engine operation modes (M1, higher torque) was 70 Nm, 2700 rpm, 20 kW, 6.0% excess oxygen, and no short-chain hydrocarbon (HC) addition, and the second engine operation mode (M2, lower torque) was 35 Nm, 3100 rpm, 12 kW, 6.3% excess oxygen and a HC addition.

A dual-fuel large-bore engine (1.4 MW, medium speed) was used in the measurements for **Paper 2**. The engine was retrofitted to enable the dual-fuel operation with natural gas and a marine gas oil (MGO) pilot injection. The engine was studied at two steady-state operation modes representing the maneuvering (40% load) and cruising (85% load) of a marine vessel. The MGO pilot quantity was also varied; it was either 4% or 6% in terms of total fuel consumption in mass for the 40% load, and either 1% or 2% for the 85% load in order to study the effect of the pilot fuel on particulate emissions.

The fuel used in all studies was high-methane-content (ca. 97%) Russian pipeline natural gas. In **Paper 2** and in Chapter 5, the results gained with natural gas operation were compared to MGO and marine diesel oil (MDO) operation. The sulfur content of the MGO and MDO was relatively low, below 0.001% and 0.1%, respectively, and the sulfur content of the NG was below 1.5 ppm.

In **Papers 3 and 4**, two different exhaust after-treatment systems were applied. The catalysts utilized were an OXICAT-x, a single reactor tailored to simultaneously oxidize CO and formaldehyde and to reduce NO_x, and a combination of a separate

methane oxidation catalyst (MOC) and an SCR. Urea was utilized for the NO_x reduction in both catalyst sets. The urea feed was adjusted at an exhaust temperature of 400 °C to an ammonia slip level <5 ppm and a NO_x conversion level of >90% for both engine operation modes, but it was not readjusted for each tested exhaust temperature. This might have led to suboptimal SCR performance at the other exhaust temperatures. There is a more detailed description of the catalysts in **Paper 3**.

Exhaust flow through the catalysts and exhaust temperature were adjusted independently of engine operation mode (Murtonen et al. 2016). The catalyst studies were performed at an exhaust temperature range of 350–500 °C, and the particle results reported were measured at an exhaust flow of 80 kg/h (excess exhaust bypassed the catalysts). The space velocities for the catalyst systems were 12,400 1/h and 8,600 1/h for the OXICAT-x and MOC+SCR, respectively.

For the particle measurements, the exhaust was sampled using a sampling system consisting of a porous tube diluter (PTD; Mikkanen et al. 2001) that introduces the dilution air gradually to the exhaust sample, a residence time tunnel, and an ejector diluter (Dekati Ltd.). Primary dilution ratios (PDR) of 6 and 12 were used, 6 in **Papers 1, 3, and 4**, and 12 in **Paper 2**. The particulate matter measured after the PTD dilution system represents the fresh exhaust particles. The PTD dilution system enables the reproduction of real-world emission formation in laboratory conditions to good accuracy: previous studies have shown that the PTD dilution system produces a similar particle size distribution to the ones in real-world ship plumes (Kuittinen et al. 2021; Ntziachristos et al. 2016) and diesel exhaust (Ntziachristos et al. 2004; Rönkkö et al. 2006).

In this thesis, the particle population is studied primarily in terms of number concentration. An engine exhaust particle sizer (EEPS, TSI Inc.; Mirme 1994), a scanning mobility particle sizer (Nano-SMPS and Long-SMPS; TSI Inc.), and a combination of a particle size magnifier (PSM; Airmodus Ltd.) and a condensation particle counter (CPC) allowed the particle number size distribution measurement at a wide range, from very small particles – even down to <5 nm — to particles of 560 nm. The total particle number concentration was measured by an ultrafine CPC or the PSM (cutoff size ca. 2.5 nm and 1 nm, respectively). All concentrations presented in this thesis were calculated back to the exhaust concentrations, i.e., corrected by the dilution ratio. In order to reduce uncertainty from different correction factors, transfer line losses were not corrected for in the calculation of the results.

In **Paper 3**, PM was collected on filters at 42–52 °C according to ISO 8178-1:2006 for the particle mass measurements. A 30 min sampling time and a dilution ratio of 10 were applied.

The chemical composition of the particles was measured with a soot particle aerosol mass spectrometer (SP-AMS; Aerodyne Research Inc., USA). The SP-AMS consists of a high-resolution time-of-flight aerosol mass spectrometer and a single-particle soot photometer (SP2; Droplet Measurement Technologies Llc.). In the calculation of the concentrations of chemical species, a collection efficiency of the default 0.5 was used in **Paper 3** and of the composition-dependent parametrization by Middlebrook et al. (2012) in **Paper 4**.

Volatility measurements were conducted with a thermodenuder (TD; Heikkilä et al. 2009) designed for nanoparticle measurements at 265 °C and with a catalytic stripper (CS; Amanatidis et al. 2013) at 350 °C. The particulate matter measured downstream of the thermodenuder or the catalytic stripper represents the primary exhaust particles, i.e., the particle population present in the undiluted exhaust. In the thermodenuder, the sample is first led through a heated section in order to evaporate the volatile fraction of the particles and then through an active charcoal section where the evaporated particulate matter is absorbed. The catalytic stripper is an oxidation catalyst followed by an absorber section (sulfur trap). The thermodenuder was also used at 7–10 different steady temperatures between 30–265 °C (**Paper 1**) or at a slowly (ca. 45 minutes) decreasing temperature (**Paper 4**) in order to gain an indication of the particle evaporation temperatures. In the data analysis, particle losses in TD and CS were corrected for.

Particles in the diluted exhaust sample were collected on holey-carbon films both with and without CS treatment. Transmission electron microscopy (TEM; JEM-2010, Jeol Ltd.) was then used to examine the particle morphology, and energy dispersive spectrometry (EDS; Noran Vantage with Si(Li) detector, Thermo Scientific Inc.) was utilized to study the elemental composition of the particles collected on the TEM grids (**Paper 2**).

The fraction of electrically charged particles was measured using an electrostatic precipitator (ESP) upstream of the Long-SMPS (**Paper 2**) or by bypassing the neutralizer upstream of the Nano-SMPS (**Paper 1**). The ESP collects the particles carrying an electric charge, thus letting only the neutral particles pass through. By subtraction of the particle size distribution without and with the ESP, the size distribution of

the naturally charged particles can be obtained. Without the neutralizer, the electric charge of the particles is not forced to equilibrium at room temperature. Therefore, the particles can be classified based on their existing charge state.

Because all the secondary aerosol formation potential of an exhaust sample cannot be directly measured or reliably evaluated using gaseous emission measurements (Gentner et al. 2017), other methods, such as flow-through oxidation chambers, need to be utilized. In **Paper 4**, a potential aerosol mass reactor (PAM; Kang et al. 2007; Lambe et al. 2011) was used to simulate the oxidation process of the exhaust representing the atmospheric aging of several (4–11) days. The particulate matter measured downstream of the PAM flow-through reactor represents the total aged aerosol with a high degree of oxidation. An oxidative environment in the PAM reactor was generated using two UV lamps emitting 85 and 254 nm radiation with a UV light voltage of 10 V. The flow through the 13L PAM reactor was a constant 5 L/min, and it was located between the PTD and ejector diluter. The measurements were done after 10–15 minutes of stabilization time after switching the UV lights on. The photochemical age simulated by the PAM chamber UV lights was calculated using the properties of the PAM chamber, measured concentrations of gaseous components (NO, NO_2, CO, methane, ethene, propane, ethene), a model based on MCM v3.3.1 via the website `http://mcm.leeds.ac.uk/MCM`, and an assumption of the average OH concentration of 1.5×10^6 molec cm^{-3} in the atmosphere (Mao et al. 2009).

During the PAM measurements, the relative humidity (RH) in the PAM reactor was very high, 80%. This was due to the very low primary dilution ratio over the PTD. However, during the background measurements, the RH was only 30%. The high humidity of the sample created uncertainty in the results and complicated reliable background subtraction: humidity in the sample enhances particulate mass formation (Lambe et al. 2011). The measured background mass was small in comparison, but the decision was made not to subtract it from the reported particle masses measured downstream of the PAM due to the comparability uncertainties.

The gaseous emissions and the dilution ratio were measured using a Fourier transform infrared spectroscopy (FTIR) analyser, a non-dispersive infrared (NDIR) analyser, and a chemiluminescence detector (CLD). A Sick Maihak SIDOR gas analyser was used to measure the CO_2 concentration of the diluted sample.

An illustration of the measurement setups is given in Figure 3.1. Note that not all the instruments in the figure were used in all the measurement campaigns. In **Paper**

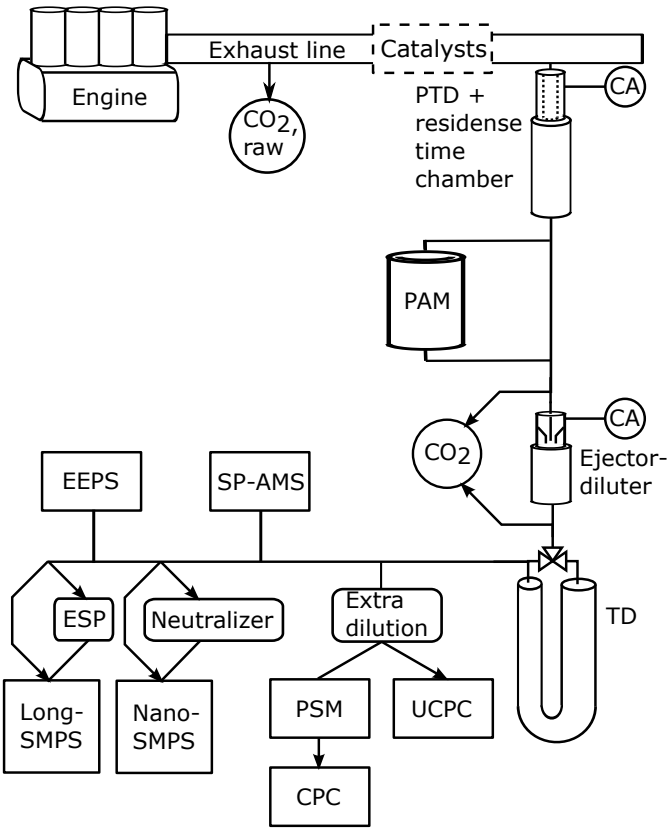

Figure 3.1 An illustration of the measurement setup used in all the measurement campaigns with small modifications. . CA = compressed air, PTD = porous tube diluter, PAM = potential aerosol mass reactor, EEPS = engine exhaust particle sizer, SP-AMS = soot particle aerosol mass spectrometer, ESP = electrostatic precipitator, TD = thermodenuder (sometimes replaced by the catalytic stripper), SMPS = scanning mobility particle sizer, PSM = particle size magnifier, UCPC/CPC = (ultrafine) condensation particle counter, Catalysts = Exhaust aftertreatment devices. Modified from **Papers 1 and 4**.

3, the sample was taken from two different positions: upstream and downstream of the catalysts and in **Paper 4**, only downstream of the catalysts.

4 RESULTS AND DISCUSSION

4.1 In the exhaust line – primary particles

The particles that are in the particulate phase in the exhaust line are called primary exhaust particles. The primary exhaust particles are relevant from the point of view of the reduction of particle emissions and the properties contributing the health and climatic effects of the particles. Because those particles in the exhaust line are non-volatile due to their existence in high exhaust temperatures, their number, size, and characteristics can be analyzed by studying the non-volatile particles of a diluted exhaust sample. In **Papers 1, 2, and 3**, the primary particles were studied by leading the diluted sample through the TD or the CS. The thermodenuded (or CS-treated) sample is assumed to best represent the primary exhaust particles. However, e.g., Ntziachristos et al. (2016) have observed that the new material condensed in the sampling process is difficult to evaporate in a thermodenuder. Also, Giechaskiel et al. (2020a) highlight that there is a risk for renucleation when using a thermodenuder, i.e., risk of producing an artefact of volatile particles downstream the TD, but the risk is lowered if a catalytic stripper is applied instead.

Figure 4.1 shows the size distributions of the particles emitted by the NG-fueled small-scale engine without any exhaust after-treatment (**Paper 1**). The size distribution of the particles led through a heated thermodenuder, i.e., the primary particles, is presented with dashed lines. With both engine operation modes, particles that were non-volatile at 265 °C were detected. The majority of these nonvolatile particles were very small, below 5 nm in diameter. The peak of the primary exhaust particle size distribution was observed at nanocluster aerosol sizes, in the size range of 1–3 nm. That size range was measured for the first time for natural gas engine exhaust and it proved to be very important. A second non-volatile particle mode with the peak at ca. 6 nm was also observed. In addition, a third particle mode at higher particle diameters of more than 20-30 nm can be seen in the size distribution figure.

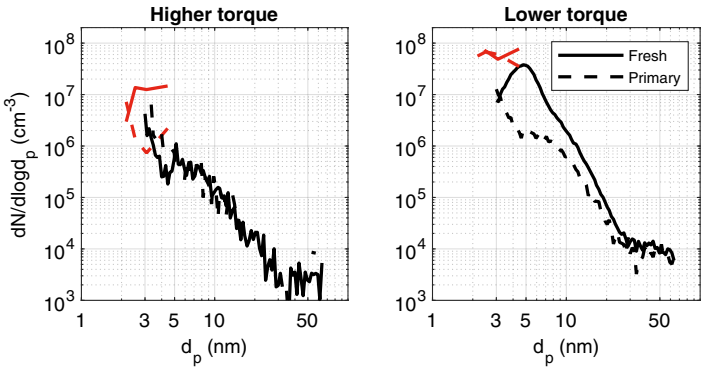

Figure 4.1 Particle size diameters of fresh (solid line) and primary (dashed line) particles measured with PSM (red) and Nano-SMPS (black) for both engine operation modes at the small-scale engine. The particle concentrations are given for the undiluted exhaust. Three primary particle modes can be seen, the peak size below 3 nm, at around 6 nm, and above 20 nm. Modified from **Paper 1**.

Figure 4.1 shows a discrepancy between the particle size distributions measured with PSM and Nano-SMPS both in diameter and concentration. This discrepancy can be at least partly explained by the calibration method of the PSM with silver particles that was used in **Paper 1**. PSM calibration links critical supersaturation levels to particle mobility diameter. This relation is material dependent; silver particles were probably less prone to grow with the condensation of diethylene glycol (working fluid used in PSM) than the exhaust particles (Kangasluoma et al. 2013). Thereby, the size distribution measured by PSM is shifted towards larger diameters if the PSM calibration is done with silver particles. This calibration method was not applied in the other papers; the default calibration of the PSM was used. The discrepancy in concentration may be due to the lower particle detection efficiency of Nano-SMPS than taken into account by the inversion algorithm of the device (Olin et al. 2019).

The primary exhaust particles were studied for the NG-fueled (with the MGO pilot) large-bore engine as well (**Paper 2**). In Figure 4.2, the particle size distributions of the exhaust samples downstream of CS are presented. The similar three particle modes were found in the exhaust of the large-bore engine also. The smallest non-volatile particles, detected by the PSM, had a diameter of below 3 nm. The middle-mode had a diameter around 10 nm, and the largest particles measured by Long-SMPS had a mean diameter of above 30 nm.

Based on the measured size distributions downstream of TD or CS, it can be concluded that solid core particles, not formed in the dilution process, already exist in the

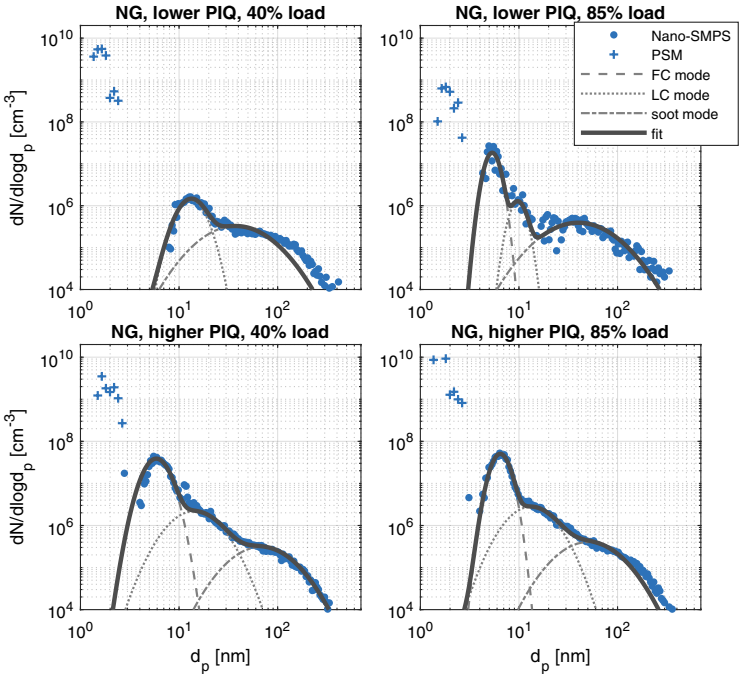

Figure 4.2 Number size distributions of the primary particles (measured downstream of the catalytic stripper) from the large-bore engine measured by PSM and SMPS. Also particle mode fits are given on the size distribution measured by SMPS. Modified from **Paper 2**. FC = fuel-originated core (mode), LC = lubricating-oil-originated core (mode), PIQ = pilot injection quantity.

exhaust line. These particles form a non-volatile core of at least a fraction of the fresh-exhaust nucleation mode particles (see the next section). In addition to these small core particles, soot particles are emitted by NG engines and exist in the particulate phase before the dilution processes.

The number of soot particles emitted by the NG engines was low. In **Paper 1**, the soot mode particles were originally not discussed due to their very low concentration (Figure 4.1). From the large-scale engine (Figure 4.2), the concentration of soot mode particles was approximately two magnitudes higher than from the small-scale engine, but still relatively low. In addition to the NG composition (low content of, e.g., aromatics and carbon-carbon bonds) (Hajbabaei et al. 2013), the well premixed mixture of the combustion air and NG before the ignition prevents large soot emissions (e.g., Majewski and Jääskeläinen 2021).

The size distributions measured with the PSM show that the size range covered by the SMPS does not reach the smallest relevant particle diameters. However, the

combination of the size distributions from the two instruments has proven difficult. Therefore, mode fitting in **Paper 2** was done to the size distributions measured with the SMPS only, following the example of Kuuluvainen et al. (2020). Three particle modes were fitted in the size distributions: FC mode (fuel-originated core mode), LC mode (lubricant-originated core mode), and soot mode. It is possible that the PSM size-range particles form one more separate particle mode in Figure 4.2. However, this study assumes that the particles in the PSM size range are a part of the FC mode. This interpretation is clearer when looking at Figure 4.1: the size distribution measured with the SMPS rises towards the small diameters and the FC mode particle distributions measured with PSM and Nano-SMPS overlap.

In the top-left image (NG with the lower pilot injection quantity, 40% load) of Figure 4.2, an FC mode was found only in the size distribution measured by the PSM, below the size range of the SMPS. Because the FC mode could be measured by the SMPS with all the other fuels (see also Chapter 5) with the higher pilot injection quantity and with the higher load (larger fuel quantity), **Paper 2** suggests the core mode would originate from the liquid pilot fuel. However, the FC mode was found in the NG only combustion of **Paper 1** as well. Therefore, the FC mode particles could also originate from incomplete NG combustion. This conclusion is supported by the study of Amirante et al. (2017b), which measured a bimodal particle size distribution (with a dominating mode at <10 nm and the other mode at around 35 nm) with NG only combustion without lubricating oil. Thus, also a fraction of the soot mode particles most probably originated from the combustion of natural gas.

The morphology of the primary particles is presented in Figure 4.3. There were 2–3 types of particles on the TEM samples collected from the large-bore engine (**Paper 2**). In Figure 4.3, examples of the soot agglomerates (indicated by EDS) are marked with purple circles, LC mode particles are marked with orange circles, and the FC mode particles are marked with a blue circle. The FC mode particles were only weakly visible on the TEM grids, which points to a carbonaceous composition. Spherical particles dominated the TEM images, their size covering a large size range from ca. 10 nm to relatively large (up to 300 nm) particles that were in the same size range as the soot agglomerates. Also Baldelli et al. (2020) found spherical particles in NG and diesel exhausts at low load and idling, and they interpreted them as originating from the lubricating oil.

The composition analysis of the TEM samples with EDS showed that the soot agglomerates contained carbon, and the spherical particles of the size range down to ca.

10 nm contained lots of lubricating oil marker elemental calcium and small amounts of, e.g., sulfur, phosphorus, and silicon. The result strongly indicates that the spherical particles were originated from the lubricating oil.

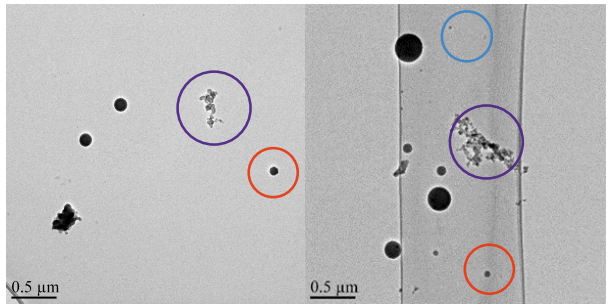

Figure 4.3 Transmission electron microscopy images of particles collected downstream of the CS (catalytic stripper) at an engine load of 40% from the larger-scale engine. Examples of soot agglomerates are circled with purple, lubricating-oil-originated particles with orange, and fuel-originated particles (only weakly visible on the grids) with blue. Spherical particles with a wide size range dominate. Modified from **Paper 2**.

Aerosol particles may become electrically charged, e.g., by ion diffusion, i.e., through collisions of particles and ions. The charge distribution at a certain temperature eventually finds an equilibrium described by the Boltzmann equation (Liu and Pui 1974). At high temperatures, the fraction of charged particles is higher than at low temperatures.

In **Paper 1**, the natural charge carried by the particles was measured by the Nano-SMPS without the neutralizer, and the gained particle size distribution was then compared to the size distribution measured with the neutralizer upstream of the Nano-SMPS, i.e., with the aerosol in an equilibrium charge state. It was observed that the exhaust particles from the small-scale engine carried approximately three times more positive electric charge than at equilibrium at room temperature. This observation indicates that the particles were formed and had gained an electric charge at a high temperature, i.e., inside or near the engine cylinders. In Figure 4.4, the theoretical charging probability $f_n(+)$ for positively charged particles was calculated using the improved Fuchs charging probability approximation formula (Wiedensohler 1988) for the neutralizer, and the natural charging probabilities of the particles $f_{ion}(+)$ were calculated by multiplying the ratio of the size distributions measured without and with the neutralizer with the theoretical charging probability. Note that even though the charging probabilities were clearly larger than at equilibrium, they were still small, less than 15%.

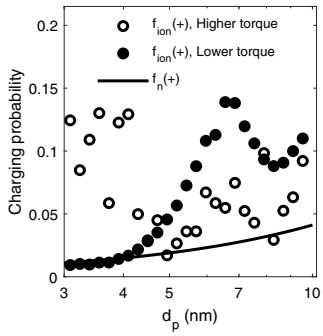

Figure 4.4 The charging probabilities for the neutralizer $f_n(+)$ (solid line; Wiedensohler 1988) and the naturally charged particles (circles). The $f_{ion}(+)$ were calculated by multiplying the average charging efficiency approximation for the neutralizer with the ratio of the size distributions measured with the Nano-SMPS with and without the neutralizer. Modified from **Paper 1**.

In the ESP method used in **Paper 2** to study the electric charge of the particles, the size distribution of neutral particles only was measured with the Long-SMPS downstream of an electrostatic precipitator. The size distribution of the neutral particles was subtracted from the size distribution of all particles (measurement without the ESP). The result was the size distribution of the naturally charged particles. It was found that a fraction of the nucleation mode particles in the large-scale engine exhaust carried an electric charge. Actually, the number of the naturally charged core mode particles was much higher than the number of naturally charged soot mode particles, although almost all soot-mode particles carried a charge (**Paper 2**: Figure 4 and related discussion). Soot mode particles are known to be formed in the engine cylinders, and the charging probability of the soot mode particles was higher due to their larger size (e.g., Wiedensohler 1988). The fraction of the naturally charged particles indicated a high particle formation temperature, although uncertainties remained. The electric charge of exhaust particles has been studied in order to determine the particle formation temperature and origin by, e.g., Lähde et al. (2009), Maricq (2006), De Filippo and Maricq (2008), and Sgro et al. (2012) for liquid fuels. In this thesis, electric charge measurements were conducted for the first time with exhaust particles from natural gas engines.

The concepts of fuel- and lubricating-oil-originated core modes were introduced by Kuuluvainen et al. (2020), and their primary particle nature is supported by multiple studies (e.g., Ushakov et al. 2013; Hallquist et al. 2013; Lähde et al. 2014; Rönkkö and Timonen 2019; Sgro et al. 2012; Seong and Choi 2014; Corbin et al. 2020;

Fushimi et al. 2011). In this study, their primary particle nature is supported by their non-volatility, TEM images, and their electric charge.

The non-volatile fraction of the NG exhaust particles, interpreted as the primary particles, consisted of a fuel-originated core (FC) mode, a lubricating-oil-originated (LC) core mode, and a soot mode. Mixed with the soot particles, larger lubricating oil particles were present in the soot mode as well. The number of the FC and LC mode particles exceeded the soot mode particles, but the mass of the FC and LC mode particles was only 2% or less of the soot mode PM (supplementary section of **Paper 2**).

With the larger-bore engine, the fuel-originated core mode particles had a mean diameter of 6–10 nm (based on Nano-SMPS measurement) or smaller (1–2 nm, based on the size distribution measurement with the PSM), and the lubricating-oil-originated core mode had a mean diameter of 10–30 nm. The non-volatile particle mode of 1–2 nm that the PSM detected is probably – but not self-evidently – part of the same fuel-originated core mode as the one detected by Nano-SMPS. With the smaller-bore engine (**Paper 1**; Figure 4.1), both core modes can be seen, too. There, the core mode of the smaller particles, assumably the fuel-originated core mode, had mean particle diameters of sub-4 nm, and the lubricating-oil-originated core mode had mean particle diameters of sub-10 nm.

As a conclusion, the solid raw exhaust particles consisted of fuel- and lubricating-oil-originated core mode particles, soot agglomerates and larger spherical lubricating-oil-originated particles. The smallest core particles were of the size of nanoclusters.

4.2 Shortly after emission – fresh emissions

Fresh exhaust particles are represented by the porous tube diluter setup. In the dilution process (sampling, release from tailpipe/stack), semivolatile matter condenses on the core particles and forms new particles by nucleation. The fresh exhaust particles are especially relevant for human health in high-traffic areas and near the emission sources.

With both of the studied engines, the fresh exhaust particle population was highly dominated in terms of particle number by small or extremely small particles. In **Paper 1**, with the small-scale engine, the highest peak at the size distribution of the

fresh exhaust particles was found at 2–5 nm (Figure 4.1), and a much lower second particle mode was detected at particle sizes of 6–10 nm. Less than 1% of all the fresh particles were over 23 nm in diameter. The shape of the fresh exhaust particle size distribution was not clearly bimodal; the primary-emission FC and LC modes were distinguishable also in the fresh exhaust. The particle size distribution of the large-bore engine (**Paper 2**) fresh exhaust particles, on the other hand, was clearly bimodal, with a dominating nucleation mode and a soot mode (Figure 4.5). With the large-scale engine, >90% of the particles, also in terms of mass concentration, were found in the nucleation mode. However, the particle diameters in the nucleation mode were somewhat larger than in the small-scale engine exhaust, 20–30 nm. Also the diameter of the soot mode particles was larger with the large-scale engine. The difference in the shape of the fresh exhaust size distributions is explained by the amount of condensing and nucleating species. With the small-scale engine, their amount was insufficient to form a clear nucleation mode similar to the nucleation mode of the large-scale engine exhaust.

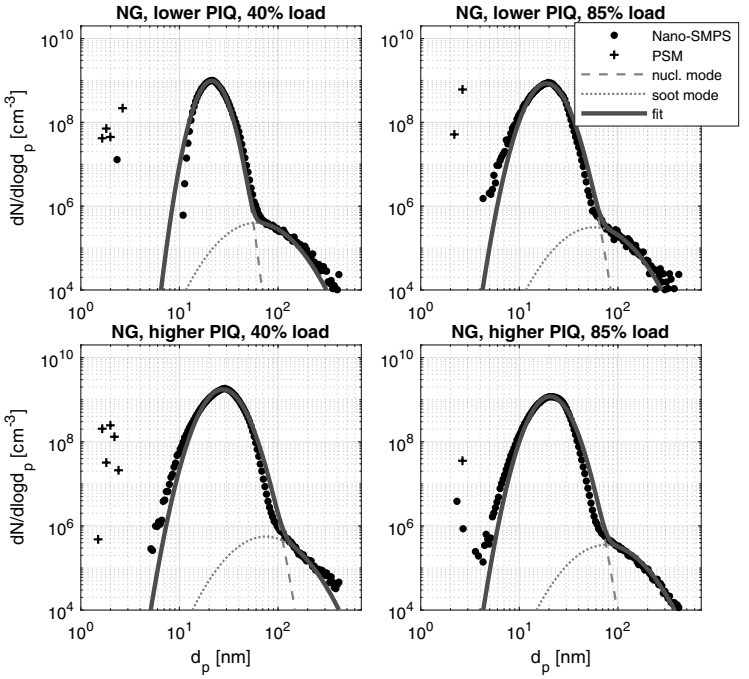

Figure 4.5 Number size distributions of the fresh exhaust particles from the large-bore engine measured with PSM (crosses) and SMPS (dots). Also particle mode fits are given on the size distribution measured by SMPS. Modified from **Paper 2**. PIQ = pilot injection quantity.

The particle population was dominated by semivolatile particles in these studies. This is shown by a comparison between Figures 4.5 and 4.2 and Figure 1 of **Paper 2** and

the right side of Figure 4.1. Nevertheless, the amount of semi-volatiles varied, being the highest with the large-bore engine and the smallest with the small-bore engine at the higher-torque operation mode. It is not clear how large a fraction of the particles were core particles and how large a fraction was formed by nucleation only. When looking at the particle size distributions and the mode fits measured by SMPS only, the fraction of all the core mode particles in the nucleation mode varied from <1% (large-scale engine, lower pilot injection quantity) to tens of percentages (small-scale engine, higher torque in Figure 4.1). However, because a significant fraction of the FC mode particles were found below the SMPS size range, the analysis becomes more complex. Catalytic stripper and thermodenuder losses for the sub-10 nm particles increases uncertainty: the total number concentrations measured by the PSM or CPC were not corrected by the size-dependent losses of CS or TD.

The lack of the FC mode on the SMPS size range at NG, lower PIQ, and 40% load case resulted in weaker particle formation and growth in the fresh exhaust nucleation mode (Figure 4.5; **Paper 2**; see also Figure 5.1). Probably because of the very small size of the FC mode particles, the semivolatile material condensing and nucleating was not enough to grow the nucleation mode to the same particle sizes and concentrations as in the case of higher PIQ and 40% load. This finding indicates that a particle filter reducing the core particle emission could also reduce the nucleation mode particle size and concentration. However, in Figure 4.5, PSM data points and some Nano-SMPS data points below 3 nm are without a certain explanation. The question arises of whether a fraction of the nanoclusters remains ungrown in the dilution process.

In the TEM image (Figure 4.6), the same types of particles were found as in the images of the primary particles. Here, however, there are very small stain-like particles clearly visible on the grids, identified as the nucleation particles. Unlike those often seen in TEM images taken with large-scale engines (e.g., Ntziachristos et al. 2016), the particles did not have a thick sulfur coating on them due to the low sulfur content of the fuels.

The primary dilution ratio over the porous tube diluter has a considerable effect on nucleation and thus the particle number concentration and size distribution. The effect of the primary dilution ratio on the small-scale engine is shown in Figure 4.7 (**Paper 1**). The primary dilution ratio of 6 strongly enhanced the particle formation. The same phenomenon has been shown by several studies. For example, Rönkkö et al. (2006) showed for a diesel exhaust by a vehicle chase study that PDR of 12 reproduced fresh exhaust particle formation in the atmosphere the best (among the

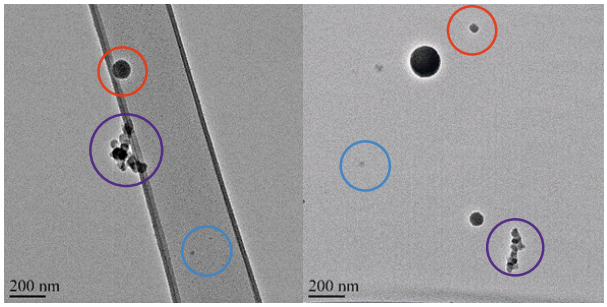

Figure 4.6 Transmission electron microscopy images of fresh exhaust particles (i.e., the sample was taken directly after the dilution system without TD or CS) at an engine load of 40% with the larger-scale engine. Examples of soot agglomerates are circled with purple, lubricating-oil-originated particles with orange, and nucleation particles with blue. Modified from **Paper 2**.

primary dilution ratios of 12, 20, and 36), although still underproducing the particle formation. Therefore, this study assumes that the PTD primary dilution ratio of 12 or lower best reproduces the particle formation and growth in atmospheric dilution.

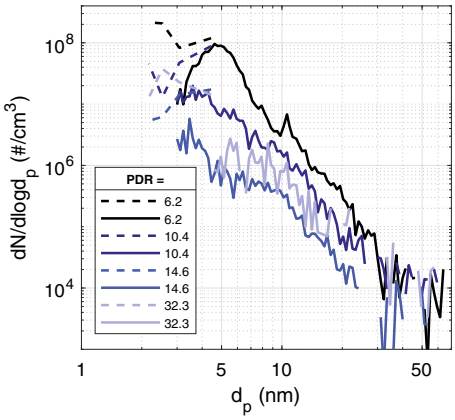

Figure 4.7 The effect of the primary dilution ratio over the porous tube diluter (PDR) on the number size distribution. A small PDR enhanced nucleation and particle growth. PSM in dashed and Nano-SMPS in solid lines. **Paper 1** campaign data.

The fresh exhaust particle emissions of the NG engines consisted of the primary exhaust particles (FC, LC, and soot) grown by the condensation of semivolatile species and nucleation particles. The nucleation mode particles most probably consisted of lubricating oil derived species. The particle size distributions measured by Amirante et al. (2017b) were very similar to the size distributions of the fresh exhaust particle emission measured in this thesis. In their study, the contribution of lubricant is clear,

because they varied the oil-fuel ratio from 0 to 5%. When the amount of lubricant oil emission increased, a nucleation mode similar to the ones measured here emerged.

4.3 The effect of catalysts

Catalysts are often needed in natural gas engines in order to meet the tightening emission legislation (see e.g., Table 2.1). Therefore, the effect of catalysts on the particulate emission needs to be studied from the viewpoint of the primary, fresh, and aged emissions. In this section, the first two are investigated. The results presented in Chapters 4.1 and 4.2 were obtained without any exhaust after-treatment. The effect of catalysts also offers information on the particle formation processes and the best emission mitigation technologies.

The effect of catalysts on natural gas exhaust particles was studied in **Paper 3**. The size distributions and particle number concentrations of the fresh and primary exhaust particles are presented in Figure 4.8 for the OXICAT-x catalyst at different temperatures. Also, the engine-out emissions sampled upstream of the catalysts are given for comparison. The size distributions were measured with PSM and EEPS, and they showed typically the same particle modes as discussed in the previous sections – three primary particle modes and the nucleation mode in the fresh exhaust. A similar shape of the particle size distribution and the dependency on exhaust temperature were measured on the oxidative-reductive MOC+SCR catalyst set also tested in the study.

The total number emission of fresh exhaust particles decreased by over 50% when the sample was collected downstream of the catalysts (oxidative + NO_x reduction catalyst) at 350 °C. The catalyst also affected the number of primary particles measured: the number of non-volatile particles with a diameter below 10 nm dropped. The drop in the smallest-diameter primary particle emission was most probably caused by diffusion losses of the primary particles in the catalysts. Fewer core particles then resulted as a lower nucleation mode particle number concentration.

On the other hand, when the exhaust temperature was higher, 400–500 °C, the number of the fresh exhaust particles increased. For example, with the OXICAT-x at 450 °C, the number emission of fresh exhaust particles was 6 times higher than when sampling the engine-out exhaust. The increase was seen as a particle mode with a peak diameter at ca. 10 nm.

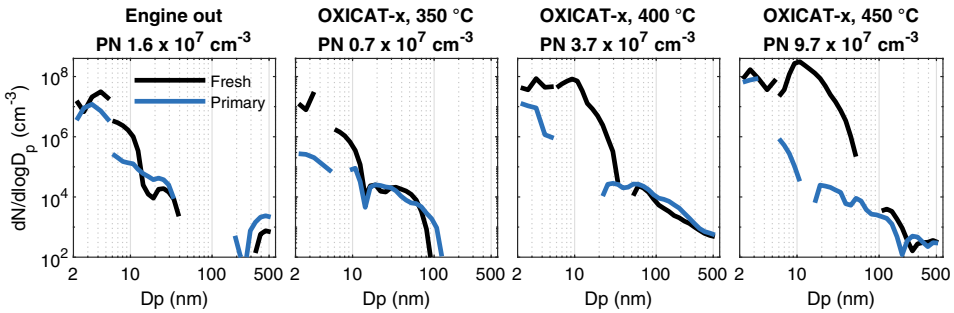

Figure 4.8 Particle number size distributions upstream of the catalyst (engine out) and after the catalyst OXICAT-x at three exhaust temperatures. The distributions are given for both primary (blue; measured downstream of the thermodenuder) and fresh (black) exhaust particles with the engine mode 2, and they were measured with PSM and EEPS. The total number concentration for fresh particles, measured by PSM, is given in the titles. Modified from **Paper 3**. PN = particle number (concentration).

However, also the number emission of the <5 nm solid particles measured downstream of TD was higher when the exhaust was led though the catalysts at the highest temperatures (400 and 450 °C for the OXICAT-x and 500 °C for the MOC+SCR). This observation contradicts the assumption that the primary exhaust particle emission is represented by the measurement downstream of the thermodenuder: some material that transferred to the particle phase during the dilution process was not entirely removed by the thermodenuder, but the particles only decreased in size, partly even below the size range of the PSM. In other words, more nanoclusters may grow to detectable sizes due to the larger amount of semivolatile species created at high catalyst temperatures, but their size does not return all the way back to the original at the thermodenuder. Another explanation would be either inefficiency of the thermodenuder to remove all volatile matter, or renucleation after the TD, that is rather commonplace according to the review article by Giechaskiel et al. (2020a).

According to the PM filter collection and SP-AMS measurement of the particle composition, the tested catalysts reduced the particle mass emission at all catalyst temperatures by decreasing the amount of organic species. The PM was the smallest at the exhaust temperature of 350 °C. Therefore, another option for the reduced fresh particle concentration is the reduction of nucleation precursors by the catalysts. That would not, however, explain the drop of the measured primary particle concentration. Also, one should note that particle mass measurements may not explain particle number measurements – the particle sizes emphasized may greatly differ in number and mass based analyses.

The higher the catalyst temperature, the more pronounced was the nucleation mode growth, i.e., the new particle formation or/and the growth of the core particles. Based on the SP-AMS measurements (see **Paper 3**: Figures 9 and 10), sulfate and ammonium were principally responsible for the catalyst-aided particle number increase. Thus, the nucleation mode particles probably consisted of ammonium sulfate and, at the highest exhaust temperatures, sulfuric acid, formed with the help of SO_2 oxidation in the catalysts. Uncertainty here is caused by the SP-AMS detection limit of ca. 50 nm — a major fraction of the particles were outside the SP-AMS detection range.

As a summary, exhaust after-treatment by catalysts may have an increasing or reducing effect on the emitted particle number concentration. The number concentration of the solid core particles was reduced by catalysts through diffusion losses, whereas the amount of particle precursors could be either reduced (especially organics) or increased (e.g., sulfur-compound precursors) by the catalysts.

4.4 Aged exhaust particle mass

The concept of secondary aerosol or secondary species refers to the particle mass of atmospherically aged exhaust. According to the measurements of, e.g., Viana et al. (2014), Cesari et al. (2014), and Huang et al. (2014), secondary aerosol, both organic and inorganic, can be at least equally significant a contributor as primary or fresh emissions to $PM_{2.5}$. The secondary aerosol formation potential is significant when evaluating the total air quality effects of an emission source, but the measurement of the secondary aerosol mass is not easy. For example, the timescale of secondary aerosol formation in the atmosphere is very long – from hours to days after the emission.

Aged aerosol was simulated by the PAM reactor with the small-scale engine in **Paper 4**. In this study, the concept "total aged" refers to the particle mass measured downstream of the PAM, i.e., the combination of the primary, fresh, and secondary particle mass. In contrast to the other papers, **Paper 4** examines the particulate mass instead of number for the reason that the number concentration and number size distribution downstream of the PAM reactor probably do not represent the reality in the atmosphere. The potential aerosol mass was developed to simulate the formation potential of the aerosol mass after an oxidation period in the atmosphere, not the number. The aerosol processes that change the size distribution over days (e.g.,

coagulation) do not necessarily take place similarly in the flow-through oxidation chamber as in the atmosphere in the presence of the pre-existing particle population.

The measurements were done at the two engine operation modes (M1 and M2) with the two sets of catalysts (OXICAT-x = C1, MOC + SCR = C2), also studied in the previous Section 4.3. Four different exhaust temperatures from 350 to 500 °C were used during the tests. In Figure 4.9, the total aged particle masses measured by SP-AMS and EEPS are given. The calculated OH exposures as equivalent atmospheric ages were rather long – 10, 10.7, 4.6, 4.7, and 9.3 days, from left to right in the figure. For comparison, the particle masses of the fresh exhaust particles are also given for the same conditions. Also, the chemical compositions measured with the SP-AMS are presented in the figure.

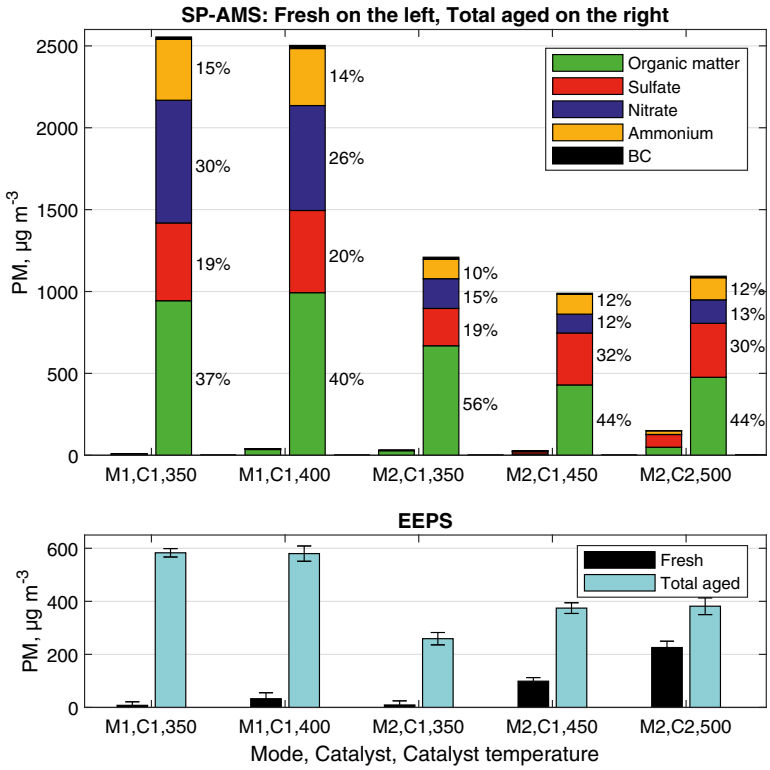

Figure 4.9 The fresh (the left-side bars) and total aged (the right-side bars) particle mass concentration measured with SP-AMS and EEPS. The fraction of black carbon was less than or equal to 1%. The calculated equivalent atmospheric ages of the total aged aerosol were 10, 10.7, 4.6, 4.7, and 9.3 days, from left to right. Unit density was used in the EEPS particle mass calculation. Modified from **Paper 4**.

The measured secondary aerosol masses were surprisingly large: the total aged particle mass was multiple times or even two magnitudes larger than the fresh particle mass emitted at the same condition. The engine operation mode M1 produced the highest total aged particle masses, but also the atmospheric ages simulated by the PAM were the longest for M1.

The total aged particle mass measured by SP-AMS exceeded the total aged particle mass of EEPS clearly, by 2–4 times. This was mostly because of the different size ranges covered by the instruments (EEPS 5.6–560 nm, SP-AMS 30–1000 nm). According to the SP-AMS size distributions (see **Paper 4**: Figure 6), the majority of the particle mass was found above 400 nm.

At the same engine operation mode, the lowest secondary particle masses appeared in conditions that produced the largest fresh exhaust particle mass, namely the highest exhaust and catalyst temperatures. One explanation could be that if the gaseous species that have secondary aerosol formation potential become oxidized already in the exhaust line, they may partly transfer to the particulate phase already when released into the atmosphere. Otherwise, they transfer to the particulate phase only after atmospheric oxidation.

The total aged aerosol was dominated by inorganic species, except in the case of M2, C1, 350 °C. The organics were the largest single species of secondary aerosol – 37–56% of the total aged aerosol mass. Secondary ammonium nitrate aerosol formation is limited by ammonia (Link et al. 2017). The mass concentration of nitrate in the total aged particles increased at the lower catalyst temperatures. This is probably caused by a larger ammonia slip at the lower exhaust temperatures – the urea feed into the NOx reduction catalyst was not adjusted to be optimal for each exhaust temperature (**Paper 3**). Even though the ammonia slip from the catalysts was below the detection limit of the FTIR analyser (2 ppm), secondary nitrate formation was notable, 12–30% of the total aged PM. Therefore, even low ammonia emissions may have importance as precursors for the secondary inorganic aerosol.

It was somewhat surprising that the secondary organic aerosol mass measured with the small-scale NG engine (9–20 mg kg_{fuel}^{-1}, photochemical age 4.7–10.7 days) was at the same level as for diesel vehicles with a working catalyst (12–20 mg kg_{fuel}^{-1}) and gasoline vehicles in hot-engine operation (13.8 mg kg_{fuel}^{-1}; ca. 8-25 mg kg_{fuel}^{-1}; 8–21 mg kg_{fuel}^{-1}) (reported by Chirico et al. 2010; Gordon et al. 2014; Karjalainen et al. 2016; Simonen et al. 2019, respectively) and higher than those of an ethanol vehicle

(<2 mg kg_{fuel}^{-1}) (Timonen et al. 2017). However, also much larger SOA formation potentials are reported in the literature, e.g., on non-road diesel engines (400–12,000 mg kg_{fuel}^{-1}), a cold start gasoline vehicle (480 mg kg_{fuel}^{-1}), and vehicle fleet (200–400 mg kg_{fuel}^{-1}) (reported by Jathar et al. 2017; Nordin et al. 2013; Tkacik et al. 2014, respectively). It must also be kept in mind that the atmospheric age varied a great deal between the different studies, which naturally affects the measured SOA formation potential.

In this study, the origin of the secondary organic aerosol formation could not be incontrovertibly solved. The options were the natural gas fuel and lubricating oil. Lubricating oil is the more probable option, because the natural gas consisted of light hydrocarbons that do not form secondary organic aerosol (Seinfeld and Pandis 2016). However, because natural gas combustion can generate primary and fresh particles (e.g., Commodo et al. 2013; Amirante et al. 2017b), it is not impossible that the combustion products could also form secondary aerosol mass. The secondary inorganic aerosol probably originated from the urea used in the SCR technology and the lubricating oil sulfur compounds. The chemical ionization mass spectrometer (CIMS) analysis of Le Breton et al. (2019) made in real-world conditions for the aged exhaust of NG buses supported this conclusion.

4.4.1 Volatility comparison

The volatility of the particles and their chemical species was studied with a combination of the thermodenuder, EEPS, and SP-AMS. The volatility measurements were conducted after the measurements for Figure 4.9, and they took approximately 45 minutes. Figure 4.10 shows the results for the volatility measurements. On the left, the mass fraction remaining at temperatures 50–250 °C measured with EEPS is given, and on the right, there is an example of the volatilities of the different chemical species measured with the SP-AMS. The different measurement technique and the different particle size range covered by the two instruments affects the volatility measurements as well as the concentration measurements.

The aged aerosol particles were found to be less volatile than the fresh exhaust particles, and the aged exhaust particles were the less volatile the higher the catalyst temperature was. The volatility was characteristic for each of the three particle types plotted in the figure in black, cyan, and blue.

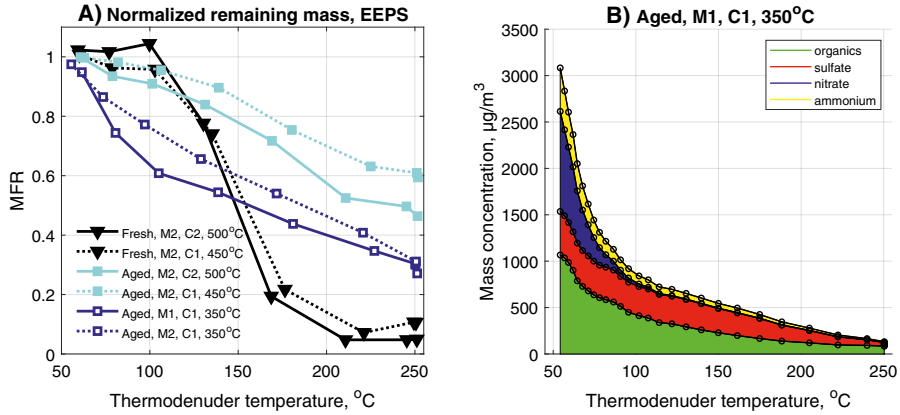

Figure 4.10 A) Comparison of the volatility of fresh and total aged exhaust particles. MFR = mass fraction remaining compared to 50 °C. B) An example of the concentration of the chemical compounds of particles remaining after the thermodenuder treatment conducted for the aged exhaust aerosol, engine mode 1, OXICAT-x at 350 °C. The mass concentrations were measured using the EEPS or SP-AMS at different thermodenuder temperatures and corrected by the dilution ratio used in the sampling system. Modified from **Paper 4**. C1 = OXICAT-x, C2 = MOC+SCR, M1 = engine mode 1 with higher torque, M2 = engine mode 2 with lower torque.

When the sample was collected downstream of the high-temperature catalysts, the total aged particle mass lessened steadily at the thermodenuder temperatures of 50–250 °C, and the mass fraction remaining at 250 °C was 46–60% (SP-AMS: 25%). The gradual evaporation was mainly due to organics and sulfates (see also **Paper 4**: Figure 4). When the catalyst temperature was the lowest, 350 °C, stronger evaporation of the total aged particle mass occurred below 110 °C, but above that the reduction of the remaining particle mass was steady (Figure 4.10 B). Now, because of this easily evaporable fraction, probably consisting of ammonium nitrate and high-volatility organics, only 30% (SP-AMS: <10%) of the total aged particle mass remained at 250 °C.

Indeed, the difference of the total aged PM volatility behavior between the catalyst temperatures was mainly related to the nitrate concentration of the particles, which is, as already mentioned, limited by the availability of ammonia. After a long stabilization of >1 hour (needed especially by the ammonia), the nitrate content of the total aged particles was higher at the low catalyst temperatures and lower at the high catalyst temperatures than shown in Figure 4.9 (See also **Paper 4**: Figure 4). Based on this result, the 10–15-minute stabilization time was insufficient for accurate nitrate concentrations due to the slow stabilization related to ammonia.

The organics of the total aged particles evaporated relatively steadily and gradually below 200 °C and remained stable at the higher temperatures (see also **Paper 4**: Figure 4). Therefore, the organic fraction of the particles probably consisted of various organic compounds with different evaporation temperatures. It was concluded that the photo-chemical aging of the NG engine exhaust generated low-volatility organics. The mean evaporation temperature of sulfate was the highest and that of nitrate the lowest among the organics, sulfate, nitrate, and ammonium. The evaporation temperature of ammonium depended on the fraction of sulfate and nitrate, confirming that the amount of ammonium determined the nitrate content of the aged particles.

The fresh particle mass, sampled downstream of the high-temperature catalysts, evaporated between 100 and 200 °C; below and above this temperature range, the particle mass fraction remaining did not change. SP-AMS data showed that the evaporated particle mass consisted of sulfate. At 250 °C, only 5–10% of the particle mass remained. The strongest evaporation of the engine-out fresh exhaust particles (measured by Nano-SMPS in **Paper 1**) occurred at temperatures from 50 to 120 °C, and ca. 40% of the total particle volume remained at 265 °C (**Paper 1**: Figure 5). Unfortunately, no SP-AMS data on the chemical composition for **Paper 1** is available.

5 COMPARISON TO LIQUID-FUEL COMBUSTION

In this chapter, the measured particle emission factors are compared to the ones reported in the literature for liquid fuel combustion, and the results obtained from the large-scale engine are compared to the low-sulfur liquid-fuel results measured from the same engine.

If the same particle size range (>23 nm) is considered (comparison to, e.g., Pirjola et al. 2017; see Table 2.1), the particle number emission from the small-scale NG engine was small – of the same magnitude or smaller compared to a diesel engine equipped with a DPF. However, the number concentration of all the fresh exhaust particles (>1 nm) emitted by the engine was significantly higher, 0.5-88 $\times 10^{13}$ kWh^{-1}. The measured total number concentrations were at the same level as from a Stage 3B (pre-2014) non-road diesel engine (Pirjola et al. 2017) or Euro IV diesel buses (Hallquist et al. 2013) measured in real-world conditions.

This result has been reported in the literature by several studies: NG combustion produces lower PN emissions than liquid fuel combustion if only solid >23 nm particles are considered, but the total number concentration of particles emitted by natural gas engines may be high. For example, Lähde and Giechaskiel (2021) measured the solid particle number (SPN) emissions from light-duty vehicles run with natural gas and liquefied petroleum gas (LPG; commonly consisting of propane, butane, and propylene), and compared the results to the SPN limit set in regulation for light-duty direct injection (DI) engines (gasoline or diesel). Their results showed that the particle emissions from natural gas engines are small compared to liquid fuel combustion if only particles >23 nm are taken into account. However, they highlighted that the emission limits set in emission legislation for the DI vehicles may be well exceeded if also sub-23 nm particles from NG vehicles are included. Toumasatos et al. (2021) compared the SPN emissions of NG vehicles to gasoline vehicles. They also found that when only the >23 nm particles were considered, SPN emissions of NG emis-

sions were considerably lower than from the gasoline vehicles but, when the particle cut-off size was lowered to >10 nm, the SPN emissions were on a similar level.

In this study, the large-scale engine emitted an especially large number of volatile particles: only 1–14% of the particles were non-volatile. With the small-scale engine, the fraction of non-volatile particles varied between 4% and 13% of the total particle number emission measured with a particle counter. However, the actual fraction of the non-volatile particles is probably somewhat higher because their number was not corrected for thermodenuder or catalytic stripper losses. The losses grow larger as the particles are smaller (Heikkilä et al. 2009). Therefore, the lack of loss correction causes more inaccuracy in the case of the small-scale engine with the smaller diameter of the emitted particles.

In **Paper 2**, the combustion of the fossil low-sulfur liquid fuels MGO and MDO (marine gas oil and marine diesel oil) was compared to dual-fuel natural gas combustion (MGO as the pilot fuel). The study was done on the large-bore laboratory engine, and the same aerosol measurements were conducted for all four fuel options.

The particle number size distributions of the liquid fuels and NG with the two pilot fuel quantities are shown in Figure 5.1, both for fresh and primary exhaust particles. The size distribution for fresh exhaust particles was bimodal for all the fuels tested, the nucleation mode highly dominating the soot mode. The nucleation modes were remarkably similar for NG and liquid fuel combustion; the NG exhaust nucleation mode concentrations and particle sizes were usually only slightly smaller. Nevertheless, the total number emission was over 45% lower for NG than for MGO or MDO.

The largest difference between the fuels was in soot emission. Soot emission from the liquid fuel combustion generated 4–12 times higher soot particle numbers than the dual-fuel NG combustion in the large-bore engine. Because the natural gas engine emitted significantly less soot and, therefore, less black carbon than the engine fueled with the liquid fuels, NG can be better for the environment. Especially in engines that operate near the poles and other snow-covered regions, soot emission should be minimized in order to slow down global heating.

The difference in the amount of soot particles was also evident on the TEM samples: spherical particles dominated the TEM images in the case of NG combustion, whereas soot agglomerates dominated in the case of liquid fuel combustion. The spherical particles were detected also on the TEM images of MDO and MGO combustion,

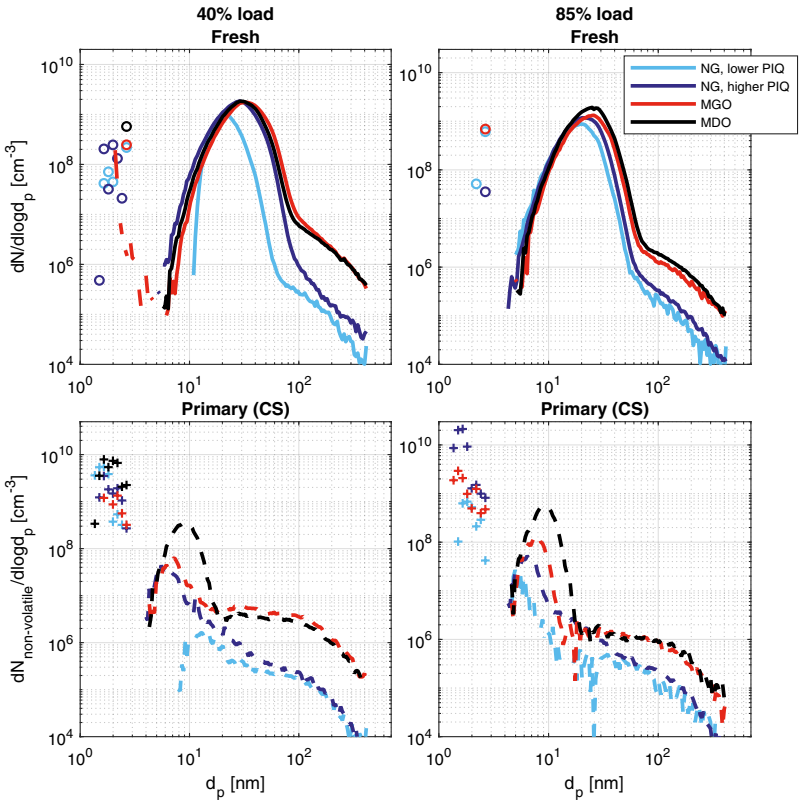

Figure 5.1 Particle number distributions for natural gas and liquid fuels MGO and MDO both for fresh (top) and primary, i.e., non-volatile (bottom) particles. Measurements with PSM with circles (fresh exhaust) and crosses (primary) and measurements with SMPS with solid and dashed lines. The load refers to engine load. NG = natural gas, PIQ = pilot injection quantity, MGO = marine gas oil, MDO = marine diesel oil. Modified from **Paper 2**.

but their relative amount when compared to NG combustion was low. Stain-like nucleation mode particles were found on the exhaust samples of all the fuels (Figure S8 of **Paper 2**).

The particle mean sizes increased slightly from gaseous to liquid fuels and from MGO to MDO (Figure 5.1). The FC core mode concentration and size were very fuel-dependent. This observation supports the finding of the FC core mode as fuel-originated. Also, the LC mode particles were larger on liquid fuel combustion than on NG combustion, but their concentration was less fuel-dependent. The lesser fuel-dependency supports the theory of their lubricant oil origin.

The LC mode particle concentration was more dependent on the engine operation mode. Based on the fitted LC mode size distributions, for all fuels except NG with

the higher PIQ, the LC mode concentration was ca. 2–8 times higher at an engine load of 40%. The engine load of 40% produced also a larger nucleation mode particle diameter than the 85% load. The other effects of engine operation mode on particle size were small.

In the EDS analysis, the sulfur signal on the lubricating-oil-originated spherical particles was higher with the highest sulfur-content fuel, MDO. The fuel, therefore, seemed to affect the elemental composition of the LC mode particles, although the origin of the LC particles was concluded to be the lubricating oil.

6 SUMMARY

This thesis characterized the particle emission from two natural gas (NG) engines in respect to number concentration, size distribution, volatility, composition, morphology, and electric charge. The effect of oxidative-reductive (OC+SCR) exhaust after-treatment on the particle formation and growth was also studied. Furthermore, the aging of the exhaust and the subsequent secondary aerosol formation potential and volatility characteristics of the total aged particulate matter were studied.

Although the natural gas engine is not a new invention, several aspects of its particle emission had not been studied before this work. Firstly, a successful measurement of the size distribution and number concentration of tiny particles as small as below 2 nm in diameter was conducted. Secondly, the atmospheric aging of natural gas engine exhaust was simulated by a potential aerosol mass reactor. Thirdly, volatility characteristics of fresh and aged exhaust particles across a large temperature range were studied using particle size distribution measurements and aerosol mass spectrometry. Fourthly, two separate primary particle core modes were identified in the NG exhaust in addition to a soot mode.

The measurements were conducted on two engines of different sizes (100 kW and 1.4 MW), both retrofitted to run with NG. The larger-bore engine was a dual-fuel engine that used an MGO pilot of 1–6 m-% of fuel consumption. The catalyst and aged exhaust tests were conducted on the smaller engine only. In addition to the NG engine tests, the larger-engine results with NG were compared to low-sulfur liquid fuels.

The number emission factors of the fresh exhaust particles were 5–880 $\times 10^{12}$ 1/kWh for the smaller and 2.7–7.1 $\times 10^{15}$ 1/kWh for the larger engine (>1.2–1.5 nm). The emission factors measured were at a similar level or higher as those reported in previous studies, probably due to the wide particle size range covered, because all fresh exhaust particles were included, not only the solid ones, and because the measured engines were retrofitted and not originally optimized for NG combustion. The number

emission factors of the non-volatile (primary) exhaust particles were 0.2–48 $\times 10^{12}$ 1/kWh for the smaller and 0.04—0.8 $\times^{15}$ for the larger engine.

Figure 6.1 shows the formation and evolution processes of natural gas exhaust particles suggested in this study. In the raw exhaust, there are solid primary particles, i.e., fuel-originated core (FC), lubricating-oil-originated core (LC), soot, and larger spherical lubricating-oil-originated particles that are initially formed in the engine cylinders. Under the diluting and cooling conditions of sampling (or upon release into the atmosphere), gaseous particle precursors transfer to the particulate phase by condensation on the existing primary particles or by forming new particles through nucleation. Nanocluster aerosol may grow to detectable sizes in the dilution process.

The number of solid primary particles and the precursors of the fresh exhaust particulate matter depend on the exhaust after-treatment. Primary nanoclusters and the smallest particles are reduced probably by diffusion losses in the catalysts, whereas the amount of particle precursors may either decrease or increase in the catalysts. For example, the higher the catalyst temperature, the more SO_2 is oxidized to SO_3 and may form, e.g., sulfuric acid and ammonium sulfate. Thus, the exhaust after-treatment may increase the fresh exhaust particle number emission due to the catalyst-aided oxidation of SO_2.

In the time frame of hours to days, more exhaust species transfer to the particulate phase through atmospheric photo-oxidation. Both organic and inorganic species form lower-volatility species by atmospheric photochemistry that then condense in the particulate phase, forming secondary aerosol mass. In this thesis, the majority of the aged exhaust particles was found to consist of organic species and inorganic species, such as ammonium sulfate and ammonium nitrate.

It was concluded that the non-volatile fuel-originated core with peak size in 1–6 nm originated from the fuel, because its particle size and concentration were dependent on the fuel, and its composition was carbonaceous because the particles were only weakly – if at all – visible on the carbonaceous transmission electron microscopy (TEM) grids. The particles on the lubricating-oil-originated core mode size range of down to 5–10 nm contained lubricating oil marker elemental calcium, and their concentration was not fuel-dependent. In the fresh exhaust size distribution, the FC and LC modes were partly (smaller engine) or totally (larger engine) overshadowed by the nucleation mode particles. Despite the name of the soot mode, the particles of the soot mode were not only soot agglomerates. Especially in the case of natural gas

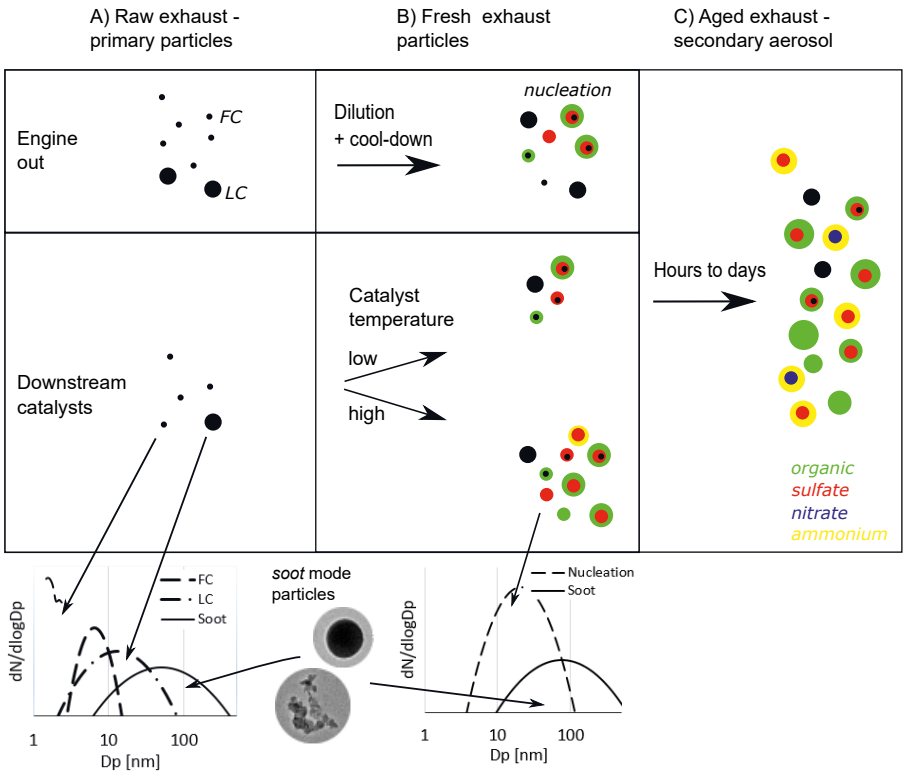

Figure 6.1 Suggested formation process of natural gas engine exhaust particles (soot mode particles excluded), the particle size distribution of primary and fresh exhaust particles, and transmission electron microscopy images of a soot agglomerate and a spherical lubricating-oil-originated soot mode particle. A) The smallest particles and nanoclusters are removed by diffusion in the catalysts. B) Sulfur compounds and hydrocarbons condense on the particles and on the nanoclusters that then grow to detectable sizes. New particles form by nucleation. The growth and nucleation depend on the catalyst temperature. C) Atmospheric photo-oxidation causes new organic and inorganic species to transfer to the particle phase. Modified from **Papers 1 and 2**.

combustion but also for the liquid fuel combustion, a significant fraction of the soot mode particles were large spherical particles derived from the lubricating oil. All the modes appeared in the exhaust of both the studied engines and also with the liquid fuels MGO and MDO.

Because also NG engines emit harmful emissions such as NOx and hydrocarbons, exhaust after-treatment devices are sometimes required. In this study, catalyst systems were tested at temperatures of 350–500 °C. The new particle formation and particle growth was the most pronounced with the highest catalyst temperatures: The number concentration of fresh exhaust particles multiplied and a nucleation mode with a particle peak diameter of ca. 10 nm formed. At the low exhaust temperatures,

the catalysts reduced the particle number of especially the primary particles with a diameter <5 nm and, consequently, the total fresh particle emission decreased due to the fewer core particles. Interestingly, however, particle mass collection on filters showed a decrease of the PM emission at all the catalyst temperatures, owing to the hydrocarbon oxidation by the catalysts.

In addition to primary and fresh exhaust particles, secondary aerosol formation causes human exposure to aerosol particles and impacts atmospheric phenomena. The secondary aerosol formation potential was found to be unexpectedly high: even 1–2 orders of magnitude higher than the fresh exhaust particle mass. Some 44–56% (or even 2/3 when measured after a long, 60-minute stabilization period) of the measured total aged PM was inorganic, largely ammonium sulfate and ammonium nitrate. Because the source of the ammonium was probably the relatively small ammonia slip (<2 ppm) from the NO_x reduction catalyst SCR rather than the engine or the fuel, it is important to minimize the ammonia slip from the SCR to reduce the inorganic aerosol formation. The secondary organic aerosol formation potential was at a low or medium level when compared to other sources, such as gasoline vehicles reported in the literature. This study assumes that engine lubricating oil was the source of the secondary organic aerosol, which implies that the lubricating oil emission must be controlled in order to reduce the secondary aerosol formation potential of the NG engine exhaust.

Particle volatility may influence the lifetime of the particles in the atmosphere and hence their impact on radiative forcing and air quality. The volatility of the NG exhaust particles in general was high – approximately <80% of the particle number was volatile. The volatility clearly depended on the exhaust after-treatment and the exhaust age. Fresh exhaust particles were measured to be more volatile than the total aged particles. It was found that the photo-chemical aging of the NG engine exhaust generated low-volatility organics and sulfates. A higher catalyst temperature or the related lower ammonia slip (in this study) reduced the volatility of the total aged aerosol by reducing the ammonium nitrate content of the particles.

The electric charge of the nucleation mode particles was measured in two ways. It was found that at least a fraction of the particles were formed at high temperatures because the particles carried approximately three times more charge than at equilibrium at room temperature. Furthermore, more nucleation mode particles carried an electric charge than the soot mode particles did, although the charging probability of soot mode particles was higher due to their larger size. The electric charge measurements

also indicate that the origin of the FC and LC mode particles was in the vicinity of engine cylinders.

Future research in the field of particle emissions from natural gas engines should study SOA formation in more detail and on a wider scale of equivalent atmospheric ages. It is interesting if the SOA formation potential is lower from natural gas engines designed for NG combustion than from the retrofitted natural gas engines. Here, the SOA formation potential was measured only downstream of the oxidative and NO_x reduction catalysts. Therefore, the effect of catalysts on the SOA formation potential remains to be studied in the future. In this study, lubricating oil consumption and ammonia slip from the SCR were found to be responsible for the secondary aerosol formation. Therefore, secondary aerosol studies on an engine with a low lubricating oil consumption and no exhaust after-treatment would be important for future research. Research questions that could be asked also include why the fuel forms both a fuel-originated core with a peak diameter of 1–9 nm and soot agglomerates; how are the fuel-originated core mode particles related to the soot agglomerates? More research on the topic of core particles needs to be undertaken before the association between the particles of different modes is clearly understood.

REFERENCES

Amanatidis, S., Ntziachristos, L., Giechaskiel, B., Katsaounis, D., Samaras, Z. and Bergmann, A. (2013). Evaluation of an oxidation catalyst ("catalytic stripper") in eliminating volatile material from combustion aerosol. *Journal of Aerosol Science* 57, 144–155. DOI: 10.1016/j.jaerosci.2012.12.001.

Amirante, R., Distaso, E., Di Iorio, S., Sementa, P., Tamburrano, P., Vaglieco, B. M. and Reitz, R. D. (2017a). Effects of natural gas composition on performance and regulated, greenhouse gas and particulate emissions in spark-ignition engines. *Energy Conversion and Management* 143, 338–347. DOI: 10.1016/j.enconman.2017.04.016.

Amirante, R., Distaso, E., Di Iorio, S., Pettinicchio, D., Sementa, P., Tamburrano, P. and Vaglieco, B. M. (2017b). Experimental Investigations on the Sources of Particulate Emission within a Natural Gas Spark-Ignition Engine. *SAE Technical Papers*. DOI: 10.4271/2017-24-0141.

Anderson, M., Salo, K. and Fridell, E. (2015). Particle- and Gaseous Emissions from an LNG Powered Ship. *Environmental Science and Technology* 49.20, 12568–12575. DOI: 10.1021/acs.est.5b02678.

Baldelli, A., Trivanovic, U., Corbin, J. C., Lobo, P., Gagné, S., Mille, J. W., Kirchen, P. and Rogak, S. (2020). Typical and atypical morphology of non-volatile particles from a diesel and natural gas marine engine. *Aerosol and Air Quality Research* 20.4, 730–740. DOI: 10.4209/aaqr.2020.01.0006.

Beelen, R., Raaschou-Nielsen, O., Stafoggia, M., Andersen, Z. J., Weinmayr, G., Hoffmann, B., Wolf, K., Samoli, E., Fischer, P., Nieuwenhuijsen, M., Vineis, P., Xun, W. W., Katsouyanni, K., Dimakopoulou, K., Oudin, A., Forsberg, B., Modig, L., Havulinna, A. S., Lanki, T., Turunen, A., Oftedal, B., Nystad, W., Nafstad, P., De Faire, U., Pedersen, N. L., Östenson, C. G., Fratiglioni, L., Penell, J., Korek, M., Pershagen, G., Eriksen, K. T., Overvad, K., Ellermann, T., Eeftens, M., Peeters, P. H., Meliefste, K., Wang, M., Bueno-De-Mesquita, B., Sugiri, D., Krämer, U., Heinrich, J., De Hoogh, K., Key, T., Peters, A., Hampel, R., Concin, H., Nagel, G., Ineichen, A., Schaffner, E., Probst-Hensch, N., Künzli, N., Schindler, C., Schikowski, T., Adam, M., Phuleria, H., Vilier, A., Clavel-Chapelon, F., Declercq, C., Grioni, S., Krogh, V., Tsai, M. Y., Ricceri, F., Sacerdote, C., Galassi, C., Migliore, E., Ranzi, A., Cesaroni, G., Badaloni, C., Forastiere, F., Tamayo, I., Amiano, P., Dorronsoro, M., Katsoulis, M., Trichopoulou, A., Brunekreef, B. and Hoek, G. (2014). Effects of long-term exposure to air pollution on natural-cause mortality: An analysis of 22 European cohorts within the multicentre ESCAPE project. *The Lancet* 383.9919, 785–795. DOI: 10.1016/S0140-6736(13)62158-3.

Bond, T. C., Doherty, S. J., Fahey, D. W., Forster, P. M., Berntsen, T., Deangelo, B. J., Flanner, M. G., Ghan, S., Kärcher, B., Koch, D., Kinne, S., Kondo, Y., Quinn, P. K., Sarofim, M. C., Schultz, M. G., Schulz, M., Venkataraman, C., Zhang, H., Zhang, S., Bellouin, N., Guttikunda, S. K., Hopke, P. K., Jacobson, M. Z., Kaiser, J. W., Klimont, Z., Lohmann, U., Schwarz, J. P., Shindell, D., Storelvmo, T., Warren, S. G. and Zender, C. S. (2013). Bounding the role of black carbon in the climate system: A scientific assessment. *Journal of Geophysical Research Atmospheres* 118.11, 5380–5552. DOI: 10.1002/jgrd.50171.

Boucher, O., Randall, D., Artaxo, P., Bretherton, C., Feingold, G., Forster, P., Kerminen, V.-M., Kondo, Y., Liao, H., Lohmann, U., Rasch, P., Satheesh, S., Sherwood, S., Stevens, B. and Zhang, X. (2013). Clouds and Aerosols. *Climate Change 2013: The Physical Science Basis. Contribution of Working Group I to the Fifth Assessment Report of the Intergovernmental Panel on Climate Change*. Ed. by T. Stocker, D. Qin, G.-K. Plattner, M. Tignor, S. Allen, J. Boschung, A. Nauels, Y. Xia, V. Bex and P. Midgley.

Bullock, D. S. and Olfert, J. S. (2014). Size, volatility, and effective density of particulate emissions from a homogeneous charge compression ignition engine using compressed natural gas. *Journal of Aerosol Science* 75, 1–8. DOI: 10.1016/j.jaerosci.2014.04.005.

Cesari, D., Genga, A., Ielpo, P., Siciliano, M., Mascolo, G., Grasso, F. M. and Contini, D. (2014). Source apportionment of PM2.5in the harbour-industrial area of Brindisi (Italy): Identification and estimation of the contribution of in-port ship emissions. *Science of the Total Environment* 497-498, 392–400. DOI: 10.1016/j.scitotenv.2014.08.007.

Chirico, R., Decarlo, P. F., Heringa, M. F., Tritscher, T., Richter, R., Prévôt, A. S. H., Dommen, J., Weingartner, E., Wehrle, G., Gysel, M., Laborde, M. and Baltensperger, U. (2010). Impact of aftertreatment devices on primary emissions and secondary organic aerosol formation potential from in-use diesel vehicles: Results from smog chamber experiments. *Atmospheric Chemistry and Physics* 10.23, 11545–11563. DOI: 10.5194/acp-10-11545-2010.

Cho, H. M. and He, B. Q. (2007). Spark ignition natural gas engines – A review. *Energy Conversion and Management* 48.2, 608–618. DOI: 10.1016/j.enconman.2006.05.023.

Cohen, A. J., Brauer, M., Burnett, R., Anderson, H. R., Frostad, J., Estep, K., Balakrishnan, K., Brunekreef, B., Dandona, L., Dandona, R., Feigin, V., Freedman, G., Hubbell, B., Jobling, A., Kan, H., Knibbs, L., Liu, Y., Martin, R., Morawska, L., Pope, C. A., Shin, H., Straif, K., Shaddick, G., Thomas, M., Dingenen, R. van, Donkelaar, A. van, Vos, T., Murray, C. J. and Forouzanfar, M. H. (2017). Estimates and 25-year trends of the global burden of disease attributable to ambient air pollution: an analysis of data from the Global Burden of Diseases Study 2015. *The Lancet* 389.10082, 1907–1918. DOI: 10.1016/S0140-6736(17)30505-6. URL: http://dx.doi.org/10.1016/S0140-6736(17)30505-6.

Commodo, M., Sgro, L. A., Minutolo, P. and D'Anna, A. (2013). Characterization of combustion-generated carbonaceous nanoparticles by size-dependent ultraviolet laser photoionization. *Journal of Physical Chemistry A* 117.19, 3980–3989. DOI: 10.1021/jp401061d.

Corbin, J. C., Peng, W., Yang, J., Sommer, D. E., Trivanovic, U., Kirchen, P., Miller, J. W., Rogak, S., Cocker, D. R., Smallwood, G. J., Lobo, P. and Gagné, S. (2020). Characterization of particulate matter emitted by a marine engine operated with liquefied natural gas and diesel fuels. *Atmospheric Environment* 220.October 2019. DOI: 10.1016/j.atmosenv.2019.117030.

De Filippo, A. and Maricq, M. M. (2008). Diesel nucleation mode particles: Semivolatile or solid?: *Environmental Science and Technology* 42.21, 7957–7962. DOI: 10.1021/es8010332.

Dimopoulos Eggenschwiler, P., Schreiber, D. and Schröter, K. (2021). Characterization of the emission of particles larger than 10 nm in the exhaust of modern gasoline and CNG light duty vehicles. *Fuel* 291.120074. DOI: 10.1016/j.fuel.2020.120074.

Distaso, E., Amirante, R., Calò, G., De Palma, P. and Tamburrano, P. (2020). Evolution of soot particle number, mass and size distribution along the exhaust line of a heavy-duty engine fueled with compressed natural gas. *Energies* 13.15. DOI: 10.3390/en13153993.

Donahue, N. M., Chuang, W., Epstein, S. A., Kroll, J. H., Worsnop, D. R., Robinson, A. L., Adams, P. J. and Pandis, S. N. (2013). Why do organic aerosols exist? Understanding aerosol lifetimes using the two-dimensional volatility basis set. *Environmental Chemistry* 10.3, 151–157. DOI: 10.1071/EN13022.

Dong, K., Sun, R., Dong, C., Li, H., Zeng, X. and Ni, G. (2018). Environmental Kuznets curve for $PM_{2.5}$ emissions in Beijing, China: What role can natural gas consumption play?: *Ecological Indicators* 93, 591–601. DOI: 10.1016/j.ecolind.2018.05.045.

Fevre, C. L. (2018). A review of demand prospects for LNG as a marine transport fuel. *Oxford Energy*, 35. DOI: https://doi.org/10.26889/9781784671143.

First registrations of motor vehicles (2021). Traficom, Finland. URL: https://trafi2.stat.fi/PXWeb/pxweb/fi/TraFi/TraFi__Ensirekisteroinnit/030_ensirek_tau_103.px/table/tableViewLayout1/ (visited on 08/21/2021).

Frailey, M., Norton, P., Clark, N. N. and Lyons, D. W. (2000). An evaluation of natural gas versus diesel in medium-duty buses. *SAE Technical Papers* 724. DOI: 10.4271/2000-01-2822.

Fushimi, A., Saitoh, K., Fujitani, Y., Hasegawa, S., Takahashi, K., Tanabe, K. and Kobayashi, S. (2011). Organic-rich nanoparticles (diameter: 10-30 nm) in diesel exhaust: Fuel and oil contribution based on chemical composition. *Atmospheric Environment* 45, 6326–6336.

Gas 2020 (2020). International energy agency (IEA), Paris. URL: https://www.iea.org/reports/gas-2020 (visited on 08/21/2021).

Gas consumption (2019). Our world in data. URL: https://ourworldindata.org/grapher/gas-consumption-by-country (visited on 05/13/2021).

Gentner, D. R., Jathar, S. H., Gordon, T. D., Bahreini, R., Day, D. A., Haddad, I. E., Hayes, P. L., Pieber, S. M., Platt, S. M., Gouw, J. D., Goldstein, A. H., Harley, R. A., Jimenez, J. L., Pre, A. S. H. and Robinson, A. L. (2017). Review of Urban Secondary Organic Aerosol Formation from Gasoline and Diesel Motor Vehicle Emissions. *Environmental Science & Technology* 51, 1074–1096. DOI: 10.1021/acs.est.6b04509.

Giechaskiel, B. (2018). Solid particle number emission factors of euro vi heavy-duty vehicles on the road and in the laboratory. *International Journal of Environmental Research and Public Health* 15.2. DOI: 10.3390/ijerph15020304.

Giechaskiel, B., Lähde, T. and Drossinos, Y. (2019). Regulating particle number measurements from the tailpipe of light-duty vehicles: The next step?: *Environmental Research* 172, 1–9. DOI: 10.1016/j.envres.2019.02.006.

Giechaskiel, B., Lähde, T., Schwelberger, M., Kleinbach, T., Roske, H., Teti, E., Bos, T. van den, Neils, P., Delacroix, C., Jakobsson, T. and Karlsson, H. L. (2019). Particle number measurements directly from the tailpipe for type approval of heavy-duty engines. *Applied Sciences* 9.20. DOI: 10.3390/app9204418.

Giechaskiel, B., Melas, A. D., Lähde, T. and Martini, G. (2020a). Non-Volatile Particle Number Emission Measurements with Catalytic Strippers: A Review. *Vehicles* 2.2, 342–364. DOI: 10.3390/vehicles2020019.

Giechaskiel, B., Schwelberger, M., Delacroix, C., Marchetti, M., Feijen, M., Prieger, K., Andersson, S. and Karlsson, H. L. (2018). Experimental assessment of solid particle number Portable Emissions Measurement Systems (PEMS) for heavy-duty vehicles applications. *Journal of Aerosol Science* 123, 161–170. DOI: 10.1016/j.jaerosci.2018.06.014.

Giechaskiel, B., Woodburn, J., Szczotka, A. and Bielaczyc, P. (2020b). Particulate Matter (PM) Emissions of Euro 5 and Euro 6 Vehicles Using Systems with Evaporation Tube or Catalytic Stripper and 23 nm or 10 nm Counters. *SAE Technical Papers* 2020-01-22.2020. DOI: 10.4271/2020-01-2203.

Gómez, A., Fernández-Yáñez, P., Soriano, J. A., Sánchez-Rodríguez, L., Mata, C., García-Contreras, R., Armas, O. and Cárdenas, M. D. (2021). Comparison of real driving emissions from Euro VI buses with diesel and compressed natural gas fuels. *Fuel* 289.119836. DOI: 10.1016/j.fuel.2020.119836.

Gordon, T. D., Presto, A. A., May, A. A., Nguyen, N. T., Lipsky, E. M., Donahue, N. M., Gutierrez, A., Zhang, M., Maddox, C., Rieger, P., Chattopadhyay, S., Maldonado, H., Maricq, M. M. and Robinson, A. L. (2014). Secondary organic aerosol formation exceeds primary particulate matter emissions for light-duty gasoline vehicles. *Atmospheric Chemistry and Physics* 14.9, 4661–4678. DOI: 10.5194/acp-14-4661-2014.

Goyal, P. and Sidhartha (2003). Present scenario of air quality in Delhi: A case study of CNG implementation. *Atmospheric Environment* 37.38, 5423–5431. DOI: 10.1016/j.atmosenv.2003.09.005.

Graves, B., Olfert, J., Patychuk, B., Dastanpour, R. and Rogak, S. (2015). Characterization of Particulate Matter Morphology and Volatility from a Compression-Ignition Natural-Gas Direct-Injection Engine. *Aerosol Science and Technology* 49.8, 589–598. DOI: 10.1080/02786826.2015.1050482.

Guo, J., Ge, Y., Hao, L., Tan, J., Li, J. and Feng, X. (2014). On-road measurement of regulated pollutants from diesel and CNG buses with urea selective catalytic reduction systems. *Atmospheric Environment* 99, 1–9. DOI: 10.1016/j.atmosenv.2014.07.032.

Hajbabaei, M., Karavalakis, G., Johnson, K. C., Lee, L. and Durbin, T. D. (2013). Impact of natural gas fuel composition on criteria, toxic, and particle emissions from transit buses equipped with lean burn and stoichiometric engines. *Energy* 62, 425–434. DOI: 10.1016/j.energy.2013.09.040.

Hallquist, Å. M., Jerksjö, M., Fallgren, H., Westerlund, J. and Sjödin, Å. (2013). Particle and gaseous emissions from individual diesel and CNG buses. *Atmospheric Chemistry and Physics* 13.10, 5337–5350. DOI: 10.5194/acp-13-5337-2013.

Heikkilä, J., Rönkkö, T., Lähde, T., Lemmetty, M., Arffman, A., Virtanen, A., Keskinen, J., Pirjola, L. and Rothe, D. (2009). Effect of open channel filter on particle emissions of modern diesel engine. *Journal of the Air & Waste Management Association (1995)* 59, 1148–1154. DOI: 10.3155/1047-3289.59.10.1148.

Hoek, G., Krishnan, R. M., Beelen, R., Peters, A., Ostro, B., Brunekreef, B. and Kaufman, J. D. (2013). Long-term air pollution exposure and cardio-respiratory mortality: A review. *Environmental Health* 12, 43. DOI: 10.1186/1476-069X-12-43.

Holmén, B. A. and Ayala, A. (2002). Ultrafine PM Emissions from Natural Gas, Oxidation-Catalyst Diesel, and Particle-Trap Diesel Heavy-Duty Transit Buses. *Environmental Science & Technology* 36.23, 5041–5050.

Holmén, B. A. and Qu, Y. (2004). Uncertainty in Particle Number Modal Analysis during Transient operation of compressed natural gas, diesel and trap-equipped diesel transit buses. *Environmental Science & Technology* 38.8, 2413–2423.

Huang, R. J., Zhang, Y., Bozzetti, C., Ho, K. F., Cao, J. J., Han, Y., Daellenbach, K. R., Slowik, J. G., Platt, S. M., Canonaco, F., Zotter, P., Wolf, R., Pieber, S. M., Bruns, E. A., Crippa, M., Ciarelli, G., Piazzalunga, A., Schwikowski, M., Abbaszade, G., Schnelle-Kreis, J., Zimmermann, R., An, Z., Szidat, S., Baltensperger, U., El Haddad, I. and Prevot, A. S. (2014). High secondary aerosol contribution to particulate pollution during haze events in China. *Nature* 514.7521, 218–222. DOI: 10.1038/nature13774.

Jääskeläinen, H. (2021). *Natural Gas Engines*. Dieselnet. URL: https://dieselnet.com/tech/engine_natural-gas.php (visited on 09/13/2021).

Jathar, S. H., Friedman, B., Galang, A. A., Link, M. F., Brophy, P., Volckens, J., Eluri, S. and Farmer, D. K. (2017). Linking Load , Fuel , and Emission Controls to Photochemical Production of Secondary Organic Aerosol from a Diesel Engine. *Environmental Science & Technology* 51, 1377–1386. DOI: 10.1021/acs.est.6b04602.

Jayaratne, E. R., Meyer, N. K., Ristovski, Z. D. and Morawska, L. (2012). Volatile properties of particles emitted by compressed natural gas and diesel buses during steady-state and transient driving modes. *Environmental Science and Technology* 46, 196–203. DOI: 10.1021/es2026856.

Jayaratne, E. R., Ristovski, Z. D., Meyer, N. and Morawska, L. (2009). Particle and gaseous emissions from compressed natural gas and ultralow sulphur diesel-fuelled buses at four steady engine loads. *Science of the Total Environment* 407.8, 2845–2852. DOI: 10.1016/j.scitotenv.2009.01.001.

Kang, E., Root, M. J., Toohey, D. W. and Brune, W. H. (2007). Introducing the concept of Potential Aerosol Mass (PAM). *Atmospheric Chemistry and Physics* 7, 5727–5744. DOI: 10.5194/acpd-7-9925-2007.

Kangasluoma, J., Junninen, H., Lehtipalo, K., Mikkilä, J., Vanhanen, J., Attoui, M., Sipilä, M., Worsnop, D., Kulmala, M. and Petäjä, T. (2013). Remarks on Ion Generation for CPC Detection Efficiency Studies in Sub-3-nm Size Range. *AIP Conference Proceedings* 1527, 192–196. ISSN: 0094243X. DOI: 10.1063/1.4803236.

Karavalakis, G., Hajbabaei, M., Durbin, T. D., Johnson, K. C., Zheng, Z. and Miller, W. J. (2013). The effect of natural gas composition on the regulated emissions, gaseous toxic pollutants, and ultrafine particle number emissions from a refuse hauler vehicle. *Energy* 50, 280–291. DOI: 10.1016/j.energy.2012.10.044.

Karjalainen, P., Timonen, H., Saukko, E., Kuuluvainen, H., Saarikoski, S., Aakko-Saksa, P., Murtonen, T., Bloss, M., Dal Maso, M., Simonen, P., Ahlberg, E., Svenningsson, B., Brune, W. H., Hillamo, R., Keskinen, J. and Rönkkö, T. (2016). Time-resolved characterization of primary particle emissions and secondary particle formation from a modern gasoline passenger car. *Atmospheric Chemistry and Physics* 16.13, 8559–8570. DOI: 10.5194/acp-16-8559-2016.

Kontses, A., Triantafyllopoulos, G., Ntziachristos, L. and Samaras, Z. (2020). Particle number (PN) emissions from gasoline, diesel, LPG, CNG and hybrid-electric light-duty vehicles under real-world driving conditions. *Atmospheric Environment* 222, 117126. DOI: 10.1016/j.atmosenv.2019.117126.

Köppel, W., Götz, M. and Graf, F. (2009). Biogas Upgrading for Injection into the Gas Grid Quality aspects, technological and ecological consideration. *gwf-Gas Erdgas, International issue* 150, 26–35.

Kuittinen, N., Jalkanen, J. P., Alanen, J., Ntziachristos, L., Hannuniemi, H., Johansson, L., Karjalainen, P., Saukko, E., Isotalo, M., Aakko-Saksa, P., Lehtoranta, K., Keskinen, J., Simonen, P., Saarikoski, S., Asmi, E., Laurila, T., Hillamo, R., Mylläri, F., Lihavainen, H., Timonen, H. and Rönkkö, T. (2021). Shipping Remains a Globally Significant Source of Anthropogenic PN Emissions even after 2020 Sulfur Regulation. *Environmental Science and Technology* 55, 129–138. DOI: 10.1021/acs.est.0c03627.

Kulmala, M., Riipinen, I., Sipilä, M., Manninen, H. E., Petäjä, T., Junninen, H., Dal Maso, M., Mordas, G., Mirme, A., Vana, M., Hirsikko, A., Laakso, L., Harrison, R. M., Hanson, I., Leung, C., Lehtinen, K. E. and Kerminen, V. M. (2007). Toward direct measurement of atmospheric nucleation. *Science* 318.5847, 89–92. DOI: 10.1126/science.1144124.

Kuuluvainen, H., Karjalainen, P., Saukko, E., Ovaska, T., Sirviö, K., Honkanen, M., Olin, M., Niemi, S., Keskinen, J. and Rönkkö, T. (2020). Nonvolatile ultrafine particles observed to form trimodal size distributions in non-road diesel engine exhaust. *Aerosol Science and Technology* 54.11, 1345–1358. DOI: 10.1080/02786826.2020.1783432.

Lähde, T. and Giechaskiel, B. (2021). Particle number emissions of gasoline, compressed natural gas (Cng) and liquefied petroleum gas (lpg) fueled vehicles at different ambient temperatures. *Atmosphere* 12.7. DOI: 10.3390/atmos12070893.

Lähde, T., Rönkkö, T., Virtanen, A., Schuck, T., Pirjola, L., Hämeri, K., Kulmala, M., Arnold, F., Rothe, D. and Keskinen, J. (2009). Heavy Duty Diesel Engine Exhaust Aerosol Particle and Ion Measurements. *Environmental Science & Technology* 43, 163–168.

Lähde, T., Virtanen, A., Happonen, M., Söderström, C., Kytö, M. and Keskinen, J. (2014). Heavy-duty, off-road diesel engine low-load particle number emissions and particle control. *Journal of the Air & Waste Management Association (Taylor & Francis Ltd)* 64.10, 1186–1194. DOI: 10.1080/10962247.2014.936985.

Lambe, A. T., Ahern, A. T., Williams, L. R., Slowik, J. G., Wong, J. P. S., Abbatt, J. P. D., Brune, W. H., Ng, N. L., Wright, J. P., Croasdale, D. R., Worsnop, D. R., Davidovits, P. and Onasch, T. B. (2011). Characterization of aerosol photooxidation flow reactors: Heterogeneous oxidation, secondary organic aerosol formation and cloud condensation nuclei activity measurements. *Atmospheric Measurement Techniques* 4.3, 445–461. DOI: 10.5194/amt-4-445-2011.

Le Breton, M., Psichoudaki, M., Hallquist, M., Watne, K., Lutz, A. and Hallquist, M. (2019). Application of a FIGAERO ToF CIMS for on-line characterization of real-world fresh and aged particle emissions from buses. *Aerosol Science and Technology* 53.3, 244–259. DOI: 10.1080/02786826.2019.1566592.

Legala, A., Premnath, V., Chadwell, M., Weber, P. and Khalek, I. (2021). Impact of Selective Catalytic Reduction Process on Nonvolatile Particle Emissions. *SAE Technical Papers*, 1–13. DOI: 10.4271/2021-01-0624.

Lehtoranta, K., Aakko-Saksa, P., Murtonen, T., Vesala, H., Ntziachristos, L., Rönkkö, T., Karjalainen, P., Kuittinen, N. and Timonen, H. (2019). Particulate Mass and Nonvolatile Particle Number Emissions from Marine Engines Using Low-Sulfur Fuels, Natural Gas, or Scrubbers. *Environmental Science and Technology* 53.6, 3315–3322. DOI: 10.1021/acs.est.8b05555.

Lelieveld, J., Evans, J. S., Fnais, M., Giannadaki, D. and Pozzer, A. (2015). The contribution of outdoor air pollution sources to premature mortality on a global scale. *Nature* 525.7569, 367–71. DOI: 10.1038/nature15371.

Lelieveld, J., Pozzer, A., Pöschl, U., Fnais, M., Haines, A. and Münzel, T. (2020). Loss of life expectancy from air pollution compared to other risk factors: A worldwide perspective. *Cardiovascular Research* 116.11, 1910–1917. DOI: 10.1093/cvr/cvaa025.

Link, M. F., Kim, J., Park, G., Lee, T., Park, T., Bin, Z., Sung, K., Kim, P., Kang, S., Soo, J., Choi, Y., Son, J., Lim, H.-j. and Farmer, D. K. (2017). Elevated production of NH4NO3 from the photochemical processing of vehicle exhaust : Implications for air quality in the Seoul Metropolitan Region. *Atmospheric Environment* 156, 95–101. DOI: 10.1016/j.atmosenv.2017.02.031.

Liu, B. and Pui, D. (1974). Equilibrium Bipolar Charge Distribution. *Journal of Colloid Interface Science* 49.305.

Majewski, W. A. and Jääskeläinen, H. (2021). *Engine Emission Control*. Dieselnet. URL: https://dieselnet.com/tech/engine_emission-control.php (visited on 09/10/2021).

Mao, J., Ren, X., Brune, W. H., Olson, J. R., Crawford, J. H., Fried, A., Huey, L. G., Cohen, R. C., Heikes, B., Singh, H. B., Blake, D. R., Sachse, G. W., Diskin, G. S., Hall, S. R. and Shetter, R. E. (2009). Airborne measurement of OH reactivity during INTEX-B. *Atmospheric Chemistry and Physics Discussions* 9, 163–173. DOI: 10.5194/acpd-8-14217-2008.

Maricq, M. M. (2006). On the electrical charge of motor vehicle exhaust particles. *Journal of Aerosol Science* 37, 858–874. DOI: 10.1016/j.jaerosci.2005.08.003.

Middlebrook, A. M., Bahreini, R., Jimenez, J. L. and Canagaratna, M. R. (2012). Evaluation of Composition-Dependent Collection Efficiencies for the Aerodyne Aerosol Mass Spectrometer using Field Data. *Aerosol Science and Technology* 46.3, 258–271. DOI: 10.1080/02786826.2011.620041.

Mikkanen, P., Moisio, M., Keskinen, J., Ristimäki, J. and Marjamäki, M. (2001). Sampling Method for Particle Measurements of Vehicle Exhaust. *SAE International Journal of Fuels and Lubricants* 724, 1–6.

Mirme, A. (1994). Electrical aerosol spectrometry. PhD thesis. Dissertationes Geophysicales Universitatis Tartuensis, No. 6, University of Tartu, Estonia.

Murtonen, T., Lehtoranta, K., Korhonen, S., Vesala, H. and Koponen, P. (2016). Imitating emission matrix of large natural catalyst studies in engine laboratory. *28th CIMAC World Congress* 107.

Nordin, E. Z., Eriksson, A. C., Roldin, P., Nilsson, P. T., Carlsson, J. E., Kajos, M. K., Hellén, H., Wittbom, C., Rissler, J., Löndahl, J., Swietlicki, E., Svenningsson, B., Bohgard, M., Kulmala, M., Hallquist, M. and Pagels, J. H. (2013). Secondary organic aerosol formation from idling gasoline passenger vehicle emissions investigated in a smog chamber. *Atmospheric Chemistry and Physics* 13.12, 6101–6116. DOI: 10.5194/acp-13-6101-2013.

Ntziachristos, L., Giechaskiel, B., Pistikopoulos, P., Samaras, Z., Mathis, U., Mohr, M., Ristimaki, J., Keskinen, J., Mikkanen, P., Casati, R., Scheer, V. and Vogt, R. (2004). Performance evaluation of a novel sampling and measurement system for exhaust particle characterization. *SAE 2004 World Congress and Exhibition* 724. DOI: 10.4271/2004-01-1439.

Ntziachristos, L., Saukko, E., Lehtoranta, K., Rönkkö, T., Timonen, H., Simonen, P. and Karjalainen, P. (2016). Particle emissions characterization from a medium-speed marine diesel engine with two fuels at different sampling conditions. *Fuel* 186, 456–465. DOI: 10.1016/j.fuel.2016.08.091.

Oberdörster, G., Sharp, Z., Atudorei, V., Elder, A., Gelein, R., Kreyling, W. and Cox, C. (2004). Translocation of Inhaled Ultrafine Particles to the Brain. *Inhalation Toxicology* 16.6-7, 437–445. DOI: 10.1080/08958370490439597.

Olin, M., Alanen, J., Palmroth, M., Rönkkö, T. and Dal Maso, M. (2019). Inversely modeling homogeneous H2SO4-H2O nucleation rate in exhaust-related conditions. *Atmospheric Chemistry and Physics* 19, 6367–6388. DOI: 10.5194/acp-19-6367-2019.

Peng, W., Yang, J., Corbin, J., Trivanovic, U., Lobo, P., Kirchen, P., Rogak, S., Gagné, S., Miller, J. W. and Cocker, D. (2020). Comprehensive analysis of the air quality impacts of switching a marine vessel from diesel fuel to natural gas. *Environmental Pollution* 266.

Pirjola, L., Rönkkö, T., Saukko, E., Parviainen, H., Malinen, A., Alanen, J. and Saveljeff, H. (2017). Exhaust emissions of non-road mobile machine: Real-world and laboratory studies with diesel and HVO fuels. *Fuel* 202. DOI: 10.1016/j.fuel.2017.04.029.

Pirjola, L., Dittrich, A., Niemi, J. V., Saarikoski, S., Timonen, H., Kuuluvainen, H., Järvinen, A., Kousa, A., Rönkkö, T. and Hillamo, R. (2016). Physical and Chemical Characterization of Real-World Particle Number and Mass Emissions from City Buses in Finland. *Environmental Science and Technology* 50, 294–304. DOI: 10.1021/acs.est.5b04105.

Pope III, C. A. and Dockery, D. W. (2006). Health Effects of Fine Particulate Air Pollution: Lines that Connect. *Journal of the Air & Waste Management Association* 56.10, 1368–1380. DOI: 10.1080/10473289.2006.10464545.

Quillen, K., Bennett, M., Volckens, J. and Stanglmaier, R. H. (2008). Characterization of particulate matter emissions from a four-stroke, lean-burn, natural gas engine. *Journal of Engineering for Gas Turbines and Power* 130.5, 3–7. DOI: 10.1115/1.2906218.

Ray, S. (2019). *Natural gas-fired reciprocating engines are being deployed more to balance renewables*. U.S. Energy Information Administration. URL: https://www.eia.gov/todayinenergy/detail.php?id=37972 (visited on 05/13/2021).

Ristovski, Z. D., Morawska, L., Hitchins, J., Thomas, S., Greenaway, C. and Gilberts, D. (2000). Particle emissions from compressed natural gas engines. *Journal of Aerosol Science* 31.4, 403–413.

Rönkkö, T., Kuuluvainen, H., Karjalainen, P., Keskinen, J., Hillamo, R., Niemi, J. V., Pirjola, L., Timonen, H., Saarikoski, S., Saukko, E., Järvinen, A., Silvennoinen, H., Rostedt, A., Olin, M., Yli-Ojanperä, J., Nousiainen, P., Kousa, A. and Dal Maso, M. (2017). Traffic is a major source of atmospheric nanocluster aerosol. *Proceedings of the National Academy of Sciences of the United States of America* 114.29, 7549–7554.

Rönkkö, T., Lähde, T., Heikkilä, J., Pirjola, L., Bauschke, U., Arnold, F., Schlager, H., Rothe, D., Yli-Ojanperä, J. and Keskinen, J. (2013). Effects of gaseous sulphuric acid on diesel exhaust nanoparticle formation and characteristics. *Environmental Science and Technology* 47.20, 11882–11889. DOI: 10.1021/es402354y.

Rönkkö, T. and Timonen, H. (2019). Overview of Sources and Characteristics of Nanoparticles in Urban Traffic-Influenced Areas. *Journal of Alzheimer's Disease* 72, 15–28. DOI: 10.3233/JAD-190170.

Rönkkö, T., Virtanen, A., Kannosto, J., Keskinen, J., Lappi, M. and Pirjola, L. (2007). Nucleation mode particles with a nonvolatile core in the exhaust of a heavy duty diesel vehicle. *Environmental Science and Technology* 41.18, 6384–6389. DOI: 10.1021/es0705339.

Rönkkö, T., Virtanen, A., Vaaraslahti, K., Keskinen, J., Pirjola, L. and Lappi, M. (2006). Effect of dilution conditions and driving parameters on nucleation mode particles in diesel exhaust: Laboratory and on-road study. *Atmospheric Environment* 40.16, 2893–2901. DOI: 10.1016/j.atmosenv.2006.01.002.

Saffaripour, M., Chan, T. W., Liu, F., Thomson, K. A., Smallwood, G. J., Kubsh, J. and Brezny, R. (2015). Effect of Drive Cycle and Gasoline Particulate Filter on the Size and Morphology of Soot Particles Emitted from a Gasoline-Direct-Injection Vehicle. *Environmental Science and Technology* 49.19, 11950–11958. DOI: 10.1021/acs.est.5b02185.

Salo, L., Hyvärinen, A., Jalava, P., Teinilä, K., Hooda, R. K., Datta, A., Saarikoski, S., Lintusaari, H., Lepistö, T., Martikainen, S., Rostedt, A., Sharma, V. P., Rahman, M. H., Subudhi, S., Asmi, E., Niemi, J. V., Lihavainen, H., Lal, B., Keskinen, J., Kuuluvainen, H., Timonen, H. and Rönkkö, T. (2021). The characteristics and size of lung-depositing particles vary significantly between high and low pollution traffic environments. *Atmospheric Environment* 255.March. DOI: 10.1016/j.atmosenv.2021.118421.

Savickis, J., Zeltins, N., Bode, I., Jansons, L., Dzelzitis, E., Koposovs, A., Selickis, A. and Ansone, A. (2020). The Biomethane Injection into the Natural Gas Networks: The EU's Gas Synergy Path. *Latvian Journal of Physics and Technical Sciences* 57, 34–50. DOI: 10.2478/lpts-2020-0020.

Schreiber, D., Forss, A. M., Mohr, M. and Dimopoulos, P. (2007). Particle Characterisation of Modern CNG, Gasoline and Diesel Passenger Cars. *SAE Technical Papers* 2007-24-01. DOI: 10.4271/2007-24-0123.

Seinfeld, J. H. and Pandis, S. N. (2016). *Atmospheric Chemistry and Physics: From Air Pollution to Climate Change*. 3rd. New York, USA: Wiley.

Seong, H. and Choi, S. (2014). Examination of nanoparticles from gasoline direct-injection (GDI) engines using transmission electron microscopy (TEM). *International Journal of Automotive Technology* 15.2, 175–181. DOI: 10.1007/s12239-014-0019-5.

Sgro, L. A., Sementa, P., Vaglieco, B. M., Rusciano, G., D'Anna, A. and Minutolo, P. (2012). Investigating the origin of nuclei particles in GDI engine exhausts. *Combustion and Flame* 159.4, 1687–1692. DOI: 10.1016/j.combustflame.2011.12.013.

Simonen, P., Kalliokoski, J., Karjalainen, P., Rönkkö, T., Timonen, H., Saarikoski, S., Aurela, M., Bloss, M., Triantafyllopoulos, G., Kontses, A., Amanatidis, S., Dimaratos, A., Samaras, Z., Keskinen, J., Dal Maso, M. and Ntziachristos, L. (2019). Characterization of laboratory and real driving emissions of individual Euro 6 light-duty vehicles – Fresh particles and secondary aerosol formation. *Environmental Pollution* 255. DOI: 10.1016/j.envpol.2019.113175.

Thiruvengadam, A., Besch, M., Yoon, S., Collins, J., Kappanna, H., Carder, D., Ayala, A., Herner, J. and Gautam, M. (2014). Characterization of particulate matter emissions from a current technology natural gas engine. *Environmental Science and Technology* 48.14, 8235–8242. DOI: 10.1021/es5005973.

Timonen, H., Karjalainen, P., Saukko, E., Saarikoski, S., Aakko-Saksa, P. and Simonen, P. (2017). Influence of fuel ethanol content on primary emissions and secondary aerosol

formation potential for a modern flex-fuel gasoline vehicle. *Atmospheric Chemistry and Physics* 17, 5311–5329. DOI: 10.5194/acp-17-5311-2017.

Tkacik, D. S., Lambe, A. T., Jathar, S., Li, X., Presto, A. A., Zhao, Y., Blake, D., Meinardi, S., Jayne, J. T., Croteau, P. L. and Robinson, A. L. (2014). Secondary Organic Aerosol Formation from in-Use Motor Vehicle Emissions Using a Potential Aerosol Mass Reactor. *Environmental Science & Technology* 48.19, 11235–11242. DOI: 10.1021/es502239v.

Toumasatos, Z., Kontses, A., Doulgeris, S., Samaras, Z. and Ntziachristos, L. (2021). Particle emissions measurements on CNG vehicles focusing on Sub-23nm. *Aerosol Science and Technology* 55.2, 182–193. DOI: 10.1080/02786826.2020.1830942.

Ushakov, S., Stenersen, D. and Einang, P. M. (2019). Methane slip from gas fuelled ships: a comprehensive summary based on measurement data. *Journal of Marine Science and Technology (Japan)* 24.4, 1308–1325. DOI: 10.1007/s00773-018-00622-z.

Ushakov, S., Valland, H., Nielsen, J. B. and Hennie, E. (2013). Particle size distributions from heavy-duty diesel engine operated on low-sulfur marine fuel. *Fuel Processing Technology* 106, 350–358. DOI: 10.1016/j.fuproc.2012.08.022.

Viana, M., Hammingh, P., Colette, A., Querol, X., Degraeuwe, B., Vlieger, I. de and Aardenne, J. van (2014). Impact of maritime transport emissions on coastal air quality in Europe. *Atmospheric Environment* 90, 96–105. DOI: 10.1016/j.atmosenv.2014.03.046.

Wang, W. G., Clark, N. N., Lyons, D. W., Yang, R. M., Gautam, M., Bata, R. M. and Loth, J. L. (1997). Emissions comparisons from alternative fuel buses and diesel buses with a chassis dynamometer testing facility. *Environmental Science and Technology* 31.11, 3132–3137. DOI: 10.1021/es9701063.

Wei, L. and Geng, P. (2016). A review on natural gas/diesel dual fuel combustion, emissions and performance. *Fuel Processing Technology* 142, 264–278. DOI: 10.1016/j.fuproc.2015.09.018.

Wiedensohler, A. (1988). An approximation of the bipolar charge distribution for particles in the submicron size range. *Journal of Aerosol Science* 19.3, 387–389. DOI: 10.1016/0021-8502(88)90278-9.

Zhu, H., McCaffery, C., Yang, J., Li, C., Karavalakis, G., Johnson, K. C. and Durbin, T. D. (2020). Characterizing emission rates of regulated and unregulated pollutants from two ultra-low NOx CNG heavy-duty vehicles. *Fuel* 277.118192. DOI: 10.1016/j.fuel.2020.118192.

PAPERS

PAPER 1

The formation and physical properties of the particle emissions from a natural gas engine

Alanen, J., Saukko, E., Lehtoranta, K., Murtonen, T., Timonen, H., Hillamo, R., Karjalainen, P., , H., Harra, J., Keskinen, J. and Rönkkö, T.

Fuel 162.(2015), 155–161
DOI: 10.1016/j.fuel.2015.09.003

Fuel 162 (2015) 155–161

Contents lists available at ScienceDirect

Fuel

journal homepage: www.elsevier.com/locate/fuel

The formation and physical properties of the particle emissions from a natural gas engine

Jenni Alanen [a,*], Erkka Saukko [a], Kati Lehtoranta [b], Timo Murtonen [b], Hilkka Timonen [c], Risto Hillamo [c], Panu Karjalainen [a], Heino Kuuluvainen [a], Juha Harra [a], Jorma Keskinen [a], Topi Rönkkö [a]

[a] Department of Physics, Tampere University of Technology, P.O. Box 599, FI-33720 Tampere, Finland
[b] VTT Technical Research Centre of Finland, P.O. Box 1000, FI-02044 VTT, Finland
[c] Atmospheric Composition Research, Finnish Meteorological Institute, P.O. Box 503, FI-00101 Helsinki, Finland

HIGHLIGHTS

- Natural gas engine particle emissions were studied in engine dynamometer.
- Exhaust particle size distribution, volatility and electric charge were measured.
- Particle features suggest that they form originally in vicinity of engine cylinders.
- Size range 1–5 nm is relevant for natural gas engine emitted particle emissions.

ARTICLE INFO

Article history:
Received 30 June 2015
Received in revised form 29 August 2015
Accepted 1 September 2015
Available online 9 September 2015

Keywords:
Fine particle emission
Particle formation
Natural gas
Internal combustion engine

ABSTRACT

Natural gas engine particle emissions were studied using an old gasoline engine modified to run with natural gas. The tests were steady-state tests performed on two different low loads in an engine dynamometer. Exhaust particle number concentration, size distribution, volatility and electric charge were measured. Exhaust particles were observed to have peak diameters below 10 nm. To get the full picture of particle emissions from natural gas engines, size range 1–5 nm is relevant and important to take into consideration. A particle size magnifier (PSM) was used in this engine application for measuring particles smaller than 3 nm and it proved to be a useful instrument when measuring natural gas engine exhaust particles. It is concluded that the detected particles probably originated from the engine cylinders or their vicinity and grew to detectable sizes in the sampling process because a small fraction of the particles were observed to carry electric charge and the particles did not evaporate totally at 265 °C.

1. Introduction

The usage of natural gas and the interest towards it have risen because of its smaller environmental effects compared to diesel and gasoline and its improved availability due to shale gas. As a fast reserve power for renewable energy sources such as wind and solar power, engine power plants have and will become more important. Natural gas is also an attracting alternative for diesel in piston engines in energy production and transport due to its potentially smaller carbon dioxide and particulate mass emissions [1].

Fine particles can possess a threat to human health. There is wide epidemiological evidence that especially particles smaller than 2.5 μm increase mortality already at moderate mass concentrations [2–4]. Mortality is connected with cardiovascular diseases and combustion related particles. Ultrafine particles smaller than 100 nm have larger surface area per unit mass and they can penetrate deeper into lungs when inhaled. Typically they do not contribute significantly to particle mass but can be significant in terms of number concentration.

Particle emissions of natural gas engines have not been studied in detail until recently, and current research in the field is concentrated on natural gas buses. Size distribution measurements have shown the size of natural gas emission particles to be in the nanoparticle size range (below 50 nm) [5–7] both in transient and in steady driving conditions. Particle size distribution peaks smaller than 12 nm have been measured by Hajbabaei et al. [8], Jayaratne et al. [1] and Hallquist et al. [9]. Limitations in instrument detection limits could be the reason for them not reporting even smaller peak diameters; especially the size distributions reported by Hajbabaei et al. [8] indicate the particles to exist also below the detection limit of the instrument. No research has been

* Corresponding author.
E-mail address: jenni.e.alanen@tut.fi (J. Alanen).

http://dx.doi.org/10.1016/j.fuel.2015.09.003
0016-2361/

reported about natural gas engine exhaust particles in the size range below 4 nm. However, if a substantial fraction of exhaust particles is smaller than 4 nm, the whole picture is not obtained if those particles are not taken into account. The smallest nanoparticles are potentially hazardous because of their ability to enter human central nervous system [10].

The number concentrations of particles emitted by natural gas engines are not necessarily small when compared to diesel engines in spite of small soot particle formation in the engines. Jayaratne et al. [11] and Hallquist et al. [9] raise a concern that particle number emissions from CNG (compressed natural gas) buses are an order of magnitude larger than from diesel buses with no after-treatment although the mass concentration of particles is substantially smaller. The maximum concentration in exhaust gas is measured to be $3 \cdot 10^5$ 1/cm^3 [5] or $1 \cdot 10^7$ 1/cm^3 [6] when the subject of experiment has been a large scale natural gas engine with maximum power more than 298 kW and $1.3 \cdot 10^6$ 1/cm^3 for a natural gas bus equipped with an oxidation catalyst at maximum load [1]. The particle number emission factors for CNG buses are of order of magnitude 10^{14} 1/km [9,1].

Physical and chemical characteristics of natural gas engine exhaust particles have previously been measured by e.g. Bullock and Olfert [12], Jayaratne et al. [7] and Yoon et al. [13]. Less than 5% of the particulate matter volume has been observed to remain non-volatile at 100 °C for a homogeneous charge compression ignition engine [12] and for CNG buses, approximately 85% of the exhaust particles are volatile at 100 °C and 98% at 250 °C [7]. The density of natural gas particulates has been found out to be 850 kg/m^3 [12]. A filter collection study by Yoon et al. [13] reveals that natural gas buses emit particles that contain elemental and organic carbon, aromatic hydrocarbons, and lubricating oil originating calcium, phosphorus, zinc, magnesium and sulfur.

Studies on natural gas combustion in flame or commercial burners can possibly provide information about natural gas engine combustion process and related particulate formation without the effect of lubricating oil. Methane fueled cook stove and burner particulates are carbonaceous nanoparticles with modal diameter at 2–4 nm [14]. According to Wagner et al. [15], the diameter of the particles emitted by natural gas fired domestic gas cookers are about 6–10 nm. On the other hand, Murr and Soto [16] defined by TEM study that natural gas burners emit particulates that are larger carbon aggregates with diameter at micron scale. Particles generated in ethylene flame have sizes of about 2–10 nm [17].

In the future the need to reduce the emissions also from natural gas engines might become more important. Therefore they need techniques to reduce their particle emissions. If the origin, formation process and the properties of the emissions are known, reducing them will be easier. In this study, detailed measurements about the primary particle emission characteristics of an engine running on natural gas were performed, including measurements of particles with diameter below 4 nm. The emissions of a natural gas engine were studied using a small-scale retrofitted natural gas engine. The original goal of the project behind the study was to imitate the emissions of a large-scale natural gas engine power plant. A small-scale engine was used in order to save space and fuel and to be able to run long detailed measurements and to test different exhaust after-treatment systems cost-efficiently in later phases of the project. This article focuses on exhaust particle formation phenomena in a natural gas engine, but not in any specific engine type.

2. Experimental

2.1. Engine, fuel and lubricating oil, and driving conditions

The engine used in the experiments was a passenger car gasoline engine that was modified to run with natural gas by installing natural gas injection nozzles in its intake manifold [18]. The original engine was an in-line, 4-cylinder, model-year 1999 engine with a total displacement of 1998 cc and maximum power 100 kW/5500 rpm. The engine was run in an engine dynamometer without exhaust after-treatment.

The engine was operated at two different engine modes which were chosen so that the gaseous emissions of the test engine were similar to the gaseous emissions of a natural gas engine power plant at two different constant loads. Carbon monoxide and NO_x levels were searched with engine adjustments but hydrocarbons were needed to add into the exhaust gas at one of the engine modes in order to produce the exhaust composition of the power plant engine that was imitated. The specification of the test engine modes are presented in Table 1. All aerosol measurements reported in this article were performed at both engine modes.

The fuel used was Russian pipeline natural gas with high methane content. It contained 97.2 vol% methane, 1.37% ethane, 0.17% propane, 0.07% other hydrocarbons, 0.9% nitrogen and 0.2% carbon dioxide. The sulfur content of the fuel was below 1.5 ppm. The lubricating oil was produced by Neste Oil Plc. The content of sulfur, calcium, phosphor and zinc were 1280 mg/kg, 2580 mg/kg, 721 mg/kg and 700 mg/kg, respectively. The mass percentage of sulfated ash was 0.97% for the lubricating oil. Viscosity at 40 °C was 68.4 mm^2/s and density was 852.7 kg/m^3.

2.2. Sampling system and measurement setup

Particle emission sampling system consisted of a porous tube diluter (PTD, [19,20]), a residence time tunnel and an ejector diluter (Dekati Ltd.). Sample was taken from the exhaust pipe after an exhaust gas heating unit to a dilution system. Residence time in the primary dilution system, i.e. in the PTD and the residence time tunnel, was 2.6 s. The dilution ratio (DR) over the porous tube diluter during the measurements was set to be as small as 6 because the particle number concentrations in the exhaust line were low and close to the detection limit of used aerosol instruments (especially EEPS and Nano-SMPS). The secondary dilution ratio over the ejector diluter was 4, resulting in a total dilution ratio of 24.

Particulate mass measurements were completed as filter collections and the sampling was done using an AVL SPC 427 Smart Sampler partial flow dilution system. The filter collections followed standard ISO 8178-1:2006(E). Particulate mass was collected on a pair of 70 mm diameter Pallflex TX40-HI20WW filters using a 1.5 g/s sample flow and a dilution ratio of 10. The sample gas temperature at the sample filter was 43–49 °C. Sample filters were weighed in a special weighing room in which the temperature and humidity were controlled according to ISO 8178-1:2006(E). Sartorius SE2-F ultramicro scale was used for filter weighing.

Particle size distribution and number concentration were measured using three instruments that together covered a wide particle mobility size range. A particle size magnifier (PSM, Airmodus Inc.) together with a condensation particle counter (CPC 3775, TSI Inc.) was used to measure size range 1.7–7.2 nm. A scanning mobility particle sizer (Nano-SMPS [21]) equipped with DMA 3085 and UCPC 3025 (TSI Inc.) was used in size range 3–60 nm.

Table 1
The specifications of the engine modes.

	Higher torque	Lower torque
Test engine torque	60 N m	35 N m
Test engine speed	2700 rpm	3100 rpm
Residual O_2	6%	6%
Combustion air consumption	100 kg/h	95 kg/h
Hydrocarbon additions	No	Yes

The sample flow was 1.5 lpm and sheath flow 15 lpm. An engine exhaust particle sizer (EEPS, TSI Inc.; originally [22]) was used to cover size range 5.6–560 nm. The EEPS default inversion matrix was applied. UCPC 3776 (TSI Inc.) was measuring beside PSM and its purpose of use was to monitor changes and support PSM total concentration data.

The measurement setup is described in Fig. 1. Thermodenuder (TD [23]) and Nano-SMPS neutralizer could be bypassed. The extra dilution before EEPS was organized using a HEPA filter and TSI Mass Flowmeter. The sample coming to PSM and UCPC was diluted with a dilution ratio 36. The particle losses of the diluter depended on particle size and the penetration curve was

$$\eta = 0.819exp(3.657\xi) + 0.097exp(22.3\xi) + 0.032exp(57\xi) \quad (1)$$

where $\xi = \pi DQL$ and D is diffusion constant of a particle, Q is flow rate through the diluter and L is the length 10.22 cm that the diluter corresponds based on fitting made on measurement data. The penetration curve follows penetration curve for diffusion losses in Gormley and May [24].

A thermodenuder at 265 °C was used to study particle volatility characteristics. Thermodenuder consists of a heated metal tube followed by an active charcoal that absorbs the evaporated compounds. The thermodenuder and the loss curve used to correct the losses in thermodenuder are described in Heikkilä et al. [25]. The used thermodenuder is designed for ultrafine particle measurements.

Nano-SMPS was used without the neutralizer to study the electric charge state of particles. After Lähde et al. [26], it will be called here Ion-SMPS (Ion-DMPS in their study). When Nano-SMPS is used without neutralizer, particles will be classified based on their existing charge state. The electric charge of particles was investigated by comparing the particle size distributions measured by Nano-SPMS and Ion-SMPS. Only a DMA with negative polarity was available in the measurements. Therefore, only particles of positive charge could be measured.

The emissions of CO_2 were measured from raw exhaust by a Non-Dispersive Infrared Analyzer (NDIR, Horiba PG-250A) and from the diluted exhaust by Sick Maihak SIDOR gas analyzer. CO_2 was used for defining the dilution ratios over both dilution systems. The SIDOR analyzer was calibrated before the measurement campaign and the NDIR analyzer every morning.

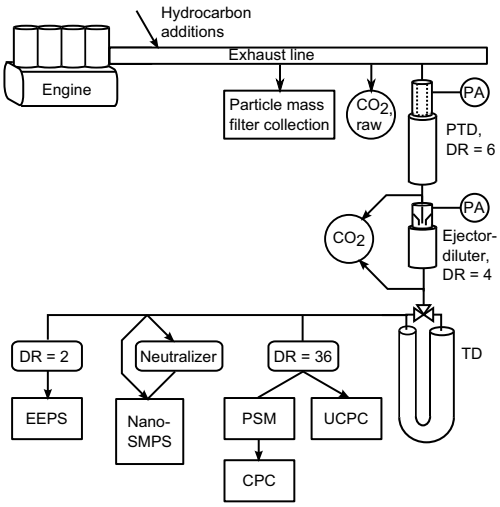

Fig. 1. A schematic diagram of the sampling system and the measurement setup.

2.3. PSM calibration

The calibration of PSM size distribution was performed using silver particles generated by an evaporation–condensation method [27] in a tube furnace. Nitrogen was used as a carrier gas. A small corona charger [28] was used to charge the particles and positively charged particles with sizes starting from 1.3 nm were selected by DMA 3085. The saturator flow of PSM was varied, which changed the growth efficiency of the particles and therefore the detection efficiency of the PSM–CPC combination that was used for measuring the concentration of the particles. The detection efficiency was calculated by first comparing the concentrations measured with each saturator flow with the concentrations with saturator flow 1 lpm and finally comparing the concentrations with the saturator flow 1 lpm with the detection efficiency curve for silver particles of positive electric charge published by Kangasluoma et al. [29]. The calibration results are shown in Fig. 2.

Presumably, silver particles do not have exactly the same density and mobility as natural gas engine exhaust particles. Also particle growth with condensing diethylene glycol (DEG, working fluid used in PSM) is material dependent; silver particles were the least prone to grow with condensation of DEG amongst ammonium sulfate, sodium chloride, tungsten oxide and silver in the study of Kangasluoma et al. [29]. However, the particle composition of the natural gas exhaust particles is still unknown. The calibration made with silver particles gives an idea in what size range the smallest particles are and provides an opportunity to gain overlapping PSM and Nano-SMPS size distributions.

3. Results and discussion

3.1. Particle size distribution and concentration

The concentration of the particles in the diluted exhaust, corrected by the dilution factor, varied between $3 \cdot 10^6$ and $35 \cdot 10^6$ 1/cm^3 depending on engine test mode (Table 2). In Table 2 mean number concentrations for all particles and particles over 23 nm are presented with calculated emission factors and standard deviations. Total number concentrations were measured using

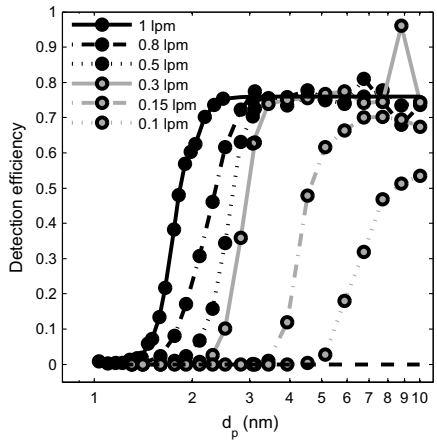

Fig. 2. Calibration of PSM with silver particles generated in a tube furnace. Saturator flow changed between 0.1 and 1 lpm.

PSM with saturator flow 1 lpm. The particle number concentration of particles with diameter over 23 nm was calculated using EEPS size distribution data. The standard deviation in EEPS size distributions and therefore also in the calculated EEPS number concentrations was large. The total mass concentration measurements were done by filter sampling.

The emission factors were calculated using information about the engine power and combustion air consumption, and assuming the density of exhaust gas to be equivalent to that of air and combustion of the natural gas to be ideal. Emission factors are practical when comparing emissions from different sources. Particle number emission emitted by power plant or ship engines is not regulated. For example in Euro 5/6 light and Euro VI heavy duty diesel emission regulations for particle number, only non-volatile particles over 23 nm are taken into account [30]. To be able to compare emission factors with vehicle engine regulations and to better understand the magnitude of the particle number concentration emitted by the test engine, particle number emission factor is calculated and presented here also for only those particles with diameter above 23 nm.

Taking into account that all particles with diameter above ~1.5 nm were counted and the dilution conditions favored generation and growth of particles [31], the observed particle number concentrations were fairly small. In addition, the engine was run at unusually low loads because of the aim to produce gaseous emissions similar to those of a natural gas engine power plant.

The number of particles with a diameter lower than 23 nm dominated clearly the total particle number concentration; less than 1% of the particles were in the particle size range above 23 nm. The particle number emission factor for particles above 23 nm was very small when compared for example to the number concentration regulation of the EU emission standard for heavy-duty diesel engines on stage Euro VI, $8 \cdot 10^{11}$ 1/kW h [32].

The particle size measured for natural gas engine exhaust particles was extremely small. Size distribution peaked at 2–5 nm (Fig. 3). Another particle mode peak with much smaller number concentration was detected at particle sizes 6–10 nm.

Observed PSM and Nano-SMPS size distributions did not correspond exactly on either size or concentration. This can result from problems in the PSM size distribution calibration with silver particles or differences in the detection efficiency of the two instruments. The losses in transfer lines have not been corrected in the results and they were somewhat larger in the transfer lines before Nano-SMPS than in transfer lines before PSM. This can explain a part of the difference between PSM and Nano-SMPS size distributions. The standard deviation of especially PSM size distribution concentrations were large. PSM still provides information of the particles with diameter below 3 nm that could not be acquired by Nano-SMPS only. Large variation in measured particle concentrations from natural gas engines has also been observed by Jayaratne et al. [1].

The concentration at the engine mode with higher torque was too low and possibly unstable in order to produce smooth Nano-SMPS size distribution curve with the scheduling used (Scan up 120 s, Retrace 30 s). At the other engine mode, the concentration was clearly larger, but also in that case the particle mode was near the lower cut point of the instrument.

Table 2
Particle number concentrations by PSM and EEPS, and mass concentrations by filter sampling at each engine operating condition.

Test engine torque Test engine speed	Higher, 60 N m 2700 rpm	Lower, 35 N m 3100 rpm
$PN_{tot} \pm \sigma$ (10^6 1/cm^3)	3.8 ± 0.6	34.6 ± 6.7
$EF_N \pm \sigma$ (10^{13} 1/kW h)	1.9 ± 0.3	25.5 ± 4.9
$PN_{>23\ nm} \pm \sigma$ (10^4 1/cm^3)	1.6 ± 1.5	3.5 ± 3.0
$EF_{>23\ nm} \pm \sigma$ (10^{10} 1/kW h)	8.3 ± 7.7	26.0 ± 22.2
PM_{tot} (mg/m^3)	4.2	6.9

3.2. Physical characteristics of the particles

The particle size shifted towards smaller sizes when sample was heated to 265 °C (Fig. 4). When the torque of the test engine was 34 N m the shift of the particle size distribution peak was from ~4.5 nm to below 2 nm. The second particle mode shifted from ~9 nm to ~6 nm.

The strongest evaporation took place at temperatures from 50 to 120 °C (Fig. 5). Approximately 40% of total volume remained at 265 °C (Fig. 5b). When the torque of the test engine was 59 N m the particle concentration was so low that the volume concentration calculated from PSM and Nano-SMPS distributions was unstable and the remaining volume in Fig. 5b did not give sensible results. The number concentration does not decrease in reality like it seems according to Fig. 5a because the losses inside the thermodenuder are significantly larger for smaller particles. When material evaporates from the surface of the particles and their size decreases, the losses grow. Jayaratne et al. [33] obtained similar results when they heated natural gas bus emission particles to 300 °C. Approximately 18% of the particles were non-volatile at that temperature which, according to them, confirms that a substantial amount of the particles consist of solid ash and metals.

Positive electric charge of the particles was measured by Nano-SMPS (with neutralizer) and Ion-SMPS (without neutralizer) and comparing them with each other. It was observed that the concentration of the particles measured by Ion-SMPS (particles unneutralized) was approximately three times higher than that measured by Nano-SMPS (Fig. 6) i.e. the particles carry approximately three times more positive electric charge than at equilibrium at room temperature. That would suggest that the particles have been generated in a higher temperature than room temperature [34]. The Ion-SMPS and Nano-SMPS distributions displayed similar modal characteristics, indicating that the charging process of particles has been independent of particle mode. This result indicates that all the particles have been generated in a similar way. All the particles at the relevant particle diameters can be assumed to carry only one elementary charge or to be neutral [35,36] because multicharging of particles with diameter less than 12 nm is negligible (in room temperature by Wiedensohler and Fissan [37]).

In Fig. 7, charging probabilities (f_{ion}) were drawn together with the average theoretical [38–40] charging probability values (f_n) for the neutralizer. The charging probabilities were calculated by multiplying the ratio of Ion-SMPS and Nano-SMPS distributions with the average charging efficiency approximation for the neutralizer made by Wiedensohler [40]. The charging probabilities were larger for particles in the sample than for particles in the neutralized sample. To evaluate the meaning of the observation, Boltzmann temperatures were solved similarly to Lähde et al. [35] and Sgro et al. [34]. It was done in the size range 3–10 nm by fitting Boltzmann charge probability equation in Fig. 7. Boltzmann temperatures calculated this way were around 1000 °C. High Boltzmann temperatures indicate that the particles have formed in high temperatures. If the particles were smaller when gaining the charge than when detected with aerosol instruments, the Boltzmann temperature indicating the generation temperature actually is even higher. Boltzmann temperatures at small particle sizes must, however, be interpreted cautiously.

3.3. Generation process of the particles

To obtain information about the generation process of the natural gas exhaust particles, particle size distribution, electric

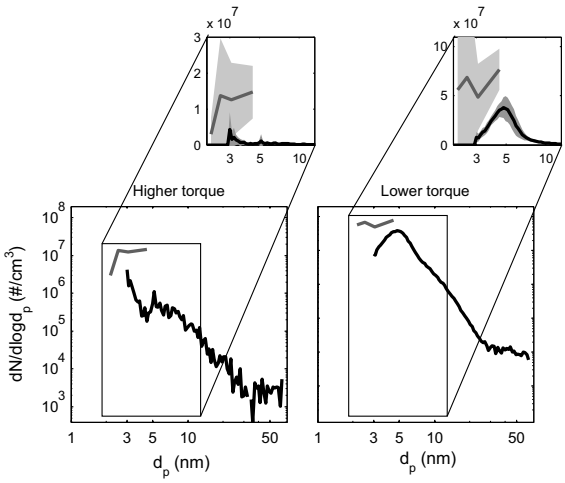

Fig. 3. Particle size distributions at the two different engine modes. PSM distributions are marked with red and Nano-SMPS with black. Standard deviation in concentrations is marked with light colors in figures with linear *y*-axis. Left: Higher test engine torque 60 N m. Right: Lower test engine torque 35 N m.

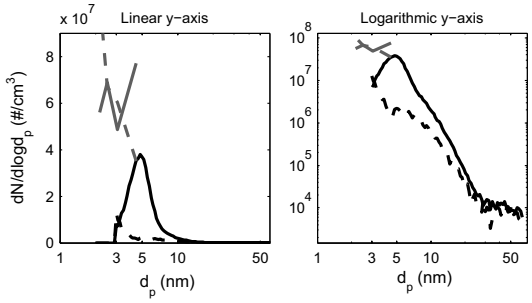

Fig. 4. Measured PSM and Nano-SMPS particle size distributions without (solid lines) and with thermodenuder (dashed lines). Lower test engine torque 35 N m. Left: Linlog scale. Right: Loglog scale.

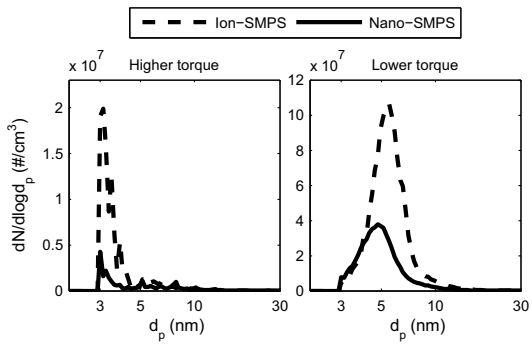

Fig. 6. Measured Nano-SMPS particle size distributions (solid lines) and Ion-SMPS results (dashed lines) obtained without neutralizer. Left: Higher test engine torque 60 N m. Right: Lower test engine torque 35 N m.

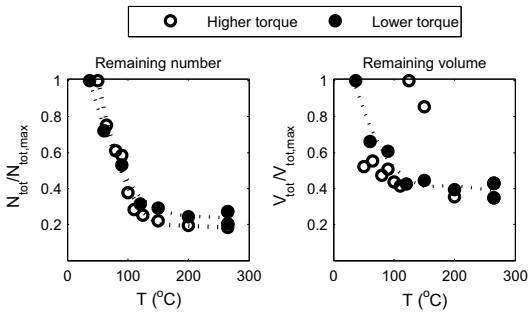

Fig. 5. Remaining particle total volume and total concentration as a function of thermodenuder temperature. Left: Remaining number concentration. Right: Remaining volume concentration. Volume calculated from combined PSM and Nano-SMPS distributions, number concentration from PSM. Losses inside the thermodenuder have been corrected only for volume concentration. The dotted lines are fits to guide the eye.

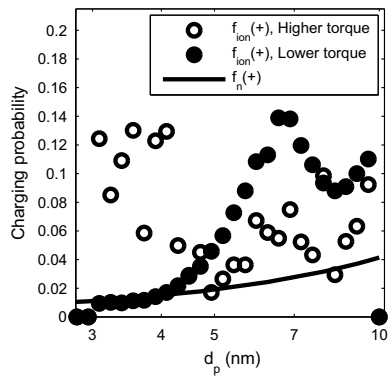

Fig. 7. Charging probabilities calculated from charging probability for the neutralizer (solid line) [40] and the ratio of Ion-SMPS and Nano-SMPS size distributions.

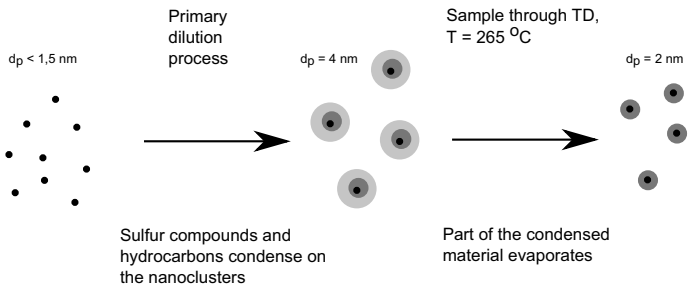

Fig. 8. Suggested formation process of nanoparticles in a natural gas engine.

charge and volatility of the particles were measured. The place of origin was investigated because it is strongly connected to the generation process and composition of the particles. The generation process and composition can for instance predict the best ways of reducing the particle emission or have an effect on the health effects of the particles. If the particles are generated during dilution and cooling process of the exhaust gases, they are likely to have been generated by sulfuric acid–water nucleation [41,42]. If the particles exist already before cooling process, their origin can be for example ash in lubricating oil or hydrocarbon combustion reactions [43,44].

A higher fraction of the particles carry an electric charge than that produced by aerosol neutralizer at room temperature. Particles carrying electric charge have been charged most probably in the high temperatures of the engine cylinders or their vicinity [45,46,34]. Especially strong evidence on this is presented in paper [46] where a particulate filter was observed to remove the charged nucleation mode particles confirming that they already exist in the tailpipe of a diesel engine.

Thermodenuder volatility measurements suggest that the particles have a non-volatile core but a notable part of their volume consists of volatile matter. Sulfuric acid evaporates at approximately 125 °C [47]. This would suggest that the material of the core of the particles is something else than sulfuric acid, since the sample was heated in this study to 265 °C in thermodenuder and the particles were not fully evaporated at that temperature. A non-volatile core is previously observed in diesel exhaust particles with diameter on nucleation mode size range for instance by Rönkkö [48] and De Filippo and Maricq [45].

The results indicate that natural gas engine exhaust particles are initially formed in engine cylinders and they increase in size during the sample dilution and cooling process (Fig. 8). The growth occurs by condensation of the gaseous compounds in exhaust gas if the conditions during primary dilution process are favorable.

The particle core composition could be e.g. nucleated metals [49] or amorphous carbon [34] and the volatile portion composition heavy hydrocarbons [12] or sulfur compounds. In earlier natural gas engine studies lubricating oil has been concluded to be the most probable source of the particles [5,7,8]. However, several laboratory flame studies performed using simple hydrocarbons such as ethylene and methane [50,51,17] show that also natural gas can be a source of carbonaceous flame-generated particles. Natural gas originated hydrocarbons can potentially condense on the already existing particles in the dilution and cooling process. Condensing compounds can also be lubricant oil originating sulfur compounds or hydrocarbons.

4. Conclusion

Particles emitted from the natural gas engine were extremely small with the particle size distribution peak at about 2–5 nm. The number of particles with a diameter larger than 23 nm was low compared to particles with smaller diameter. This was the first time the electrical charge of the particle emission of a natural gas engine was investigated or particles under 4 nm in the particle emission of a natural gas engine were measured. Also the observation of particle size reduction at 265 °C rather than complete evaporation was made for the first time in this work for natural gas engine particle emission. The usage of PSM in particle size distribution measurements helped to confirm the behavior of the particle size when the sample was heated.

The origin of the particles is probably engine cylinder or its vicinity. Our hypothesis is that the core of the particles consist of compounds originated from lubricating oil such as metals, or non-volatile carbonaceous combustion products of natural gas or lubricating oil. Natural gas originated hydrocarbons, and lubricating oil originated hydrocarbons and sulfur compounds can magnify the already existing particles in dilution and cooling process (sampling).

This study produced a base for understanding on how the natural gas engine exhaust particles are formed. In the future work this can be used when even more environmentally friendly solutions for natural gas based traffic and energy production, such as exhaust after-treatment devices and lubricant oils, are developed. For instance, in this work it was observed that the lubricating oil is possibly a significant contributor to the particles, and thus the potential of modification of lubricating oil composition in emission reduction should be investigated. In addition, because most research in the field of natural gas engines has been done for buses and also this work was done using a small-scale engine, future studies should include also the particle emissions from large scale engines such as natural gas engine power plants or ship engines.

Acknowledgments

This study was funded by Tekes, the Finnish Funding Agency for Innovation, Neste Oil, AGCO Power, Wärtsilä, Dinex Ecocat, Dekati, Suomi Analytics and Viking Line. Jenni Alanen acknowledges Gasum kaasurahasto for financial support.

The engine was operated by Timo Murtonen and Hannu Vesala (VTT).

References

[1] Jayaratne ER, Ristovski ZD, Meyer N, Morawska L. Particle and gaseous emissions from compressed natural gas and ultralow sulphur diesel-fuelled buses at four steady engine loads. Sci Total Environ 2009;407:2845–52.
[2] Beelen R, Raaschou-Nielsen O, Stafoggia M, Andersen ZJ, et al. Effects of long-term exposure to air pollution on natural-cause mortality: an analysis of 22 European cohorts within the multicentre ESCAPE project. Lancet 2014;383:785–95.
[3] Hoek G, Krishnan RM, Beelen R, Peters A, Ostro B, Brunekreef B, et al. Long-term air pollution exposure and cardio-respiratory mortality: a review. Environ Health 2013;12:43.

[4] Brunekreef B, Holgate ST. Air pollution and health. The Lancet 2002;360:1233–42.
[5] Quillen K, Bennet M, Volckens J, Stanglmaier RH. Characterization of particulate matter emissions from a four-stroke, lean-burn, natural gas engine. J Eng Gas Turb Power 2008;130:447–53.
[6] Ristovski ZD, Morawska L, Hitchinds J, Thomas S, Greenaway C, Gilbert D. Particle emissions from compressed natural gas engines. J Aerosol Sci 2000;31(4):403–13.
[7] Jayaratne ER, Meyer NK, Ristovski ZD, Morawska L. Volatile properties of particles emitted by compressed natural gas and diesel buses during steady-state and transient driving modes. Environ Sci Technol 2012;46:196–203.
[8] Hajbabaei M, Karavalakis G, Johnson KC, Lee L, Durbin TD. Impact of natural gas fuel composition on criteria, toxic, and particle emissions from transit buses equipped with lean burn and stoichiometric engines. Energy 2013;62:425–34.
[9] Hallquist ÅM, Jerksjö M, Fallgren H, Westerlund J, Sjödin Å. Particle and gaseous emissions from individual diesel and CNG buses. Atmos Chem Phys 2013;13:5337–50.
[10] Oberdörster G, Sharp Z, Atudorei V, Elder A, Gelein R, Kreyling W, et al. Translocation of inhaled ultrafine particles to the brain. Inhal Toxicol 2004;16:437–45.
[11] Jayaratne ER, Meyer NK, Ristovski ZD, Morawska L, Mioljevic B. Critical analysis of high particle number emissions from accelerating compressed natural gas buses. Environ Sci Technol 2010;44:3724–31.
[12] Bullock DS, Olfert JS. Size, volatility, and effective density of particulate emissions from a homogeneous charge compression ignition engine using compressed natural gas. J Aerosol Sci 2014;75:1–8.
[13] Yoon S, Hu S, Kado NY, Thiruvengadam A, Collins JF, Gautam M, et al. Chemical and toxicological properties of emissions from CNG transit buses equipped with three-way catalysts compared to lean-burn engines and oxidation catalyst technologies. J Aerosol Sci 1988;19:387–9.
[14] D'Anna A. Combustion-formed nanoparticles. Proc Combust Inst 2009;32:593–613.
[15] Wagner AY, Livbjerg H, Kristensen PG, Glarborg P. Particle emissions from domestic gas cookers. Combust Sci Technol 2010;182:1511–27.
[16] Murr LE, Soto KF. A TEM study of soot, carbon nanotubes, and related fullerene nanopolyhedra in common fuel-gas combustion sources. Mater Charact 2005;55:50–65.
[17] Mätzing H, Baumann W, Bockhorn H, Paur H-R, Seifert H. Detection of electrically charged soot particles in laminar premixed flames. Combust Flame 2012;159:1082–9.
[18] Murtonen T, Lehtoranta K, Korhonen S, Vesala H. Imitating emission matrix of a large natural gas engine opens new possibilities for catalyst studies in engine laboratory. In: CIMAC congress, June 6–10, 2016; 2016.
[19] Mikkanen P, Moisio M, Keskinen J, Ristimäki J, Marjamäki M. Sampling method for particle measurements of vehicle exhaust. Society of automoive engineers (SAE) technical paper 2001-01-0219.
[20] Ntziachristos L, Giechaskiel B, Pistikopoulos P, Samaras Z, Mathis U, Mohr M, et al. Performance evaluation of a novel sampling and measurement system for exhaust particle characterization. Society of automoive engineers (SAE) technical paper 2004-01-1439.
[21] Wang SC, Flagan RC. Scanning electrical mobility spectrometer. Aerosol Sci Technol 1990;13:230–40.
[22] Mirme A. Electrical aerosol spectrometry, Ph.D. thesis, University of Trtu; 1994.
[23] Burtscher H, Baltensperger U, Bukowiecki N, Cohn P, Häglin C, Mohr M, et al. Separation of volatile and non-volatile aerosol fractions by thermodesorption: instrumental development and applications. J Aerosol Sci 2001;32:427–42.
[24] Gormley PG, May FG. Diffusion from a stream flowing through a cylindrical tube. Proc Roy Irish Acad 1949;52A:163–9.
[25] Heikkilä J, Rönkkö T, Lähde T, Lemmetty M, Arffman A, Virtanen A, et al. Effect of open channel filter on particle emissions of modern diesel engine. J Air Waste Manage Assoc 2009;59:1148–54.
[26] Lähde T, Rönkkö T, Happonen M, Söderström C, Virtanen A, Solla A, et al. Effect of fuel injection pressure on a heavy-duty diesel engine nonvolatile particle emission. Environ Sci Technol 2011;45:2504–9.
[27] Scheibel HG, Porstendörfer J. Generation of monodisperse Ag- and NaCl-aerosols with particle diameters between 2 and 300 nm. J Aerosol Sci 1983;14:113–26.
[28] Arffman A, Yli-Ojanperä J, Kalliokoski J, Harra J, Pirjola L, Karjalainen P, et al. High-resolution low-pressure cascade impactor. J Aerosol Sci 2014;78:97–109.
[29] Kangasluoma J, Junninen H, Lehtipalo K, Mikkilä J, Vanhane J, Attoui M, et al. Remarks on ion generation for CPC detection efficiency studies in sub-3-nm size range. Aerosol Sci Technol 2013;47:556–63.
[30] Giechaskiel B, Chirico R, DeCarlo PF, Clairotte M, Adam T, Martini G, et al. Evaluation of the particle measurement programme (PMP) protocol to remove the vehicles' exhaust aerosol volatile phase. Sci Total Environ 2010;408:5106–16.
[31] Keskinen J, Rönkkö T. Can real-world diesel exhaust particle size distribution be reproduced in the laboratory? A critical review. J Air Waste Manage Assoc 2010;60:1245–55.
[32] DieselNet. Emission Standards [WWW]; 2015. <https://www.dieselnet.com/standards/eu/hd.php> [cited 05.06.15].
[33] Jayaratne ER, He C, Ristovski ZD, Morawska L, Johnson GR. A comparative investigation of ultrafine particle number and mass emissions from a fleet of on-road diesel and CNG buses. Environ Sci Technol 2008;42:6736–42.
[34] Sgro LA, Sementa P, Vaglieco BM, Rusciano G, D'Anna A. Investigating the origin of nuclei particles in GDI enginen exhaust. Combust Flame 2012;159:1687–92.
[35] Lähde T, Virtanen A, Happonen M, Söderström C, Kytö M, Keskinen J, et al. Heavy-duty, off-road diesel engine low-load particle number emissions and particle control. J Air Waste Manage Assoc 2014;64:1186–94.
[36] Maricq MM. On the electrical charge of motor vehicle exhaust particles. J Aerosol Sci 2006;37:858–74.
[37] Wiedensohler A, Fissan HJ. Bipolar charge distributions of aerosol particles in high-purity argon and nitrogen. Aerosol Sci Technol 1991;14:358–64.
[38] Fuchs NA. On the stationary charge distribution on aerosol particles in a bipolar ionic atmosphere. Pure Appl Geophys 1963;56:185–93.
[39] Hoppel WA, Frick GM. Ion-aerosol attachment coefficients and the steady-state charge distribution on aerosols in a bipolar environment. Aerosol Sci Technol 1986;5:1–21.
[40] Wiedensohler A. An approximation of the bipolar charge distribution for particles in the submicron size range. J Aerosol Sci 1988;19:387–9.
[41] Kittelson DB. Engines and nanoparticles: a review. J Aerosol Sci 1998;29:575–88.
[42] Shi JP, Harrison RM. Investigation of ultrafine particle formation during diesel exhaust dilution. Environ Sci Technol 1999;33:3730–6.
[43] Sakurai H, Tobias H, Park K, Zarling D, Docherty KS, Kittelson DB, et al. On-line measurements of diesel nanoparticle composition and volatility. Atmos Environ 2003;37:1199–210.
[44] Sgro LA, Borghese A, Speranza L, Barone AC, Minutolo P, Bruno A, et al. Measurements of nanoparticles of organic carbon and soot in flames and vehicle exhausts. Environ Sci Technol 2008;42:859–63.
[45] De Filippo A, Maricq MM. Diesel nucleation mode particles: semivolatile or solid? Environ Sci Technol 2008;42:7957–62.
[46] Lähde T, Rönkkö T, Virtanen A, Schuck TJ, Pirjola L, Hämeri K, et al. Heavy duty diesel engine exhaust aerosol particle and ion measurements. Environ Sci Technol 2009;43:163–8.
[47] Schmid O, Eimer B, Hagen DE, Whitefield PD. Investigation of volatility method for measuring aqueous sulfuric acid on mixed aerosols. Aerosol Sci Technol 2002;36:877–89.
[48] Rönkkö T, Virtanen A, Kannosto J, Keskinen J, Lappi M, Pirjola L. Nucleation mode particles with a nonvolatile core in the exhaust of a heavy duty diesel vehicle. Environ Sci Technol 2007;41:6384–9.
[49] Jung H, Kittelson DB. Measurement of electrical charge on diesel particles. Aerosol Sci Technol 2005;39:1129–35.
[50] Buchta C, D'Alessio A, D'Anna A, Gambi G, Minutolo P, Russo S. The optical characterization of high molecular mass carbonaceous structures produced in premixed laminar flames across the soot threshold limit. Planet Space Sci 1995;43:1227–32.
[51] Commodo M, Sgro LA, Minutolo P, D'Anna A. Characterization of combustion-generated carbonaceous nanoparticles by size-dependent ultraviolet laser photoionization. J Phys Chem A 2013;117:3980–9.

PAPER 2

Physical Characteristics of Particle Emissions from a Medium Speed Ship Engine Fueled with Natural Gas and Low-Sulfur Liquid Fuels

Alanen, J., Isotalo, M., Kuittinen, N., Simonen, P., Martikainen, S., Kuuluvainen, H., Honkanen, M., Lehtoranta, K., Nyyssönen, S., Vesala, H., Timonen, H., Aurela, M., Keskinen, J. and Rönkkö, T.

Environmental Science and Technology 54.(2020), 5376–5384
DOI: 10.1021/acs.est.9b06460

Environmental Science & Technology

pubs.acs.org/est

Article

Physical Characteristics of Particle Emissions from a Medium Speed Ship Engine Fueled with Natural Gas and Low-Sulfur Liquid Fuels

Jenni Alanen, Mia Isotalo, Niina Kuittinen, Pauli Simonen, Sampsa Martikainen, Heino Kuuluvainen, Mari Honkanen, Kati Lehtoranta, Sami Nyyssönen, Hannu Vesala, Hilkka Timonen, Minna Aurela, Jorma Keskinen, and Topi Rönkkö*

Cite This: *Environ. Sci. Technol.* 2020, 54, 5376−5384

Read Online

ACCESS | Metrics & More | Article Recommendations | Supporting Information

ABSTRACT: Particle emissions from marine traffic affect significantly air quality in coastal areas and the climate. The particle emissions were studied from a 1.4 MW marine engine operating on low-sulfur fuels natural gas (NG; dual-fuel with diesel pilot), marine gas oil (MGO) and marine diesel oil (MDO). The emitted particles were characterized with respect to particle number (PN) emission factors, PN size distribution down to nanometer scale (1.2−414 nm), volatility, electric charge, morphology, and elemental composition. The size distribution of fresh exhaust particles was bimodal for all the fuels, the nucleation mode highly dominating the soot mode. Total PN emission factors were 2.7×10^{15}−7.1×10^{15} #/kWh, the emission being the lowest with NG and the highest with MDO. Liquid fuel combustion generated 4−12 times higher soot mode particle emissions than the NG combustion, and the harbor-area-typical lower engine load (40%) caused higher total PN emissions than the higher load (85%). Nonvolatile particles consisted of nanosized fuel, and spherical lubricating oil core mode particles contained, e.g., calcium as well as agglomerated soot mode particles. Our results indicate the PN emissions from marine engines may remain relatively high regardless of fuel sulfur limits, mostly due to the nanosized particle emissions.

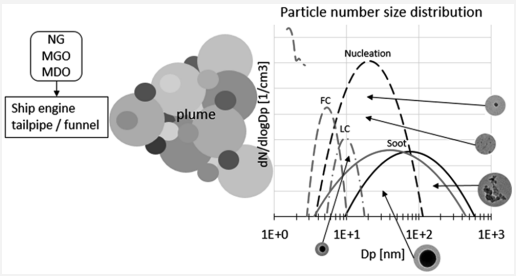

■ INTRODUCTION

The particulate emissions from marine vessels have significant impacts on air quality and climate change, e.g, through the cloud condensation nuclei they generate[1] and their soot emissions.[2,3] Particulate emissions cause adverse health effects and premature mortality[4,5] connected to respiratory and heart diseases. Moreover, ultrafine particles (<100 nm) can enter human blood circulation and even the brain,[6,7] and they are shown to have a link to, e.g., Alzheimer's disease.[8] Although the evidence of the connection between adverse health effects and elevated particle concentrations is the heaviest for $PM_{2.5}$, ultrafine particles, typically high in number concentration, and soot particles are also shown to be hazardous.[9,10] Also ship exhaust particulates cause adverse health effects on humans.[11,12] Particle emissions from shipping contribute to $PM_{2.5}$ up to 30% in coastal areas depending on the activity of the shipping,[13] albeit 60−70% of the total shipping $PM_{2.5}$ comes from the secondary particulate matter formation from shipping exhaust.[14−16]

Historically, a typical number size distribution of fresh exhaust particles has been considered to consist of a nucleation mode with smaller (mean diameter typically <30 nm), volatile particles, and a soot mode with larger (mean diameter typically 30−70 nm), solid soot agglomerates. By fresh exhaust, we refer to the exhaust that has just been emitted to the atmosphere but has already met the ambient conditions with respect to temperature and humidity. Thus, in addition to primary exhaust particles such as soot, the exhaust compounds that nucleate or condense to the particulate phase in the cooling dilution of exhaust exist in the particulate phase in fresh exhaust. This concept, however, has been challenged by several studies showing that the nucleation mode can consist of both semivolatile particles and particles with a nonvolatile core.[17,18] For example, Ushakov et al.[19] concluded that the nucleation mode of marine fuel exhaust consists mainly of nonvolatile particles, and Hallquist et al.[20] found that on some operation conditions half of the particles by number had a nonvolatile core. The existence of these core particles in exhaust depends, e.g., on exhaust after-treatment[21,22] and lubricating oil

Received: October 28, 2019
Revised: April 3, 2020
Accepted: April 6, 2020
Published: April 6, 2020

https://dx.doi.org/10.1021/acs.est.9b06460
Environ. Sci. Technol. 2020, 54, 5376−5384

composition.[23] Kuuluvainen et al.[17] found that there are two kinds of core particles, their difference being the source of the particles, namely, fuel and lubricating oil. The fuel-originated core mode particles had a diameter below 10 nm, and the spherical lubricating-oil-originated core mode particles were mainly observed in particle sizes below 50 nm. Other studies support the result.[24] For instance, the studies of Sgro et al.[25] and Seong et al.[26] indicate that the core particles consist of amorphous carbonaceous compounds, possibly from fuel combustion, and Corbin et al.,[27] Fushimi et al.,[28] and Lähde et al.[23] link the core particles to a lubricating oil origin.

Several research groups have studied the volatility of ship exhaust particles. According to Moldanová et al.,[29] Petzold et al.,[1] Jonsson et al.[30] and Pirjola et al.,[31] 33−66% of ship exhaust particles are volatile. Anderson et al.[32] gave a very large range of volatile fraction of ∼1−100%, depending on engine load (0−35%) and fuel. Ntziachristos et al.[33] reported that particles emitted from a marine engine only shrank to sub-30 nm in a thermodenuder but did not disappear. This observation indicates that ship exhaust also contains nonvolatile core particles. The nonvolatile particles are interpreted to represent the primary particles present in the exhaust line or funnel already before the atmospheric dilution and cooling processes.

Shipping emissions and fuel characteristics are being increasingly regulated. The fuel sulfur content regulations of the International Maritime Organization will probably force more marine vessels to abandon heavy fuel oil (HFO) and lead to replacement of HFO by lighter fuels.[34] From 2020, the allowed sulfur content is reduced to 0.5%. This transition will increase the interest to study the particle emissions from the combustion of low-sulfur liquid and gaseous fuels. For instance, Lehtoranta et al.[35] observed that both the nonvolatile >23 nm particle number (PN) and the particle mass (PM) emissions can be reduced by the transition to low-sulfur liquid fuels. These interests are linked with other effects of fuel changes; e.g., NG engines emit lower CO_2 emissions due to the smaller carbon content of NG and lower soot emissions than liquid fuel combustion. Unfortunately, the methane and total hydrocarbon emissions from NG engines and therefore their CO_2-equivalent greenhouse gas emissions can be high.[36,37] Soot emissions are especially relevant in the marine engines because marine vessels are not equipped with particle filters. Soot particles are carbonaceous agglomerates that form during combustion processes and contribute to global warming, being the second largest climate change agent after CO_2.[3] They are especially harmful for snow- and ice-covered surfaces through changing the albedo of the layers from reflecting to absorbing.

Characterization of emissions is needed to understand the effects of particle emissions on climate and human health and to develop sustainable solutions for marine traffic and new emission regulations. Although several papers concern the emissions from HFO fueled ships,[32,33,38] relatively few publications focus on emissions from low-sulfur fuels, especially gaseous fuels such as NG.[27,35,39] In this paper, we compare the PN emissions and their physical properties from a large-bore ship engine fueled by three low-sulfur fuels. We present the particle size distributions down to 1.2 nm, emission factors (EF) of the particles, and transmission electron microscope (TEM) images of the particles. Furthermore, the studied physical characteristics of the particles, such as volatility and electric charge, provide understanding of the particles' lifetime in the atmosphere, as well as of their origin and formation process.

■ MATERIALS AND METHODS

The particulate emission measurements were conducted on a Wärtsilä Vasa 4R32 engine that was retrofitted to enable dual-fuel operation (see Lehtoranta et al.[35] for description of the retrofitting). The engine was a 1.4 MW 4-cylinder medium-speed dual-fuel marine engine with no exhaust after-treatment systems. These kinds of engines are typically auxiliary engines in open-sea marine vessels. The engine operated at two steady-state operation modes at 40% and 85% load at 750 rpm, representing maneuvering and open-sea cruising of a marine vessel, respectively. The engine was operated in dual-fuel mode with NG and pilot fuel or using marine gas oil (MGO) or marine diesel oil (MDO). NG was high methane content (96.4%) compressed natural gas (CNG), and MGO was used as the pilot to ignite the natural gas−air mixture in engine cylinders. With respect to emissions, the CNG is seen to represent the liquefied natural gas (LNG) used in several ship applications. To study the impact of the pilot fuel on particulate emissions in dual-fuel operation, the pilot injection quantity (PIQ) was adjusted to be either 3.8% or 5.9% ("lower PIQ" or "higher PIQ") of the total fuel consumption in terms of mass for 40% engine load and 1.2% or 2.2% for 85% load. The sulfur content of the MGO and the MDO was low, smaller than 0.001% and 0.1%, respectively.[35] The lubricating oil used was Shell Argina XL 40.

Particle size distribution in the size range 1.2−414 nm was measured by a Nano-SMPS, a Long-SMPS (Scanning Mobility Particle Sizer; TSI Inc.; Models 3776 and 3775) and a PSM (Particle Size Magnifier; Airmodus Oy; Model A11) that was coupled with Airmodus CPC (A20). The total particle concentration was studied by an ultrafine CPC (Condensation Particle Sizer; TSI Inc.; Model 3025) and the PSM. The particle number size distribution data measured by the Nano-SMPS was diffusion corrected, and a detection efficiency correction factor of 1.25 was applied in the PSM particle concentration data. The PSM measured PN concentration in the scanning mode where the saturation flow rate of the instrument was scanned in the range of 0.1−1.2 lpm, providing the particle size distribution in the range of 1.2−3 nm. Detected particle concentration depends on the saturation flow rate because the larger the saturation flow rate is, the smaller the particles are magnified to be then detected by the CPC downstream the PSM. The detailed PSM data inversion is described in the Supporting Information.

The charged fraction of particles was measured using an electrostatic precipitator (ESP) upstream the Long-SMPS. The difference of the size distributions with and without the ESP gave the size distribution and concentration of naturally charged particles in the exhaust. This subtraction method only works for relatively high charged particle fractions. The Boltzmann temperature, i.e., the formation temperature, was calculated from the charged fraction for each fuel case at 85% load. The formation temperature was calculated both with the assumption that the particles received their charge before the dilution process, i.e., at nonvolatile particle mean size measured using the CS, and with the assumption that the particles first grew by condensation and then received the charge.

Ambient dilution of exhaust was simulated by a partial-flow exhaust sampling and dilution system that consists of a porous tube diluter (PTD)[40] that introduces the dilution air gradually

https://dx.doi.org/10.1021/acs.est.9b06460
Environ. Sci. Technol. 2020, 54, 5376−5384

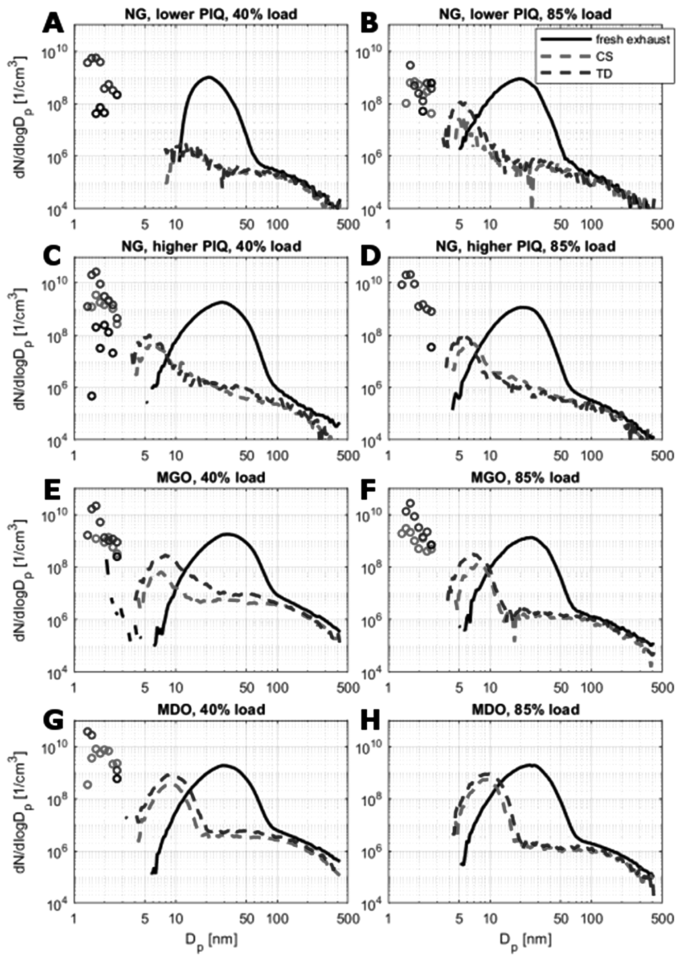

Figure 1. Particle number size distributions of fresh exhaust particles and nonvolatile particles (treated by CS or TD) measured by SMPS (lines) and PSM (circles). Data is missing in the cases: PSM+CS in NG, lower pilot injection quantity (PIQ), 40% (A), PSM+CS in NG, higher PIQ, 85% (D), and all PSM data in MDO, 85% (H). Fuel-originated core (FC) mode particles had peak size < 10 nm, lubricating-oil-originated core (LC) mode particles 10−30 nm, nucleation mode particles ∼ 20−30, and soot mode particles > 60 nm. The concentrations are dilution ratio corrected, i.e., calculated back to the undiluted raw exhaust.

to the exhaust sample, a residence time chamber, and a following ejector diluter (Dekati Oy). Previous laboratory experiments for ship engine exhaust with the PTD dilution system with a primary dilution ratio of 12 have shown that the system produces a similar particle size distribution to the ones in real world ship plumes.[33] The volatility of the exhaust particles was measured using a catalytic stripper (CS)[41,42] at 350 °C and a thermodenuder (TD)[21] at a slowly decreasing temperature from ∼265 °C downward. The SMPS and PSM size distributions were corrected for the TD and CS losses. Particle morphology was examined with TEM (JEM-2010, Jeol) and their elemental composition with energy dispersive spectrometry (EDS; Noran Vantage with Si(Li) detector, Thermo Scientific) by collecting a diluted exhaust sample on copper TEM grids with a holey-carbon film (Agar Scientic) both with and without CS treatment.

EFs were calculated similarly to Pirjola et al.,[31] by utilizing the measured CO_2 concentration, engine power, and total fuel consumption and the CO_2 emission factor. The total number of concentrations was measured by the CPC (MDO, 85%; because the PSM data was missing) or the PSM (all the other cases). Due to the complications in combining PSM and SMPS particle size distributions, SMPS data was utilized only when the fractions of particles in each particle size mode were calculated.

■ RESULTS

Particle Size Distribution of Exhaust Particles. The exhaust particle size distributions were measured after the partial flow sampling and dilution both with and without the TD or CS. When measured with the TD or CS, the size distributions and concentrations represented nonvolatile

https://dx.doi.org/10.1021/acs.est.9b06460
Environ. Sci. Technol. 2020, 54, 5376−5384

particles, i.e., primary exhaust particles. Instead, when the particle size distributions and concentrations were measured without thermal treatment, the results represent fresh exhaust, where a fraction of the semivolatile compounds exists in the particulate phase.

PN size distributions of the fresh exhaust, measured by the combination of the Nano-SMPS and the Long-SMPS, showed two particle modes: a nucleation mode (particle diameter < 100 nm) and a soot mode (particle diameter > ∼50 nm) (Figure 1). The shapes of the distributions were remarkably similar to all the measured fuels, the nucleation mode particles highly dominating the PN. Majority of the particles were found in the ultrafine particle size range (<100 nm), as previously seen, e.g., for MGO and MDO fueled ships.[29,32] The fuel change from the liquid fuels to NG predominantly decreased the number concentration of the soot mode particles, whereas the differences between the nucleation modes between fuels were smaller. The difference between the soot emissions from the two liquid fuels was small, as well as the difference between the soot emissions of the two different pilot quantities of NG combustion (see also Figure S1).

The particle size distributions of the nonvolatile particles revealed that not all the nucleation mode particles of fresh exhaust were totally volatile; CS treatment maintained a significant number of core particles with a diameter below 30 nm. TD studies confirmed the same observation: nonvolatile particle modes with a diameter below 30 nm were present in the exhaust with a similar size distribution shape. Possibly due to inaccuracies in loss corrections of sub-10 nm particles, the concentrations measured with the TD were higher than with the CS.[21,42] In addition to the soot mode, we found the two core modes previously introduced by Kuuluvainen et al.[17] (see also Figures S1 and S2). One of the core modes had a mean diameter of 10−30 nm, and the other could be found in smaller sizes of 6−10 nm (or smaller). From here on, we name these modes with the concepts adapted from previous study,[17] i.e., lubricating-oil-originated core (LC) mode, and fuel-originated core (FC) mode, respectively.

An important observation is that the smaller core mode was missing from the number size distribution measured by the SMPS in the case of NG, lower PIQ, at the lower engine load of 40%. This observation of such fuel dependency suggests the core mode could originate from liquid fuel. This interpretation is supported by previous studies.[17] The mode, however, was not nonexisting; the size distributions measured by the PSM reveal that the particle diameter of these fuel-originated core particles in that case was below the Nano-SMPS size range (Figure 1A). The very small size of the FC mode particles seems to affect also the fresh exhaust nucleation mode; the nucleation mode mean particle size in the NG, lower PIQ, 40% case, was located in smaller particle sizes than with all other fuels, whereas in all other cases the nucleation modes were relatively alike (Figure S1).

For simplicity, the particle mode fitting (Figure S2) in the size distributions was done using the particle size distributions measured by the SMPS, without including the PSM size distributions (Table 1). Roughly, the fitted modes show that particle mean size increased from gaseous to liquid fuels and from MGO to MDO. LC mode particles were larger when the engine run with the liquid fuels was compared to that of NG. However, their size did not depend on engine load. MGO combustion generated the largest nucleation and soot particles and MDO the largest FC and LC particles. The engine load increase decreased the diameter of the nucleation mode particles but caused no other significant changes in particle sizes. This is probably because the lower engine load emitted more unburned hydrocarbons[35] that condensed in the dilution process and increased the nucleation particle size.

Table 1. Geometric Mean Diameters (GMDs) of Particle Modes and the Volatile Fraction of the Particle Number in Each Engine Load and Fuel[a]

GMD [nm]	NG, lower PIQ	NG, higher PIQ	MGO	MDO
Engine Load 40%				
fuel-originated core	NaN	6	7	9
lubricating-oil-originated core	13	14	21	28
nucleation	21	28	33	30
soot	60	75	80	90
Engine Load 85%				
fuel-originated core	5	6	8	9
lubricating-oil-originated core	10	13	21	28
nucleation	19	21	23	24
soot	57	75	80	85

[a]The modes were fitted in size distributions measured with SMPS. According to the PSM data, the actual peak diameter of the fuel-originated core particle mode was 1−2 nm, and it was present with all the fuels.

Particle size distributions were measured by the PSM in all the cases except for in the MDO, 85%, case and with CS in the NG, lower PIQ, 40%, and NG, higher PIQ, 85%, cases (Figure 1). There were especially nonvolatile particles in the exhaust also below the SMPS size range. There was an ∼1 nm gap between the PSM and SMPS size ranges, and the detection efficiency of SMPS and PSM might differ at the smallest particle sizes, which complicates the analysis.[43,44] It is not self-evident if the FC mode detected by SMPS is the same as the one detected by PSM or if there is one more particle mode existing in the PSM size range. However, because of the observations made in previous studies,[35,45] we assume the same core mode was detected both with PSM and with SMPS. According to the PSM data, the actual peak diameter of the fuel-originated core particle mode was ∼1−2 nm, and it was present with all the fuels.

In the case of fresh exhaust, the PSM data inversion was sensitive to, e.g., the chosen particle diameter limits, because there was no clear dependence between the post-PSM CPC concentration and the PSM saturation flow—the lonely black dots in Figure 1D−G could have been removed by a different selection of the particle diameter limits. In the cases of nonvolatile particles, the PSM size distributions are more reliable because there the inversion was not sensitive to the data handling methods tested.

Emission Factors and Particle Number Concentrations. Work-specific PN emission factors for different fuels (NG, lower PIQ, NG, higher PIQ, MGO, MDO) are given in Figure 2, and the fuel-consumption-specific EFs are found in Figure S5. The EFs for total PN were in the range of 2.7×10^{15}−7.1×10^{15} #/kWh. The nucleation and soot particle EFs were calculated using fitted modes in fresh exhaust measurements, and they were in the range of 2.7×10^{15}−7.0×10^{15} #/kWh and 1.9×10^{12}−4.3×10^{13} #/kWh, respectively. The FC and LC particle EFs were calculated using mode fitting for nonvolatile (CS treatment) particle size distribution, and they

https://dx.doi.org/10.1021/acs.est.9b06460
Environ. Sci. Technol. 2020, 54, 5376−5384

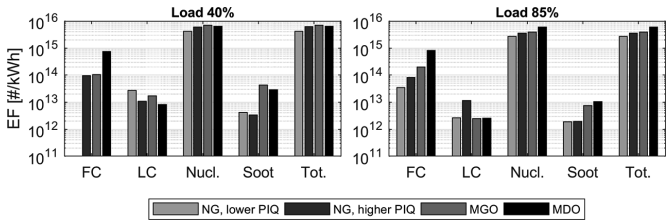

Figure 2. Emission factors of particles in the SMPS size range (2.5−414 nm); the total particle number concentration was measured by PSM, and fractions of the particles in each particle size mode were measured by SMPS. Emission factors from left to right: Nonvolatile fuel-originated core particle number, nonvolatile lubricating-oil-originated core particle number, fresh exhaust nucleation particle number, fresh exhaust soot particle number, and fresh exhaust total particle number. Note that the *y*-axis is logarithmic.

were in the range of 9.5×10^{11}−1.4×10^{13} #/kWh and 1.1×10^{12}−1.7×10^{13} #/kWh, respectively. The EFs of total particle emissions for the low-sulfur liquid fuels (MGO and MDO) in our study were 2−3 times higher than the EFs found by Moldanová et al.[29] and 4−6 times higher than those found by Ntziachristos et al.[33] The difference could be explained by the detection efficiency of the instrument used; in our study, the total particle concentration was measured with a PSM with cutoff size as low as 1.2 nm. The number emissions of soot particles matched those measured by Moldanová et al.[29]

Similarly to Ntziachristos et al.,[33] we found that all fuels that load 40% produced higher total PN emission than those that load 85%. In addition, LC, nucleation, and soot particle number emissions were all higher at the lower load. Because low-load engine operation is typical in harbor areas and therefore more relevant to people's health in coastal areas, the elevated PN concentrations at the lower engine load are of greater concern, and special attention should be paid to the mitigation of those emissions.

The soot particle EFs of the liquid fuels (7.5×10^{12}−4.3×10^{13} #/kWh) were substantially—4−12 times—larger than those of NG (dual-fuel; 1.9×10^{12}−4.2×10^{12} #/kWh) at the same engine load, which encourages the use of NG engines in marine vessels. In the atmosphere, soot particles absorb solar radiation and cause climate warming. Therefore, from the viewpoint of soot particle emissions and global warming, the transition to NG fueled ships can be welcomed, especially close to snow- and ice-covered regions.

The volatile fraction of the particle number was calculated to be 86−99%, but because the total PN concentrations could not be corrected with the size-dependent penetration efficiency of TD or CS, the actual volatility fraction could be smaller. The fraction of nucleation mode particles was over 99% of the total emitted fresh exhaust PN with all the used fuels. Although the importance of soot particles is undeniable, the nucleation mode particles should also be paid attention to because of their huge number concentrations. The majority (>70%) of particle mass in the SMPS size range, too, was emitted in the form of the nucleation mode particles, especially in case of NG (>90%) (see Figure S6).

Fuel heavily influenced the FC mode PN and was especially large when MDO was used as the fuel. This indicates the FC mode particles consisted of fuel-originated compounds. The FC mode particles formed the majority of the number of the nonvolatile particles (over 70%). In the mass-based consideration, soot mode particles formed most of the nonvolatile PM (93−99.6%).

When compared to the fuel-originated core mode PN, the lubricating-oil-originated core mode PN was much less dependent on fuel but more influenced by engine operation, indicating those particles could consist of lubricating oil. The observation that the oil-derived LC mode PN was larger at the lower load is in contrast with the previous studies[17,46] stating that the concentration of oil markers in PM samples increases with higher engine loads. However, the number emission of oil droplets in the nanoparticle size range does not necessarily follow the oil consumption or the total mass emission of oil.

Lehtoranta et al.[35] measured the particle mass emissions from the engine with the same fuels by filter weighing and sampling according to the ISO standard 8178-1:2006. They found the liquid fuel combustion produced higher PM emission than the NG combustion. We calculated the PM emission from the engine using SMPS size distribution data and by assuming spherical particles and unit density. The PMs measured by the two different methods were on a similar level. The PM emission was 2−13 times higher with the liquid fuels than with NG. Also, our SMPS measurement supported their observation that the lower engine load produced larger PM emissions than the higher load.

Morphology and Elemental Composition of the Particles. Figure 3 shows the TEM images of the solid particles (CS treatment at ∼350 °C) collected from all the fuels' exhausts at an engine load of 40%. The particles observed on the TEM grids can be divided into two groups—soot agglomerates (indicated by EDS; larger magnification image in Figure S9) and spherical particles with diameter from 10 to 300 nm. The smallest spherical particles are in the same range of the LC mode while the largest spherical particles are more clearly in sizes of the soot agglomerates, thus possibly not seen in particle number size distributions. The smallest (diameter < 10 nm) core particles can also be seen on the TEM grids (Figure S9), but that observation is not entirely without doubt due to the very small size of the probably carbonaceous particles on a carbon film. We remind the reader that the collection efficiency on the TEM grids depends on the aerodynamic properties of the particles such as their size[17] and that the different particle types can be internally mixed (e.g., the largest spherical particles in the soot mode). Therefore, the particle size distribution in the TEM images is not identical to the particle size distributions measured by SMPS. However, the three-modal particle size distribution seen by SMPS and our interpretation of each mode is supported by the TEM images.

Fuel had an effect on the particle population: the portion of soot agglomerates increases from A and B to C and D in Figure

https://dx.doi.org/10.1021/acs.est.9b06460
Environ. Sci. Technol. 2020, 54, 5376−5384

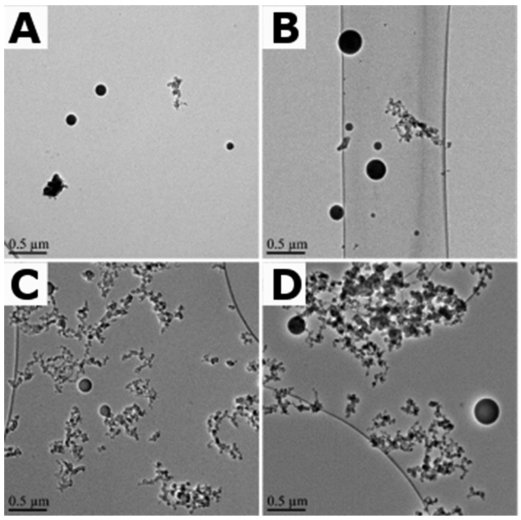

Figure 3. TEM images of particles when using (A) NG, lower PIQ, (B) NG, higher PIQ, (C) MGO, and (D) MDO. With respect to the total particle number, the fraction of soot agglomerates increases from A to D. The engine load was 40%, and the aerosol sample was treated with CS before particle sampling on TEM grids. The long string-like structures on the TEM images are edges of the holey TEM grid holes.

3. Spherical particles dominated in the NG exhaust; in contrast, MGO and MDO exhaust contained more soot agglomerates than spherical particles. The EDS analysis showed that the spherical particles always contained abundantly elemental calcium, a lubricating oil marker, and a small amount of S, P, Si, C, and O. Therefore, it is concluded that they were droplets from lubricating oil. No calcium was observed in the soot agglomerates. Fuel affected the elemental composition of particles: with MDO, the fuel with the largest sulfur content, sulfur, was clearly present in the spherical particles. According to the EDS analysis, soot consisted mainly of carbon and a small amount of sulfur. Lieke et al.[47] interpreted ship engine emitted spherical particles in the 30−50 nm size range to compose crystalline salts because they sometimes observed "hexagonal habitus", because the particles restructured under the electron beam during EDS analysis and they detected only minor amounts of Ca in those particles. Our observations, however, point to lubricant droplets due to the spherical structure and high calcium content of the particles. Moldanová et al.[29] also detected lubricating oil derived spherical particles containing calcium, zinc, and phosphorus traces and fuel (MGO) originated soot particles mainly composed of carbon in their electron microscopy study on ship exhaust.

Figure S8 shows the images of carbonized TEM samples taken of fresh exhaust (without the CS). The samples were carbonized to prevent the evaporation of the volatile particles during the TEM studies. The particle population is similar in the two cases (fresh vs CS-treated exhaust), but there are more very small stain-like particles among the fresh exhaust particles (Figure S8) compared to the solid particles (Figure 3). We identify them as nucleation particles due to their appearance in the fresh exhaust samples. Because of the low sulfur content of the fuels used, the particles did not have a thick sulfur coating on them, often met in TEM images taken of HFO exhaust particles.[33] Lehtoranta et al.[35] reported that the PM emitted by the studied engine consisted mainly of organic carbon; in liquid fuel operation, also elemental carbon (i.e., soot); and in MDO operation, 4% of sulfates.

Formation Temperature of the Core Mode Particles. The measurement of the particle charge states was done by subtracting the neutral particle size distributions, measured by the Long-SMPS downstream the ESP, from the size distributions measured without the ESP, thus gaining the particle size distribution of naturally charged particles. More nucleation mode particles (in absolute terms) were electrically charged than soot particles, although most soot particles carried a charge.

Figure 4 shows the size distributions of the naturally charged particles in the exhaust of all studied fuels at the engine load of

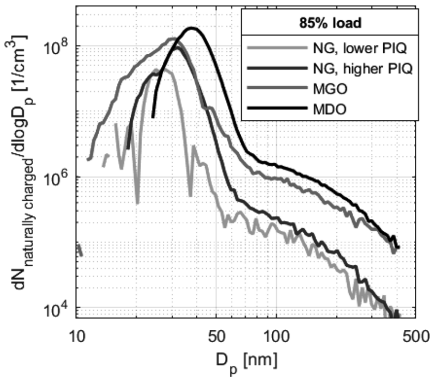

Figure 4. Size distribution of the naturally charged particles at 85% load for all the measured fuels.

85%. The charged fraction at the 40% load was too low for the subtraction method (see Figure S7). The higher combustion temperature (see in-cylinder pressures in Figure S4) may have been a reason for the larger fraction of the charged nucleation mode particles at the higher engine load. The formation temperature (Boltzmann temperature) was calculated from the electric charge measurement data. To eliminate the influence of the charge carried by soot particles, the fit made in soot mode was subtracted from the size distribution of the naturally charged particles. This slightly overestimated the charging probability of soot particles because the actual charging efficiency of the soot particles lies around 0.9.

The Boltzmann temperature analysis reveals the charging temperatures of the nucleation mode particles were 774, 822, 903, and 1115 °C for fuels NG, lower PIQ, NG, higher PIQ, MGO, and MDO, respectively. The size distribution of the MDO, 85% load, case was the clearest (i.e., the highest number concentration, the most regular shape of the size distribution) and therefore the most reliable because the sizes of the nucleation mode particles fit the best on the long SMPS size range. These Boltzmann temperatures were obtained with an assumption that the particles were charged before dilution when their mean diameter was the diameter of the core particles (without hydrocarbon or sulfate condensation on the particles). If an assumption that particles were charged when already grown was used (nucleation mode GMDs), the

https://dx.doi.org/10.1021/acs.est.9b06460
Environ. Sci. Technol. 2020, 54, 5376−5384

Boltzmann temperatures would be −20, 25, 43, and 154 °C. The weakness of the latter assumption is, however, the ion origin.[22] The charge measurements conducted do not prove that the particles were formed and charged in high temperatures. However, together with the TEM studies and volatility studies, they give an indication of the formation temperature of the particles. Maricq[48] has studied the charge of <20 nm particles using Boltzmann distribution, and Sgro et al.[49] found that the charge fractions of flame-generated sub-10 nm particles agree with those calculated from the Boltzmann charge distribution at maximum flame temperature. Furthermore, the facts that nucleaton mode particles carried electric charge and the higher-combustion-temperature load produced more charged particles than the 40% load indicate that a significant fraction of the particles formed in the vicinity of the engine cylinders and not in the tailpipe or the sample dilution system.[23,25,50]

■ DISCUSSION

The particle size distributions and TEM images showed that the particulate emission from ship exhaust consisted of four particle types: first, soot agglomerates with a mean diameter of 60−100 nm, second, nonvolatile fuel-originated core particles with a mean diameter below 10 nm, third, nonvolatile spherical lubricating oil originated particles with a mean diameter of 10−30 nm, and finally, stain-like nucleation particles in the exhaust that together with the grown core particles had a mean diameter of 20−30 nm. It was concluded that the smallest core particles originated from fuel because their size and number were fuel dependent and they were hard to detect in the TEM samples, which indicates they were carbonaceous. With the PSM measurement, the peak diameter of the FC particles was measured to be as low as 1−2 nm. The larger spherical particles originated from lubricating oil because they consisted of, e.g., calcium, a lubricant oil marker, and their number was engine load dependent and not fuel dependent. TEM images revealed the LC particles could have a diameter of up to at least 300 nm. The spherical particles dominated the TEM images in NG combustion and soot particles dominated in liquid fuel combustion. The nucleation mode particle emission was very high, especially at the low-load operation representative of maneuvering in coastal areas. Although the majority of the particles emitted were volatile, the core mode particles cannot be neglected. Their number emission was higher than that of soot particles, and the importance of soot emissions is undeniable. The effect of fuel type on soot emissions was significant. NG emitted the lowest soot emissions, which supports NG as an attractive fuel option for marine vessels. Particles existing in the funnel, including both soot and core particles, could be efficiently reduced by exhaust filtration.

A question arises why NG combustion formed soot. The soot emissions of NG + pilot combustion were 9−30% of those of MGO combustion, although the pilot fuel flows were only 1−6% of the MGO fuel flows in MGO only combustion. If soot mode particles formed from pilot fuel, combustion of MGO deteriorated when used as the pilot compared to the MGO only combustion. This is supported by the observation that an increased pilot amount reduced rather than increased soot emissions. If the lubricating oil was the main source of NG particles, it would mean that a significant fraction of MGO soot mode particles, too, originated from lubricating oil. This is also possible—Eichler et al.[51] specified that a dominant fraction of ship exhaust particles originate from lubricating oils, and Carbone et al.[52] reported that, in a locomotive diesel engine, diesel fuel and lubricating oil produced comparable PM emissions.

In addition to the primary particulate mass emission, also secondary aerosol formation from the ship exhaust should be considered when discussing the effects of particle emissions. Further studies covering this area are needed because of the high fraction of secondary particulate matter in the total aerosol PM.[14,53] From the secondary aerosol formation point of view, the transition to lower-sulfur fuels is interesting because less sulfur in the fuel may lead to lower secondary aerosol formation potential.[54] Furthermore, atmospheric processes such as the secondary aerosol formation and mixing with other ambient aerosols potentially change the relative existence of different exhaust particle types and size distribution and composition of particles, thus affecting, e.g., the health and climatic effects of the emissions.

■ ASSOCIATED CONTENT

Supporting Information

The Supporting Information is available free of charge at https://pubs.acs.org/doi/10.1021/acs.est.9b06460.

PN size distributions to ease the comparison between fuels; mode fitting examples on number size distributions; exhaust temperature and engine cylinder peak pressure; particle number and mass EFs in additional units; the effect of the ESP on particle number size distributions; TEM images of fresh exhaust samples and soot; and more detailed description of PSM inversion (PDF)

■ AUTHOR INFORMATION

Corresponding Author

Topi Rönkkö − *Aerosol Physics Laboratory, Physics Unit, Faculty of Engineering and Natural Sciences, Tampere University, FI-33014 Tampere, Finland;* orcid.org/0000-0002-1555-3367; Email: topi.ronkko@tuni.fi

Authors

Jenni Alanen − *Aerosol Physics Laboratory, Physics Unit, Faculty of Engineering and Natural Sciences, Tampere University, FI-33014 Tampere, Finland;* orcid.org/0000-0002-5316-7133

Mia Isotalo − *Aerosol Physics Laboratory, Physics Unit, Faculty of Engineering and Natural Sciences, Tampere University, FI-33014 Tampere, Finland*

Niina Kuittinen − *Aerosol Physics Laboratory, Physics Unit, Faculty of Engineering and Natural Sciences, Tampere University, FI-33014 Tampere, Finland*

Pauli Simonen − *Aerosol Physics Laboratory, Physics Unit, Faculty of Engineering and Natural Sciences, Tampere University, FI-33014 Tampere, Finland;* orcid.org/0000-0002-4267-6098

Sampsa Martikainen − *Aerosol Physics Laboratory, Physics Unit, Faculty of Engineering and Natural Sciences, Tampere University, FI-33014 Tampere, Finland*

Heino Kuuluvainen − *Aerosol Physics Laboratory, Physics Unit, Faculty of Engineering and Natural Sciences, Tampere University, FI-33014 Tampere, Finland*

Mari Honkanen − *Tampere Microscopy Center, Tampere University, FI-33014 Tampere, Finland*

Kati Lehtoranta − *VTT Technical Research Centre of Finland, FI-02044 Espoo, Finland;* orcid.org/0000-0001-9822-2565
Sami Nyyssönen − *VTT Technical Research Centre of Finland, FI-02044 Espoo, Finland*
Hannu Vesala − *VTT Technical Research Centre of Finland, FI-02044 Espoo, Finland*
Hilkka Timonen − *Atmospheric Composition Research, Finnish Meteorological Institute, FI-00101 Helsinki, Finland;* orcid.org/0000-0002-7987-7985
Minna Aurela − *Atmospheric Composition Research, Finnish Meteorological Institute, FI-00101 Helsinki, Finland;* orcid.org/0000-0001-7561-2974
Jorma Keskinen − *Aerosol Physics Laboratory, Physics Unit, Faculty of Engineering and Natural Sciences, Tampere University, FI-33014 Tampere, Finland;* orcid.org/0000-0002-2807-8593

Complete contact information is available at: https://pubs.acs.org/10.1021/acs.est.9b06460

Notes

The authors declare no competing financial interest.

■ ACKNOWLEDGMENTS

This research was done in HERE (40330/13), funded by Tekes (Business Finland), AGCO Power Oy, Dekati Oy, Dinex Ecocat Oy, Neste Oyj, Pegasor Oy, and Wärtsilä Oy. This work utilized Tampere Microscopy Center facilities at Tampere University.

■ REFERENCES

(1) Petzold, A.; Weingartner, E.; Hasselbach, J.; Lauer, P.; Kurok, C.; Fleischer, F. Physical Properties, Chemical Composition, and Cloud Forming Potential of Particulate Emissions from a Marine Diesel Engine at Various Load Conditions. *Environ. Sci. Technol.* **2010**, *44*, 3800−3805.
(2) Aakko-Saksa, P.; Koponen, P.; Aurela, M.; Vesala, H.; Piimäkorpi, P.; Murtonen, T.; Sippula, O.; Koponen, H.; Karjalainen, P.; Kuittinen, N.; Panteliadis, P.; Rönkkö, T.; Timonen, H. Considerations in analysing elemental carbon from marine engine exhaust using residual, distillate and biofuels. *J. Aerosol Sci.* **2018**, *126*, 191−204.
(3) Bond, T. C.; Doherty, S. J.; Fahey, D. W.; Forster, P. M.; Berntsen, T.; Deangelo, B. J.; Flanner, M. G.; Ghan, S.; Kärcher, B.; Koch, D.; Kinne, S.; Kondo, Y.; Quinn, P. K.; Sarofim, M. C.; Schultz, M. G.; Schulz, M.; Venkataraman, C.; Zhang, H.; Zhang, S.; Bellouin, N.; Guttikunda, S. K.; Hopke, P. K.; Jacobson, M. Z.; Kaiser, J. W.; Klimont, Z.; Lohmann, U.; Schwarz, J. P.; Shindell, D.; Storelvmo, T.; Warren, S. G.; Zender, C. S. Bounding the role of black carbon in the climate system: A scientific assessment. *J. Geophys. Res. Atmos.* **2013**, *118*, 5380−5552.
(4) Lelieveld, J.; Evans, J. S.; Fnais, M.; Giannadaki, D.; Pozzer, A. The contribution of outdoor air pollution sources to premature mortality on a global scale. *Nature* **2015**, *525*, 367−371.
(5) Lelieveld, J.; Klingmüller, K.; Pozzer, A.; Pöschl, U.; Fnais, M.; Daiber, A.; Münzel, T. Cardiovascular disease burden from ambient air pollution in Europe reassessed using novel hazard ratio functions. *Eur. Heart J.* **2019**, *40*, 1590−1596.
(6) Oberdörster, G.; Sharp, Z.; Atudorei, V.; Elder, A.; Gelein, R.; Kreyling, W.; Cox, C. Translocation of Inhaled Ultrafine Particles to the Brain. *Inhalation Toxicol.* **2004**, *16*, 437−445.
(7) Wilker, E. H.; Preis, S. R.; Beiser, A. S.; Wolf, P. A.; Au, R.; Kloog, I.; Li, W.; Schwartz, J.; Koutrakis, P.; Decarli, C.; Seshadri, S.; Mittleman, M. A. Long-Term Exposure to Fine Particulate Matter, Residential Proximity to Major Roads and Measures of Brain Structure. *Stroke* **2015**, *46*, 1161−1166.
(8) Heusinkveld, H. J.; Wahle, T.; Campbell, A.; Westerink, R. H. S.; Tran, L.; Johnston, H.; Stone, V.; Cassee, F. R.; Schins, R. P. F. Neurodegenerative and neurological disorders by small inhaled particles. *NeuroToxicology* **2016**, *56*, 94−106.
(9) Oberdörster, G. Pulmonary effects of inhaled ultrafine particles. *Int. Arch. Occup. Environ. Health* **2000**, *74*, 1−8.
(10) Janssen, N. A. H.; Gerlofs-Nijland, M. E.; Lanki, T.; Salonen, R. O.; Cassee, F.; Hoek, G.; Fischer, P.; Brunekreef, B.; Krzyzanowski, M. *Health Effects of Black Carbon*; World Health Organization: Copenhagen, Denmark, 2012.
(11) Corbett, J. J.; Winebrake, J. J.; Green, E. H.; Kasibhatla, P.; Eyring, V.; Lauer, A. Mortality from Ship Emissions: A Global Assessment. *Environ. Sci. Technol.* **2007**, *41*, 8512−8518.
(12) Sofiev, M.; Winebrake, J. J.; Johansson, L.; Carr, E. W.; Prank, M.; Soares, J.; Vira, J.; Kouznetsov, R.; Jalkanen, J. P.; Corbett, J. J. Cleaner fuels for ships provide public health benefits with climate tradeoffs. *Nat. Commun.* **2018**, *9*, 406.
(13) Liu, Z.; Lu, X.; Feng, J.; Fan, Q.; Zhang, Y.; Yang, X. Influence of Ship Emissions on Urban Air Quality: A Comprehensive Study Using Highly Time-Resolved Online Measurements and Numerical Simulation in Shanghai. *Environ. Sci. Technol.* **2017**, *51*, 202−211.
(14) Viana, M.; Hammingh, P.; Colette, A.; Querol, X.; Degraeuwe, B.; Vlieger, I. de; van Aardenne, J. Impact of maritime transport emissions on coastal air quality in Europe. *Atmos. Environ.* **2014**, *90*, 96−105.
(15) Mazzei, F.; D'Alessandro, A.; Lucarelli, F.; Nava, S.; Prati, P.; Valli, G.; Vecchi, R. Characterization of particulate matter sources in an urban environment. *Sci. Total Environ.* **2008**, *401*, 81−89.
(16) Cesari, D.; Genga, A.; Ielpo, P.; Siciliano, M.; Mascolo, G.; Grasso, F. M.; Contini, D. Source apportionment of PM2.5 in the harbour-industrial area of Brindisi (Italy): Identification and estimation of the contribution of in-port ship emissions. *Sci. Total Environ.* **2014**, *497*−*498*, 392−400.
(17) Kuuluvainen, H.; Karjalainen, P.; Saukko, E.; Ovaska, T.; Sirviö, K.; Honkanen, M.; Olin, M.; Niemi, S.; Keskinen, J.; Rönkkö, T. Non-volatile ultrafine particles observed to form trimodal size distributions in non-road diesel engine exhaust. *Aerosol Sci. Technol.* **2020**, submitted.
(18) Rönkkö, T.; Virtanen, A.; Kannosto, J.; Keskinen, J.; Lappi, M.; Pirjola, L. Nucleation Mode Particles with a Nonvolatile Core in the Exhaust of a Heavy Duty Diesel Vehicle. *Environ. Sci. Technol.* **2007**, *41*, 6384−6389.
(19) Ushakov, S.; Valland, H.; Nielsen, J. B.; Hennie, E. Particle size distributions from heavy-duty diesel engine operated on low-sulfur marine fuel. *Fuel Process. Technol.* **2013**, *106*, 350−358.
(20) Hallquist, Å. M.; Fridell, E.; Westerlund, J.; Hallquist, M. Onboard Measurements of Nanoparticles from a SCR-Equipped Marine Diesel Engine. *Environ. Sci. Technol.* **2013**, *47*, 773−780.
(21) Heikkilä, J.; Rönkkö, T.; Lähde, T.; Lemmetty, M.; Arffman, A.; Virtanen, A.; Keskinen, J.; Pirjola, L.; Rothe, D. Effect of open channel filter on particle emissions of modern diesel engine. *J. Air Waste Manage. Assoc.* **2009**, *59*, 1148−1154.
(22) Lähde, T.; Rönkkö, T.; Virtanen, A.; Schuck, T.; Pirjola, L.; Hämeri, K.; Kulmala, M.; Arnold, F.; Rothe, D.; Keskinen, J. Heavy Duty Diesel Engine Exhaust Aerosol Particle and Ion Measurements. *Environ. Sci. Technol.* **2009**, *43*, 163−168.
(23) Lähde, T.; Virtanen, A.; Happonen, M.; Söderström, C.; Kytö, M.; Keskinen, J. Heavy-duty, off-road diesel engine low-load particle number emissions and particle control. *J. Air Waste Manage. Assoc.* **2014**, *64*, 1186−1194.
(24) Rönkkö, T.; Timonen, H. Overview of sources and characteristics of nanoparticles in urban traffic-influenced areas. *J. Alzheimer's Dis.* **2019**, *72*, 15−28.
(25) Sgro, L. A.; Sementa, P.; Vaglieco, B. M.; Rusciano, G.; D'Anna, A.; Minutolo, P. Investigating the origin of nuclei particles in GDI engine exhausts. *Combust. Flame* **2012**, *159*, 1687−1692.

(26) Seong, H.; Choi, S.; Lee, K. Examination of nanoparticles from gasoline direct-injection (GDI) engines using transmission electron microscopy (TEM). *Int. J. Automot. Techn.* **2014**, *15*, 175−181.
(27) Corbin, J. C.; Peng, W.; Yang, J.; Sommer, D. E.; Trivanovic, U.; Kirchen, P.; Miller, J. W.; Rogak, S.; Cocker, D. R.; Smallwood, G. J.; Lobo, P.; Gagné, S. Characterization of particulate matter emitted by a marine engine operated with liquefied natural gas and diesel fuels. *Atmos. Environ.* **2020**, *220*, 117030.
(28) Fushimi, A.; Saitoh, K.; Fujitani, Y.; Hasegawa, S.; Takahashi, K.; Tanabe, K.; Kobayashi, S. Organic-rich nanoparticles (diameter: 10−30 nm) in diesel exhaust: Fuel and oil contribution based on chemical composition. *Atmos. Environ.* **2011**, *45*, 6326−6336.
(29) Moldanová, J.; Fridell, E.; Winnes, H.; Holmin-Fridell, S.; Boman, J.; Jedynska, A.; Tishkova, V.; Demirdjian, B.; Joulie, S.; Bladt, H.; Ivleva, N. P.; Niessner, R. Physical and chemical characterisation of PM emissions from two ships operating in European emission control areas. *Atmos. Meas. Tech.* **2013**, *6*, 3577−3596.
(30) Jonsson, Å. M.; Westerlund, J.; Hallquist, M. Size-resolved particle emission factors for individual ships. *Geophys. Res. Lett.* **2011**, DOI: 10.1029/2011GL047672.
(31) Pirjola, L.; Pajunoja, A.; Walden, J.; Jalkanen, J. P.; Rönkkö, T.; Kousa, A.; Koskentalo, T. Mobile measurements of ship emissions in two harbour areas in Finland. *Atmos. Meas. Tech.* **2014**, *7*, 149−161.
(32) Anderson, M.; Salo, K.; Hallquist, Å. M.; Fridell, E. Characterization of particles from a marine engine operating at low loads. *Atmos. Environ.* **2015**, *101*, 65−71.
(33) Ntziachristos, L.; Saukko, E.; Lehtoranta, K.; Rönkkö, T.; Timonen, H.; Simonen, P.; Karjalainen, P.; Keskinen, J. Particle emissions characterization from a medium-speed marine diesel engine with two fuels at different sampling conditions. *Fuel* **2016**, *186*, 456−465.
(34) Kalli, J.; Karvonen, T.; Makkonen, T. *Sulphur content in ships bunker fuel in 2015 - A study on the impacts of the new IMO regulations and transportation costs*; Ministry of Transport and Communications: Helsinki, Finland, 2009.
(35) Lehtoranta, K.; Aakko-Saksa, P.; Murtonen, T.; Vesala, H.; Ntziachristos, L.; Rönkkö, T.; Karjalainen, P.; Kuittinen, N.; Timonen, H. Particulate Mass and Nonvolatile Particle Number Emissions from Marine Engines Using Low-Sulfur Fuels, Natural Gas, or Scrubbers. *Environ. Sci. Technol.* **2019**, *53*, 3315−3322.
(36) Wei, L.; Geng, P. A review on natural gas/diesel dual fuel combustion, emissions and performance. *Fuel Process. Technol.* **2016**, *142*, 264−278.
(37) Johnson, D. R.; Heltzel, R.; Nix, A. C.; Clark, N.; Darzi, M. Greenhouse gas emissions and fuel efficiency of in-use high horsepower diesel, dual fuel, and natural gas engines for unconventional well development. *Appl. Energy* **2017**, *206*, 739−750.
(38) Murphy, S.; Agrawal, H.; Sorooshian, A.; Padró, L. T.; Gates, H.; Hersey, S.; Welch, W. A.; Jung, H.; Miller, J. W.; Cocker, D. R.; Nenes, A.; Jonsson, H. H.; Flagan, R. C.; Seinfeld, J. H. Comprehensive simultaneous shipboard and airborne characterization of exhaust from a modern container ship at sea. *Environ. Sci. Technol.* **2009**, *43*, 4626−4640.
(39) Anderson, M.; Salo, K.; Fridell, E. Particle- and Gaseous Emissions from an LNG Powered Ship. *Environ. Sci. Technol.* **2015**, *49*, 12568−12575.
(40) Giechaskiel, B.; Ntziachristos, L.; Samaras, Z.; Scheer, V.; Casati, R.; Vogt, R. Formation potential of vehicle exhaust nucleation mode particles on-road and in the laboratory. *Atmos. Environ.* **2005**, *39*, 3191−3198.
(41) Amanatidis, S.; Ntziachristos, L.; Giechaskiel, B.; Katsaounis, D.; Samaras, Z.; Bergmann, A. Evaluation of an oxidation catalyst ('catalytic stripper') in eliminating volatile material from combustion aerosol. *J. Aerosol Sci.* **2013**, *57*, 144−155.
(42) Amanatidis, S.; Ntziachristos, L.; Karjalainen, P.; Saukko, E.; Simonen, P.; Kuittinen, N.; Aakko-Saksa, P.; Timonen, H.; Keskinen, J.; Rönkkö, T. Comparative performance of a thermal denuder and a catalytic stripper in sampling laboratory and marine exhaust aerosols. *Aerosol Sci. Technol.* **2018**, *52*, 420−432.
(43) Rönkkö, T.; Kuuluvainen, H.; Karjalainen, P.; Keskinen, J.; Hillamo, R.; Niemi, J. V.; Pirjola, L.; Timonen, H. J.; Saarikoski, S.; Saukko, E.; Järvinen, A.; Silvennoinen, H.; Rostedt, A.; Olin, M.; Yli-Ojanperä, J.; Nousiainen, P.; Kousa, A.; Dal Maso, M. Traffic is a major source of atmospheric nanocluster aerosol. *Proc. Natl. Acad. Sci. U. S. A.* **2017**, *114*, 7549−7554.
(44) Olin, M.; Alanen, J.; Palmroth, M. R. T.; Rönkkö, T.; Dal Maso, M. Inversely modeling homogeneous H_2SO_4 - H_2O nucleation rate in exhaust-related conditions. *Atmos. Chem. Phys.* **2019**, *19*, 6367−6388.
(45) Alanen, J.; Saukko, E.; Lehtoranta, K.; Murtonen, T.; Timonen, H.; Hillamo, R.; Karjalainen, P.; Kuuluvainen, H.; Harra, J.; Keskinen, J.; Rönkkö, T. The formation and physical properties of the particle emissions from a natural gas engine. *Fuel* **2015**, *162*, 155−161.
(46) Sippula, O.; Stengel, B.; Sklorz, M.; Streibel, T.; Rabe, R.; Orasche, J.; Lintelmann, J.; Michalke, B.; Abbaszade, G.; Radischat, C.; Gröger, T.; Schnelle-Kreis, J.; Harndorf, H.; Zimmermann, R. Particle emissions from a marine engine: Chemical composition and aromatic emission profiles under various operating conditions. *Environ. Sci. Technol.* **2014**, *48*, 11721−11729.
(47) Lieke, K. I.; Rosenørn, T.; Pedersen, J.; Larsson, D.; Kling, J.; Fuglsang, K.; Bilde, M. Micro- and nanostructural characteristics of particles before and after an exhaust gas recirculation system scrubber. *Aerosol Sci. Technol.* **2013**, *47*, 1038−1046.
(48) Maricq, M. M. The dynamics of electrically charged soot particles in a premixed ethylene flame. *Combust. Flame* **2005**, *141*, 406−416.
(49) Sgro, L. A.; D'Anna, A.; Minutolo, P. Charge Distribution of Incipient Flame-Generated Particles Charge Distribution of Incipient Flame-Generated Particles. *Aerosol Sci. Technol.* **2010**, *44*, 651−662.
(50) De Filippo, A.; Maricq, M. M. Diesel nucleation mode particles: Semivolatile or solid? *Environ. Sci. Technol.* **2008**, *42*, 7957−7962.
(51) Eichler, P.; Muller, M.; Rohmann, C.; Stengel, B.; Orasche, J.; Zimmermann, R.; Wisthaler, A. Lubricating Oil as a Major Constituent of Ship Exhaust Particles. *Environ. Sci. Technol. Lett.* **2017**, *4*, 54−58.
(52) Carbone, S.; Timonen, H. J.; Rostedt, A.; Happonen, M.; Rönkkö, T.; Keskinen, J.; Ristimaki, J.; Korpi, H.; Artaxo, P.; Canagaratna, M. R.; Worsnop, D.; Canonaco, F.; Prévôt, A. S. H.; Hillamo, R.; Saarikoski, S. Distinguishing fuel and lubricating oil combustion products in diesel engine exhaust particles. *Aerosol Sci. Technol.* **2019**, *53*, 594−607.
(53) Alanen, J.; Simonen, P.; Saarikoski, S.; Timonen, H.; Kangasniemi, O.; Saukko, E.; Hillamo, R.; Lehtoranta, K.; Murtonen, T.; Vesala, H.; Keskinen, J.; Rönkkö, T. Comparison of primary and secondary particle formation from natural gas engine exhaust and of their volatility characteristics. *Atmos. Chem. Phys.* **2017**, *17*, 8739−8755.
(54) Karjalainen, P.; Rönkkö, T.; Simonen, P.; Ntziachristos, L.; Juuti, P.; Timonen, H.; Teinilä, K.; Saarikoski, S.; Saveljeff, H.; Lauren, M.; Happonen, M.; Matilainen, P.; Maunula, T.; Nuottimäki, J.; Keskinen, J. Strategies To Diminish the Emissions of Particles and Secondary Aerosol Formation from Diesel Engines. *Environ. Sci. Technol.* **2019**, *53*, 10408−10416.

Supporting Information

Physical characteristics of particle emissions from a medium speed ship engine fueled with natural gas and low-sulfur liquid fuels

Authors: Jenni Alanen[1, #], Mia Isotalo[1], Niina Kuittinen[1], Pauli Simonen[1], Sampsa Martikainen[1], Heino Kuuluvainen[1], Mari Honkanen[2], Kati Lehtoranta[3], Sami Nyyssönen[3], Hannu Vesala[3], Hilkka Timonen[4], Minna Aurela[4], Jorma Keskinen[1], Topi Rönkkö[1,*]

[1] Aerosol Physics Laboratory, Faculty of Engineering and Natural Sciences, Tampere University, P.O. Box 692, FI-33014 Tampere University, Finland
[2] Tampere Microscopy Center, Tampere University, P.O. Box 692, FI-33014 Tampere University, Finland
[3] VTT Technical Research Centre of Finland, P.O. Box 1000, FI-02044 VTT Espoo
[4] Atmospheric Composition Research, Finnish Meteorological Institute, P.O. Box 503, FI-00101 Helsinki, Finland

[#] currently also: AGCO Power Oy, Linnavuorentie 8-10, FI-37240 Linnavuori, Finland
* corresponding author: Topi Rönkkö, Aerosol Physics Laboratory, Faculty of Engineering and Natural Sciences, Tampere University, P.O. Box 692, FI-33014 Tampere University, Finland, topi.ronkko@tuni.fi

Number of pages: 9
Number of figures: 10
Number of tables: 0

Contents:

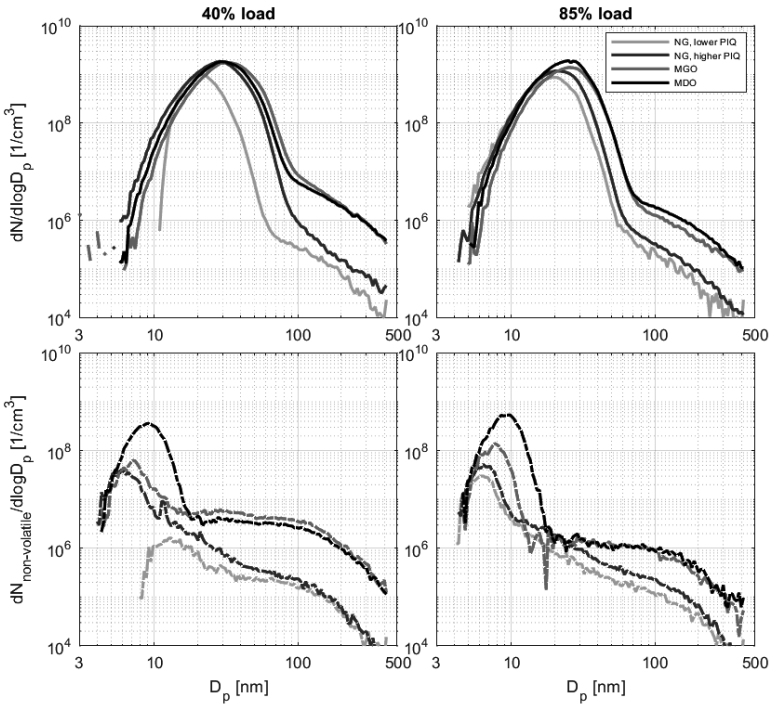

S1 The particle size distribution of fresh exhaust particles on top with solid lines and the particle size distribution of non-volatile particles on bottom with a dash-dot line. The latter was measured using CS. On the left, engine load was 40% and on the right, it was 85%

Mode fitting

Mode fitting was done for the fresh exhaust and CS treated SMPS size distributions using Excel Solver tool and least squares method. Two modes were found in fresh and 2-3 modes were found in CS treated exhaust sample. In S2 there are four examples of the mode fittings.

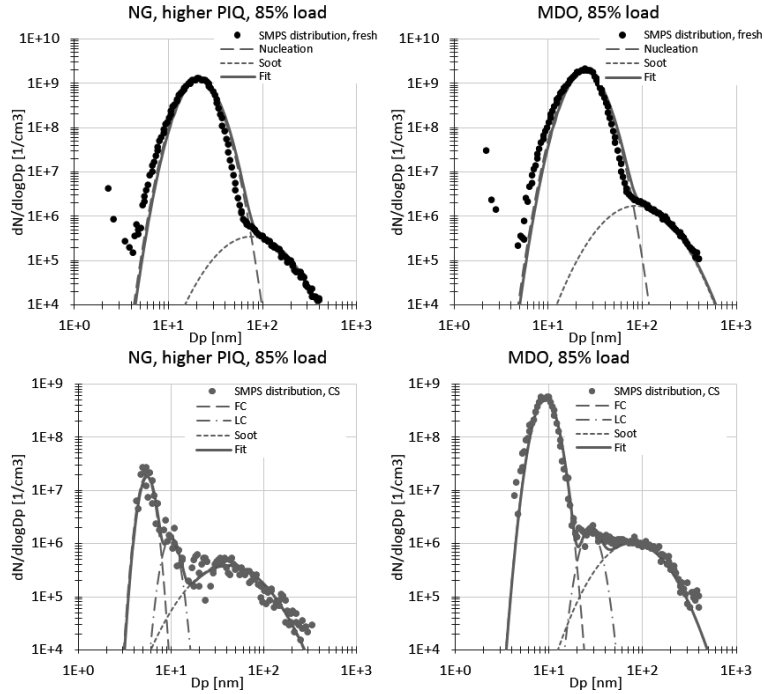

S2 Examples of the mode fitting in SMPS size distributions of fresh and CS treated exhaust sample.

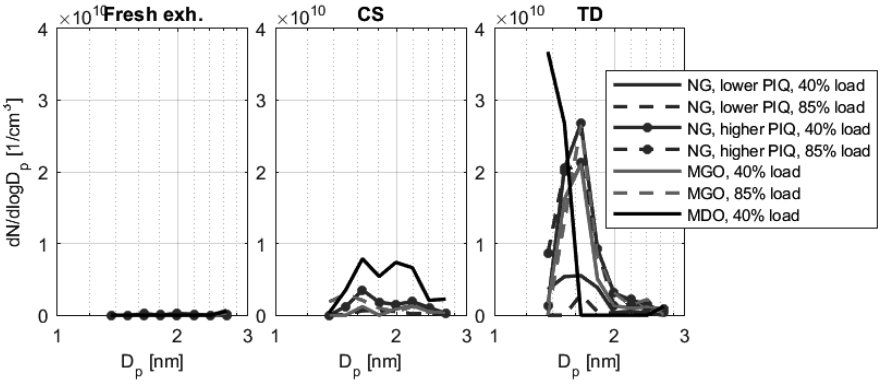

S3 PSM size distributions

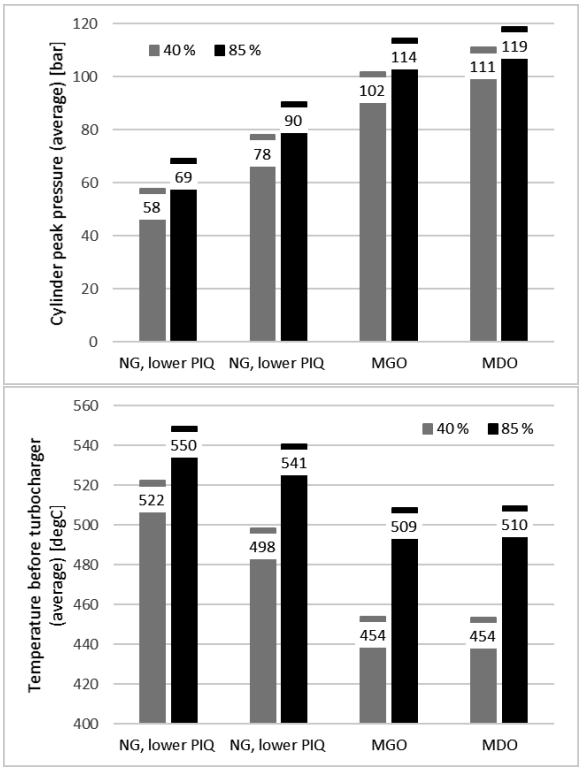

S4 On the left: In-cylinder peak pressures, the average of the four cylinders. The cylinder pressure curves were measured 3-14 Times, here the averages given. On the right: The exhaust gas temperatures upstream turbo varied in the range 454-550 °C, the highest pre turbo temperatures produced by natural gas combustion and the 85% engine load.

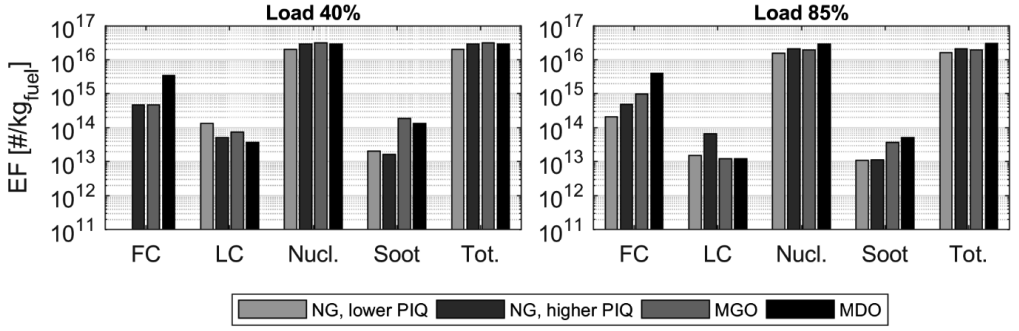

S5 Particle number emission factors in unit #/kg$_{fuel}$

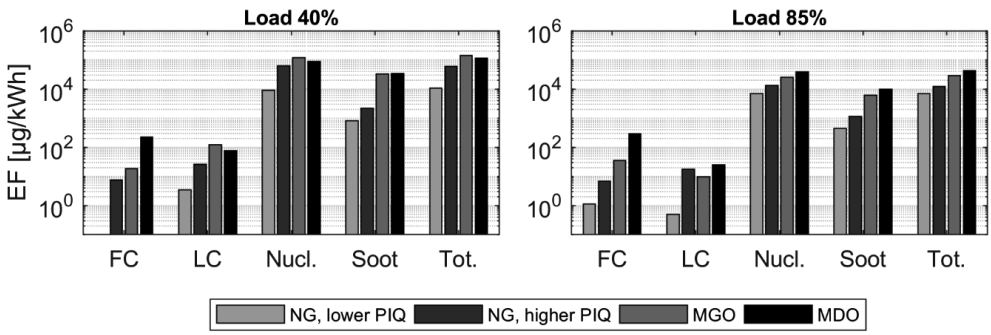

		EF [µg/kWh]		
Load 40%	NG, lower PIQ	NG, higher PIQ	MGO	MDO
FC	-	7.5E+0	1.9E+1	2.3E+2
LC	3.5E+0	2.6E+1	1.2E+2	7.5E+1
Nucl.	9.1E+3	6.3E+4	1.2E+5	8.9E+4
Soot	8.1E+2	2.2E+3	3.3E+4	3.4E+4
Tot.	1.1E+4	6.0E+4	1.4E+5	1.1E+5
Load 85%	NG, lower PIQ	NG, higher PIQ	MGO	MDO
FC	1.1E+0	6.8E+0	3.6E+1	2.9E+2
LC	5.1E-1	1.8E+1	9.7E+0	2.5E+1
Nucl.	7.1E+3	1.3E+4	2.5E+4	3.8E+4
Soot	4.5E+2	1.1E+3	6.2E+3	9.7E+3
Tot.	7.0E+3	1.2E+4	2.9E+4	4.3E+4

S6 Particle mass emission factors in unit µg/kWh. Calculated using SMPS particle size distributions. Unit density and spherical particles assumed. The particulate mass emission factors are on a similar level as reported by Lehtoranta et al. (2019). They collected PM samples on filters according to the ISO standard 8178-1:2006 and weighed the filters.

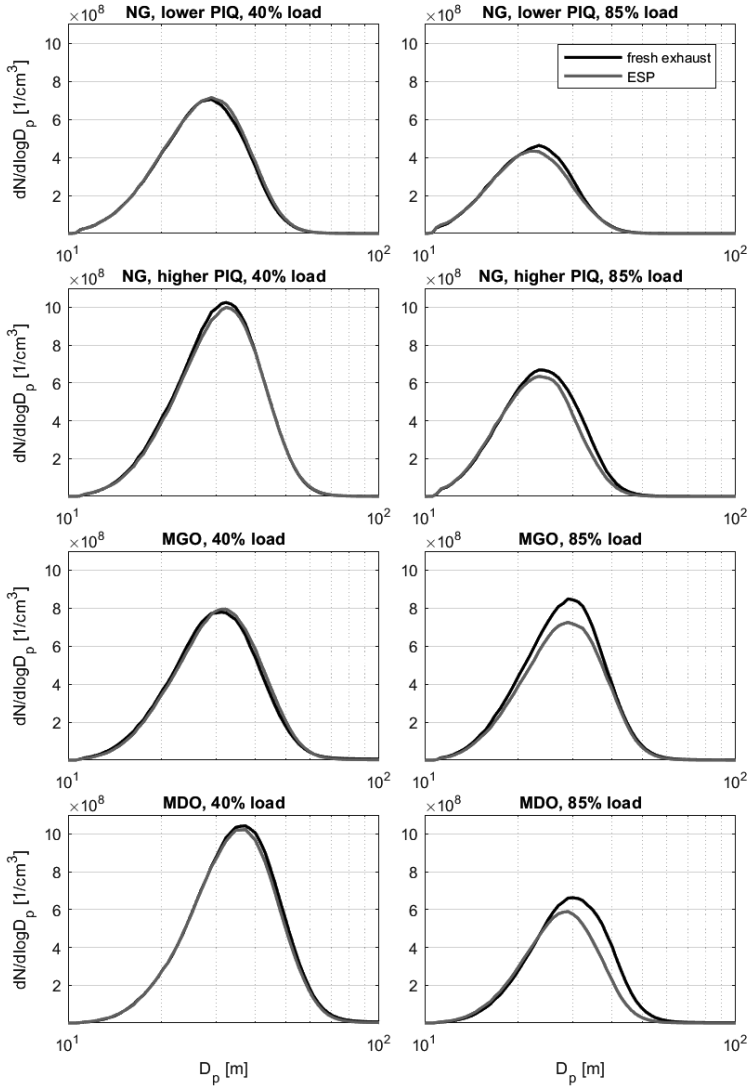

S7 Size distributions measured both without (fresh exhaust) and with electrostatic precipitator (ESP). 40% load produced more nucleation mode particles with fewer charges. 40% load case has a too low fraction of naturally charged particles, which causes "negative concentrations of charged particles", i.e., makes the analysis impossible.

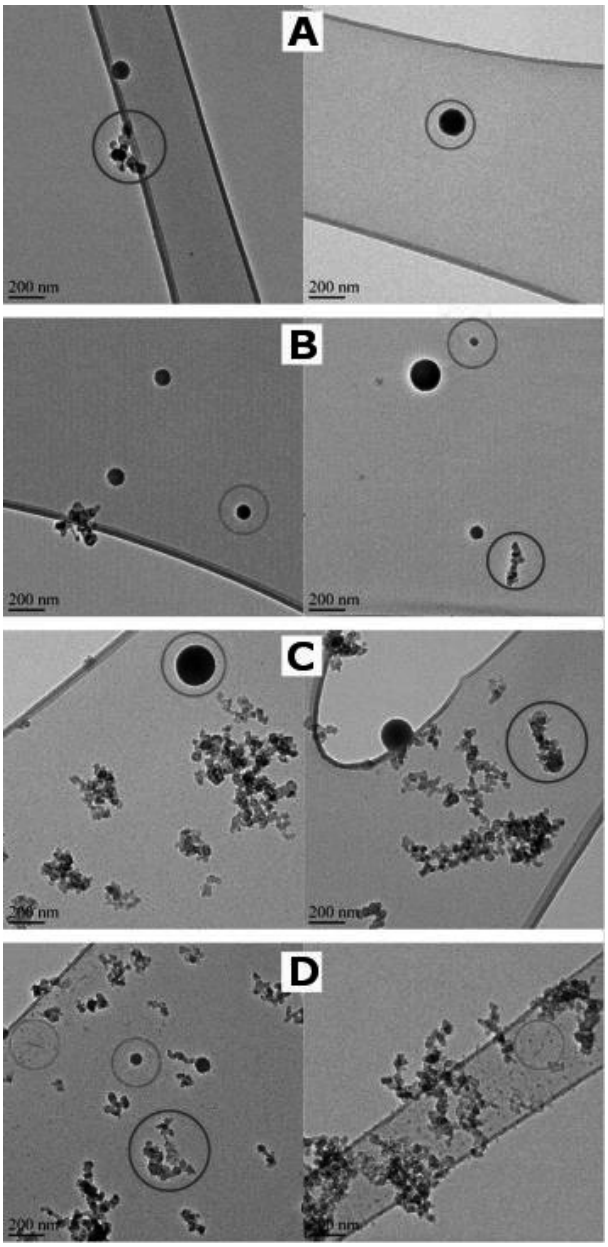

S8 TEM images of fresh exhaust particles (i.e. the sample was taken directly after the dilution system without TD or CS). Engine load was 40% in all collected TEM samples. A) Natural gas, lower PIQ B) Natural gas, higher PIQ C) MGO D) MDO. Examples of different particle types are circulated with different colors: spherical LC particles with orange, soot particles with purple and the stain-like particles with light blue.

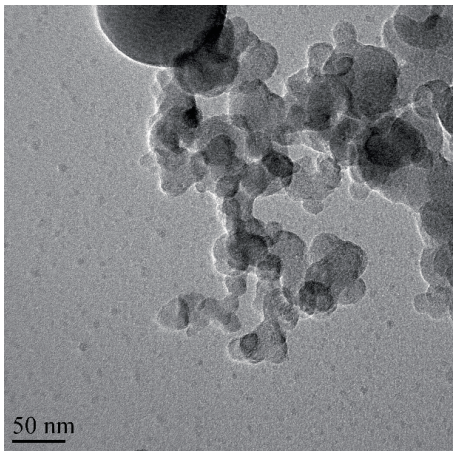

S9 Higher magnification image of a soot agglomerate, a spherical particle and possibly fuel originated core particles

PSM inversion

First, the particle concentration data was plotted in saturation flow–cumulative particle concentration figure (See S10) and the saturation flow was converted to 50% cut-off diameters using the Airmodus' calibration data. Then, a fit to the data was made that forced the measured cumulative particle number concentration to be monotonic and smoothed the noise in the data but did not force the shape of the curve. This was done using Matlab's *smooth* function with as large a span as possible (= 249 because the length of the data was minimum 250 s). The cumulative concentrations corresponding to the particle sizes > 3 nm were treated as their average and addressed to particle size 3 nm, because otherwise "smooth" would have been too much affected by the individual data points at the largest particle sizes. Then, 10 particle diameters with a ratio of 1.1 and starting point 1.18 were selected and the cumulative concentrations at those particle diameters were found in the smoothed cumulative particle number concentration data. Finally, the quantity $dN/dlogD_p$ at the geometric mean particle diameters was calculated.

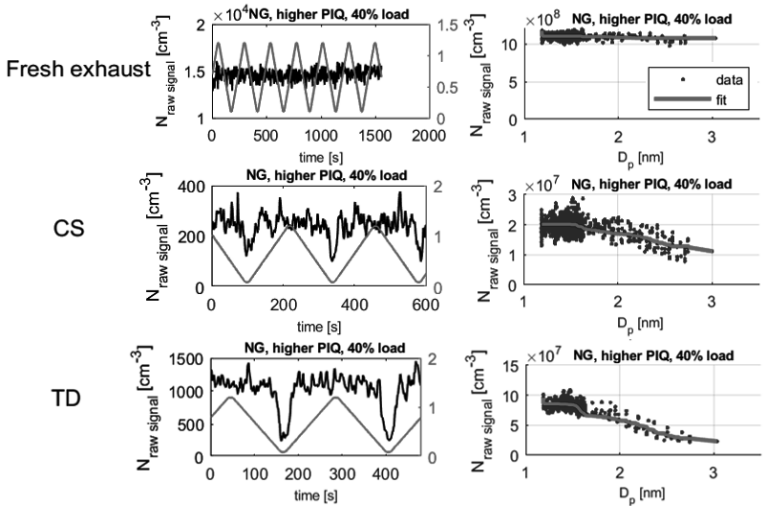

S10 On the left: PSM raw data timeseries with fresh exhaust particles, CS treatment and TD treatment for one example case NG, higher PIQ, 40% load. On the right: Particle concentration raw signal of PSM and a made fit at the different cut-off particle diameters. Saturation flow was turned into to particle 50% cut diameter the calibration of Airmodus: Saturation flow limits = [0.1020, 0.1110, 0.1540, 0.1910, 0.2270, 0.2620, 0.2980, 0.8110, 1.0710, 1.2220] lpm. Corresponding D_p limits = [3.0700, 2.7600, 2.4100, 2.2100, 1.9800, 1.8200, 1.6300, 1.4200, 1.3000, 1.1700] nm. The fit was plotted using functions fit and smooth in Matlab.

PAPER 3

Natural Gas Engine Emission Reduction by Catalysts

Lehtoranta, K., Murtonen, T., Vesala, H., Koponen, P., Alanen, J., Simonen, P., Rönkkö, T., Timonen, H., Saarikoski, S., Maunula, T., Kallinen, K. and Korhonen, S.

Emission Control Science and Technology 3.(2017), 142–152
DOI: 10.1007/s40825-016-0057-8

Emiss. Control Sci. Technol. (2017) 3:142–152
DOI 10.1007/s40825-016-0057-8

Natural Gas Engine Emission Reduction by Catalysts

Kati Lehtoranta[1] · Timo Murtonen[1] · Hannu Vesala[1] · Päivi Koponen[1] · Jenni Alanen[2] · Pauli Simonen[2] · Topi Rönkkö[2] · Hilkka Timonen[3] · Sanna Saarikoski[3] · Teuvo Maunula[4] · Kauko Kallinen[4] · Satu Korhonen[5]

Received: 17 May 2016 / Revised: 5 December 2016 / Accepted: 7 December 2016 / Published online: 23 December 2016

Abstract In order to meet stringent emission limits, aftertreatment systems are increasingly utilized in natural gas engine applications. In this work, two catalyst systems were studied in order to clarify how the catalysts affect, e.g. hydrocarbons, NO_x and particles present in natural gas engine exhaust. A passenger car engine modified to run with natural gas was used in a research facility with possibilities to modify the exhaust gas properties. High NO_x reductions were observed when using selective catalytic reduction, although a clear decrease in the NO_x reduction was recorded at higher temperatures. The relatively fresh methane oxidation catalyst was found to reach reductions greater than 50% when the exhaust temperature and the catalyst size were sufficient. Both the studied catalyst systems were found to have a significant effect on particulate emissions. The observed particle mass reduction was found to be due to a decrease in the amount of organics passing over the catalyst. However, especially at high exhaust temperatures, high nanoparticle concentrations were observed downstream of the catalysts together with higher sulphate concentrations in particles. This study contributes to understanding emissions from future natural gas engine applications with catalysts in use.

✉ Kati Lehtoranta
kati.lehtoranta@vtt.fi

[1] VTT Technical Research Centre of Finland, Espoo, Finland

[2] Aerosol Physics, Tampere University of Technology, Tampere, Finland

[3] Aerosol Research, Finnish Meteorological Institute, Helsinki, Finland

[4] Dinex Ecocat Oy, Vihtavuori, Finland

[5] Wärtsilä Finland Oy, Helsinki, Finland

Keywords Natural Gas · Engine emissions · Methane oxidation · NO_x reduction · Nanoparticles

1 Introduction

Natural gas (NG) engines are used worldwide in energy production, vehicle applications and increasingly also in marine applications. The increased availability of natural gas (e.g. extraction of shale gas), increasing fuel prices as well as the ever more stringent emission legislations boost the use of natural gas. Furthermore, and importantly, the use of natural gas can lead to lower CO_2 emissions compared to conventional liquid fossil fuels. This is due to the chemical properties of NGs, with their high H/C ratio, as natural gas is primarily composed of methane (CH_4; e.g. [6]).

Although NG combustion applications have clear benefits when compared to conventional liquid fossil fuels, NG engines also produce emissions that have adverse environmental and health effects. In general, the formation of NO in combustion processes occurs mainly at high temperatures. When compared, e.g. to diesel engines, in NG engines, lower levels of NO_x can be achieved (in lean burn conditions with premixed combustion) due to the relatively low temperature of combustion of NG engines. On the other hand, lean burn conditions of an NG engine can lead to relatively high CO and HC emissions if the emissions are compared with stoichiometric combustion. Several studies have shown that NG engines have higher CO and HC emissions compared with liquid fuel engines (e.g. diesel engines; see, for example, [1, 6, 11, 19]). Methane is the principal hydrocarbon species emitted by NG engines. Since methane is a potential greenhouse gas, its emissions should be minimized. Another important emission component found in NG engine emissions is formaldehyde, a toxic compound which is hazardous even in low concentrations.

Formaldehyde can be emitted from NG engines as a product of incomplete combustion, mostly due to partial oxidation events in the engine [23, 27].

Particle emissions from NG engines are known to be low, e.g. when compared to conventional diesel engines. This is because of the lower soot particle formation in combustion. However, recent studies indicate that particle number emissions of NG engines, especially nanoparticle emissions, are not necessarily low [2, 12]. Particle emissions are known to have a negative impact on human health, and especially the smallest particles (nanoparticles) can penetrate into the lungs and blood-vascular system (e.g. [32]).

In order to diminish the environmental and health effects and to comply with tightening emission limits, exhaust aftertreatment systems will, in future, also be increasingly utilized in natural gas engine applications. The oxidation catalysts for lean burn natural gas engines have mainly been designed to oxidize CO and non-methane hydrocarbons (and formaldehyde). In order to oxidize methane, a highly efficient catalyst is needed. One significant challenge in the development of methane oxidation catalysts for lean NG applications is the catalyst deactivation since, e.g. both sulphur and water have been found to inhibit the oxidation of methane (e.g. [16, 30]). To the best of the authors' knowledge, no commercially available methane oxidation catalysts for lean conditions currently exist.

One option to further reduce NO_x from NG engines is a selective catalytic reduction (SCR) method which has been proven to be very effective in many applications (vehicles, ships and stationary applications). The SCR uses a catalyst and ammonia to reduce NO_x. Several chemical reactions can occur in the SCR system, the dominant one involving nitrogen monoxide, ammonia and oxygen reacting to produce nitrogen and water (e.g. [20]). Due to the toxicity and handling problems associated with pure ammonia, an aqueous solution of urea is widely used as an ammonia source. Typically, urea is injected into the exhaust gas well upstream of the catalyst itself in order to have enough time for the urea to decompose into ammonia before entering the catalyst.

In the present study, we investigated the efficiencies of two different catalysts with real NG engine exhaust gas in a facility with possibilities to adjust the exhaust gas temperature, flow and composition independently. For catalyst studies, we see this as a relevant intermediate step, between the catalyst laboratory tests with synthetic gases and the actual target real application test. We examined two different catalyst systems (combinations of oxidation catalyst and SCR) to determine how they affect gaseous and particle emissions from a natural gas engine in different operating conditions. The experiment for the decomposition of urea in the exhaust is included in the study. A methane oxidation catalyst, still under development, was also studied.

2 Experimental

The research facility included a passenger car gasoline engine that was modified to run with natural gas. The selection of driving conditions was based on the emission levels. The target was to mimic the emission levels of a relevant power plant engine. Acceptable carbon monoxide and nitrogen oxide levels were achieved with engine adjustments. However, in order to achieve acceptable hydrocarbon levels, HC additions into the exhaust gas were also made. The engine with the test facility was presented in detail in Murtonen et al. [24]. The engine was operated with a lean air-to-fuel mixture.

For the present study, two different engine driving modes were utilized. These are presented in Table 1 along with the engine out O_2, CO and NO_x levels. The exhaust gas flow and temperature (measured upstream of the catalysts) were adjusted independently, and therefore, it was possible to keep these constant even when changing the driving mode.

Natural gas from the Nord Stream pipeline has high methane content. In the present study, the gas analysis results were: 97.2% methane, 1.37% ethane, 0.17% propane, 0.07% other hydrocarbons, 0.9% nitrogen and 0.2% carbon dioxide. The sulphur content of the gas was below 1.5 ppm. The lubricating oil sulphur content was 1760 mg/kg, density was 852.3 kg/m^3, and viscosity at 100 °C was 12.0 mm^2/s.

Two different catalyst setups were utilized in the present study. Both utilized urea for NO_x reduction, but the oxidation targets were different. The first setup consisted of a combination of a separate oxidation catalyst and an SCR catalyst. The oxidation catalyst, placed upstream of the SCR (and upstream of the urea injection), was targeted for methane oxidation (methane oxidation catalyst, MOC). The MOC utilized platinum–palladium (1:4) as active metals on a tailored coating developed for lean NG applications and supported on a metallic substrate. The volume of MOC was 1.69 dm^3. The SCR catalyst was a stabilized TiO_2–WO_3-based vanadium catalyst supported on a metallic substrate with a volume of 5.5 dm^3. The other setup consisted of only one catalyst reactor (OXICAT-x, placed similarly to the SCR in the first catalyst setup; see Fig. 1), which targeted to the oxidation of carbon

Table 1 Driving modes

	Mode 1	Mode 2
Torque (Nm)	70	35
Speed (rpm)	2700	3100
Power (kW)	20	12
O_2 (%)	6.0	6.3
NO_x (ppm)	190	50
CO (ppm)	400	430
Hydrocarbon additions	No	Yes

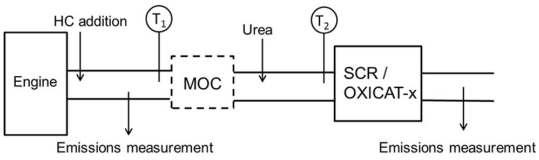

Fig. 1 Test setup

monoxide and formaldehyde and at the same time could utilize ammonia for NO_x reduction. This OXICAT-x utilized a fibre-reinforced noble metal–vanadium–tungsten–titania catalyst. The volume of OXICAT-x was 5 dm^3.

In order to study the performance of catalysts, the exhaust gas temperature and the space velocity are essential parameters. In the test facility of the present study, the exhaust gas temperature and the exhaust gas flow were adjustable [24]. Studies were conducted in an exhaust gas temperature range of 350–500 °C and with two exhaust gas flows (80 and 40 kg/h). The higher temperatures are needed for methane oxidation and would also mean that the catalyst placement in any real application would be first in line downstream of the engine, even pre-turbocharger. The utilized flows result to space velocities (1/h) of 8600 and 4300 for the MOC + SCR system and 12,400 and 6200 for the OXICAT-x system. A minimum of three test repetitions were made for each test condition in order to obtain reliable results.

Before conducting any actual tests, the catalysts were preconditioned by ageing for 48 h in mode 1 (with an exhaust gas temperature of 400 °C and exhaust flow of 80 kg/h; Table 1), without any urea feed. After the preconditioning, preliminary tests were performed for both catalyst setups in order to determine the urea feed to be utilized in subsequent tests. Aqueous 32.5% urea solution was used. The urea feed was selected to have a condition in which no (or only minor, i.e. below 5 ppm) ammonia slip was formed in the catalyst and the NO_x reduction was still clearly above 90%. The used NH_3/NO_x ratios were 1.12 and 1.17 in mode 1 and mode 2 (see Table 1), respectively. This preliminary test was made only at an exhaust temperature of 400 °C, and in further tests in different exhaust temperatures, the urea feed was kept the same. It should be noted that this most probably did not result in the SCR's best possible performance in all the selected temperature modes.

The emission measurement setup consisted of a chemiluminescence detector, used to measure the NO_x (NO and NO_2) and a non-dispersive infrared analyser to measure CO and CO_2. A Fourier transform infrared spectroscopy (FTIR) analyser was used to measure water, methane, NH_3 and HNCO concentrations. The FTIR as well as the sampling line and the filter prior to the FTIR spectrometer were heated to 180 °C. In addition, the methane, ethane, propane and ethylene components were measured from a diluted exhaust gas sample with a gas chromatograph (GC). Aldehyde samples were collected from diluted exhaust gas by using the dinitrophenyl hydrazine cartridges. In the cartridges, aldehydes form hydrazine derivatives which are then analyzed by high-performance liquid chromatography. The sample for GC and aldehyde measurement was taken from the FTIR output, utilizing a T-branch diluter and a tracer (sulphur hexafluoride, SF_6) to define the exact dilution ratio. This was observed to be 9–13. All these measurements of gaseous emissions were made upstream and downstream of the catalyst setups.

For the measurements of particle number, size distribution and composition, the exhaust was sampled using a sampling system consisting of a porous tube diluter (PTD), a residence time tunnel and an ejector diluter (Dekati Ltd.) [22, 25]. The system was the same as in the study of [2], but now the exhaust sample was taken from two different positions, as indicated in Fig. 1 (upstream and downstream of the catalyst). Residence time in the primary dilution system, i.e. in the PTD and the residence time tunnel, was 2.6 s, and the dilution ratio in the PTD was as low as 6 (to ensure concentration levels high enough for the EEPS and the Nano-SMPS). The secondary dilution ratio over the ejector diluter was 4, resulting in a total dilution ratio of 24 after two dilution stages. Both the primary and secondary dilution ratios were calculated from CO_2 measurements conducted for undiluted exhaust and diluted exhaust samples. After the secondary dilution, the particle size distribution of the exhaust sample was measured using the Engine Exhaust Particle Sizer (EEPS, TSI Inc.), the scanning mobility particle sizer (Nano-SMPS, consisting of DMA 3085 and CPC 3025, TSI Inc.) and the electrical low pressure impactor ELPI+ (Dekati Inc.), and the chemical composition of the particles was measured using a soot particle aerosol mass spectrometer (SP-AMS, Aerodyne Research Inc., USA). SP-AMS is a combination of two instruments: an Aerodyne high-resolution time-of-flight aerosol mass spectrometer and a single-particle soot photometer (SP2; Droplet Measurement Technologies, CO, USA), and it is capable of measuring refractory and non-refractory particulate materials [29]. In this study, the SP-AMS was operated in V-mode with a time resolution of 1 min. Both the laser and tungsten vaporizer were used and the concentrations of chemical species were calculated by using a default collection efficiency of 0.5. Particle number concentration measurements were conducted by the CPC 3776 (TSI Inc.) and the Particle Size Magnifier (PSM, Airmodus Ltd.) combined with the CPC 2775 (TSI Inc.). The exhaust sample was further diluted by a factor of 36. PSM was also used for sub-5-nm particle size distribution measurements in scanning mode (saturation flow scanning between 0.1 and 1 lpm). Volatility measurements for particle emission were made using a thermodenuder that was designed for nanoparticle measurements [10]. In the thermodenuder, aerosol sample is heated up to 265 °C in order to evaporate the volatile fraction of the particles and then led

through an active charcoal section where the evaporated particulate matter is absorbed and cooled. When total particle number emission was measured, the thermodenuder was bypassed.

The effect of the catalysts on particulate matter (PM) was studied by sampling PM both before and after the catalyst with a sampling according to international standard ISO 8178-1:2006. According to this standard, the PM is measured as any material collected on a filter after diluting exhaust gas with clean, filtered air to a temperature higher than 42 °C and less than or equal to 52 °C, as measured at a point immediately upstream of the filter. A dilution ratio of 10 and a sampling time of 30 min were used. Samples were collected on TX40HI20-WW filters (Ø = 47 mm).

3 Results and Discussion

In order to determine how the injected urea is decomposed to ammonia, measurements were made upstream of the SCR, but downstream of the urea injection. These measurements were made using the FTIR. Urea decomposition occurs in phases (e.g. [14, 37]). First, the water from the urea solution droplets is evaporated. Then, the urea is thermally decomposed into ammonia (NH_3) and isocyanic acid (HNCO). Hence, 1 mol of urea produces 1 mol of ammonia and 1 mol of isocyanic acid. The isocyanic acid is quite stable in the gas phase, but readily hydrolyzes on the surface of a metal oxide catalyst, producing ammonia and carbon dioxide. The measurements showed that at a temperature of 350 °C, approximately 50% of the urea was decomposed to ammonia and isocyanic acid, whereas at higher temperatures, the decomposition rate was clearly higher: at 400–450 °C, almost 80% of the urea was decomposed (Fig. 2). This is clearly better than the results reported earlier for the decomposition of urea for automotive

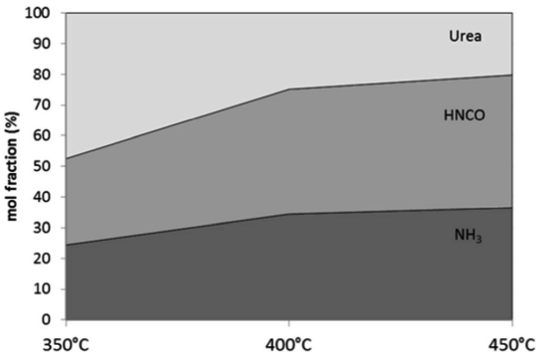

Fig. 2 Urea, isocyanic acid and ammonia measured upstream of the catalyst (downstream of the urea injection), i.e. at the catalyst entrance. The three measurement points (350, 400 and 450 °C) and the lines are to guide the eyes only

SCR systems by Koebel and Strutz [14], who found that only about 50% of urea decomposed at 400 °C when the residence time from urea injection to catalyst entrance was 0.09 s. In the present study, the residence time was longer: at 400 °C, the residence time was 0.13 s. The time available from the injection to the catalyst entrance is one of the key issues when discussing urea decomposition [14] and also one possible reason for the differences in urea decomposition between the present study and the study by Koebel and Strutz [14]. Other possible reasons could be a smaller droplet size or a better mixing of urea with the exhaust gas. One should also note that the accurate measurement of HNCO with FTIR can be challenging (e.g. due to interferences with other compounds existing in the exhaust gas). According to our experience, with the FTIR spectrometers we have utilized, especially the low HNCO levels (roughly below 30 ppm) cannot be measured accurately. In the present study, in the case of Fig. 2, the measured HNCO levels were between 64 and 100 ppm.

Good urea decomposition is a basis for efficient SCR operation and for avoiding misuse of the catalyst itself for water evaporation and urea decomposition.

Furthermore, the urea decomposition as well as the droplet size and mixing of urea with exhaust gas should be similar to those occurring in a real application case in order to make the present studies in an engine laboratory comparable with real application cases. For example, in the present study, the distance from the urea injection to the catalyst entrance and the nozzle utilized for urea injection were selected on the basis of the authors' knowledge of real application setups.

In the two different driving modes, the engine out NO_x levels were 190 and 50 ppm in mode 1 and mode 2, respectively. NO_2/NO_x was found to be 0.25 and 0.4 in modes 1 and 2, respectively. Exhaust from most combustion sources contains NO_x composed primarily of NO. However, leaner burn conditions tend to change the NO_2/NO_x ratio so that a higher fraction of NO_2 is emitted (e.g. [28]). In good correlation with the present results, significant fractions of NO_2 have earlier been reported for natural gas engines (e.g. [28, 33]).

The NO_x reduction, calculated from the NO_x measurements upstream and downstream of the catalyst, is presented as a function of temperature (measured upstream of the SCR or 'OXICAT-x', i.e. T_2 in the setup figure) in Fig. 3 at constant urea feed. The conventional SCR (placed downstream of the MOC) appears to operate similarly in both driving modes and the NO_x efficiency (in per cent) to depend rather little on the temperature between 350 and 450 °C.

The NO_x efficiency of OXICAT-x, however, was found to depend greatly on the temperature since a clearly lower efficiency was measured at the highest test temperature of 450 °C, especially in the case of mode 2. The lower NO_x reduction by 'OXICAT-x' was probably due to the competing reactions that actually oxidize the injected ammonia to NO rather than to the reaction between ammonia and NO resulting in N_2. It should

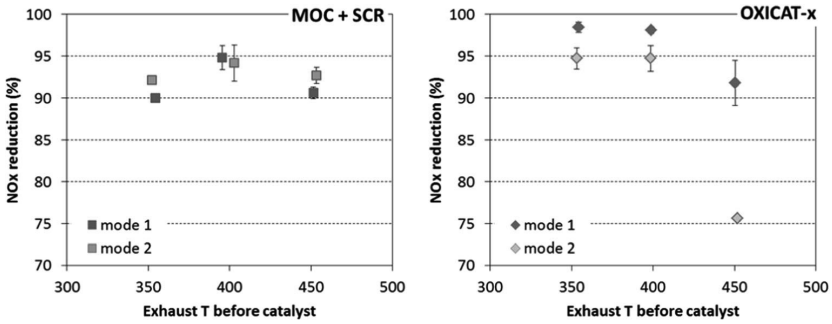

Fig. 3 NO_x reduction as a function of exhaust temperature. *Error bars* show the standard deviation of a minimum of three test repetitions

also be noted that the urea injection was not optimized for the different temperatures but was constant.

Since the two catalyst systems are different, e.g. in compositions, volumes and catalyst loadings, differences in NO_x reductions could also be anticipated. At an exhaust temperature of 400 °C, catalyst systems appeared to operate rather similarly (with the same urea feeds), reaching NO_x reductions close to 95% (OXICAT-x performs even better in mode 1), and as anticipated, differences were observed at the other test temperatures. In standard SCR catalyst, the optimal operation window depends greatly, e.g. on the catalyst (vanadium) loading (e.g. [8, 17, 18]). High vanadium loading increases NO_x reduction at low temperatures, but the higher the vanadium loading is, the more the SCR also oxidizes NH_3 at high temperatures. For example, in a recent study of differently loaded vanadium SCR performance (in heavy fuel oil application), a rather similar NO_x efficiency was observed with all the tested catalyst loadings at 350–450 °C, but at lower temperatures, the highest loaded catalyst gave significantly better NO_x removal efficiency than the lower loaded catalysts [17].

The oxidation catalysts most probably also have an effect on the NO_2/NO ratio. Both increase and decrease of NO_2 over an oxidation catalyst have earlier been reported [28]. In each test of the present study, the SCR method was utilized simultaneously with the oxidation catalyst, resulting in very low NO_x levels downstream of the catalysts. Practically no NO_2 was measured downstream of either of the catalyst systems.

The CO levels downstream of both catalyst setups in all test conditions were low. The highest value, 15 ppm, still implying a CO reduction of 96.5% over the catalyst, was recorded downstream of 'OXICAT-x' in mode 2 with the lowest test temperature (350 °C). At temperatures of 400 °C and higher, the CO reduction over both catalyst systems was 98–99%.

The measured methane concentrations (in mode 1) are shown in Fig. 4 as a function of the exhaust temperature measured upstream of the oxidation catalyst (T_1 for MOC and T_2 for OXICAT-x—see setup figure). For both catalyst setups, three different exhaust temperature modes were studied, as well as a lower exhaust flow mode in one selected temperature case. The OXICAT-x was not designed for methane oxidation and therefore was not expected to have any effect on the methane levels. This was found to be true on the basis of the measurement since the OXICAT-x had practically no effect on methane in either of the studied exhaust temperatures or flows. The MOC + SCR, with the methane oxidation catalyst, had a minor decreasing effect on the methane at ~400 °C, but at ~500 °C, approximately 50% methane decrease was observed. Furthermore, the lower exhaust flow studied at 450 °C increased the methane conversion from 38% (measured with 80 kg/h exhaust flow) to 65% (with 40 kg/h).

In order to have a fair idea of how the present results fit in with earlier published laboratory-based studies, we make here some comparisons. It should however be kept in mind that, e.g. the noble metal loading and catalyst sizing can have a significant effect on catalyst performance, making the comparison of different studies difficult. Ottinger et al. [30] reported light-off curves for CH_4 over Pd-based oxidation catalyst with an initial T_{50} (the temperature for 50% conversion) value of 480 °C, and some lower light-off temperatures were reported by, e.g. Corro et al. [7], Venezia et al. [36] and Gelin et al. [9]. By comparison, the methane conversion result of 50%

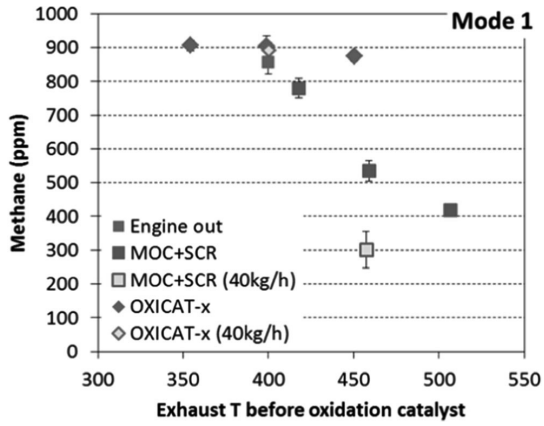

Fig. 4 Methane concentration as a function of exhaust temperature in mode 1

(present study, steady-state condition) required a higher temperature (i.e. 500 °C) than in the case of the T_{50} values reported earlier. However, the earlier studies have been carried out with simplified gas mixtures in laboratories and not with real exhaust gas as in the present study, which most probably had an effect on the results together with the differences in catalyst materials and amounts. Furthermore, the preconditioning procedure utilized in the present study (48 h) might have had a significant effect on the oxidation activity (the fresh catalyst was not measured in the present study).

The effect of sulphur on the methane oxidation catalyst performance can be crucial since as little as 1 ppm SO_2 present in the exhaust has already been found to inhibit the oxidation of methane (e.g. [16, 30]). In this study we did not observe any significant change in the catalyst performance during the tests. The possible SO_2 originates from the sulphur in natural gas and the lubricating oil. Assuming that all this sulphur (from gas and oil) ends up as SO_2, the SO_2 present in the exhaust gas would still be below 0.2 ppm in the driving modes of the present study. Furthermore, the test times in the present study were rather short, only tens of hours (after the 48-h preconditioning), which might be too short to observe any significant catalyst deactivation by the sulphur amount in the present study.

In addition to methane, other hydrocarbon species, i.e. ethane, propane and ethylene, were also studied. The ethane and propane concentrations as a function of exhaust temperature in mode 2 are presented in Fig. 5. The OXICAT-x started to oxidize these hydrocarbon species at the exhaust T of 450 °C, whereas at lower temperatures, practically no effect was found. At the same temperature (450 °C), the MOC, as expected, oxidized ethane and propane more effectively than OXICAT-x, and the oxidation also increased with the temperature increase (500 °C). At 450 °C, the ethane conversions were 37% with OXICAT-x and 65% with MOC, and the propane conversions were 75% with OXICAT-x and 88% with MOC. Thus, the alkane reactivity proceeds in the order $C_3H_8 > C_2H_6 > CH_4$, which is as was expected and similar to the observations of, e.g. Lambert et al. [16] and Ottinger et al. [30]. Ethylene was the easiest to oxidize, and practically no ethylene was measured downstream of either of the catalyst setups.

The engine out formaldehyde concentration was ~50 ppm in both driving modes. Downstream of MOC + SCR, the measured formaldehyde levels were below 1 ppm in all test conditions. Downstream of OXICAT-x, the highest formaldehyde level was measured in mode 2 with an exhaust T of 350 °C, resulting in ~3 ppm, whereas at higher temperatures, the measured formaldehyde level was below 2 ppm. This 1–2 ppm was also rather close to the measurement accuracy of the aldehyde measurement in the present study. Since formaldehyde is hazardous even in small concentrations, these 1–2 ppm levels (or even below) will possibly need a relevant measurement method in the near future.

3.1 Particles

One standard (ISO 8178) method was utilized to study the particle mass emission. Since the PM method measures the total mass, larger particles can contribute to the result much more than smaller ones (nanoparticles).

Engine out PM results had a rather high variation of 17% (standard deviation of four to five samples; Fig. 6). The effect of the catalysts was however obvious, and both catalyst systems clearly decreased the total PM in all test conditions. The PM reduction was of the order of 45–73%. Since catalysts commonly have a decreasing effect only on the volatile (organic) fraction of the PM mass, this alone indicates that a large part of the engine out PM is some volatile material present in the gaseous phase at the catalyst temperatures.

However, the PM results measured downstream of the catalysts appeared to correlate with the exhaust temperature as higher PM levels were measured at higher exhaust temperatures (with 'the mode 1 and 500 °C' case forming an exception to this pattern; see Fig. 6). Sulphate formation contributing to PM increase is seen over many catalysts (ammonium sulphates in the case of SCR) and could be one explanation for the PM increase with temperature increase, although in the present study the total amount of sulphur available from the fuel and oil was very low.

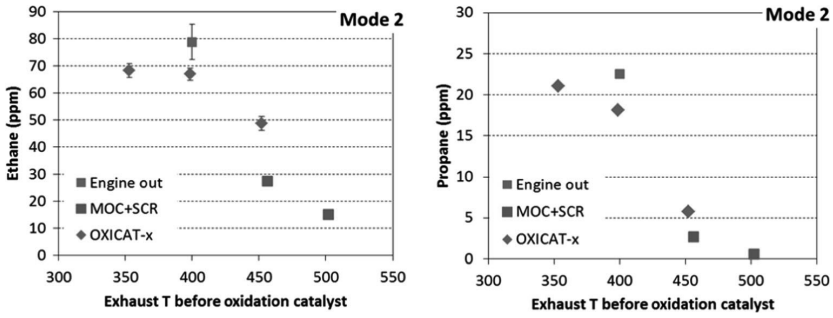

Fig. 5 Ethane and propane concentrations as a function of exhaust temperature (measured upstream of the oxidation catalysts) in mode 2

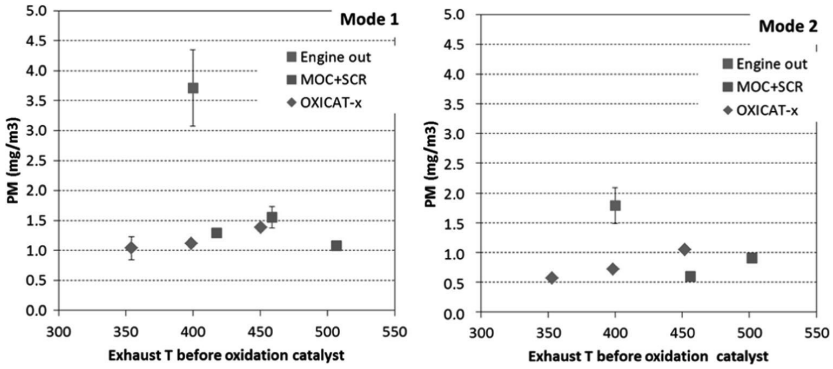

Fig. 6 PM emissions measured from engine out and downstream of the two catalyst systems in both driving modes and at all test temperatures

According to Alanen et al. [2], the particle number emissions of a natural gas engine are dominated by nanoparticles when the engine is not equipped with a catalyst or other exhaust after-treatment system. These nanoparticles, being even smaller than 5 nm in diameter, were reported to be initially formed already in high temperature conditions. In this study, the research engine was the same as in the study of Alanen et al. [2]. Only some very minor modifications were made to the engine. Engine out returned qualitatively similar results for particle number to those obtained previously (see Fig. 7); particle number size distribution was dominated by nanoparticles smaller than 10 nm, and especially the smallest particles were observed to be non-volatile. The thermodenuder treatment was observed to decrease the concentration of larger particles (diameter > 5 nm), shifting the mean particle size to a smaller level, which indicates that the particles also contained some semi-volatile compounds.

When the exhaust was sampled for particle measurements downstream from the catalyst, the exhaust temperature was observed to significantly affect the particle number (see Fig. 8) and number size distribution (Fig. 7). First, at the lowest temperature, the measured particle numbers were lower than those in the sample from upstream of the catalyst. The catalyst was observed to affect all particle sizes. However, the particle number was also dominated by nanoparticles downstream from the catalyst. When the exhaust temperature was increased, both the mean particle size and the particle number concentration (measured downstream from the catalyst) increased. At the highest temperature point (500 °C), the particle size distribution was dominated by particles larger than 10 nm

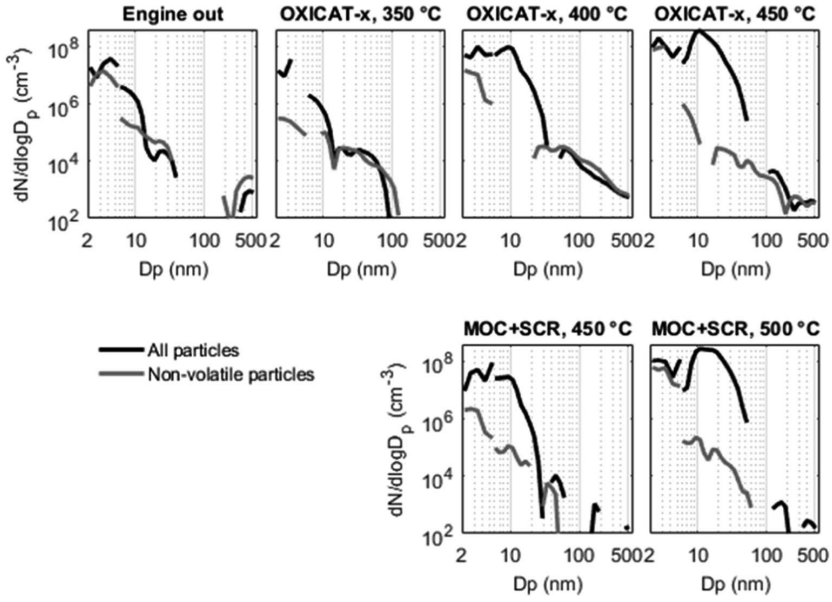

Fig. 7 Particle number size distributions upstream from the catalyst (engine out) and after the catalyst at different exhaust temperatures. Both the distributions measured without the thermodenuder (all particles) and with the thermodenuder (non-volatile particles) are shown. Size distributions were measured by the combination of PSM and CPC and by the EEPS in mode 2. Note: The discontinuity in the charts results from the low particle number concentrations and the subtracting of background levels, which can produce negative concentrations seen as a discontinuity in the logarithmic scale

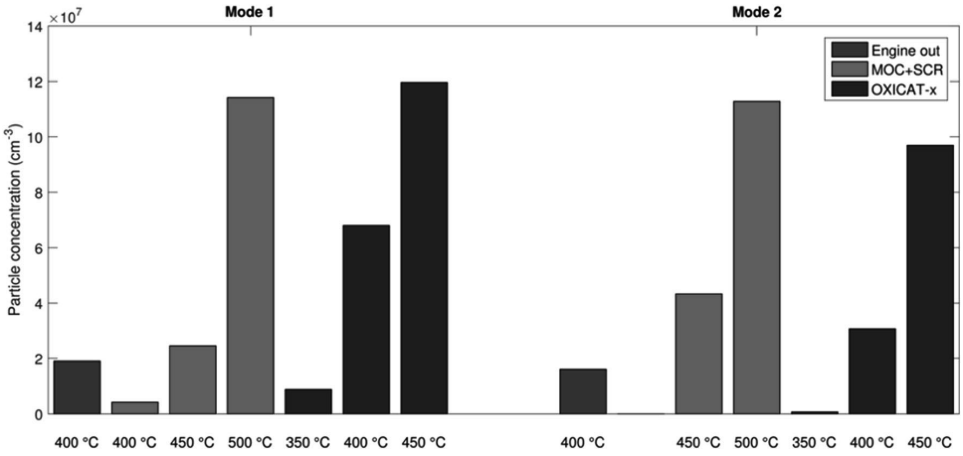

Fig. 8 Total particle number concentration of natural gas engine exhaust when the exhaust was sampled upstream from the catalyst (engine out) and after the catalyst. Particle concentrations were measured by the combination of PSM and CPC

and the total particle number (measured by PSM, particles larger than ~1 nm) was up to 20 times higher than the concentration at the lowest temperature point and more than five times higher than the particle number in the sample taken upstream from the catalyst.

The increase in particle number as a function of exhaust temperature was caused by volatile particles; the thermodenuder treatment for the exhaust sample totally removed the particle mode at 10 nm (Fig. 7). Based on previous studies, conducted mostly for diesel engines, the volatile exhaust particles have

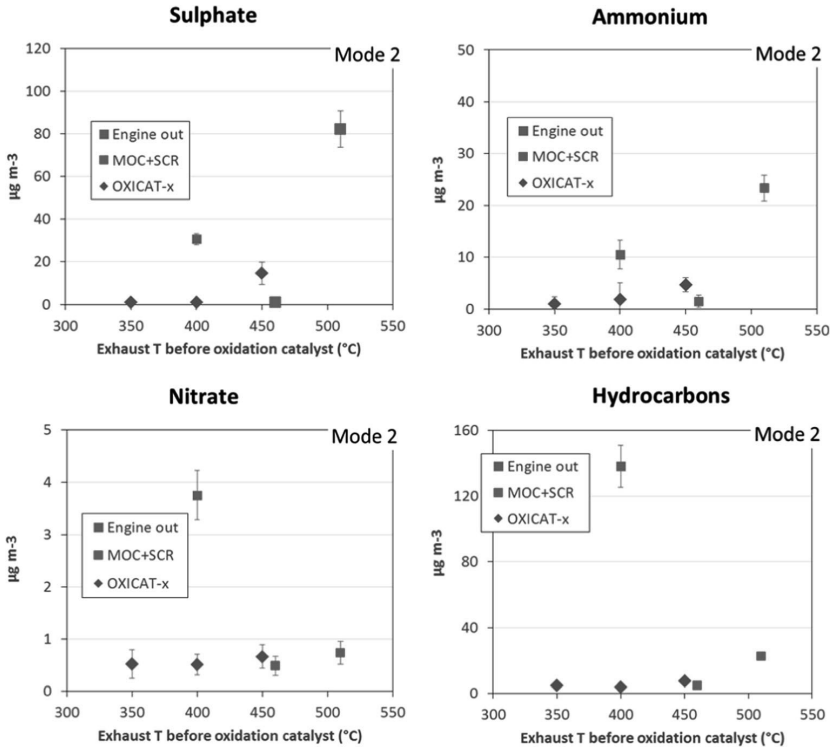

Fig. 9 Sulphate, ammonium, nitrate and hydrocarbon concentrations as a function of exhaust temperature (measured upstream of the oxidation catalysts) for mode 2

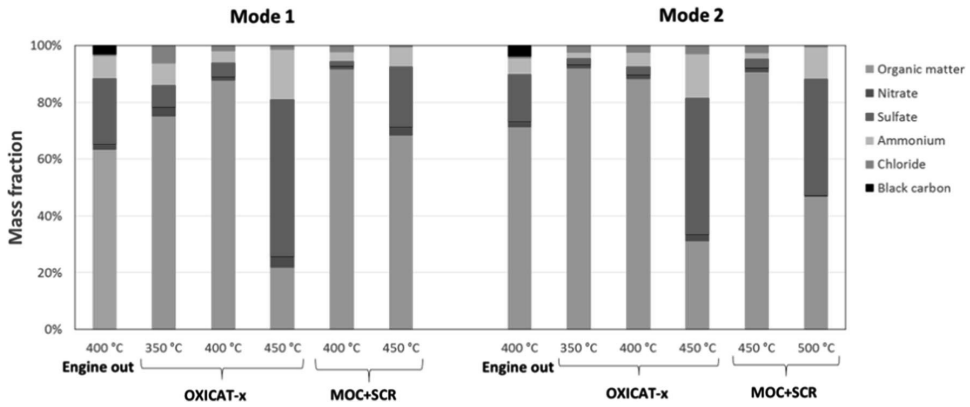

Fig. 10 Chemical compositions of particles at various measurement points

been observed to be formed during cooling and dilution of exhaust [15, 34], especially when the engine is equipped with an oxidative exhaust after-treatment device [13, 15, 21, 35]. One possible precursor for nanoparticle formation is sulphuric acid, which is present in the gaseous phase at typical exhaust temperatures and tends to nucleate in exhaust sampling systems (see, e.g. [26, 31]), forming new particles. However, organic acids have also been proposed to participate in this process [3]. The observations of this study are qualitatively similar to those of studies in which the role of sulphuric acid in particle formation has been measured; nanoparticles are volatile, they exist in the sample taken after the catalyst, and an increase of exhaust temperature increases particle concentration and size. The particle composition measurements (see the text below) support the notion that sulphur compounds may explain these observations.

Based on the SP-AMS results, the concentration of sulphate increased with higher catalyst temperature (Fig. 9). Sulphate was clearly higher at 450 °C for OXICAT-x and MOC + SCR in mode 1 and at 500 °C for MOC + SCR in mode 2. At an exhaust temperature ≤450 °C, the sulphate concentration measured downstream from the catalyst was lower than that measured upstream of the catalyst, but at 500 °C (MOC + SCR), it was more than double that measured upstream of the catalyst. Ammonium had similar temperature dependence to that of sulphate. Sulphate appeared to be mostly neutralized with ammonia as their ratio was close to that calculated for ammonium sulphate. Only at the highest catalyst temperatures (and sulphate concentrations) was there excess sulphate, suggesting that a part of the sulphate was in the form of sulphuric acid in particles. The amount of sulphuric acid ranged from 12 to 27% of the measured sulphate, corresponding to sulphuric acid concentrations of 2–22 μg m^{-3}. However, it should be noted here that the SP-AMS can detect particles only above ~50 nm in size, meaning that only the tail of the particle mode shown in the particle number size distributions of Fig. 7 was measured by the SP-AMS. In addition to sulphate and ammonium, nitrate concentration also increased with the catalyst temperature increase, although the catalysts decreased the concentration of nitrate by as much as 87% on average.

In addition to sulphate, ammonium and nitrate, particles contained organic matter, chloride and black carbon (Fig. 10). Excluding the measurement points with high sulphate concentrations, most of the particle mass consisted of organic matter. The concentration of organic matter had no clear dependence on the catalyst temperature, but the catalysts

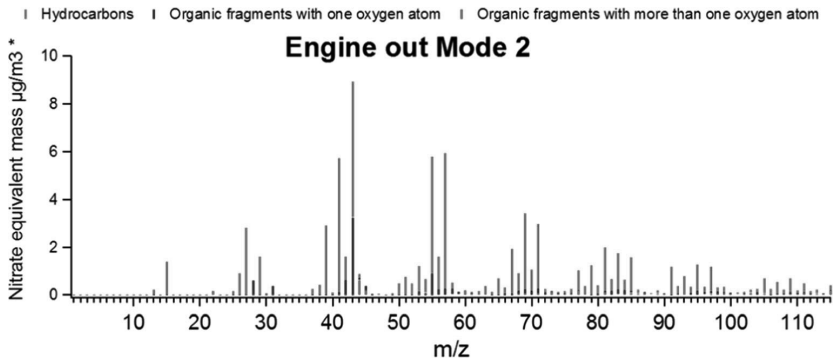

Fig. 11 Mass spectra for particulate organic matter measured without the catalysts in mode 2

reduced organic matter by, on average, 86% (OXICAT-x) and 55% (MOC-SCR). This is in good correlation with the PM results, showing that the total mass was clearly reduced by the catalysts. Chloride also showed no trend with the catalyst temperature, and the concentration of chloride was only slightly lower with the catalysts. Black carbon was observed to exist in the exhaust only in engine out measurements.

Organic matter in the gas engine emission particles was mostly composed of hydrocarbon fragments (Fig. 11). The largest hydrocarbon fragments according to the mass spectra (MS) of organic matter were $C_3H_5^+$ (at m/z 41), $C_3H_7^+$ (at m/z 43), $C_4H_7^+$ (at m/z 55) and $C_4H_9^+$ (at m/z 57), typical for, e.g. vehicle emissions (e.g. [4, 5]). Similar to sulphate, ammonium and nitrate, the sum of hydrocarbon fragments increased with the catalyst temperature (Fig. 8), but the catalyst decreased the concentration of hydrocarbons much more than those of inorganics. As well as the hydrocarbon fragments, there were some oxidized organic fragments, e.g. $C_2H_3O^+$ (at m/z 43) in the MS. In general, no change in the oxidation state of organics was observed as a result of the catalysts.

4 Conclusions

The growing trend in the use of natural gas (and also biogas) as energy sources enhances the sustainable use of natural resources and can lead to lower CO_2 levels. However, gas combustion is not emission-free. Emissions such as hydrocarbons, especially methane, and formaldehyde, NO_x and particles, all known to have effects on the environment and on human health, are found from natural gas exhausts. In order to deal with the more stringent emission legislation, after-treatment systems, such as catalysts, are increasingly utilized in natural gas applications. In the present study, we made a comprehensive emission study from a natural gas engine exhaust both upstream and downstream of two different catalyst systems in order to determine the effects of the catalysts on different emission components.

The SCR was found to be effective in reducing NO_x. In the present study, the SCR was utilized in two different ways: as a separate catalyst reactor downstream of an oxidation catalyst and integrated into an oxidation catalyst. For the integrated system, the oxidation reactions and NO_x reduction reactions were suggested to be competing with each other, resulting in lower NO_x efficiencies at high temperatures. This might imply limitations for utilization; however, this greatly depends on the required NO_x reduction as well as on the possibilities to further optimize the behaviour in different temperature windows. In real applications with, e.g. limited spaces and the need to control the expenses of the catalyst systems, this kind of system can be more attractive compared to two separate catalysts.

The results indicated that the oxidation catalyst developed for methane reduction can reach methane reduction levels better than 50% in real natural gas engine exhaust gas applications if the temperature is high and the catalyst sizing is correct. However, further studies are needed to solve the long-term performance and the possible deactivation by sulphur.

The particle emission studies indicated that nanoparticles dominate the particle number size distribution. Catalysts were found to have a significant influence on particle emissions. Downstream of the catalyst, the particle formation was found to depend greatly on the exhaust temperature. At higher temperatures, higher numbers of volatile nanoparticles were found, indicating that sulphur compounds are involved in the particle formation. The composition studies support this interpretation as more sulphate was observed at higher catalyst temperatures. Both the studied catalyst systems had a clearly decreasing effect on total particle mass emissions, which, together with the composition study results, indicates a decrease in the organics (hydrocarbons). This might be one more relevant issue in the future, with the growing environmental and human health concerns of particle emissions. Future research needs to include solving the origin of the particles (e.g. lubrication oil versus the natural gas) and the possibilities to control these particle emissions.

In addition to the present results, studies in real natural gas combustion applications, both vehicle and power plant applications, are needed in order to confirm the emission levels and the catalyst operation in real-world conditions. In addition to pure natural gas combustion applications, the results of the present study may also be important when planning biogas utilization, which is expected to grow significantly in the near future, and when considering the emissions from biogas engines. Further studies are needed in order to be able to develop suitable systems for biogas emissions since, e.g. biogas impurities may play a major role in the catalyst performance.

Acknowledgements The study was conducted in a research project funded by Tekes (Finnish Funding Agency for Technology and Innovation) and industrial partners: Wärtsilä Finland, Dinex Ecocat, Dekati, Neste, Suomi Analytics and AGCO Power. Sanna Saarikoski acknowledges the Academy of Finland (grant no. 259016). Jenni Alanen acknowledges Gasum kaasurahasto for financial support. The authors also thank Pekka Piimäkorpi at VTT for his contribution to the emission measurements and analyses.

Compliance with ethical standards The authors declare no competing financial interest.

References

1. Abdelaal, M.M., Hegab, A.H.: Combustion and emissions characteristics of a natural gas-fueled diesel engine with EGR. Energy Convers. Manag. **64**, 301–312 (2012)
2. Alanen, J., Saukko, E., Lehtoranta, K., Murtonen, T., Timonen, H., Hillamo, R., Karjalainen, P., Kuuluvainen, H., Harra, J., Keskinen, J., Rönkkö, T.: The formation and physical properties of the particle emissions from a natural gas engine. Fuel **162**, 155–161 (2015)

3. Arnold, F., Pirjola, L., Rönkkö, T., Reichl, U., Schlager, H., Lähde, T., Heikkilä, J., Keskinen, J.: First on-line measurements of sulphuric acid gas in modern heavy duty diesel engine exhaust: implications for nanoparticle formation. Environ. Sci. Technol. **46**, 11227–11234 (2012)
4. Canagaratna, M.R., Jayne, J.T., Ghertner, D.A., Herndon, S., Shi, Q., Jimenez, J.L., Silva, P.J., Williams, P., Lanni, T., Drewnick, F., Demerjian, K.L., Kolb, C.E., Worsnop, D.R.: Chase studies of particulate emissions from in-use New York City vehicles. Aerosol Sci. Technol. **38**, 555–573 (2004)
5. Chirico, R., Prevot, A.S.H., DeCarlo, P.F., Heringa, M.F., Richter, R., Weingartner, E., Baltensperger, U.: Aerosol and trace gas vehicle emission factors measured in a tunnel using an aerosol mass spectrometer and other on-line instrumentation. Atmos. Environ. **45**, 2182–2192 (2011)
6. Cho, H.M., He, B.-Q.: Spark ignition natural gas engines—a review. Energy Convers. Manag. **48**, 608–618 (2007)
7. Corro, G., Cano, C., Fierro, J.L.G.: A study of Pt-Pd/γ-Al_2O_3 catalysts for methane oxidation resistant to deactivation by sulfur poisoning. J. Mol. Catal. A Chem. **315**, 35–42 (2010)
8. Forzatti, P., Lietti, L.: Recent advances in De-NO_xing catalysis for stationary applications. Heterog. Chem. Rev. **3**, 33–51 (1996)
9. Gelin, P., Urfels, L., Primet, M., Tena, E.: Complete oxidation of methane at low temperature over Pt and Pd catalysts for the abatement of lean-burn natural gas fuelled vehicles emissions: influence of water and sulphur containing compounds. Catal. Today **83**, 45–57 (2003)
10. Heikkilä, J., Rönkkö, T., Lähde, T., Lemmetty, M., Arffman, A., Virtanen, A., Keskinen, J., Pirjola, L., Rothe, D.: Effect of open channel filter on particle emissions of modern diesel engine. J. Air Waste Manage. Assoc. **59**(10), 1148–1154 (2009)
11. Hesterberg, T.W., Lapin, C.A., Bunn, W.B.: A comparison of emissions from vehicles fuelled with diesel or compressed natural gas. Environ. Sci. Technol. **42**, 6437–6445 (2008)
12. Jayaratne, E.R., Ristovski, Z.D., Meyer, N., Morawska, L.: Particle and gaseous emissions from compressed natural gas and ultralow sulphur diesel-fuelled buses at four steady engine loads. Sci. Total Environ. **407**, 2845–2852 (2009)
13. Kittelson, D.B., Watts, W.F., Johnson, J.P., Thorne, C., Higham, C., Payne, M., Goodier, S., Warrens, C., Preston, H., Zink, U., Pickles, D., Goersmann, C., Twigg, M.V., Walker, A.P., Boddy, R.: Effect of fuel and lube oil sulfur on the performance of a diesel exhaust gas continuously regenerating trap. Environ. Sci. Technol. **42**, 9276–9282 (2008)
14. Koebel, M., Strutz, E.O.: Thermal and hydrolytic decomposition of urea for automotive selective catalytic reduction systems: thermochemical and practical aspects. Ind. Eng. Chem. Res. **42**, 2093–2100 (2003)
15. Lähde, T., Rönkkö, T., Virtanen, A., Schuck, T., Pirjola, L., Hämeri, K., Kulmala, M., Arnold, F., Rothe, D., Keskinen, J.: Heavy duty diesel engine exhaust aerosol particle and ion measurements. Environ. Sci. Technol. **43**, 163–168 (2009)
16. Lambert, J.K., Kazi, M.S., Farrauto, R.J.: Palladium catalyst performance for methane emissions abatement from lean burn natural gas vehicles. Appl. Catal. B Environ. **14**, 211–223 (1997)
17. Lehtoranta, K., Vesala, H., Koponen, P., Korhonen, S.: Selective catalytic reduction operation with heavy fuel oil: NO_x and NH_3, and particle emissions. Environ. Sci. Technol. **49**, 4735–4741 (2015)
18. Lietti, L., Nova, I., Forzatti, P.: Selective catalytic reduction of NO by NH_3 over TiO_2-supported V_2O_5-WO_3 and V_2O_5-MoO_3 catalysts. Top. Catal. **11**, 111–122 (2000)
19. Liu, J., Yang, F., Wang, H., Ouyang, M., Hao, S.: Effects of pilot fuel quantity on the emissions characteristics of a CNG/diesel dual fuel engine with optimized pilot injection timing. Appl. Energy **110**, 201–206 (2013)
20. Majewski, W.A., Khair, M.K.: Diesel emissions and their control. SAE International, Warrendale (2006)
21. Maricq, M.M., Chase, R.E., Xu, N., Laing, P.M.: The effects of the catalytic converter and fuel sulfur level on motor vehicle particulate matter emissions: light duty diesel vehicles. Environ. Sci. Technol. **36**, 283–289 (2002)
22. Mikkanen, P, Moisio, M, Keskinen, J, Ristimäki, J, Marjamäki, M.: Sampling method for particle measurements of vehicle exhaust. Society of Automotive Engineers (SAE) Technical Paper 2001-01-0219
23. Mitchell, C.E., Olsen, D.B.: Formaldehyde formation in large bore natural gas engines part 1: formation mechanisms. J. Eng. Gas Turbines Power **122**, 603–610 (2000)
24. Murtonen, T., Lehtoranta, K., Korhonen, S., Vesala, H., Koponen, P.: Imitating emission matrix of large natural gas engine opens new possibilities for catalyst studies in engine laboratory. CIMAC Pap. pp. 107 (2016)
25. Ntziachristos, L., Giechaskiel, B., Pistikopoulos, P., Samaras, Z., Mathis, U., Mohr, M., et al.: Performance evaluation of a novel sampling and measurement system for exhaust particle characterization. Society of Automotive Engineers (SAE) Technical Paper 2004-01-1439
26. Olin, M., Rönkkö, T., Dal Maso, M.: CFD modeling of a vehicle exhaust laboratory sampling system: sulfur-driven nucleation and growth in diluting diesel exhaust. Atmos. Chem. Phys. **15**, 5305–5323 (2015)
27. Olsen, D.B., Mitchell, C.E.: Formaldehyde formation in large bore natural gas engines part 2: factors affecting measured CH_2O. J. Eng. Gas Turbines Power **122**, 611–616 (2000)
28. Olsen, D.B., Kohls, M., Arney, G.: Impact of oxidation catalysts on exhaust NO_2/NO_x ratio from lean-burn natural gas engines. J. Air Waste Manage. Assoc. **60**, 867–874 (2010)
29. Onasch, T.B., Trimborn, A., Fortner, E.C., Jayne, J.T., Kok, G.L., Williams, L.R., Davidovits, P., Worsnop, D.R.: Soot particle aerosol mass spectrometer: development, validation, and initial application. Aerosol Sci. Technol. **46**, 804–817 (2012)
30. Ottinger, N., Veele, R., Xi, Y., Liu, Z. G.: Desulfation of Pd-based oxidation catalysts for lean-burn natural gas and dual-fuel applications. SAE Tech. Pap. Ser. 2015, SAE paper 2015-01-0991
31. Pirjola, L., Karl, M., Rönkkö, T., Arnold, F.: Model studies of volatile diesel exhaust particle formation: are organic vapours involved in nucleation and growth? Atmos. Chem. Phys. **15**, 10435–10452 (2015)
32. Pope III, C.A., Dockery, D.W.: Health effects of fine particulate air pollution: lines that connect. J. Air Waste Manag. Assoc. **56**, 709–742 (2006)
33. Ristovski, Z.D., Morawska, L., Hitchins, J., Thomas, S., Greenway, C., Gilbert, D.: Particle emissions from compressed natural gas engines. J. Aerosol Sci. **31**, 403–413 (2000)
34. Rönkkö, T., Lähde, T., Heikkilä, J., Pirjola, L., Bauchke, U., Arnold, F., Rothe, D., Yli-Ojanperä, J., Keskinen, J.: Effects of gaseous sulphuric acid on diesel exhaust nanoparticle formation and characteristics. Environ. Sci. Technol. **47**, 11882–11889 (2013)
35. Vaaraslahti, K., Virtanen, A., Ristimäki, J., Keskinen, J.: Nucleation mode formation in heavy-duty diesel exhaust with and without a particulate filter. Environ. Sci. Technol. **38**, 4884–4890 (2004)
36. Venezia, A.M., Di Carlo, G., Pantaleo, G., Liotta, L.F., Melaet, G., Kruse, N.: Oxidation of CH_4 over Pd supported on TiO_2-doped SiO_2: effect of Ti(IV) loading and influence of SO_2. Appl. Catal. B **88**, 430–437 (2009)
37. Yim, S.D., Kim, S.K., Baik, J.B., Nam, I.-S., Mok, Y.S., Lee, J.-H., Cho, B.K., Oh, S.H.: Decomposition of urea into NH_3 for the SCR process. Ind. Eng. Chem. Res. **43**, 4856–4863 (2004)

PAPER 4

Comparison of primary and secondary particle formation from natural gas engine exhaust and of their volatility characteristics

Alanen, J., Simonen, P., Saarikoski, S., Timonen, H., Kangasniemi, O., Saukko, E., Hillamo, R., Lehtoranta, K., Murtonen, T., Vesala, H., Keskinen, J. and Rönkkö, T.

Atmospheric Chemistry and Physics 17.(2017), 8739–8755
DOI: 10.5194/acp-17-8739-2017

Atmos. Chem. Phys., 17, 8739–8755, 2017
https://doi.org/10.5194/acp-17-8739-2017

Atmospheric Chemistry and Physics Open Access EGU

Comparison of primary and secondary particle formation from natural gas engine exhaust and of their volatility characteristics

Jenni Alanen[1], Pauli Simonen[1], Sanna Saarikoski[2], Hilkka Timonen[2], Oskari Kangasniemi[1], Erkka Saukko[1], Risto Hillamo[2], Kati Lehtoranta[3], Timo Murtonen[3], Hannu Vesala[3], Jorma Keskinen[1], and Topi Rönkkö[1]

[1]Aerosol Physics, Faculty of Natural Sciences, Tampere University of Technology, P.O. Box 692, Tampere, Finland
[2]Atmospheric Composition Research, Finnish Meteorological Institute, P.O. Box 503, Helsinki, Finland
[3]VTT Technical Research Centre of Finland Ltd., P.O. Box 1000, Espoo, Finland

Correspondence to: Topi Rönkkö (topi.ronkko@tut.fi)

Received: 26 January 2017 – Discussion started: 8 February 2017
Revised: 15 May 2017 – Accepted: 6 June 2017 – Published: 18 July 2017

Abstract. Natural gas usage in the traffic and energy production sectors is a growing trend worldwide; thus, an assessment of its effects on air quality, human health and climate is required. Engine exhaust is a source of primary particulate emissions and secondary aerosol precursors, which both contribute to air quality and can cause adverse health effects. Technologies, such as cleaner engines or fuels, that produce less primary and secondary aerosols could potentially significantly decrease atmospheric particle concentrations and their adverse effects. In this study, we used a potential aerosol mass (PAM) chamber to investigate the secondary aerosol formation potential of natural gas engine exhaust. The PAM chamber was used with a constant UV-light voltage, which resulted in relatively long equivalent atmospheric ages of 11 days at most. The studied retro-fitted natural gas engine exhaust was observed to form secondary aerosol. The mass of the total aged particles, i.e., particle mass measured downstream of the PAM chamber, was 6–268 times as high as the mass of the emitted primary exhaust particles. The secondary organic aerosol (SOA) formation potential was measured to be 9–20 mg kg_{fuel}^{-1}. The total aged particles mainly consisted of organic matter, nitrate, sulfate and ammonium, with the fractions depending on exhaust after-treatment and the engine parameters used. Also, the volatility, composition and concentration of the total aged particles were found to depend on the engine operating mode, catalyst temperature and catalyst type. For example, a high catalyst temperature promoted the formation of sulfate particles, whereas a low catalyst temperature promoted nitrate formation. However, in particular, the concentration of nitrate needed a long time to stabilize – more than half an hour – which complicated the conclusions but also indicates the sensitivity of nitrate measurements on experimental parameters such as emission source and system temperatures. Sulfate was measured to have the highest evaporation temperature, and nitrate had the lowest. The evaporation temperature of ammonium depended on the fractions of nitrate and sulfate in the particles. The average volatility of the total aged particles was measured to be lower than that of primary particles, indicating better stability of the aged natural gas engine-emitted aerosol in the atmosphere. According to the results of this study, the exhaust of a natural gas engine equipped with a catalyst forms secondary aerosol when the atmospheric ages in a PAM chamber are several days long. The secondary aerosol matter has different physical characteristics from those of primary particulate emissions.

1 Introduction

Primary aerosol particles are directly emitted into the atmosphere by various anthropogenic sources, such as vehicles, engines and power plants, and biogenic sources. Secondary aerosol particle mass forms as a consequence of the atmospheric oxidation of emitted precursor gases. In this process, the saturation vapor pressure of the organic and inorganic gases becomes lower, thus allowing them to transfer into particle phase through condensation and nucleation (Hallquist et al., 2009; Murphy et al., 2014). In addition to biogenic sources, also traffic and other anthropogenic sources con-

tribute to secondary aerosol formation (Kanakidou et al., 2005).

Fine particles ($< 2.5\,\mu m$) are found to cause adverse health effects and premature mortality in people (Dockery and Pope III, 1994; Lelieveld et al., 2015). The relative contribution of primary and secondary particles to these health effects is still unknown, but there are indications that secondary particles can be even more hazardous than primary particles (Künzi et al., 2015; McWhinney et al., 2011; Rager et al., 2011). Therefore, both primary and secondary particle emissions must be taken into consideration when evaluating the health effects of particle emissions.

Aerosols play an important role in the climate as well. Fine particles in the atmosphere affect the radiative balance of the atmosphere by either warming or cooling it, depending on their properties (Myhre et al., 2013); however, large uncertainties remain regarding the contribution of particles to climate change and its prevention. Clouds also contribute to the atmosphere's radiative balance. Aging of an aerosol can lead to increased hygroscopicity of the particles (Kanakidou et al., 2005) and a higher likelihood that they act as cloud condensation nuclei. The preservation and lifetime of the particles in the atmosphere partly define how large their impact is on the climate.

The formation process of secondary inorganic aerosol can be modeled rather accurately because the number of different inorganic precursors is small and their oxidation reactions are well known. Secondary organic aerosol (SOA) is a more complex subject area due to the vast number of different organic compounds, their potential reactions and the still unknown participation of all compounds in secondary aerosol formation (Hallquist et al., 2013; Jimenez et al., 2009). SOA has been a hot topic in aerosol science during the past decade (Huang et al., 2014; Robinson et al., 2007; Virtanen et al., 2010), but there are still many open questions in considering, for example, the SOA formation from vehicle emissions (Gentner et al., 2017). Also, the relative fractions of secondary organic and inorganic aerosol from various emission sources still need to be studied. Both secondary organic and secondary inorganic aerosol can contribute significantly to air quality deterioration (Huang et al., 2014).

Particle number and mass emission regulations for passenger cars and heavy-duty engines have substantially decreased the primary particle emissions from vehicles (e.g., May et al., 2014; Johnson, 2009). Secondary particle precursor emissions or secondary aerosol formation potential are not directly regulated, but some of the current emission regulations affect secondary particle precursor emissions indirectly. For instance, oxidative catalysts reduce the total hydrocarbon emissions and thus probably the emissions of secondary organic aerosol precursors; simultaneously, they also change the oxidation state of inorganic compounds. Furthermore, the mandatory national targets of 10 % biofuel (ethanol) in gasoline in EU may have decreased the SOA formation in the atmosphere (Timonen et al., 2017). In general, vehicles emit a substantial fraction of anthropogenic precursors for SOA formation (Gentner et al., 2017), and the amount of potential SOA often exceeds the emissions of primary organic aerosol. For instance, gasoline vehicles emit 9–15 times or even 2 orders of magnitude higher secondary organic particulate matter than primary organic particle mass (Karjalainen et al., 2016; Nordin et al., 2013; Platt et al., 2013; Tkacik et al., 2014). Indeed, Bahreini et al. (2012) found that secondary organic aerosol originating from gasoline engines forms the majority of the SOA in and downwind of large metropolitan areas. From diesel vehicles without a particle filter, the SOA mass formation potential is of the same magnitude as or lower than the primary particle mass emission (Jathar et al., 2017; Gordon et al., 2014b; Weitkamp et al., 2007).

Exhaust after-treatment can reduce secondary aerosol formation potential from engine exhaust, especially SOA formation potential. In general, diesel fuel has the strongest secondary organic aerosol formation potential amongst diesel, jet fuel, gasoline and the Fischer–Tropsch fuels from natural gas (NG) and coal (Jathar et al., 2013). However, diesel vehicles equipped with oxidation catalysts or catalytic particle filters have been reported to be minor secondary particle emitters (Chirico et al., 2010; Gordon et al., 2014b; Samy and Zielinska, 2010). In gasoline engine functioning, exhaust after-treatment can also clearly reduce secondary particle formation (Karjalainen et al., 2016). The secondary aerosol precursor emissions of engines and vehicles are also strongly dependent on the driving conditions, which should be taken into account in emission comparisons.

For instance, Tkacik et al. (2014) showed that the secondary inorganic mass often exceeds the amount of the secondary organic aerosol in a highway tunnel, even by a factor of 2. The main contributor to secondary inorganic aerosol in their study was ammonium nitrate, which originates from NO_x and ammonia emissions. According to Karjalainen et al. (2016), large fractions of nitrate in the secondary inorganic particles are characteristic for highway driving, and the inorganic species concentrations are relatively low when compared with the secondary organic aerosol formed during other parts of the New European Driving Cycle (NEDC), which they tested. Idling is another engine operation mode that can produce significant amounts of secondary inorganic aerosol from gasoline vehicle exhaust (Nordin et al., 2013).

Natural gas usage as a fuel in combustion engines, both in energy production and traffic, is a growing trend worldwide. Natural gas engines emit little primary particle mass and less CO_2 than engines fueled with conventional fuels (Anderson et al., 2015; Bielaczyc et al., 2014) but their particle number emission can be significant (Hallquist et al., 2013; Jayaratne et al., 2010). In addition, the size of the majority of the particles emitted by natural gas engines can be below the detection limits of traditional exhaust particle measurement devices (Alanen et al., 2015). Natural gas engine exhaust particles are highly volatile (Bullock and Olfert, 2014; Jayaratne et al., 2012) or they can consist of volatile mat-

ter condensed on non-volatile cores (Alanen et al., 2015; Graves et al., 2015; Pirjola et al., 2016). The evaporation of the particles is largest at temperatures below 100 °C (Alanen et al., 2015; Jayaratne et al., 2012). Primary particles from natural gas engines mainly consist of organic matter (Pirjola et al., 2016), but the composition depends on exhaust after-treatment (Lehtoranta et al., 2017). In the study of Lehtoranta et al. (2017), high catalyst temperatures were found to increase the fraction of sulfate in particles when a combination of oxidative and reductive catalysts was employed. Also, increased ammonium concentrations were found in particles at high catalyst temperatures.

To the authors' knowledge, there are no published studies on secondary particle formation from natural gas engine emissions, its chemical or physical properties or the effect of exhaust after-treatment on exhaust's secondary particle formation. Goyal and Sidhartha (2003) recorded a notable improvement in the air quality of Delhi when a portion of vehicles were changed to natural gas vehicles in 2001. In our study, the secondary aerosol formation potential of natural gas engine exhaust was investigated using a flow-through reactor, and the chemical and physical characteristics of particles were investigated by aerosol instruments. The results were compared to those of primary particle emissions, but because the primary particle emissions of the same engine have already been discussed in two earlier publications (Alanen et al., 2015; Lehtoranta et al., 2017), they are not a focus of this paper. In general, the aim of this study is to report the total particulate emissions of natural gas engines, i.e., primary and secondary particles, to ensure that shifting to natural gas from diesel and gasoline will not cause unexpected environmental or health issues, and to define the possible benefits of the shift. Volatility studies on both primary and secondary particles enabled an evaluation of the stability and residence time of the particles in the atmosphere. The study of chemical composition can help solve their origin and find ways to reduce the particulate emissions.

2 Methods

2.1 Engine and after-treatment

A small (2.0 L displacement) spark-ignited passenger car engine was used for the measurements with Russian pipeline natural gas as fuel. The methane content of the fuel was 97 %, other hydrocarbon content was 1.6 % and nitrogen content was 0.9 %. The sulfur content was below 1 ppm. The engine was run at two steady-state engine operation modes with torque of 70 Nm and speed of 2700 rpm (mode 1, M1) and torque of 35 Nm and speed of 3100 rpm (mode 2, M2). In engine mode 2, short-chain hydrocarbons were added into the exhaust to make it resemble the exhaust of a power plant NG engine. The exhaust gas composition in two operation modes simulated typical natural gas power plant exhaust gas composition. The engine, natural gas and lubricating oil properties as well as the engine operation modes have been described in more detail by Murtonen et al. (2016), Alanen et al. (2015) and Lehtoranta et al. (2017).

Two separate after-treatment systems were applied in the measurements, both consisting of a reductive and an oxidative section. The after-treatment has been described in more detail by Lehtoranta et al. (2017). The first catalyst (catalyst 1, C1) consisted of only one reactor, which targeted both oxidation of carbon compounds and NO_x reduction through urea injection in the same catalyst reactor. The second catalyst system (catalyst 2, C2) consisted of a palladium- and platinum-containing methane oxidation catalyst followed by urea injection and a vanadium-SCR (selective catalyst reduction) catalyst, which were supported on metallic honeycomb substrates. Catalyst 1 was used in three different exhaust temperatures in the range of 350–450 °C in order to study its performance and its influence on secondary particle formation potential of the engine exhaust. The temperature of the catalyst 2 was 500 °C. Catalyst performance depends on the exhaust temperature (e.g., Lehtoranta et al., 2017). By using the catalysts at different temperatures, effects of catalyst temperature on the formation and characteristics of primary and total aged particulate matter could be studied. The catalyst temperatures were measured upstream of the oxidation catalysts. The temperature prior to the SCR of catalyst 2 was approximately 50 °C lower than prior to the oxidation catalyst. The exhaust flow through the catalysts was kept constant at 80 kg h^{-1} by leading only a part of the exhaust gas flow through them (Murtonen et al., 2016).

2.2 Instrumentation and data analysis

The sampling system or the particle measurement instruments consisted of a porous tube diluter (PTD, Mikkanen et al., 2001; Ntziachristos et al., 2004) with a dilution ratio (DR) of 6, followed by a residence time chamber with a residence time of 6 s. The low primary dilution ratio was used because of the very low primary particle emission concentrations (see Alanen et al., 2015). The dilution air was heated to 30 °C to achieve constant dilution conditions. A second dilution stage was carried out with an ejector diluter (Dekati Ltd.) with DR 4. The dilution ratio over the PTD was adjusted using a bypass flow mass flow controller placed downstream of the residence time chamber (Fig. 1). The dilution ratios were calculated from CO_2 concentrations in the raw and diluted exhaust samples and they could be used to calculate tailpipe concentrations of particle emissions. The aerosol sampling was done downstream of the exhaust after-treatment system.

A potential aerosol mass (PAM) chamber (Kang et al., 2007, 2011; Lambe et al., 2011, 2015) was used to simulate the aging process of an aerosol in the atmosphere. In the PAM, an oxidative environment (O_3, OH and HO_2, UV light) was produced using two UV lamps emitting 185 and 254 nm radiation, respectively, in a small (13 L) flow-through cham-

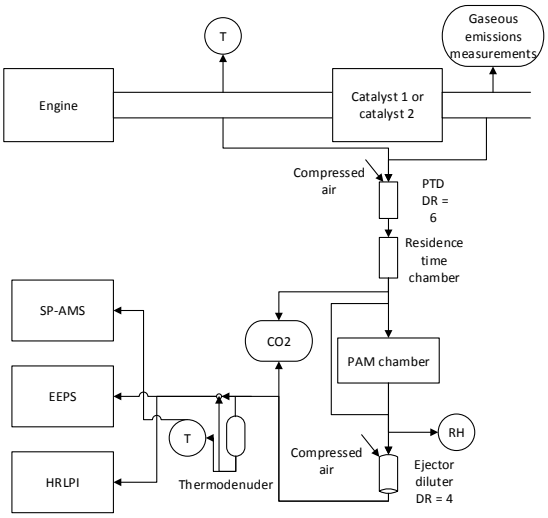

Figure 1. A schematic picture of the measurement setup.

ber. The PAM chamber was placed between the two dilution stages, and the flow through it was a constant 5 L min^{-}1 (residence time 156 s), measured by a bubble flow meter (Gilibrator, Sensidyne Inc.) and adjusted by a pressure regulator of the compressed air flow to the ejector diluter. The PAM chamber could be either bypassed or used to measure the properties of primary and secondary aerosols, respectively.

The approximate atmospheric age, i.e., the photochemical age simulated by the PAM chamber UV lights, was modeled using the properties of the PAM chamber and the measured concentrations of gaseous components that cause external OH reactivity in the chamber. The model used for calculating the OH exposures was based on the degradation mechanism extracted from the Master Chemical Mechanism or MCM v3.3.1 (Jenkin et al., 1997, 2003; Saunders et al., 2003) via the website http://mcm.leeds.ac.uk/MCM and translated to Matlab code using the kinetic preprocessor or KPP (Damian et al., 2002). The model has been tested against SO_2 reduction measurements in the PAM chamber.

MCM is a near-explicit chemical mechanism that describes the atmospheric degradation of volatile organic compounds in gas phase. MCM describes the degradation of a given volatile organic compound (VOC) through different generations of products until CO_2 is ultimately formed. It contains about 17 000 reactions for 6700 different species (Jenkin et al., 1997, 2003; Saunders et al., 2003). To be able to use these mechanisms with the PAM chamber, the photolysis rates have been calculated for ultraviolet light with wavelengths of 185 and 254 nm. The absorption cross section and quantum yield values needed for this are IUPAC recommendations (Atkinson et al., 2007) supplemented with the Jet Propulsion Laboratory (JPL) data evaluation number 18 (Burkholder et al., 2015) when necessary. Some photolysis reactions that are relevant to the PAM chamber but missing from the tropospheric MCM schemes have also been added.

KPP is a software tool for translating kinetic chemical mechanisms into Fortran 77, Fortran 90, C or MATLAB simulation code. The generated code produces concentrations of each species present as a function of time (Damian et al., 2002). For the model used, the KPP source code was modified to fix certain conflicts involving the MCM mechanism and the photolysis rate calculations written for the PAM chamber, as well as to allow large chemical schemes typical to MCM.

In this paper, we describe the PAM OH exposure as photochemical age, which is the equivalent time in the atmosphere in which the sample would reach the same OH exposure as in the PAM chamber. Thus,

$$\text{Photochemical age (days)} = \frac{\text{OH exposure}}{1.5\times10^{6}\,\text{molec cm}^{-3}}\frac{1}{3600\,\text{h}^{-1}\,\text{s}\times24\,\text{d}^{-1}\,\text{h}}, \quad (1)$$

where 1.5×10^{6} molec cm^{-3} is the average OH concentration in the atmosphere (Mao et al., 2009).

Relative humidity (RH) was measured downstream of the PAM chamber. The RH was high, about 80 %, due to the low primary dilution ratio that was applied during the experiments. The high RH of the sample complicated the evaluation of the PAM background mass levels – i.e., the particulate mass that was generated by only compressed air and UV lights – because the high RH could not be reproduced in the compressed air by the available instrumentation. The background levels were measured using both dry compressed air and compressed air with RH $\sim$ 30 %.

NO_x concentration was measured with a chemiluminescence detector (CLD), CO and CO_2 concentrations in raw exhaust were measured with a non-dispersive infrared (NDIR) analyzer and CO_2 concentrations in diluted exhaust were measured with a Sick Maihak SIDOR gas analyzer. Water, methane, NH_3, HNCO and the ratio of NO and NO_2 were measured with a Fourier transform infrared spectroscopy (FTIR, Gasmet Cr-2000) analyzer, and methane, ethane, propane and ethylene were measured with a gas chromatograph (GC).

Aerosol instruments covered a large range of particle mobility and aerodynamic size as well as measurements of the particles' chemical composition. An engine exhaust particle sizer (EEPS, TSI Inc., Mirme, 1994) and a high-resolution low-pressure impactor (HRLPI, Arffman et al., 2014) were employed, both on 1 s time resolution, to measure the particle number, mass and size. The EEPS measures the size distribution and concentration of particles with a mobility diameter of 5.6–560 nm, and the HRLPI measures the aerodynamic size distribution of particles with diameter of $\sim$ 5–200 nm. The mass of the particles was calculated under assumptions

of unit density and spherical particles. EEPS default inversion was applied.

A soot particle aerosol mass spectrometer (SP-AMS, Aerodyne Research Inc., US) – a combination of a high-resolution time-of-flight aerosol mass spectrometer and a single particle soot photometer (Droplet Measurement Technologies) – was used to measure the chemical composition and oxidative state of the aerosol sample. The SP-AMS measures both refractory and non-refractory particulate matter. It operated in V mode with a 1 min time resolution, measuring half of the time in mass spectra (MS) mode and the other half in particle size (pToF) mode. Both laser and tungsten vaporizers were used. The collection efficiency applied in the calculations was calculated using the parameterization by Middlebrook et al. (2012). The CO_2 gas interference in the AMS data was corrected by using the CO_2 concentrations measured with the Sick Maihak SIDOR gas analyzer. The impact of ammonium nitrate interference on CO_2^+, O : C and H : C ratios was evaluated to be small (less than 5 % for O : C and H : C; Pieber et al., 2016). Therefore, a correction of ammonium nitrate interference was not applied for organics or O : C data.

Volatility measurements were made with a thermodenuder (TD) described in the publication by Heikkilä et al. (2009). When the remaining mass of particles was measured as a function of TD temperature, the thermodenuder was heated up to 265 °C and then switched off, with the sample flow still flowing through it. The decreasing temperature was recorded for at least half an hour until the temperature was below 50 °C.

Emission factors were calculated from fuel composition and engine performance information. Residual O_2 in the exhaust was 6.2–6.3 %, the power of the engine was 12 and 20 kW and the combustion air flow into the engine was approximately 100 and 115 $kg\,h^{-1}$ in engine modes 1 and 2, respectively. Calculated from the fuel composition information, the emission factor for CO_2 EF_{CO_2} was 2730 $g\,kg_{fuel}^{-1}$, and the carbon intensity was 0.74 $kg_C\,kg_{fuel}^{-1}$.

3 Results and discussion

3.1 Secondary particle formation and chemical composition

The concept "total aged" here comprises all particle mass measured downstream of the PAM chamber, i.e., both primary and secondary particle mass. In general, primary particle mass has not been subtracted from the mass measured downstream of the PAM (total aged) to calculate the secondary particle mass separately because doing so would have created inconsistency in representation of the results, since, for example, particle size distributions or volatility behavior cannot be presented in this way. For the same reasons, the PAM background mass – i.e., the particle mass generated in the PAM chamber from clean compressed air – has not been subtracted but is instead presented separately in the Supplement of this paper. To enable a comparison to literature, an exception is made when presenting secondary particle production factors (PFs).

Figure 2 contains particulate mass measurement results derived from the three aerosol instruments. The chemical compositions from SP-AMS are also presented. The cases (engine mode, catalyst and catalyst temperature) included in this paper cover all of the tested exhaust temperatures and both engine operation modes, and they have data collected with all available instruments of both the primary and total aged aerosol measurements. In most cases in our measurements, primary exhaust particle mass concentrations from the natural gas engine were close to the detection limits of the instruments EEPS, HRLPI and SP-AMS (Alanen et al., 2015; Lehtoranta et al., 2017). Exceptions were made by the high temperature catalyst cases (M2, C2, 500 °C and M2, C1, 450 °C) during which more primary particle mass was formed, especially on the size ranges of the HRLPI and EEPS: a high catalyst temperature favors the conversion of SO_2 into SO_3 and further into sulfuric acid, which can nucleate and condense on existing particles in the sampling process or when released into the atmosphere (see, e.g., Arnold et al., 2012; Rönkkö et al., 2013). The primary particle formation phenomena and concentrations have been discussed in more detail in Lehtoranta et al. (2017) while this paper focuses on secondary aerosol formation and the total aged particle emissions.

The formed secondary particle mass concentrations were found to be significantly high in comparison with the primary particle mass emissions. In all of the investigated cases, particle mass increased when the sample was led through the PAM chamber. The increase in mass could be magnitudes larger than the primary particle mass emission (Table 1). The relative increase in mass in the PAM chamber could not be specified for all of the HRLPI measurements because of the very low primary particle mass. The total aged aerosol mass produced by natural gas engine exhaust was 0.99–2.6 $mg\,m^{-3}$ according to SP-AMS, leading to secondary mass production of 0.96–2.5 $mg\,m^{-3}$.

The secondary aerosol formation – i.e., the ratio of the total aged particulate mass to the primary particulate mass – was lower in the cases that already produced more primary particle mass, i.e., in the cases with a high catalyst temperature. It is possible that if the catalyst conditions are favorable, the particulate matter that would otherwise condense on particles in the PAM chamber condenses on the particle phase already in the cooling and dilution processes. In other words, if the catalyst sufficiently oxidizes the exhaust gases, thus lowering their saturation vapor pressure, they condense or nucleate already when released from the tailpipe and not later on in the atmosphere. A high catalyst temperature promoted larger total aged aerosol formation, according to the EEPS and HRLPI measurements. However, the total aged

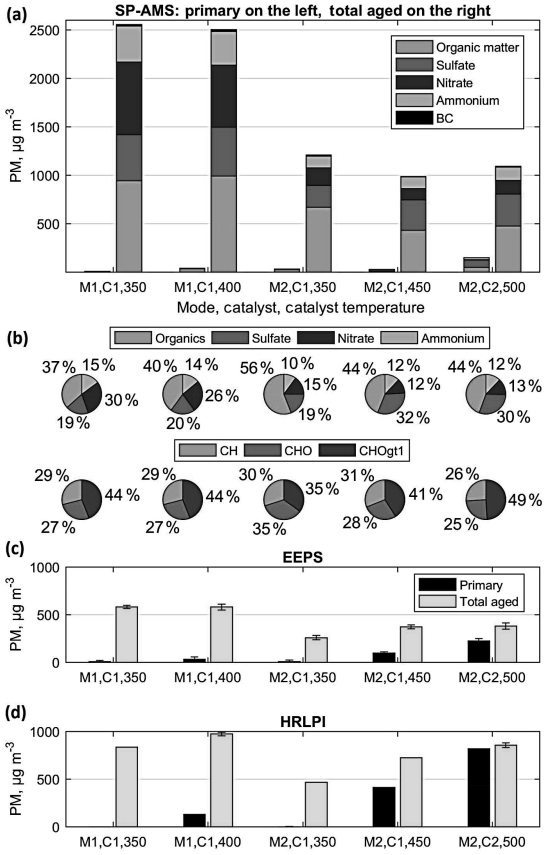

Figure 2. Exhaust primary and total aged particle mass concentrations measured by **(a)** SP-AMS, **(c)** EEPS and **(d)** HRLPI at different engine modes and catalyst temperatures. All values have been corrected by dilution ratio used in the sampling system. Secondary particle mass can be calculated by subtracting primary from total aged emission. The composition of the total aged particulate matter and the organic particulate matter is presented as pie charts **(b)**. The fraction of black carbon is less than or equal to 1 % and therefore left out from the pie charts.

mass concentrations of the SP-AMS did not increase as catalyst temperature increased. The differences in the instruments' showings are discussed in Sect. 3.3. Also, the variation in the atmospheric ages increases uncertainty in the comparison of the catalyst temperature on secondary aerosol formation potential.

The total aged aerosol of the natural gas engine exhaust consisted of both organic and inorganic matter at the tested operating conditions (Fig. 2, Table 1). Approximately half of the total aged aerosol particle mass detected by SP-AMS consisted of organic matter. The fraction of sulfate and nitrate was measured to be 34–49 % in total, with their ratio depending on the case, and the fraction of ammonium varied between 10 and 15 %. Link et al. (2017) found that even high NO_x emissions can produce negligible amounts of secondary nitrate aerosol if related ammonia emissions are small. Because secondary ammonium nitrate aerosol formation is limited by ammonia, its formation is probably more related to the exhaust after-treatment than the fuel. The exact ammonia concentrations in the raw exhaust cannot be given because they were below the instrument detection limit of 2 ppm. According to these measurements, also low ammonia emissions may have atmospheric importance as secondary inorganic aerosol precursors.

The organic fraction of the total aged aerosol consisted of hydrocarbon fragments (C_xH_y), fragments with one oxygen atom (C_xH_yO) and fragments with more than one oxygen atom ($C_xH_yO_{z,z>1}$); there was little or no C_xH_yN fragments (hydrocarbons with nitrogen) in the total aged particles. The main secondary organic ions detected by the SP-AMS were CO_2^+, CHO^+ and $C_2H_3O^+$. The composition of the organic aerosol was similar in all of the cases: the $C_xH_yO_{z,z>1}$ group was the largest, followed by C_xH_y and C_xH_yO. The source of the secondary organic aerosol could be either the natural gas or the lubricating oil. However, we are not able to tell the source based on these measurements. The fuel mainly consisted of light hydrocarbons that are unable to form secondary organic aerosol (e.g., Seinfeld and Pandis, 2016, pp. 575). For example, Thiruvengadam et al. (2014) and Eichler et al. (2017) have suspected engine lubricating oil to be responsible for a large portion of engine-emitted particles. Therefore, we believe that also lubricating oil is a potential candidate for the source of secondary aerosol.

The O : C ratios of the total aged aerosol measured by SP-AMS were between 0.9 and 1.2. The O : C ratio of the primary aerosol in the case with the largest concentration was slightly smaller (1.1) than the O : C ratio of the total aged aerosol in the same case (M2, C2, 500 °C). In all of the other primary aerosol measurements, the particle mass concentrations in the sample were too low for O : C ratio analysis. In comparison with a secondary aerosol emission study on gasoline engines by Karjalainen et al. (2016), the observed O : C ratios in the total aged aerosol from the PAM chamber were rather high.

The emission factors or secondary aerosol production factors in different units can be calculated from the presented particle mass concentrations by using the following factors. If a unit factor in $\mathrm{mg\,kg_{fuel}^{-1}}$ is needed, a factor of approximately $22\,\mathrm{m^3\,kg_{fuel}^{-1}}$ can be applied to multiply the particle concentration (calculation, e.g., in Jathar et al., 2017; Gordon et al., 2014b). In order to obtain emission and production factors in units of $\mathrm{kWh^{-1}}$, a factor of $2.7\,\mathrm{m^3\,kWh^{-1}}$ (mode 1) or $4\,\mathrm{m^3\,kWh^{-1}}$ (mode 2) can similarly be used. These factors are derived from the fuel composition and engine performance information provided in Sect. 2.1 and 2.2 and the exhaust CO_2 concentration.

Table 1. (a) Particle mass concentrations of primary and total aged particles (SP-AMS), increase of particle mass (%) in PAM chamber, calculated atmospheric ages simulated by PAM chamber and O : C ratios measured by SP-AMS. If no increase in PAM is presented, it is larger than 100 000 %. **(b)** The particle mass of species (SP-AMS) in all cases is also presented in the table as well as **(c)** the concentrations of gaseous emissions in raw exhaust (published already in Lehtoranta et al., 2017). Values have been corrected by the dilution ratio used in the sampling system.

(a)	M1, C1, 350 °C	M1, C1, 400 °C	M2, C1, 350 °C	M2, C1, 450 °C	M2, C2, 500 °C
Primary PM, $\mu g\,m^{-3}$, SP-AMS	9	40	31	28	150
Total aged PM, $\mu g\,m^{-3}$, SP-AMS	2554	2503	1210	989	1093
Increase in PAM %, SP-AMS	26 800	6210	3840	3440	630
Increase in PAM %, EEPS	7130	1660	2680	278	69
Increase in PAM %, HRLPI	–	643	22 800	75	4
Atmospheric age, days	10.0	10.7	4.6	4.7	9.3
O : C	1	1.1	1	0.9	1.2
(b) Total aged PM of species, $\mu g\,m^{-3}$, SP-AMS					
Organic	944	993	669	430	476
Sulfate	475	502	228	317	330
Nitrate	749	641	182	115	143
Ammonium	372	348	119	121	135
(c) Concentrations of gaseous emissions, ppm					
NO_x	3	4	3	12	4
CO	14	7	14	8	4
Methane	906 ± 16	904 ± 30	2232 ± 74	2238 ± 51	1360 ± 7
Ethane	18	17	68	49	15
Propane	1	1	21	6	1
Ethene	0	0	2	0	0

Table 2. SOA production factors calculated from the SP-AMS data in this study and in literature (age is OH exposure / (1.5×10^6 molec cm^{-3})). Primary organic aerosol has been subtracted from the total aged organic aerosol.

Source	Age	PF (mg kg_{fuel}^{-1})	Reference
NG engine:			
M1, C1, 350 °C	10 days	19	This study
M1, C1, 400 °C	10.7 days	20	This study
M2, C1, 350 °C	4.6 days	12	This study
M2, C1, 450 °C	4.7 days	9	This study
M2, C2, 500 °C	9.3 days	9	This study
Diesel/biodiesel non-road engine, idling	1.5 days	5300–12000	Jathar et al. (2017)
Diesel/biodiesel non-road engine, 50 % load	0.8 days	400–900	Jathar et al. (2017)
Ethanol vehicle, NEDC cycle	∼ 1–8 days	< 2*	Timonen et al. (2017)
Gasoline vehicle, parts of NEDC cycle	∼ 1–8 days	7–155*	Karjalainen et al. (2016)
Vehicle fleet in highway tunnel	5.4 days	350	Tkacik et al. (2014)
Gasoline vehicle, hot start	3 h	13.8	Gordon et al. (2014a)
Gasoline vehicle, cold start	3 h	19–60	Gordon et al. (2014a)
Gasoline vehicles, idling	3–6 h	5–90	Nordin et al. (2013)
Gasoline vehicles, cold start	Unknown	480	Nordin et al. (2013)
Gasoline vehicle, NEDC cycle	8 h	345	Platt et al. (2013)
Small two-stroke off-road engine	1–7 h	240–1400	Gordon et al. (2013)
Small four-stroke off-road engine	1 h	100–130	Gordon et al. (2013)
Diesel vehicle, deactivated catalyst	Unknown	230–560	Chirico et al. (2010)
Diesel vehicle, catalyst working	Unknown	12–20	Chirico et al. (2010)

* Calculated assuming gasoline density 0.75 $kg\,l^{-1}$ and consumption 7.9 L $(100\,km)^{-1}$.

The production factors of secondary organic aerosol have been calculated and collected in Table 2, in units of kg_{fuel}^{-1}. To be able to compare the SOA production factors, here primary organic aerosol was subtracted from the total aged organic aerosol. Table 2 also contains SOA production factors of secondary organic aerosol for different diesel and gasoline vehicles obtained from the literature. Although the total aged particulate matter production of the investigated NG engine was much larger than its primary particle emissions, it was smaller than SOA production from in-use diesel and gasoline vehicles in the literature (Tkacik et al., 2014). The SOA formation potential from the NG engine, measured by SP-AMS, was similar to that of a diesel vehicle equipped with a catalytic converter or to that of a hot-start gasoline vehicle. On the other hand, the photochemical age that was simulated by a chamber in the different studies varied greatly. This is why the comparison of the SOA production factors should be done very carefully, if at all. The longest atmospheric ages in the literature collected in Table 2 were achieved in our study.

Palm et al. (2016), Tkacik et al. (2014) and Kang et al. (2011) have seen with an oxidation flow reactor – such as the PAM chamber in our experiments – that the highest potential secondary organic aerosol formation takes place at the photochemical age of a few days and starts decreasing after that. For example, in the vehicle fleet emission study in a highway tunnel of Tkacik et al. (2014), the peak secondary aerosol production took place after 4–10 days of equivalent atmospheric oxidation ($[OH] = 1.5 \times 10^6$ molec cm^{-3}), and larger OH exposures started to reduce the secondary mass. In our study, the simulated atmospheric, or photochemical, ages in the investigated cases varied between 4.6 and 10.7 days, depending on the external OH reactivity, which was affected by the concentrations of gaseous emissions (Table 1) entering the PAM chamber and by the relative humidity of the sample. The largest total aged particle concentrations were achieved with the longest atmospheric ages and the lowest particle concentrations were achieved with the shortest atmospheric ages. However, the secondary aerosol formation potential may have also been affected by the engine parameters and not only the achieved photochemical age: the total aged particle concentrations were the highest in engine operation mode 2 (M2).

3.2 Volatility of primary and secondary particle mass

The volatility of the particles was studied with a thermodenuder. Mass fraction remaining (MFR) stands for the fraction of the particle mass at a given thermodenuder temperature and the particle mass at room temperature. In Fig. 3, the particle mass fraction remaining has been calculated for two representative cases of primary emissions and four representative cases of total aged particle emissions, selected from among the cases already introduced. Figure 3 only shows data from EEPS, since the curves obtained from HRLPI were similar. Here, the curves have been smoothed by a moving average but the original 1 s resolution figure can be found in the Supplement. For the total aged emissions, the cases with both higher and lower catalyst temperature are presented. For primary particle emissions, only the case with the higher catalyst temperature is presented. This is because an accurate examination of the volatility of primary particles in low catalyst temperatures could not be done, due to the insufficient primary particle mass concentrations for high-quality analysis. In the figure, the "starting point", i.e., the temperature where the mass fraction remaining is one, is 50 °C and not lower because of the decelerated cooling of the thermodenuder toward the room temperature and related time limitations.

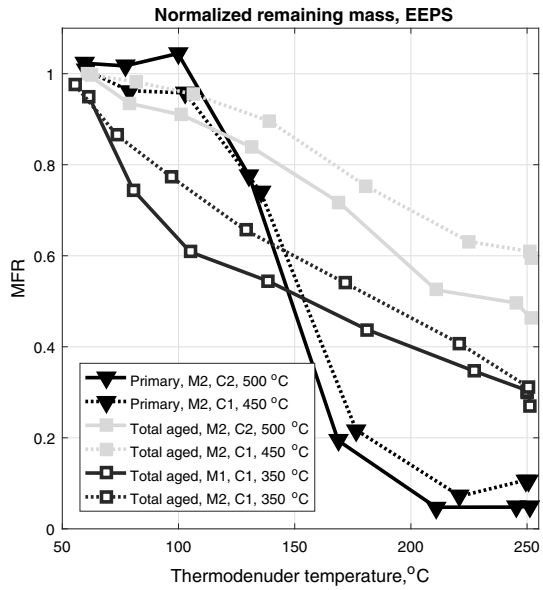

Figure 3. Results of particle volatility measurements. Particle mass fraction remaining (MFR) after the thermodenuder treatment for the exhaust aerosol sample of three different types of particle emissions from the natural gas engine. MFR values were calculated from the size distributions measured by EEPS with unit mass assumption.

The MFR curves for each type of particles are characteristic, i.e., each particle type can easily be distinguished by their evaporation behavior. To highlight this, the primary particle evaporation is marked with black, and the total aged particle evaporation curves are marked with cyan and blue in Fig. 3. The volatility of the particles from the natural gas engine clearly changed when the particles were aged. At high catalyst temperature, the primary particles (black triangles in Fig. 3) were more volatile than the total aged particles (cyan squares). Approximately half (46–60 % in EEPS, 43–53 % in HRLPI) of the total aged particle mass remained at a thermodenuder temperature of 250 °C, whereas only 5–10 % (1–

4 % in HRLPI) of the primary particle mass remained at that temperature. Also, the catalyst temperature had an impact on the volatility of the total aged particles (blue vs. cyan). An easily evaporable fraction of the total aged particles was formed in the case of a low catalyst temperature, which evaporated below 110 °C. Because of this easily evaporable fraction, the MFR of total aged particles at 250 °C was 30 % in the low catalyst temperature cases, while in the high catalyst temperature cases the MFR of total aged particles at 250 °C was 46–60 %.

The thermodenuder used in this study has been designed to minimize nanoparticle losses by reducing the residence time (Heikkilä et al., 2009). For example, in this study, the residence time in the heated zone of the thermodenuder was less than 1 s. An et al. (2007) measured the volatility of secondary organic aerosol produced during α-pinene photooxidation and observed that only half of the secondary particle mass evaporates in a thermodenuder (100 °C) if the residence times in the heated zone of the thermodenuder are less than a few seconds. With longer residence times, the remaining mass downstream of the thermodenuder decreases to less than 3 %. This means that the remaining fraction of particle mass in our study could have been smaller with longer residence times in the thermodenuder. On the other hand, a longer residence time in the thermodenuder would have increased the nanoparticle losses. In this study, with the use of a thermodenuder, we could observe the volatility differences between the different types of particle emissions emitted by a natural gas engine.

In Fig. 4, the remaining mass fractions are plotted for different chemical species of the particles drawn from the SP-AMS. In the primary emission case, approximately one-third of the particle mass – consisting mainly of organics – remained at TD temperature of 250 °C. The low concentrations and particle size below the detection limit of SP-AMS degrade the analysis in the case M2, C1, 450 °C, which was seen as a fluctuating signal. About 25 % of the total aged particle mass in the high catalyst temperature cases and less than 10 % of the total aged particle mass in low catalyst temperature cases remained at 250 °C, according to SP-AMS. The remaining particle matter consisted of organics, sulfate and ammonium, in this order.

The composition information reveals that the high-volatility fraction of the total aged particles in the low temperature catalyst cases consisted of nitrates, possibly of ammonium nitrate and high-volatility organics. The primary particle sulfate evaporated at thermodenuder temperatures between 100 and 170 °C, and the total aged particle sulfate evaporated more gradually above 120 °C. In all types of particles, the evaporation of organics was steady and gradual below 200 °C, indicating various organic compounds with different evaporation temperatures. Above 200 °C, the evaporation of organics decreased. This combined SP-AMS and EEPS/HRLPI derived thermodenuder temperature ramp information can be used in future measurements for particle composition analysis: the evaporation temperature of the particles can give valuable information about the composition of the particles also without access to SP-AMS.

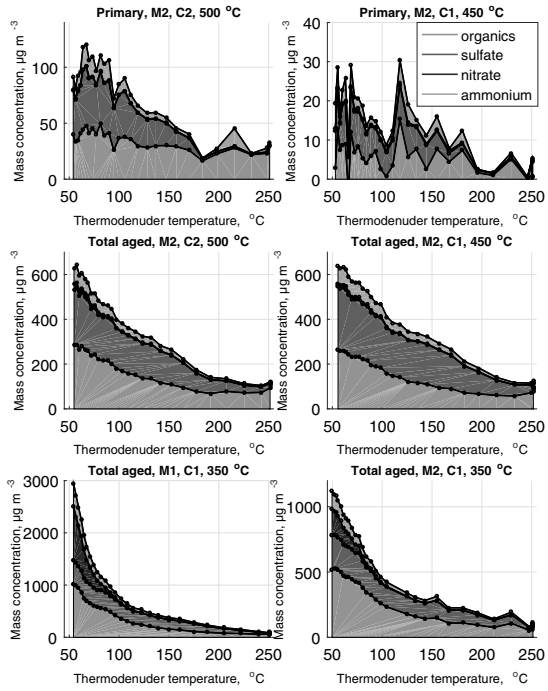

Figure 4. Concentration of different chemical compounds of particles remaining after the thermodenuder treatment conducted for the exhaust aerosol. The mass concentrations were measured using the SP-AMS at different thermodenuder temperatures and corrected by the dilution ratio used in the sampling system.

The temperatures at which 50 % of the volatile fraction of the chemical compounds of the particles were remaining are collected in Table 3. The case "primary, M2, C1, 450 °C" had particle mass concentrations that were too low (see Fig. 4) for this kind of examination. The evaporation temperatures of sulfate and nitrate were the highest and the lowest, respectively, in all of the analyzed cases (all catalyst temperatures; primary and total aged particles). Similarly to Huffman et al. (2009), who measured ambient aerosol volatility in megacities with a thermodenuder and an SP-AMS, we found that nitrate had the highest volatility and sulfate had the lowest.

Robinson et al. (2007) and Huffman et al. (2009) proposed that all organic aerosol should be considered semivolatile. Our results on primary and PAM-chamber-generated organic aerosols point in that direction as well. The evaporation temperature of the volatile fraction ($T_{\mathrm{volatile,\,50\,\%}}$) of organic matter remained between the $T_{\mathrm{volatile,\,50\,\%}}$ of nitrate and sulfate in all cases. Also, a significant fraction of the mass concentration of the organic matter did not evaporate. More exact

Table 3. The temperatures where 50 % of the volatile fraction of species has evaporated.

$T_{\text{volatile, 50 \%}}$ (°C)	Primary M2, C2, 500 °C	Primary M2, C1, 450 °C	Total aged M2, C2, 500 °C	Total aged M2, C1, 450 °C	Total aged M1, C1, 350 °C	Total aged M2, C1, 350 °C
Organics	115	–	99	104	87	93
Sulfate	125	–	152	168	120	147
Nitrate	72	–	80	84	65	65
Ammonium	104	–	97	112	70	79

specifications of the volatility cannot be given, but there is room left for speculation if part of the organic matter in secondary particles is semi-volatile (SV-SOA) or low volatility (LV-SOA) secondary organic aerosol (Murphy et al., 2014).

The ammonium in total aged particles evaporated at higher thermodenuder temperatures when the catalyst temperature was high. The theory that the sulfate–nitrate trade-off phenomenon that determines the formation of nitrates is ammonium bound is supported by the evaporation temperatures of ammonium. Ammonium evaporated at approximately 20 °C higher thermodenuder temperatures in the high catalyst temperature cases (Table 3); thus, its evaporation temperature was closer to the evaporation temperature of sulfate when the sulfate concentration of the particles was larger. By contrast, in the low catalyst temperature cases where the nitrate concentration was higher, the evaporation temperature of ammonium was closer to that of nitrate.

The nitrate concentrations measured during the thermodenuder temperature ramp (Fig. 4) in low thermodenuder temperatures differed from the nitrate concentrations that were measured without a thermodenuder (Fig. 2a and b) in total aged particles. A possible explanation is that a long time is needed for the nitrate concentration to stabilize. In our measurement protocol, we waited 10–15 min after switching the PAM UV lights on, followed by a 10 min steady-state measurement with the aerosol instruments. After this, a thermodenuder ramp was started, which took approximately 45 min. Based on the results, the 10–15 min wait was insufficient if accurate nitrate concentrations were desired. Therefore, the chemical compound measurements performed at low thermodenuder temperature can give a truer picture of the secondary aerosol formation than the measurements presented in Fig. 2. The change in concentrations between the steady-state measurements and the thermodenuder ramp measurements was the largest for nitrate, but the concentrations of other compounds also differed slightly from each other. Because the nitrate concentrations were found to be the slowest to stabilize and the most sensitive to changes in the system, such as to changes in temperature, special attention should be given to measurements of nitrate, especially when a PAM chamber is being used. We note that because nitrate formation is limited by ammonium, the slow stabilization is probably related to ammonia.

According to our thermodenuder temperature ramp experiments, the catalyst temperature affected the total aged particle composition. With a decreasing catalyst temperature, the mass concentration and fraction of sulfate in total aged particles decreased (Fig. 4, Table 1). This was expected: at lower catalyst temperatures the oxidation of SO_2 to SO_3 decreases and less sulfuric acid (sulfates) can form (Arnold et al., 2012). The mass concentration of nitrate in secondary particles increased as the catalyst temperature decreased. This could not be explained by catalyst performance improvement: gaseous NO_x levels remained similar at all catalyst temperatures or rose as catalyst temperature increased (see Lehtoranta et al., 2017). Because ammonia concentrations after catalyst were low, below 2 ppm in all cases, the effect of catalyst temperature on ammonia emission could not be measured. However, ammonium concentrations measured by SP-AMS correlated rather well with nitrate concentrations. Therefore, we suggest that ammonium increase was related to the nitrate increase. Also, the sulfate concentrations could partly explain the behavior of the nitrate concentrations. If enough gaseous sulfuric acid is available, ammonium sulfate forms, and if not, more ammonium nitrate can form instead. A similar behavior of nitrate and sulfate trade-off has been measured by Ntziachristos et al. (2016) for two different marine fuels, namely heavy fuel oil (HFO) and light fuel oil (LFO).

3.3 Differences between instruments and mass size distributions

Slightly unexpectedly, the total aged particle mass measured by SP-AMS was 2–4 times larger than the total mass measured by EEPS and 1–3 times larger than that measured by HRLPI (Fig. 2). There could be several reasons for this. In EEPS and HRLPI, unit density and spherical particles were assumed in the mass calculations. Natural gas engine primary particles have a density of 0.85 g cm^{-3} (Bullock and Olfert, 2014), but the densities of natural gas engine secondary particles can be larger than the unit density. For example, the density of ammonium nitrate, ammonium sulfate and sulfuric acid is approximately 1.5, 1.5 and 1.8 g m^{-3}, respectively (Clegg and Wexler, 2011). Particle density does not completely explain the difference in instrument readings. Also, the collection efficiency (CE) estimation used in the SP-AMS calculation is probably not the reason for the differences be-

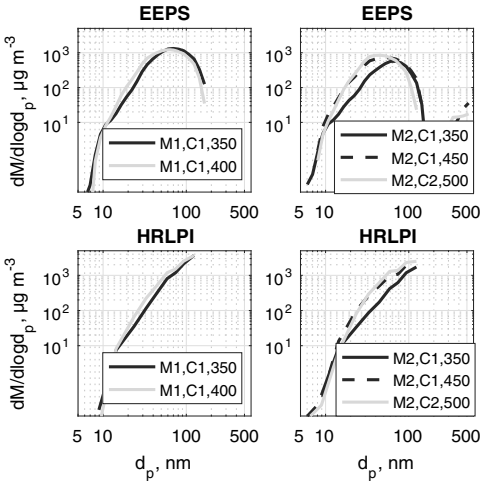

Figure 5. Particle mass size distributions measured by EEPS and HRLPI and corrected by the dilution ratios. Cases M1, C1 are on the left, and cases M2, C1 and M2, C2 are on the right. Cyan curves stand for the higher catalyst temperatures and blue for the lower ones.

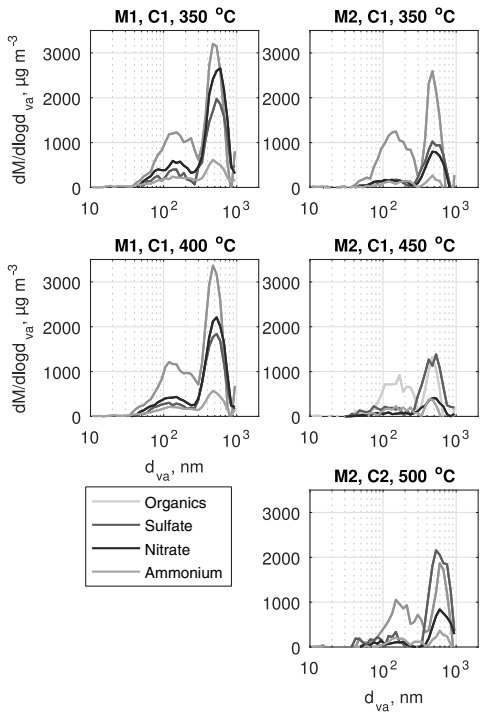

Figure 6. Component-wise particle mass size distributions measured by SP-AMS and corrected by the dilution ratios.

tween the instrument results in this study. Evaluation of the CE following the procedure of Middlebrook et al. (2012) revealed that CE equal to 0.45 was the correct value for the studied total aged particles in the cases in Fig. 1.

However, the detection efficiency and size range varied among the aerosol instruments (EEPS 5.6–560 nm, HRLPI ∼ 5–200 nm, SP-AMS ∼ 30–1000 nm) and can explain the differences in results; HRLPI can detect a larger fraction of the primary particles than SP-AMS because of the more suitable size range of the instrument and, correspondingly, SP-AMS can detect a larger fraction of the total aged particles formed in the PAM chamber because of its more suitable size range. Also, particle losses may play a role in the differences between instruments; particle losses in the PAM chamber were larger in the HRLPI size range than in the SP-AMS size range. Nevertheless, most probably, the largest role was played by the differences in instrument size ranges.

Mass size distributions of the total aged aerosol, measured with EEPS and HRLPI, are plotted in Fig. 5. HRLPI suggests that a part of the particle mass lies above the instrument size range, which was confirmed by SP-AMS mass size distributions in Fig. 6. According to SP-AMS, the mass size distributions of total aged particles were bimodal, with the size of the larger mode being 480–840 nm and the smaller being 150–200 nm. The mode with smaller particle size was dominated by organics. Although the mass concentration of the total aged particles was better recorded by SP-AMS, a portion of the particles on the smallest particle sizes was missed due to the lower limit of SP-AMS size range at 30–50 nm. The best overall picture is therefore gained with a combination of SP-AMS and HRLPI. See the Supplement for a comparison of the size distributions measured by different instruments in the same figure. The two instruments that measure the aerodynamic diameter of the particles (HRLPI and SP-AMS) compare quite well with each other in the size range 47–124 nm.

We can also see a difference between the EEPS and HRLPI mass size distributions. The difference is probably due to the inversion of EEPS, which forces the size distributions to follow a log-normal shape. EEPS also underestimated the mass of particles with diameter above 200 nm (see the Supplement). The different measurement principles of the instruments must also be kept in mind. EEPS measures the mobility size and HRLPI measures the aerodynamic size of the particles.

3.4 PAM artifacts and losses

The so-called smog chambers are an established method of measuring SOA formation. An oxidation flow chamber such as PAM provides some advantages in comparison to smog chambers, such as a higher degree of oxidation, smaller phys-

ical size and a short residence time, which allows measurements with higher time resolution. Smog chamber walls may also cause large wall losses and influence the chemistry in the chamber (Bruns et al., 2015). On the other hand, smog chambers may simulate the atmospheric oxidation of organic precursors better than oxidation flow chambers due to their more tropospheric oxidant concentrations and longer residence times (Lambe et al., 2011).

The PAM method has been designed to produce the maximum potential aerosol mass from precursor gases (Kang et al., 2007). In that stage, the oxidation products of precursors have condensed into the particle phase and formed secondary aerosol. However, because the oxidant concentrations are unrealistically high in PAM, the UV-light intensity used is non-tropospheric and the residence times are much shorter than in the atmosphere (e.g., Simonen et al., 2017), precursor oxidation products also have other possible fates; they can be oxidized too far and form non-condensable oxidation products before condensation (accelerated chemistry) and they can exit the reactor before the condensation occurs. Also, precursor oxidation products can be lost on the PAM walls although the losses on the walls are minimized by the chamber design (Lambe et al., 2011). The fates other than condensing on particle phase are viewed here as PAM artifacts and losses.

The losses of condensable organic oxidation products and artifact effects of the accelerated chemistry in the PAM have been evaluated following the method of Palm et al. (2016) for the cases in Fig. 2. HRLPI number size distributions were used to calculate the condensation sink needed in the loss calculation. A molar mass of $200\,\mathrm{g\,mol^{-1}}$, a diffusion coefficient of $7 \times 10^{-6}\,\mathrm{m^2\,s^{-1}}$ (Tang et al., 2015) and a rate constant for reaction with OH of 1×10^{-11} (Ziemann and Atkinson, 2012) were applied. For sticking coefficient selection $\alpha = 1$ (assumed by Palm et al., 2016), the fraction of oxidation products that condensed into the particle phase was 0.94 ± 0.03, but for $\alpha = 0.1$ the fraction of oxidation products that condensed into the particle phase was 0.64 ± 0.15.

The losses of sulfuric acid were also calculated in the same way. A diffusion coefficient of 1×10^{-5} (Hanson and Eisele, 2000), α of 0.65 (Pöschl et al., 1998) and molar mass of $98.079\,\mathrm{g\,mol^{-1}}$ were used for sulfuric acid. The fraction of sulfuric acid that condensed into the particle phase was 0.98 ± 0.01. According to Lambe et al. (2011), SO_2 losses in the PAM are negligible. It can be concluded that the effect of precursor losses and artifacts in the PAM was not substantial in our measurements. The measurement of ammonium nitrate and ammonium sulfate is difficult because ammonia sticks on the walls of sampling systems and instruments (Suarez-Bertoa et al., 2015; Heeb et al., 2012, 2008), which may result in wall losses or an artifact on subsequent measurements. The penetration of ammonia could not be calculated, but the measured ammonium concentrations varied clearly from one case to another, implicating that the source of the ammonia was indeed the exhaust line instead of, e.g., the walls of the PAM. However, longer times for the stabilization of the SP-AMS concentration would have been advantageous for the reliability of ammonium and, as a consequence, nitrate particle formation.

Karjalainen et al. (2016) and Timonen et al. (2017) estimated the effect of particle losses in a similar PAM chamber to be small. The particle losses measured by Karjalainen et al. (2016) depend on particle size and are below 10 % at the particle sizes with most particle mass. An exact calculation of the particle losses in the PAM chamber is not possible because the particle size and number increase while the aerosol sample flows through the chamber. An estimation for the particle mass losses in the chamber can be given, calculated using the average of HRLPI particle number size distributions before and after the chamber (similarly to the precursor-loss calculation by Palm et al., 2016) and the PAM particle loss curve. The particle mass loss according to this examination was 20.3 ± 3.7 %. Most probably, however, the actual particle mass losses in the chamber were smaller because majority of the mass actually was located at larger particle sizes that HRLPI is unable to measure, where particle losses are smaller.

No loss corrections were done based on these calculations on the results presented in this article. If corrections had been made, the presented secondary aerosol productions and production factors would be slightly higher (less than 10 %) in Figs. 2 and 4–6, and in Tables 1 and 2.

4 Conclusions

Natural gas engines emit very little particle mass, which can make them less harmful to human health than corresponding gasoline-, diesel- or marine-fuel-oil-fueled engines. However, secondary aerosol formation also increases human exposure to aerosol particles. When natural gas engines become more common in traffic and energy production, their potential for secondary particle formation will become more important and an even more relevant object for research. Therefore, it is important to study the potential reduction of the total aerosol particle mass and related health and climate effects when shifting from liquid fuels to natural gas or biogas in combustion engines is important.

In this study, a retro-fitted natural gas engine equipped with exhaust after-treatment was studied in a laboratory in an engine test bench, using steady-state engine operation modes, i.e., constant engine speed and torque. The secondary aerosol formation was studied using a (PAM) chamber. Estimates for the atmospheric ages achieved by the PAM chamber were 4.6–10.7 days. In this study, the secondary aerosol mass potential of natural gas emission was measured to be at a small or medium level but was well measurable. Compared to the primary particle mass emissions from the same engine, the secondary aerosol formation potential was substantial – approximately 1–2 orders of magnitude higher than the pri-

mary aerosol mass. However, the very small primary particle masses in some of the observed engine and catalyst operation modes complicated this comparison. To give a rough estimate to the quantity of the NG engine exhaust's SOA formation potential, it was on the same level as or lower than the SOA formation potential of a diesel vehicle equipped with an oxidation catalyst or that of warm (hot-start) gasoline vehicles. However, the photochemical age that was produced by the PAM chamber in our study was longer (several days) than the photochemical ages achieved in the previous studies (several hours). Therefore, the SOA formation potential must not be directly compared. Also, despite the attempts to model PAM-related losses and artifacts, and to estimate particle losses in PAM, the measurements performed with PAM still involve uncertainties.

The total aged aerosol, i.e., the combined primary and secondary aerosol (downstream of a PAM chamber) of the NG engine, consisted of organic matter, nitrate, sulfate and ammonium, roughly in this order. It was found that aging of the exhaust generates low-volatility organics. However, the composition of the secondary aerosol was, for the most part, inorganic; the fraction of organic matter in the secondary particles varied between 37 and 56 %.

Exhaust after-treatment was found to have an effect on the secondary aerosol composition. High catalyst temperature promoted the formation of sulfate particles in total aged aerosol, whereas low catalyst temperatures promoted nitrate formation. Because the amount of NO_x emissions was reduced at the lower catalyst temperatures, it was concluded that the formation of nitrate in particles (total aged) depended on the ammonia concentration and sulfate particle formation rather than the NO_x emissions. Sulfate and nitrate are likely to exist in the forms of ammonium sulfate and ammonium nitrate. Therefore, what limits the nitrate mass in particles is most likely the availability of ammonia which is more related to the exhaust after-treatment than fuel or combustion processes.

The total aged nanoparticles formed from the natural gas exhaust were found to be less volatile than the primary particles. This can affect their lifetime in the atmosphere and therefore their impact on the radiative balance of the atmosphere or their potential to act as cloud nuclei. A higher catalyst temperature impacts the total aged particles by decreasing their volatility or by decreasing their volatile fraction.

In our study, only one constant PAM UV-light voltage could be used. With improved instrumentation, a broader variation in light intensity could be achieved, thus improving our knowledge regarding the evolution of the secondary aerosol. Also, because natural gas is not the only widely used gaseous fuel, the secondary aerosol formation potential of a more extensive fuel selection would be interesting to study. The role of lubricating oil is not known yet either – studies performed at different natural gas combustion sites and with various lubricating oils would reveal its significance to secondary aerosol formation.

Code and data availability. The data and code of this study are available from the authors upon request.

The Supplement related to this article is available online at https://doi.org/10.5194/acp-17-8739-2017-supplement.

Competing interests. The authors declare that they have no conflict of interest.

Acknowledgements. This study was funded by Tekes, the Finnish Funding Agency for Innovation, Neste, AGCO Power, Wärtsilä, Dinex Ecocat, Dekati, Suomi Analytics and Viking Line. Jenni Alanen acknowledges Gasum's gas funding for financial support. Pauli Simonen acknowledges the TUT Graduate School for its funding. Oskari Kangasniemi acknowledges the Nessling Foundation for its funding. Topi Rönkkö acknowledges the financial support from the Academy of Finland (ELTRAN project, grant no. 293437).

Edited by: Rob MacKenzie
Reviewed by: two anonymous referees

References

Alanen, J., Saukko, E., Lehtoranta, K., Murtonen, T., Timonen, H., Hillamo, R., Karjalainen, P., Kuuluvainen, H., Harra, J., Keskinen, J., and Rönkkö, T.: The formation and physical properties of the particle emissions from a natural gas engine, Fuel, 162, 155–161, https://doi.org/10.1016/j.fuel.2015.09.003, 2015.

An, W. J., Pathak, R. K., Lee, B. H., and Pandis, S. N.: Aerosol volatility measurement using an improved thermodenuder: application to secondary organic aerosol, J. Aerosol Sci., 38, 305–314, https://doi.org/10.1016/j.jaerosci.2006.12.002, 2007.

Anderson, M., Salo, K., and Fridell, E.: Particle- and gaseous emissions from an LNG powered ship, Environ. Sci. Technol., 49, 12568–12575, https://doi.org/10.1021/acs.est.5b02678, 2015.

Arffman, A., Yli-Ojanperä, J., Kalliokoski, J., Harra, J., Pirjola, L., Karjalainen, P., Rönkkö, T., and Keskinen, J.: High-resolution low-pressure cascade impactor, J. Aerosol Sci., 78, 97–109, https://doi.org/10.1016/j.jaerosci.2014.08.006, 2014.

Arnold, F., Pirjola, L., Rönkkö, T., Reichl, U., Schlager, H., Lähde, T., Heikkilä, J., and Keskinen, J.: First online measurements of sulfuric acid gas in modern heavy-duty diesel engine exhaust: implications for nanoparticle formation, Environ. Sci. Technol., 46, 11227–11234, https://doi.org/10.1021/es302432s, 2012.

Atkinson, R., Baulch, D., Cox, R., Crowley, J., Hampson, R., Hynes, R., Jenkin, M., Kerr, J., Rossi, M., and Troe, J.: IUPAC Subcommittee for gas kinetic data evaluation, Evaluated kinetic data, available at: http://www.iupac-kinetic.ch.cam.ac.uk (last access: 13 December 2016), 2007.

Bahreini, R., Middlebrook, A. M., Brock, C. A., Gouw, J. A. D., Mckeen, S. A., Williams, L. R., Daumit, K. E., Lambe, A. T.,

Massoli, P., Canagaratna, M. R., Ahmadov, R., Carrasquillo, A. J., Cross, E. S., Ervens, B., Holloway, J. S., Hunter, J. F., Onasch, T. B., Pollack, I. B., Roberts, J. M., Ryerson, T. B., Warneke, C., Davidovits, P., Worsnop, D. R., and Kroll, J. H.: Mass spectral analysis of organic aerosol formed downwind of the deepwater horizon oil spill: field studies and laboratory confirmations, Environ. Sci. Technol., 46, 8025–8034, https://doi.org/10.1126/science.1200320, 2012.

Bielaczyc, P., Woodburn, J., and Szczotka, A.: An assessment of regulated emissions and CO_2 emissions from a European light-duty CNG-fueled vehicle in the context of Euro 6 emissions regulations, Appl. Energ., 117, 134–141, https://doi.org/10.1016/j.apenergy.2013.12.003, 2014.

Bruns, E. A., El Haddad, I., Keller, A., Klein, F., Kumar, N. K., Pieber, S. M., Corbin, J. C., Slowik, J. G., Brune, W. H., Baltensperger, U., and Prévôt, A. S. H.: Inter-comparison of laboratory smog chamber and flow reactor systems on organic aerosol yield and composition, Atmos. Meas. Tech., 8, 2315–2332, https://doi.org/10.5194/amt-8-2315-2015, 2015.

Bullock, D. S. and Olfert, J. S.: Size, volatility, and effective density of particulate emissions from a homogeneous charge compression ignition engine using compressed natural gas, J. Aerosol Sci., 75, 1–8, https://doi.org/10.1016/j.jaerosci.2014.04.005, 2014.

Burkholder, J. B., Sander, S. P., Abbatt, J., Barker, J. R., Huie, R. E., Kolb, C. E., Kurylo, M. J., Orkin, V. L., Wilmouth, D. M., and H., W. P.: Chemical Kinetics and Photochemical Data for Use in Atmospheric Studies, Evaluation No. 18, JPL Publication 15-10, Jet Propulsion Laboratory, Pasadena, available at: http://jpldataeval.jpl.nasa.gov (last access: 13 December 2016), 2015.

Chirico, R., DeCarlo, P. F., Heringa, M. F., Tritscher, T., Richter, R., Prévôt, A. S. H., Dommen, J., Weingartner, E., Wehrle, G., Gysel, M., Laborde, M., and Baltensperger, U.: Impact of aftertreatment devices on primary emissions and secondary organic aerosol formation potential from in-use diesel vehicles: results from smog chamber experiments, Atmos. Chem. Phys., 10, 11545–11563, https://doi.org/10.5194/acp-10-11545-2010, 2010.

Clegg, S. L. and Wexler, A. S.: Densities and apparent molar volumes of atmospherically important electrolyte solutions. 2. The systems H^+–HSO_4^-–SO_4^{2-}–H_2O from 0 to 3 mol kg^{-1} as a function of temperature and H^+–NH_4^+–HSO_4^-–SO_4^{2-}–H_2O from 0 to 6 mol kg^{-1} at 25 °C using a pitzer ion interaction model, and NH_4HSO_4–H_2O and $(NH_4)_3H(SO_4)_2$–H_2O over entire concentration range, J. Phys. Chem.-US, 115, 3461–3474, https://doi.org/10.1021/jp1089933, 2011.

Damian, V., Sandu, A., Damian, M., Potra, F., and Carmichael, G. R.: The kinetic preprocessor KPP-a software environment for solving chemical kinetics, Comput. Chem. Engin., 26, 1567–1579, https://doi.org/10.1016/S0098-1354(02)00128-X, 2002.

Dockery, D. and Pope III, A.: Acute respiratory effects of particulate air pollution, Annu. Rev. Publ. Health, 15, 107–132, 1994.

Eichler, P., Muller, M., Rohmann, C., Stengel, B., Orasche, J., Zimmermann, R., and Wisthaler, A.: Lubricating oil as a major constituent of ship exhaust particles, Environ. Sci. Tech. Let., 4, 54–58, 2017.

Gentner, D. R., Jathar, S. H., Gordon, T. D., Bahreini, R., Day, D. A., Haddad, I. E., Hayes, P. L., Pieber, S. M., Platt, S. M., Gouw, J. D., Goldstein, A. H., Harley, R. A., Jimenez, J. L., Prévôt, A. S. H., and Robinson, A. L.: Review of urban secondary organic aerosol formation from gasoline and diesel motor vehicle emissions, Environ. Sci. Technol., 51, 1074–1096, https://doi.org/10.1021/acs.est.6b04509, 2017.

Gordon, T. D., Tkacik, D. S., Presto, A. A., Zhang, M., Jathar, S. H., Nguyen, N. T., Massetti, J., Truong, T., Cicero-Fernandez, P., Maddox, C., Rieger, P., Chattopadhyay, S., Maldonado, H., Maricq, M. M., and Robinson, A. L.: Primary gas- and particle-phase emissions and secondary organic aerosol production from gasoline and diesel off-road engines, Environ. Sci. Technol., 47, 14137–14146, https://doi.org/10.1021/es403556e, 2013.

Gordon, T. D., Presto, A. A., May, A. A., Nguyen, N. T., Lipsky, E. M., Donahue, N. M., Gutierrez, A., Zhang, M., Maddox, C., Rieger, P., Chattopadhyay, S., Maldonado, H., Maricq, M. M., and Robinson, A. L.: Secondary organic aerosol formation exceeds primary particulate matter emissions for light-duty gasoline vehicles, Atmos. Chem. Phys., 14, 4661–4678, https://doi.org/10.5194/acp-14-4661-2014, 2014a.

Gordon, T. D., Presto, A. A., Nguyen, N. T., Robertson, W. H., Na, K., Sahay, K. N., Zhang, M., Maddox, C., Rieger, P., Chattopadhyay, S., Maldonado, H., Maricq, M. M., and Robinson, A. L.: Secondary organic aerosol production from diesel vehicle exhaust: impact of aftertreatment, fuel chemistry and driving cycle, Atmos. Chem. Phys., 14, 4643–4659, https://doi.org/10.5194/acp-14-4643-2014, 2014b.

Goyal, P. and Sidhartha: Present scenario of air quality in Delhi: a case study of CNG implementation, Atmos. Environ., 37, 5423–5431, https://doi.org/10.1016/j.atmosenv.2003.09.005, 2003.

Graves, B., Olfert, J., Patychuk, B., Dastanpour, R., and Rogak, S.: Characterization of particulate matter morphology and volatility from a compression-ignition natural-gas direct-injection engine, Aerosol Sci. Tech., 49, 589–598, https://doi.org/10.1080/02786826.2015.1050482, 2015.

Hallquist, M., Wenger, J. C., Baltensperger, U., Rudich, Y., Simpson, D., Claeys, M., Dommen, J., Donahue, N. M., George, C., Goldstein, A. H., Hamilton, J. F., Herrmann, H., Hoffmann, T., Iinuma, Y., Jang, M., Jenkin, M. E., Jimenez, J. L., Kiendler-Scharr, A., Maenhaut, W., McFiggans, G., Mentel, Th. F., Monod, A., Prévôt, A. S. H., Seinfeld, J. H., Surratt, J. D., Szmigielski, R., and Wildt, J.: The formation, properties and impact of secondary organic aerosol: current and emerging issues, Atmos. Chem. Phys., 9, 5155–5236, https://doi.org/10.5194/acp-9-5155-2009, 2009.

Hallquist, Å. M., Jerksjö, M., Fallgren, H., Westerlund, J., and Sjödin, Å.: Particle and gaseous emissions from individual diesel and CNG buses, Atmos. Chem. Phys., 13, 5337–5350, https://doi.org/10.5194/acp-13-5337-2013, 2013.

Hanson, D. R. and Eisele, F.: Diffusion of H_2SO_4 in humidified nitrogen: hydrated H_2SO_4, J. Phys. Chem.-US, 104, 1715–1719, 2000.

Heeb, N. V., Saxer, C. J., Forss, A.-m., and Brühlmann, S.: Trends of NO-, NO_2-, and NH_3 -emissions from gasoline-fueled Euro-3- to Euro-4-passenger cars, Atmos. Environ., 42, 2543–2554, https://doi.org/10.1016/j.atmosenv.2007.12.008, 2008.

Heeb, N. V., Haag, R., Seiler, C., Schmid, P., Zennegg, M., Wichser, A., Ulrich, A., Honegger, P., Zeyer, K., Emmeneg-

ger, L., Zimmerli, Y., Czerwinski, J., Kasper, M., and Mayer, A.: Effects of a combined Diesel Particle Filter-DeNOx System (DPN) on reactive nitrogen compounds emissions: a parameter study, Environ. Sci. Technol., 46, 13317–13325, 2012.

Heikkilä, J., Rönkkö, T., Lähde, T., Lemmetty, M., Arffman, A., Virtanen, A., Keskinen, J., Pirjola, L., and Rothe, D.: Effect of open channel filter on particle emissions of modern diesel engine, J. Air Waste Manage., 59, 1148–1154, https://doi.org/10.3155/1047-3289.59.10.1148, 2009.

Huang, R. J., Zhang, Y., Bozzetti, C., Ho, K. F., Cao, J. J., Han, Y., Daellenbach, K. R., Slowik, J. G., Platt, S. M., Canonaco, F., Zotter, P., Wolf, R., Pieber, S. M., Bruns, E. A., Crippa, M., Ciarelli, G., Piazzalunga, A., Schwikowski, M., Abbaszade, G., Schnelle-Kreis, J., Zimmermann, R., An, Z., Szidat, S., Baltensperger, U., El Haddad, I., and Prévôt, A. S.: High secondary aerosol contribution to particulate pollution during haze events in China, Nature, 514, 218–222, https://doi.org/10.1038/nature13774, 2014.

Huffman, J. A., Docherty, K. S., Aiken, A. C., Cubison, M. J., Ulbrich, I. M., DeCarlo, P. F., Sueper, D., Jayne, J. T., Worsnop, D. R., Ziemann, P. J., and Jimenez, J. L.: Chemically-resolved aerosol volatility measurements from two megacity field studies, Atmos. Chem. Phys., 9, 7161–7182, https://doi.org/10.5194/acp-9-7161-2009, 2009.

Jathar, S. H., Miracolo, M. A., Tkacik, D. S., Donahue, N. M., Adams, P. J., and Robinson, A. L.: Secondary organic aerosol formation from photo-oxidation of unburned fuel: experimental results and implications for aerosol formation from combustion emissions, Environ. Sci. Technol., 47, 12886–12893, 2013.

Jathar, S. H., Friedman, B., Galang, A. A., Link, M. F., Brophy, P., Volckens, J., Eluri, S., and Farmer, D. K.: Linking load, fuel, and emission controls to photochemical production of secondary organic aerosol from a diesel engine, Environ. Sci. Technol., 51, 1377–1386, https://doi.org/10.1021/acs.est.6b04602, 2017.

Jayaratne, E. R., Meyer, N. K., Ristovski, Z. D., Morawska, L., and Miljevic, B.: Critical analysis of high particle number emissions from accelerating compressed natural gas buses, Environ. Sci. Technol., 44, 3724–3731, 2010.

Jayaratne, E. R., Meyer, N. K., Ristovski, Z. D., and Morawska, L.: Volatile properties of particles emitted by compressed natural gas and diesel buses during steady-state and transient driving modes, Environ. Sci. Technol., 46, 196–203, https://doi.org/10.1021/es2026856, 2012.

Jenkin, M. E., Saunders, S. M., and Pilling, M. J.: The tropospheric degradation of volatile organic compounds: a protocol for mechanism development, Atmos. Environ., 31, 81–104, https://doi.org/10.1016/S1352-2310(96)00105-7, 1997.

Jenkin, M. E., Saunders, S. M., Wagner, V., and Pilling, M. J.: Protocol for the development of the Master Chemical Mechanism, MCM v3 (Part B): tropospheric degradation of aromatic volatile organic compounds, Atmos. Chem. Phys., 3, 181–193, https://doi.org/10.5194/acp-3-181-2003, 2003.

Jimenez, J. L., Canagaratna, M. R., Donahue, N. M., Prevôt, A. S. H., Zhang, Q., Kroll, J. H., Decarlo, P. F., Allan, J. D., Coe, H., Ng, N. L., Aiken, A. C., Ulbrich, I. M., Grieshop, A. P., Duplissy, J., Wilson, K. R., Lanz, V. A., Hueglin, C., Sun, Y. L., Tian, J., Laaksonen, A., Raatikainen, T., Rautiainen, J., Vaattovaara, P., Ehn, M., Kulmala, M., Tomlinson, J. M., Cubison, M. J., Dunlea, E. J., Alfarra, M. R., Williams, P. I., Bower, K., Kondo, Y., Schneider, J., Drewnick, F., Borrmann, S., Weimer, S., Demerjian, K., Salcedo, D., Cottrell, L., Takami, A., Miyoshi, T., Shimono, A., Sun, J. Y., Zhang, Y. M., Dzepina, K., Sueper, D., Jayne, J. T., Herndon, S. C., Williams, L. R., Wood, E. C., Middlebrook, A. M., Kolb, C. E., Baltensperger, U., and Worsnop, D. R.: Evolution of organic aerosols in the atmosphere, Science, 326, 1525–1529, 2009.

Johnson, T. V.: Review of diesel emissions and control, Int. J. Engine Res., 10, 275–285, 2009.

Kanakidou, M., Seinfeld, J. H., Pandis, S. N., Barnes, I., Dentener, F. J., Facchini, M. C., Van Dingenen, R., Ervens, B., Nenes, A., Nielsen, C. J., Swietlicki, E., Putaud, J. P., Balkanski, Y., Fuzzi, S., Horth, J., Moortgat, G. K., Winterhalter, R., Myhre, C. E. L., Tsigaridis, K., Vignati, E., Stephanou, E. G., and Wilson, J.: Organic aerosol and global climate modelling: a review, Atmos. Chem. Phys., 5, 1053–1123, https://doi.org/10.5194/acp-5-1053-2005, 2005.

Kang, E., Root, M. J., Toohey, D. W., and Brune, W. H.: Introducing the concept of Potential Aerosol Mass (PAM), Atmos. Chem. Phys., 7, 5727–5744, https://doi.org/10.5194/acp-7-5727-2007, 2007.

Kang, E., Toohey, D. W., and Brune, W. H.: Dependence of SOA oxidation on organic aerosol mass concentration and OH exposure: experimental PAM chamber studies, Atmos. Chem. Phys., 11, 1837–1852, https://doi.org/10.5194/acp-11-1837-2011, 2011.

Karjalainen, P., Timonen, H., Saukko, E., Kuuluvainen, H., Saarikoski, S., Aakko-Saksa, P., Murtonen, T., Dal Maso, M., Ahlberg, E., Svenningsson, B., Brune, W. H., Hillamo, R., Keskinen, J., and Rönkkö, T.: Time-resolved characterization of primary and secondary particle emissions of a modern gasoline passenger car, Atmos. Chem. Phys., 16, 8559–8470, https://doi.org/10.5194/acp-16-8559-2016, 2016.

Künzi, L., Krapf, M., Daher, N., Dommen, J., Jeannet, N., Schneider, S., Platt, S., Slowik, J. G., Baumlin, N., Salathe, M., Prévôt, A. S. H., Kalberer, M., Strähl, C., Dümbgen, L., Sioutas, C., Baltensperger, U., and Geiser, M.: Toxicity of aged gasoline exhaust particles to normal and diseased airway epithelia, Sci. Rep.-UK, 5, 11801, https://doi.org/10.1038/srep11801, 2015.

Lambe, A. T., Ahern, A. T., Williams, L. R., Slowik, J. G., Wong, J. P. S., Abbatt, J. P. D., Brune, W. H., Ng, N. L., Wright, J. P., Croasdale, D. R., Worsnop, D. R., Davidovits, P., and Onasch, T. B.: Characterization of aerosol photooxidation flow reactors: heterogeneous oxidation, secondary organic aerosol formation and cloud condensation nuclei activity measurements, Atmos. Meas. Tech., 4, 445–461, https://doi.org/10.5194/amt-4-445-2011, 2011.

Lambe, A. T., Chhabra, P. S., Onasch, T. B., Brune, W. H., Hunter, J. F., Kroll, J. H., Cummings, M. J., Brogan, J. F., Parmar, Y., Worsnop, D. R., Kolb, C. E., and Davidovits, P.: Effect of oxidant concentration, exposure time, and seed particles on secondary organic aerosol chemical composition and yield, Atmos. Chem. Phys., 15, 3063–3075, https://doi.org/10.5194/acp-15-3063-2015, 2015.

Lehtoranta, K., Murtonen, T., Vesala, H., Koponen, P., Alanen, J., Simonen, P., Rönkkö, T., Timonen, H., Saarikoski, S., Maunula, T., Kallinen, K., and Korhonen, S.: Natural Gas Engine Emission Reduction by Catalysts, Emiss. Control Sci. Technol., 3, 142–152, https://doi.org/10.1007/s40825-016-0057-8, 2017.

Lelieveld, J., Evans, J. S., Fnais, M., Giannadaki, D., and Pozzer, A.: The contribution of outdoor air pollution sources to premature mortality on a global scale, Nature, 525, 367–71, https://doi.org/10.1038/nature15371, 2015.

Link, M. F., Kim, J., Park, G., Lee, T., Park, T., Bin, Z., Sung, K., Kim, P., Kang, S., Soo, J., Choi, Y., Son, J., Lim, H.-j., and Farmer, D. K.: Elevated production of NH_4NO_3 from the photochemical processing of vehicle exhaust: implications for air quality in the Seoul Metropolitan Region, Atmos. Environ., 156, 95–101, https://doi.org/10.1016/j.atmosenv.2017.02.031, 2017.

Mao, J., Ren, X., Brune, W. H., Olson, J. R., Crawford, J. H., Fried, A., Huey, L. G., Cohen, R. C., Heikes, B., Singh, H. B., Blake, D. R., Sachse, G. W., Diskin, G. S., Hall, S. R., and Shetter, R. E.: Airborne measurement of OH reactivity during INTEX-B, Atmos. Chem. Phys., 9, 163–173, https://doi.org/10.5194/acp-9-163-2009, 2009.

May, A. A., Nguyen, N. T., Presto, A. A., Gordon, T. D., Lipsky, E. M., Karve, M., Gutierrez, A., Robertson, W. H., Zhang, M., Brandow, C., Chang, O., Chen, S., Cicero-fernandez, P., Dinkins, L., Fuentes, M., Huang, S.-m., Ling, R., Long, J., Maddox, C., Massetti, J., Mccauley, E., Miguel, A., Na, K., Ong, R., Pang, Y., Rieger, P., Sax, T., Truong, T., Vo, T., Chattopadhyay, S., Maldonado, H., Maricq, M. M., and Robinson, A. L.: Gas- and particle-phase primary emissions from in-use, on-road gasoline and diesel vehicles, Atmos. Environ., 88, 247–260, 2014.

McWhinney, R. D., Gao, S. S., Zhou, S., and Abbatt, J. P. D.: Evaluation of the effects of ozone oxidation on redox-cycling activity of two-stroke engine exhaust particles, Environ. Sci. Technol., 45, 2131–2136, https://doi.org/10.1021/es102874d, 2011.

Middlebrook, A. M., Bahreini, R., Jimenez, J. L., and Canagaratna, M. R.: Evaluation of composition-dependent collection efficiencies for the aerodyne aerosol mass spectrometer using field data, Aerosol Sci. Tech., 46, 258–271, https://doi.org/10.1080/02786826.2011.620041, 2012.

Mikkanen, P., Moisio, M., Keskinen, J., Ristimäki, J., and Marjamäki, M.: Sampling method for particle measurements of vehicle exhaust, SAE Tech. Pap. Ser. 2001, No. 2001-01-0219, https://doi.org/10.4271/2001-01-0219, 2001.

Mirme, A.: Electrical aerosol spectrometry, PhD thesis, Dissertationes Geophysicales Universitatis Tartuensis, No. 6, University of Tartu, Estonia, 1994.

Murphy, B. N., Donahue, N. M., Robinson, A. L., and Pandis, S. N.: A naming convention for atmospheric organic aerosol, Atmos. Chem. Phys., 14, 5825–5839, https://doi.org/10.5194/acp-14-5825-2014, 2014.

Murtonen, T., Lehtoranta, K., Korhonen, S., and Vesala, H.: Imitating emission matrix of large natural catalyst studies in engine laboratory, CIMAC congress, 6–10 June 2016, Helsinki, Finland, 2016.

Myhre, G., Shindell, D., Bréon, F. M., Collins, W., Fuglestvedt, J., Huang, J., Koch, D., Lamarque, J. F., Lee, D., Mendoza, B., Nakajima, T., Robock, A., Stephens, G., Takemura, T., and Zhang, H.: Anthropogenic and Natural Radiative Forcing, in: Climate Change 2013: The Physical Science Basis. Contribution of Working Group I to the Fifth Assessment Report of the Intergovernmental Panel on Climate Change, edited by: Stocker, T. F., Qin, D., Plattner, G.-K., Tignor, M., Allen, S. K., Boschung, J., Nauels, A., Xia, Y., Bex, V., and Midgley, P. M., Cambridge University Press, Cambridge, UK and New York, NY, USA, 659–740, 2013.

Nordin, E. Z., Eriksson, A. C., Roldin, P., Nilsson, P. T., Carlsson, J. E., Kajos, M. K., Hellén, H., Wittbom, C., Rissler, J., Löndahl, J., Swietlicki, E., Svenningsson, B., Bohgard, M., Kulmala, M., Hallquist, M., and Pagels, J. H.: Secondary organic aerosol formation from idling gasoline passenger vehicle emissions investigated in a smog chamber, Atmos. Chem. Phys., 13, 6101–6116, https://doi.org/10.5194/acp-13-6101-2013, 2013.

Ntziachristos, L., Giechaskiel, B., Pistikopoulos, P., Samaras, Z., Mathis, U., Mohr, M., Ristimaki, J., Keskinen, J., Mikkanen, P., Casati, R., Scheer, V., and Vogt, R.: Performance evaluation of a novel sampling and measurement system for exhaust particle characterization, SAE 2004 World Congress and Exhibition, 14 January 2004, Detroit, USA, https://doi.org/10.4271/2004-01-1439, 2004.

Ntziachristos, L., Saukko, E., Rönkkö, T., Lehtoranta, K., Timonen, H., Hillamo, R., and Keskinen, J.: Impact of sampling conditions and procedure on particulate matter emissions from a marine diesel engine, CIMAC congress, 6–10 June 2016, Helsinki, Finland, 2016.

Palm, B. B., Campuzano-Jost, P., Ortega, A. M., Day, D. A., Kaser, L., Jud, W., Karl, T., Hansel, A., Hunter, J. F., Cross, E. S., Kroll, J. H., Peng, Z., Brune, W. H., and Jimenez, J. L.: In situ secondary organic aerosol formation from ambient pine forest air using an oxidation flow reactor, Atmos. Chem. Phys., 16, 2943–2970, https://doi.org/10.5194/acp-16-2943-2016, 2016.

Pieber, S. M., Haddad, I. E., Slowik, J. G., Canagaratna, M. R., Jayne, J. T., Platt, S. M., Bozzetti, C., Daellenbach, K. R., Fro, R., Vlachou, A., Klein, F., Dommen, J., Miljevic, B., Jime, J. L., Worsnop, D. R., Baltensperger, U., and Prévôt, A. S. H.: Inorganic salt interference on CO_2^+ in aerodyne AMS and ACSM organic aerosol composition studies, Environ. Sci. Technol., 50, 10494–10503, https://doi.org/10.1021/acs.est.6b01035, 2016.

Pirjola, L., Dittrich, A., Niemi, J. V., Saarikoski, S., Timonen, H., Kuuluvainen, H., Järvinen, A., Kousa, A., Rönkkö, T., and Hillamo, R.: Physical and Chemical Characterization of Real-World Particle Number and Mass Emissions from City Buses in Finland, Environ. Sci. Technol., 50, 294–304, https://doi.org/10.1021/acs.est.5b04105, 2016.

Platt, S. M., El Haddad, I., Zardini, A. A., Clairotte, M., Astorga, C., Wolf, R., Slowik, J. G., Temime-Roussel, B., Marchand, N., Ježek, I., Drinovec, L., Močnik, G., Möhler, O., Richter, R., Barmet, P., Bianchi, F., Baltensperger, U., and Prévôt, A. S. H.: Secondary organic aerosol formation from gasoline vehicle emissions in a new mobile environmental reaction chamber, Atmos. Chem. Phys., 13, 9141–9158, https://doi.org/10.5194/acp-13-9141-2013, 2013.

Pöschl, U., Canagaratna, M., Jayne, J. T., Molina, L. T., Worsnop, D. R., Kolb, C. E., and Molina, M. J.: Mass accommodation coefficient of H_2SO_4 vapor on aqueous sulfuric acid surfaces and gaseous diffusion coefficient of H_2SO_4 in N_2/H_2O, J. Phys. Chem.-US, 102, 10082–10089, 1998.

Rager, J. E., Lichtveld, K., Ebersviller, S., Smeester, L., Jaspers, I., Sexton, K. G., and Fry, R. C.: A toxicogenomic comparison of primary and photochemically altered air pollutant mixtures, Environ. Health Persp., 119, 1583–1589, https://doi.org/10.1289/ehp.1003323, 2011.

Robinson, A. L., Donahue, N. M., Shrivastava, M. K., Weitkamp, E. A., Sage, A. M., Grieshop, A. P., Lane, T. E., Pierce, J. R., and Pandis, S. N.: Rethinking organic aerosols: semivolatile emissions and photochemical aging, Science, 315, 1259–1262, https://doi.org/10.1126/science.1133061, 2007.

Rönkkö, T., Lähde, T., Heikkilä, J., Pirjola, L., Bauschke, U., Arnold, F., Schlager, H., Rothe, D., Yli-Ojanperä, J., and Keskinen, J.: Effects of gaseous sulphuric acid on diesel exhaust nanoparticle formation and characteristics, Environ. Sci. Technol., 47, 11882–11889, https://doi.org/10.1021/es402354y, 2013.

Samy, S. and Zielinska, B.: Secondary organic aerosol production from modern diesel engine emissions, Atmos. Chem. Phys., 10, 609–625, https://doi.org/10.5194/acp-10-609-2010, 2010.

Saunders, S. M., Jenkin, M. E., Derwent, R. G., and Pilling, M. J.: Protocol for the development of the Master Chemical Mechanism, MCM v3 (Part A): tropospheric degradation of non-aromatic volatile organic compounds, Atmos. Chem. Phys., 3, 161–180, https://doi.org/10.5194/acp-3-161-2003, 2003.

Seinfeld, J. H. and Pandis, S. N.: Atmospheric Chemistry and Physics: From Air Pollution to Climate Change, 3 edn., Wiley, New York, USA, 2016.

Simonen, P., Saukko, E., Karjalainen, P., Timonen, H., Bloss, M., Aakko-Saksa, P., Rönkkö, T., Keskinen, J., and Dal Maso, M.: A new oxidation flow reactor for measuring secondary aerosol formation of rapidly changing emission sources, Atmos. Meas. Tech., 10, 1519–1537, https://doi.org/10.5194/amt-10-1519-2017, 2017.

Suarez-Bertoa, R., Zardini, A. A., Lilova, V., Meyer, D., Nakatani, S., Hibel, F., Ewers, J., Clairotte, M., Hill, L., and Astorga, C.: Intercomparison of real-time tailpipe ammonia measurements from vehicles tested over the new world-harmonized light-duty vehicle test cycle (WLTC), Environ. Sci. Pollut. R., 22, 7450–7460, 2015.

Tang, M. J., Shiraiwa, M., Pöschl, U., Cox, R. A., and Kalberer, M.: Compilation and evaluation of gas phase diffusion coefficients of reactive trace gases in the atmosphere: Volume 2. Diffusivities of organic compounds, pressure-normalised mean free paths, and average Knudsen numbers for gas uptake calculations, Atmos. Chem. Phys., 15, 5585–5598, https://doi.org/10.5194/acp-15-5585-2015, 2015.

Thiruvengadam, A., Besch, M., Yoon, S., Collins, J., Kappanna, H., Carder, D., Ayala, A., Herner, J., and Gautam, M.: Characterization of particulate matter emissions from a current technology natural gas engine, Environ. Sci. Technol., 48, 8235–8242, https://doi.org/10.1021/es5005973, 2014.

Timonen, H., Karjalainen, P., Saukko, E., Saarikoski, S., Aakko-Saksa, P., Simonen, P., Murtonen, T., Dal Maso, M., Kuuluvainen, H., Bloss, M., Ahlberg, E., Svenningsson, B., Pagels, J., Brune, W. H., Keskinen, J., Worsnop, D. R., Hillamo, R., and Rönkkö, T.: Influence of fuel ethanol content on primary emissions and secondary aerosol formation potential for a modern flex-fuel gasoline vehicle, Atmos. Chem. Phys., 17, 5311–5329, https://doi.org/10.5194/acp-17-5311-2017, 2017.

Tkacik, D. S., Lambe, A. T., Jathar, S., Li, X., Presto, A. A., Zhao, Y., Blake, D., Meinardi, S., Jayne, J. T., Croteau, P. L., and Robinson, A. L.: Secondary organic aerosol formation from in-use motor vehicle emissions using a potential aerosol mass reactor, Environ. Sci. Technol., 48, 11235–11242, https://doi.org/10.1021/es502239v, 2014.

Virtanen, A., Joutsensaari, J., Koop, T., Kannosto, J., Yli-Pirilä, P., Leskinen, J., Mäkelä, J. M., Holopainen, J. K., Pöschl, U., Kulmala, M., Worsnop, D. R., and Laaksonen, A.: An amorphous solid state of biogenic secondary organic aerosol particles. SI, Nature, 467, 824–7, https://doi.org/10.1038/nature09455, 2010.

Weitkamp, E. A., Sage, A. M., Pierce, J. R., Donahue, N. M., and Robinson, A. L.: Organic aerosol formation from photochemical oxidation of diesel exhaust in a smog chamber, Environ. Sci. Technol., 41, 6969–6975, https://doi.org/10.1021/es070193r, 2007.

Ziemann, P. J. and Atkinson, R.: Kinetics, products, and mechanisms of secondary organic aerosol formation, Chem. Soc. Rev., 41, 6582–6605, https://doi.org/10.1039/c2cs35122f, 2012.

Supplement of Atmos. Chem. Phys., 17, 8739–8755, 2017
https://doi.org/10.5194/acp-17-8739-2017-supplement

Atmospheric Chemistry and Physics Open Access

Supplement of

Comparison of primary and secondary particle formation from natural gas engine exhaust and of their volatility characteristics

Jenni Alanen et al.

Correspondence to: Topi Rönkkö (topi.ronkko@tut.fi)

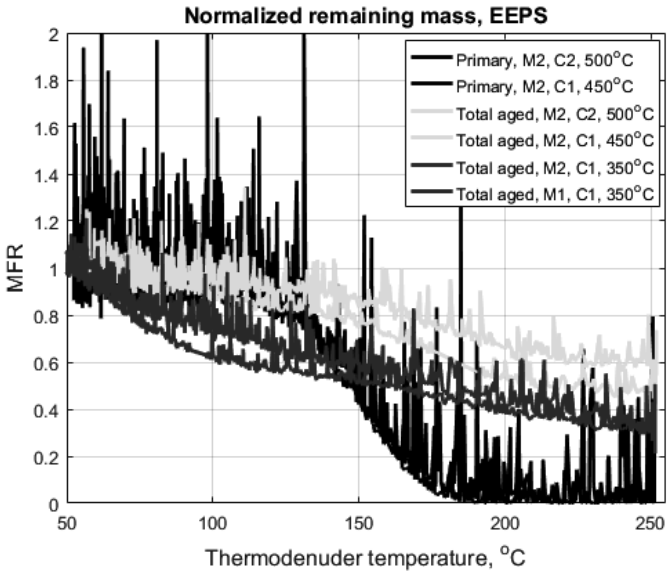

S1 Original one-second-resolution results of particle volatility measurements. Particle mass fraction remaining (MFR) after the thermodenuder treatment for the exhaust aerosol sample of three different types of particle emission from the natural gas engine. MFR values were calculated from the size distributions measured by EEPS with unit mass assumption.

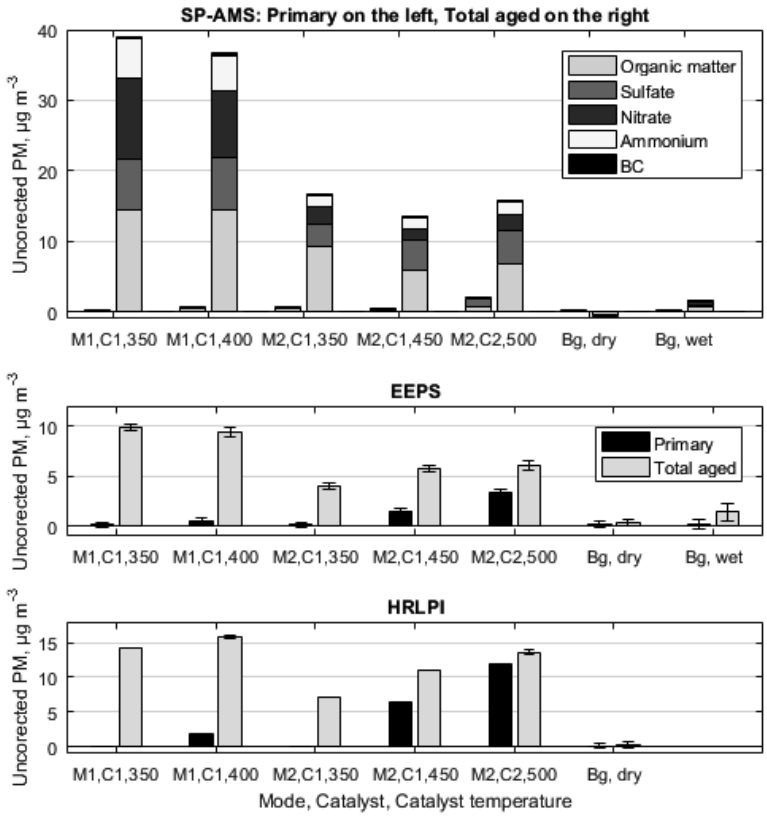

S2 Exhaust primary and total aged particle mass concentrations, compared with blank measurements, measured by SP-AMS, EEPS and HRLPI at different engine modes and catalyst temperatures.

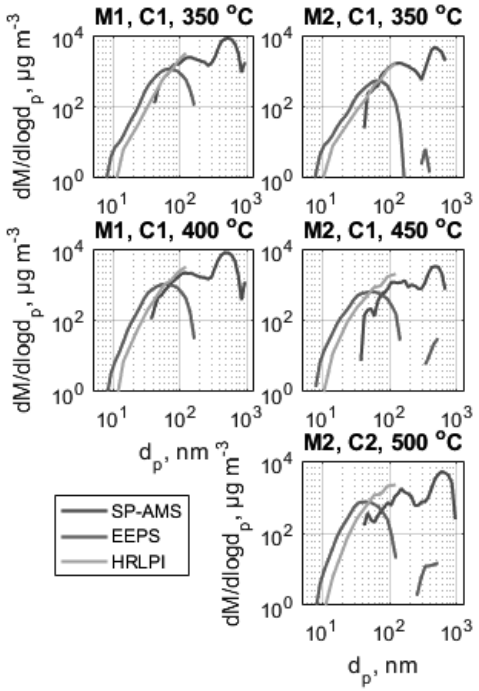

S3 Particle mass size distributions measured with SP-AMS, HRLPI and EEPS. Note that d_p stands for aerodynamic diameter for HRLPI, vacuum aerodynamic diameter for SP-AMS and mobility diameter for EEPS.